THE IONIC CONDUCTIVITY OF PURE AND MANGANESE DOPED SODIUM CHLORIDE

Thesis Submitted for the Degree of
Doctor of Philosophy

by

D.L. KIRK.
B.Sc. A.R.C.S. (LONDON) 1964

SEPTEMBER 1968

Department of Physical Metallurgy,
Imperial College of
Science and Technology,
University of London.

Contents Index.

PART I.

A determination of the parameters of ionic motion in single crystals of pure and manganese doped sodium chloride and their possible dependence upon the mechanical state of the crystal.

PART II

The state of aggregation and dispersion of divalent manganese. in single crystals of sodium chloride.

PART III.

The references quoted at the ends of PART I and II are more numerous than those used in the text. They are divided into a subject grouping and will provide the reader with a more detailed background than that discussed in the literature surveys.

ABSTRACT

The present research has been divided into two separate investigations: firstly, an examination of the parameters of ionic motion in pure, single crystals of sodium chloride and their dependence upon the line and surface defects in the crystal; secondly, an examination of the state of aggregation of divalent manganese in sodium chloride.

The initial investigation has shown that intrinsic conductivity is sensitive to the presence of grain and sub-grain boundaries and possibly dislocations. The parameters of ionic motion concerning the cation vacancy bear a close similarity to the values obtained for similar ionic motion in potassium chloride. The resolution of the aggregated phase of manganese was studied as a function of temperature using the techniques of ionic conductivity, dielectric absorption and relaxation and ionic thermocurrent measurement. The ionic thermocurrent technique has been used as a powerful tool for studying the dielectric relaxation processes in ionic materials; for the particular case of impurity-vacancy dipole relaxation, the technique was found to be superior to that of dielectric absorption in both resolution and sensitivity. Having obtained the impurity in solution by a suitable heat treatment, the different forms and associated states of the impurity ion were investigated using the above mentioned techniques and the parameters concerned with the association and aggregation reactions derived.

GLOSSARY OF SYMBOLS USED IN PART I

Q_I, Q_{III}	Apparent slopes of conductivity plot.
σ_1, σ_2	Cation and anion vacancy's contribution to ionic conductivity.
α_1, α_2	Molar concentration of cation and anion vacancies.
n_1, n_2	Number of cation and anion vacancies/c.c.
μ_1, μ_2	Cation and anion vacancy mobilities.
ϕ	Mobility ratio, $(\phi = \mu_2/\mu_1)$.
N	Number of anions or cations/c.c.
M, ρ	Molecular weight and density of sodium chloride.
D_1, D_2	Diffusivity of cation and anion vacancy.
g, h, s	Gibbs free energy, enthalpy and entropy of formation of Schottky pair.
Δg_1, Δh_1, Δs_1	Gibbs free energy, enthalpy and entropy of motion of cation vacancy.
Δg_2, Δh_2, Δs_2	Gibbs free energy, enthalpy and entropy of motion of anion vacancy.
ν_1, ν_2	Jump frequencies of cation and anion vacancy.
ν_p, ν_L	Jump frequencies of ion in perfect lattice and ion next to a point defect.
c	Divalent cation impurity content, mole fraction.
c_o	Background anion impurity content.

(i) The Scope and Aim of PART I

The aim of the introduction and discussion is not to present a complete and critical literature survey of ionic conduction and matter transport in non-metals, but rather to deal with the recent advances in the field which are of any significance or interest to the present work. For a detailed account of earlier experimental investigations, the reader is referred to the very extensive and thorough treatises of Lidiard [1] Howard and Lidiard [2] and Friauf.[3] For the initial considerations of point defects in solids and the nature of substitutional and interstitial defects, the references of Schottky [4] and Frenkel [5] are supplied.

(ii) Introduction and Survey of Literature

(1) Intrinsic Conduction

The study of point defects and their reactions in alkali halide single crystals constitutes one of the more widely investigated fields of solid state physics. The techniques of ionic conductivity and self diffusion have yielded valuable information about the parameters of motion and formation of these defects. Ionic conductivity has produced the widest divergence of results, probably due to systematic errors appearing between different groups of investigators.

The Arrhenius plot of ionic conductivity in Fig.(1.1), is the normal method of presenting conductivity data and this shows the

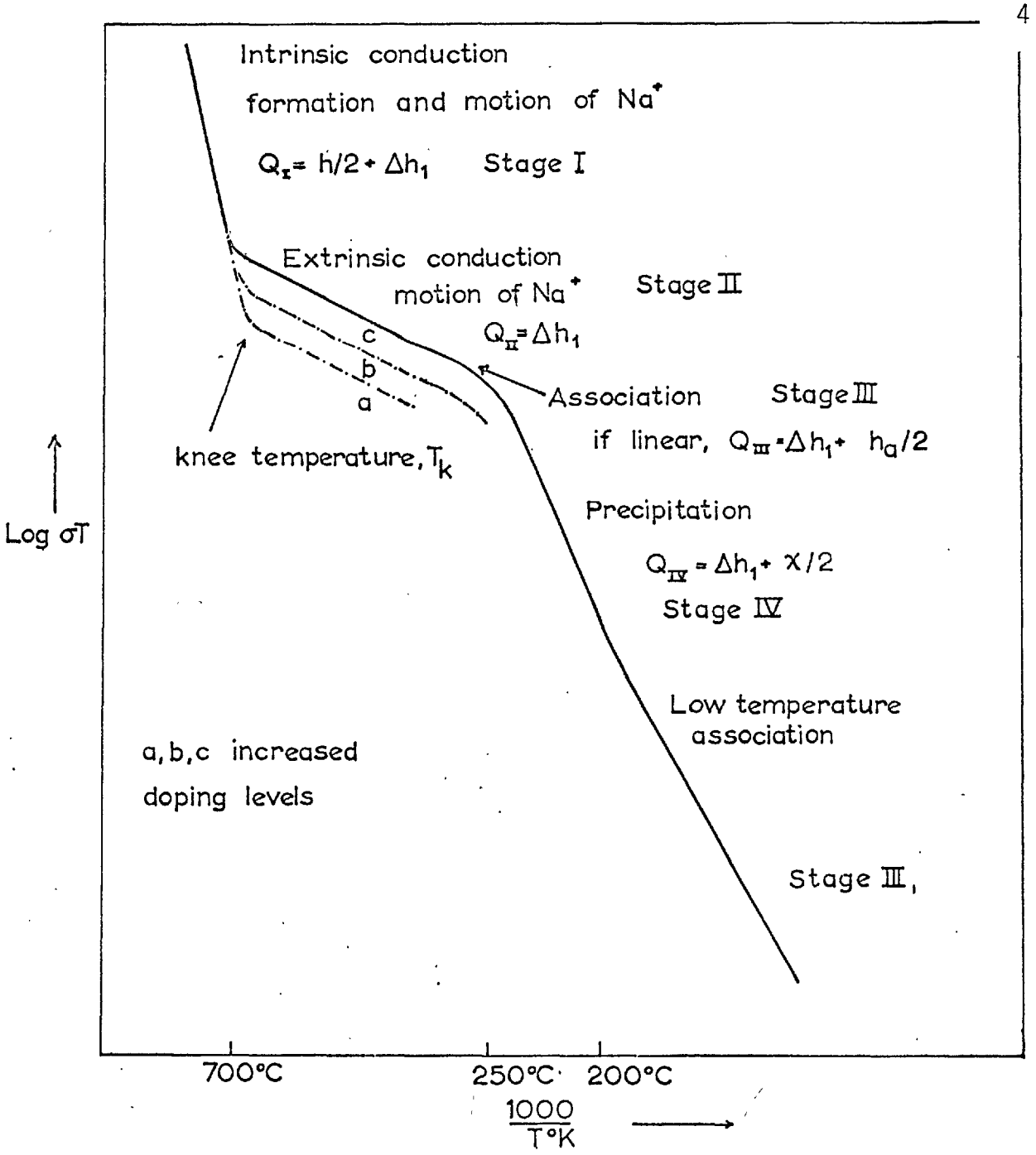

Fig. 1.1 Qualitative features of Arrhenius conductivity plot.

ENTHALPIES OF FORMATION OF THE SCHOTTKY PAIR AND MOTION OF THE CATION VACANCY - FOR SODIUM CHLORIDE

Source	heV	Δh_1eV.	Technique
Taylor [163]	2.04	0.69	D.C.
Jain et al.[110]	2.30	0.69 - 0.75	Pulsed D.C.
Graham[129]	1.70	0.80	D.C.
	2.14	0.79	A.C.
Dreyfus et al.[54]	2.12	0.79	D.C.
Etzel et al.[104]	2.02	0.85	Pulsed D.C.
Mapother et al.[56]	2.12	0.77-0.83	Diffusion
Bierman [164]	2.19	0.74	D.C. (Q_{II})
		0.85	D.C. Isotherms)
Fumi et al.[165]	2.12	-	Theoretical
Boswarva et al.[162]	2.138	-	Theoretical
Schamp et al.[66]	-	0.86	Diffusion
Bean [106]	-	0.78	A.C.
Laurent et al.[58]	-	0.60	Diffusion
Redfern et al.[100]	-	0.69 - 0.72	D.C.
Haven [57]	-	0.72	A.C.
Kobayashi et al.[166]	-	0.74	A.C.
Itoh et al.[85]	-	0.74	N.M.R.
Reif et al.[91]	-	0.66	N.M.R.
Guccione et al.[167]	-	0.87	Theoretical

characteristic regions with their appropriate nomenclature. Table (1.1) shows the enthalpies of formation of the Schottky pair and of motion of the cation vacancy in sodium chloride, as determined by earlier workers using different experimental techniques.

Lehfeldt [6] successfully resolved the intrinsic and extrinsic regions of ionic conduction whilst working on single crystals of the Li, Na, K, Rb halides, whilst Koch and Wagner [7] showed that the magnitude of the extrinsic conductivity was sensitive to the level of doping with a divalent cation impurity. Density studies performed by Pick and Weber [8] on potassium chloride single crystals, doped with calcium and strontium chlorides, indicated that the divalent ions occupied substitutional positions on the cation sub-lattice, while Kelting and Witt [9] used the knee temperature to determine the divalent cation impurity contents.

It has often been assumed that intrinsic conductivity is solely due to the formation and motion of cation vacancies, the anion mobility being negligible. This simple assumption is questioned when the transport number determinations of Kerkhoff [12] and Tubandt [13] are compared with conductivity data. These measurements were performed upon pellets of potassium chloride, hot pressed from the powder, and they show a considerable contribution appearing from the motion of the anion vacancy in the intrinsic region of conduction, with a possible electronic contribution of about 5% which appeared to be independent of temperature. Tubandt's work on sodium chloride, prepared in the same manner, also showed a structure sensitive anion contribution to matter transport. The most recent transport number determinations are those of Haven.[14]

Using the classical method of weighing, he replaced the hot pressed powders of the previous workers by three plates of single crystals of sodium or potassium chloride and used graphite electrodes. Within the temperature range 690°C - 715°C, the cation transport number t_1 had a value of 0.86 for sodium chloride, with little evidence of an electronic contribution. This anion contribution was larger than the previous determinations and because of the single crystal nature of the specimens, is probably more representative of matter transport through the bulk of the material. The results also suggest a difference of 0.15eV. between the enthalpies of motion of the anion and cation vacancy.

The magnitude and source of a possible electronic contribution to the bulk conductivity has been a point of some discussion in the past. The band gap in sodium chloride is approximately 10.0eV.[15] if exciton and other impurity levels are neglected. This precludes any significant electronic conduction by thermal production of electron-hole pairs. Electrons may appear in the conduction band from alternative sources, namely uncompensated bonds present in dislocation cores [16], impurity ions, F centres [17] formed at the electrode-crystal interface or by possible deviations from stoichiometry caused by variations of the partial pressure of one particular component in a surrounding atmosphere.[18] All these factors will introduce donor levels of varying concentration between the valence and conduction bands.

In contrast, the anion contribution to the intrinsic conduction is a matter that has received considerable attention. Allnatt and Jacobs [50] were the first to attribute a curvature of the

intrinsic region in potassium chloride to anion motion. Transport numbers and mobility ratios determined from Allnatt's data, showed fair agreement with the transport numbers of Kerkhoff [12] and diffusion data of Laurent and Benard.[58] The earlier conductivity data of Phipps and Partridge [51] had also shown a curvature of the intrinsic region, but this had been ignored and a straight line drawn through the conductivity points. In contrast, Aschner's [62] conductivity data for the same material had a linear intrinsic region up to the melting point. Fig. (1.2). When Aschner's results are compared with Allnatt's, there is agreement as to the slope of the high temperature end of intrinsic conductivity, although there is a small systematic difference in its magnitude. This agreement disappears at the lower temperatures. Aschner's conductivity determinations were made upon well annealed single crystals, whilst Allnatt's crystals probably contained many sub-grains and possibly grain boundaries as a result of growing the crystals by the Stockbarger technique and then annealing them in the conductivity rig at high temperatures for long periods of time. As a consequence of the design of the rig, the crystals experienced considerable plastic deformation at these temperatures. Beaumont and Jacobs,[52] using the same crystals and conductivity rig as Allnatt et al., have suggested that intrinsic conductivity is in fact represented by a smooth curve up to the melting point. They have managed to fit their data to a theoretical curve compounded from the eight variables connected with the intrinsic, extrinsic and association regions of ionic conductivity. To do this they used a least squares minimization routine written into a computer

A Comparison of the conductivity data for KCl.

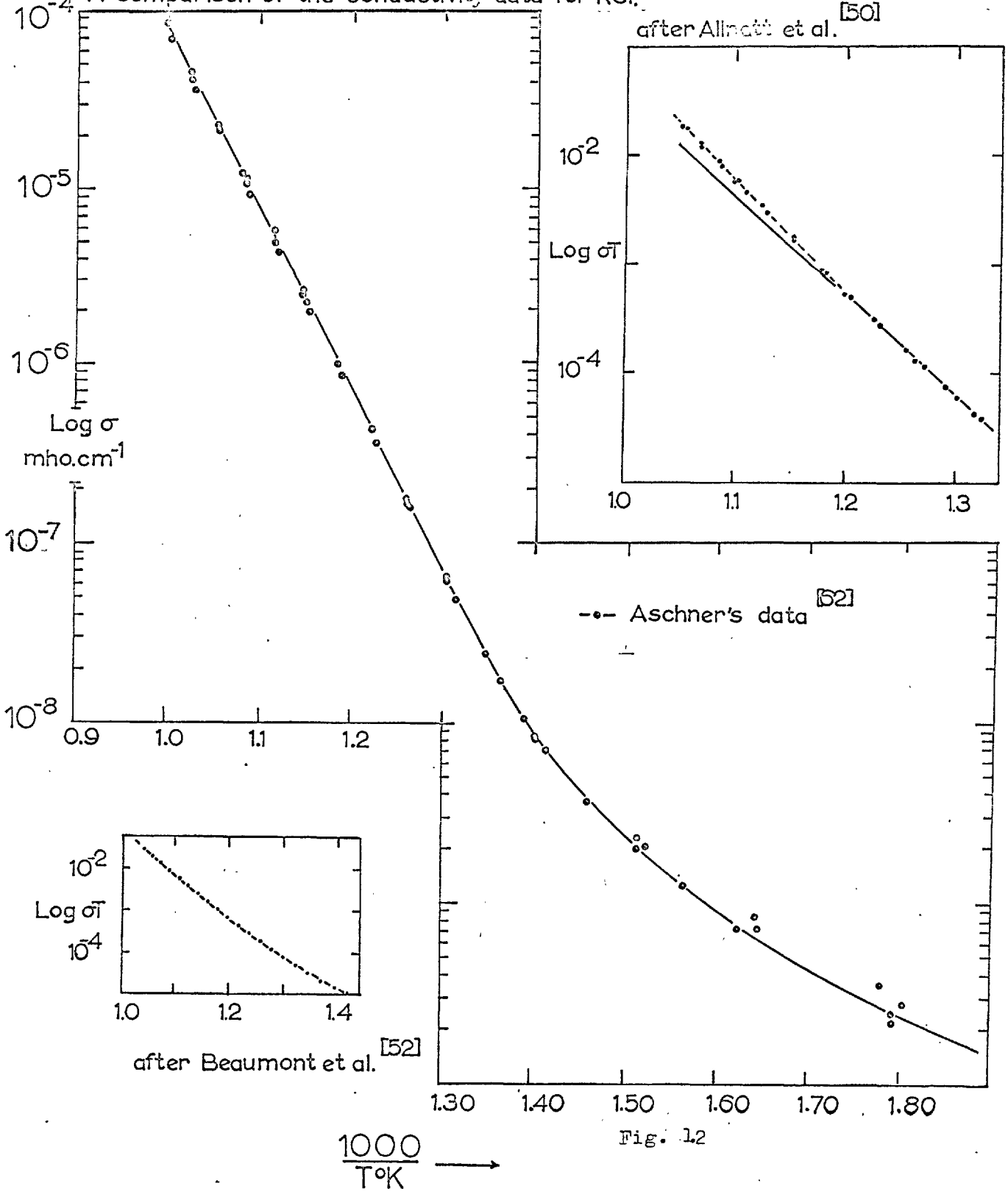

Fig. 1.2

programme. Their results are in good agreement with the diffusion studies of Fuller, [53] who submitted his results to the same form of analysis. A feature neither worker discusses is the large variation in the entropy of anion motion which appears from specimen to specimen. This variation is not reproduced in the entropy of motion for the cation vacancy. This could be interpreted either as a true change in entropy for anion motion in the bulk of the crystal, or a variable magnitude in the anion vacancy's contribution to ionic conduction, both of which would appear as a variation in a pre-exponential term.

The intrinsic conductivity of the sodium chloride lattice has not been so carefully investigated as that of potassium chloride. Dreyfus and Nowick [54] have attempted a compilation of the results of various workers for the intrinsic and extrinsic regions of conductivity for sodium chloride. Not too much significance can be attached to their conclusions because they have neglected to take into account

(i) The experimental method of obtaining conductivity results (D.C. measurements give consistently low values for Q_1 compared with A.C. measurements).

(ii) The possible effects of an anion contribution steepening Q_1. Although a curvature of the intrinsic region has never been reported in sodium chloride, Jain [55] has suggested a value of 1.92eV. for Q_1. This is very large, possibly due to the effects of an anion contribution.

(iii) The effects of association reactions steepening the slope of the extrinsic regions to give high values for Q_{II}.

(2) Diffusion

Mapother, Crooks and Maurer [56] were the first to measure the diffusion of Na^{24} into single crystals of sodium bromide and chloride and then to compare this with the ionic conductivity using the Nernst-Einstein equation

$$\sigma_1 / D_1 = \frac{N e^2}{kT}$$

The increased diffusion, over and above that calculated from the conductivity, which occurred below 500°C, was cited as evidence for vacancy-pairs, or a possible correlation effect. Both these suggestions were subsequently rejected as a correlation effect would have depressed the diffusion below the conductivity and vacancy-pairs would have required a larger anion diffusivity than was observed. The effect was due to the diffusion of divalent cation-vacancy pairs, which contribute to diffusion but not to conductivity. Although the Nernst-Einstein equation was satisfied in the intrinsic regions of conductivity, Haven, [57] performing a similar comparison in pure sodium chloride, found the above relationship was not valid. In many cases, the ratio between the conductivity and diffusion was just that expected from a consideration of correlation effects. A correlation effect appears when the defect mechanisms of diffusion are considered. The assumption that diffusion occurs by random jumps is not correct for either the vacancy or interstitialcy mechanisms. Suppose that an ion has just made one jump by exchange with a vacancy. The possible directions for the next jump are clearly not of an equal probability.

The vacancy is more likely to effect a movement by a reverse jump of the ion. Similarly the probability is less than random that the second jump will take place in the same direction as the first. The effect of this is to introduce a correlation factor f into the theoretical expression for D, calculated on the assumption of a random migration of ions. f depends upon the lattice geometry, type of jump mechanism (interstitial or vacancy) and when two or more species diffuse on the same lattice, on their relative rates of jumping.

Laurent and Benard (58,59) made a study of the self diffusion of both the cations and anions in single and polycrystals of the alkali halides. Also as a function of grain size over a temperature range of 400°C to the melting point. In all the crystals, except those based upon caesium, they found that the activation energies of self diffusion appropriate to the anion or cation were independent of grain size. Further, the magnitude of the cation diffusion was not affected by grain size. This was in marked contrast to the anion diffusion coefficient, which increased in magnitude with decreasing grain size. They correlated this increase in anion diffusivity with the relative polarization of the ions: the greater the polarization of the ion, the greater the influence of the grain and sub-grain boundaries upon its movement. In the caesium salts, the cation diffusion was also enhanced by a decrease in grain size. Their work suffered in two respects: firstly, no attempt was made to keep the grain boundaries free from anion impurities. In particular $(OH)^-$ ions were present in the poly-crystals formed by sintering cold pressed powders; secondly, they

used a method of analysis devised by Fisher and Whipple [60,61] which is only applicable to a semi-infinite slab of homogeneous, crystalline material. The Whipple analysis does not account for the diffusion processes occurring down grain boundaries.

Cabane [62] rectified these faults by preparing polycrystalline specimens from hot pressed powders which had been subjected to a prolonged heat treatment at 400°C, to remove any moisture. This treatment produced crystals that were transparent with polycrystalline densities near the theoretical limit. To measure true grain boundary diffusion, Cabane developed an auto-radiographic technique and modified the Fisher-Whipple analysis to the situation of diffusion down a grain boundary. In grain boundaries free of the $(OH)^-$ ion the activation energy for diffusion was similar to that for diffusion through the bulk of the material. When the $(OH)^-$ ion was present in the boundaries, the activation energy for diffusion was much lower.

Aschner [63] measured conductivity and cation diffusion in crystals of pure and cadmium doped sodium chloride. Good agreement between conductivity and diffusion was observed in the doped crystal when a degree of association for the particular doping level and temperature was introduced into the correlation factor. This work showed a general feature of cation diffusion in crystals doped with divalent cations in so far as diffusivities exceed the values calculated from conductivity by the greatest amount, at the lowest temperatures and highest doping levels, the conditions under which the impurity-vacancy dipole concentration is greatest. Lidiard [1] has performed a critical analysis of Aschner's data and has obtained a correlation factor for tracer diffusion in the sodium chloride

lattice in terms of the jump frequencies of the associated impurity ions and cation vacancies.

Anion diffusion studies in the alkali halides were initiated by Chemla,[64,65] who measured the diffusion of the isotope Cl^{36} in sodium chloride over a limited range of temperatures. Laurent and Bénard [58,59] repeated these measurements, extending the range of temperature investigated from 400°C to the melting point. Little progress was made in extending the determination of anion diffusivities to lower temperatures until the introduction of the radio-active gas exchange technique. This method involved the monitoring of the rate of exchange of radio-active Cl^{36} (produced by neutron irradiation) from the solid state into a surrounding atmosphere of chlorine gas. It enabled the measurement of diffusion coefficients several orders of magnitude smaller than that obtainable with the usual sectioning techniques. Harrison, Morrison and Rudham, [69] using this technique, observed that the chlorine ion diffusion in sodium chloride presented a knee at 500°C, similar to that of ionic conductivity and cation diffusivity. They suggested that divalent anion impurities caused the anion vacancy concentration to become fixed at this temperature, similar to the extrinsic regions of ionic conductivity. Lidiard [70] pointed out that this was a contradiction of the Law of Mass Action and suggested that the diffusion might be occurring via vacancy pairs. If this were true, the presence of divalent impurities would decrease the free anion vacancy diffusion, but not affect the vacancy pair diffusion. These conclusions were subsequently verified by Morrison and Rudham, [71] who showed that above a certain doping level, the anion diffusion coefficient of potassium chloride was

insensitive to the presence of divalent cations, indicating that vacancy pair diffusion was occurring in doped crystals. Laurance [72] measured anion diffusion in pure sodium chloride and crystals doped with varying amounts of calcium over the temperature range 520°C to 740°C, and found that anion diffusion in pure crystals occurred with an energy of 2.12eV. The diffusion coefficient in crystals containing calcium was smaller than that of pure crystals by a factor of 5 to 10 and had an activation energy of 2.5eV. The results were explained upon the basis of diffusion occurring by free anion vacancies and vacancy pairs, the energy of migration of the vacancy pair being similar to that of the free anion vacancy. By using a theoretical value of 0.6eV. for the pair-binding energy [73] he deduced a value of 1.07eV. for its enthalpy of migration. This value would suggest that there is no pair contribution to cation diffusion, because the motional energy of the vacancy pair is significantly larger than that of the cation vacancy. Barr, Morrison and Schroeder [74] measured anion diffusion in sodium chloride between 300°C and 700°C and then found the concentration of the divalent, cation impurity by measuring the ionic conductivity of the specimens. They managed to resolve their diffusion plots into a sum of two exponential processes, representing a free anion vacancy and a pair contribution, which were of the form

$$D_2 = 1.1 \exp - (1.92/kT) \text{ cm}^2/\text{sec.}$$

$$D_p = 363 \exp - (2.37/kT) \text{ cm}^2/\text{sec.}$$

This is to be compared with Laurance's [72] pair diffusion of

$$D_p = 1{,}280 \exp - (2.49/kT) \text{ cm}^2/\text{sec.}$$

Although the energy for pair-diffusion was in good agreement with that of Laurance's results for doped crystals, there was a discrepancy in the magnitude of D_o both for pair and free anion vacancy diffusion. It was suggested that a precipitated phase of $CaCl_2$ was producing considerable strains in the lattice, resulting in the formation of dislocations in the bulk of the crystal, these offering paths of easy diffusion for the anions or vacancy pairs. This variation in the magnitude of the anion diffusivity is present in all the data of the previous workers. The summary of their quantitative results is presented in Table (1.2) and for a fixed temperature, the large variations in the values of D_2 can only suggest that the anion diffusion is structure sensitive. Barr et al also found that the magnitude of the anion diffusion coefficient was sensitive to the previous thermal history of the crystal. Barr, Hoodless, Morrison and Rudham [75] have observed that a reduction in the diffusivity and change in activation energy, which occurred below the intrinsic regions, could be correlated with a decrease in dislocation density, as determined by etching techniques.

Fuller [53] has recently measured the anion diffusion in potassium chloride and has produced essentially the same features observed in sodium chloride. Quantitatively his results were:

$$D_2 = 36.5 \exp - (2.10/kT) \text{ cm}^2/\text{sec.}$$

$$D_p = 8.56 \exp - (2.65/kT) \text{ cm}^2/\text{sec.}$$

with values of 0.95eV. for Δh_2 and 2.31eV. for h.

TABLE (1.2)

ACTIVATION ENERGIES FOR ANION VACANCY DIFFUSION IN SODIUM CHLORIDE

$$D = D_o \exp - Q/kT \ cm^2/sec.$$

Q eV	D_o cm^2/s	Temperature range °C	Interpretation	Reference and Authors
2.23	110	600 - 730	Free vacancy	(58, 59) Laurent et al.
2.49	1,280	585 - 730	Free vacancy and pair motion in doped crystals	(72) Laurance
2.70	3,000	650 - 760	Free vacancy	(64, 65) Chemla
2.12	56	520 - 745	Free vacancy and pair motion in pure crystals	(72) Laurance
2.3 - 2.6	-	400	Pair and free vacancy	(75) Barr et al.
2.29	490	450 - 690	Free vacancy	(69) Harrison et al.
1.92	1.1	500	Free vacancy	(74)
2.37	363		Vacancy pair	Barr et al.

Additional evidence for the existence of the vacancy pair appears in the dielectric absorptions observed in the megacycle range of frequencies by Sastry and Srinivasan [76] and Sack and Smith.[77] Sastry et al. observed a dielectric absorption in the temperature range of 600°C to the melting point in potassium chloride. They also observed that the dipolar contribution to the dielectric loss was unaffected by additions of strontium chloride. The addition of divalent cation impurity is known to affect the free anion and cation vacancy concentration, so the observation would suggest that the dipolar loss was caused by the vacancy pair. Unfortunately, the concentration of vacancy pairs derived from the loss data was unreasonably large. At 700°C, the calculated concentration of vacancy pairs was 25% of the total concentration of ion pairs. The large concentrations of point defects required to explain these effects have never been observed in specific heat determinations at elevated temperatures.[80] Theoretical refinements to the predicted equilibrium concentration of vacancy pairs made by Boswarva and Franklin [81] have shown that the vacancy pair concentration could never exceed 3% of the total lattice sites. The discrepancy between theory and experiment still exists. Sack et al. [77] measured the dielectric losses of NaCl, KCl, AgCl and AgBr at a fixed frequency of 24 kilomegacycles/sec., over a temperature range from room temperature to just below the melting point. The dielectric losses were fitted to two components, one representing the tail of a reststrahlen absorption peak, and the other resulting from the reorientation of vacancy pairs.

(3) Extrinsic Conductivity

From a knowledge of Q_I and Q_{II}, the enthalpy of formation of a Schottky pair and the enthalpy of motion of the cation vacancy may be calculated. Figures quoted for Δh_I, Table (1.1), obtained from region II, have a wide scatter and are often dependent on the divalent, cation impurity present in the crystal; in contrast to theory, which predicts that Q_{II} should be independent of the impurity ion added. The divergence of results is due to the combined effects of the association reaction and a prolonged changeover from extrinsic to intrinsic conduction, both of which make extrinsic conductivity an ill defined region of the Arrhenius plot.

Whilst the addition of divalent cation impurities enhances ionic conduction, divalent anion additions are seen to depress it: Rolfe (99) has attempted to suppress the cation impurity concentration, so that anion conduction becomes the predominant process. This was achieved by doping potassium bromide with potassium carbonate, the carbonate radical acting as a divalent anion $(CO_3)^{--}$. Enthalpies of motion of $\Delta h_1 = 0.665$, $\Delta h_2 = 0.87$, for the anion and cation vacancies were obtained. Anion additions may act as either substitutional defects or complexing centres. The anions $(CO_3)^{--}$, $(SO_4)^{--}$ are divalent in nature and play a substitutional role similar to that of the divalent cation impurities Cd^{++}, Ca^{++}. Redfern and Pratt (100) doped sodium chloride with O^{--} and $(SO_4)^{--}$ ions. These suppressed the magnitude of the extrinsic conductivity, but the apparent slope Q_{II} remained the same as that of the pure crystal, showing that the cation vacancy was still the predominant charge carrying defect,

although their concentration had been greatly reduced by the addition of the anions. Anger, Fritz and Luty [101] have doped crystals of potassium chloride with $(OH)^-$ ions, and then studied their properties using the techniques of bulk density measurements, ionic conductivity and optical absorption. The absorption measurements were made at 2.04mμ and 2.8μ. It was found that the $(OH)^-$ ion occupies a substitutional position and complexes with divalent cations. It is the latter reaction which probably reduces the number of free cation vacancies. The $(OH)^-$ ion does not produce any charge anomaly, as compared with $(SO_4)^{--}$ and O^{--} and will not reduce the cation vacancy concentration through the condition of charge neutrality. It is interesting to note that the $(OH)^-$ ion or possibly the (H_2O) molecule has a profound effect upon the precipitation reactions of divalent cations M^{++} [102].

Etzel and Maurer studied the extrinsic and association regions of ionic conductivity in cadmium doped sodium chloride. Their enthalpy of cation motion 0.85eV., although rather high, was obtained by a critical analysis of the conductivity isotherms. Dreyfus and Nowick [105] made an extensive study of the D.C. conductivity in the extrinsic and low temperature association and precipitation regions of sodium chloride doped with different divalent cations. Although having a large scatter in the values of Q_{II} (0.70 - 0.83eV.) their results did not show any systematic dependence upon the radius of the impurity ion. An independent estimate of the enthalpy of motion of the cation vacancy of 0.79 ± 0.02eV. was also obtained by quenching pure and doped crystals from 100°C to -60°C and then measuring the enhanced conductivity as a function of temperature, during a heating

of the crystal. This method assumed that the cation vacancy concentration, frozen in by the heat treatment, remained essentially constant below room temperatures, the conditions for true extrinsic conduction. The data had to be corrected for the annealing out of these non-equilibrium vacancies.

(4) Paths of Enhanced Conductivity and Diffusion

Dislocations in ionic crystals can affect the conductivity by modifying the distribution of free cation vacancies and by acting as possible paths of enhanced diffusion. Pratt [112] first pointed out that dislocations in an ionic crystal could become charged by having an excess of jogs of one sign lying on the dislocation core with a sheath or charge cloud of vacancies of predominantly opposite sign surrounding it. The first attempt to determine the form of the potential associated with the space-charge and its interactions was made by Eshelby, Newey, Pratt and Lidiard [113], who also tried to correlate their findings with the temperature dependence of the yield stress in pure sodium chloride. They argued for the existence of an impurity controlled isoelectric temperature, where the charge on the dislocation core is zero. This "temperature" arises from the cation concentration being controlled by the divalent, cation content, the isoelectric temperature occurring when the cation and anion vacancy concentrations became equal. Below the isoelectric temperature, the dislocation core has an excess of negative jogs (sodium ion vacancies on dislocation cores) with a positive charge cloud surrounding it. Above this temperature, the situation is reversed. There is considerable experimental evidence for the

existence of this space charge cloud, in particular the light scattering experiments of Plint, Theimer and Sibley [114] show the existence of the space charge cylinder and an isoelectric point in pure sodium chloride. Many observations of isoelectric temperatures have been made in ionic crystals subjected to flexural vibrations and bending experiments.[115, 116]

As well as modifying the defect distribution, dislocations may act as paths of enhanced diffusion. If a grain or sub-grain boundary is considered to be made up of an array of dislocations, then the grain boundaries may also act as a path of high diffusivity. Enhanced diffusion along grain boundaries has been observed many times in polycrystalline metals.[123, 124]

Conductivity studies of dislocation cores in lithium fluoride by Tucker and Laskar [125] have shown that cations (Na^+) may diffuse down both edge and screw dislocations with an activation energy of 0.3eV. This work was extended by Moment and Gordon [126] to sub-grain and grain boundaries with misorientations from $4^\circ 20'$ to $53^\circ 30'$. The activation energy of 0.32eV. for the sodium ion diffusion down the grain boundary was found to be independent of the boundary's degree of misorientation, over a temperature range of $225^\circ C$ to $325^\circ C$.

An investigation of the dependence of ionic conductivity upon grain size in polycrystalline sodium chloride has been made by Graham,[129] using both A.C. and D.C. methods. His work may be summarized in the following manner:-

(i) The contribution of the chlorine ion vacancy to the total conductivity is significant in the intrinsic regions of conductivity, even for single crystals.

(ii) The chlorine ion vacancy's contribution to conductivity is reciprocally dependent upon grain size.

(iii) The sodium ion vacancy conduction is nearly independent of grain size.

(iv) The layer thickness providing the enhanced conductivity is approximately 0.1 microns thick at 350°C.

(5) The Effect of Deformation upon Ionic Conductivity

The measured conductivity of alkali halide single crystals is known to change when the crystal is subjected to homogeneous plastic deformation. Temporary increases in conductivity are observed during deformation, followed by a decay in the conductivity when the deformation ceases. This is the so-called Gyulai-Hartly [130] effect and its explanation is based upon isolated vacancies, generated by plastic deformation, producing the excess conductivity. This then dies away as the vacancies are annealed out by migration to the dislocations, surfaces and grain boundaries, or by clustering into vacancy platelets. The situation occurring during plastic deformation is made complex by the presence of a charge flow associated with dislocation movement, this being independent of the applied electric field. This causes a potential to be developed across the crystal during the course of deformation. Many authors have dealt with the various aspects of this charge flow, in particular the papers of Whitworth [131] and Davidge [132] deal in detail with the charges appearing upon the edge and screw dislocations, which are forced to move by various modes of deformation.

Few attempts have been made to correlate the excess conductivity with the details of plastic deformation. Caffyn and Goodfellow [138] studied the increase of conductivity in crystals deformed by loads of increasing magnitude. The excess conductivity was found to be proportional to the increments of applied stress. Taylor and Pratt [139] emphasized that squat specimens showed a sizeable conductivity increase only when considerable strains were achieved, whereas thin tall specimens did not display extra conduction even at high levels of deformation. This showed that inter-penetration of the different slip systems must occur before substantial vacancy production becomes possible.

Camagni and Manara [141] extended this study by observing the excess conductivity of alkali halide single crystals during homogeneous deformation at low and constant strain rates. Using potassium chloride and bromide crystals they found that a steady state enhancement of conductivity only occurred when deformation into the plastic region was performed, and this enhancement disappeared rapidly as soon as the plastic deformation was interrupted. By studying the dependence of this conductivity enhancement upon temperature, a migrational energy of less than 0.35eV. was obtained for the excess carriers in both salts. The suggested carriers were either an anion interstitial or a dislocation charge cloud vacancy having a low migrational energy.

(iii) The Basic Theoretical Equations Concerning Ionic Conduction

(1) Intrinsic Conduction

At high temperatures in a pure crystal the conduction is intrinsic and the vacancy concentration is a consequence of the thermal statistics of the lattice only and independent of impurity doping level. The equations governing this intrinsic conduction are:-

$$\sigma = \sigma_1 + \sigma_2 \qquad \text{——— (1)}$$

$$x_1 x_2 = \exp -g/kT = Xo^2 \qquad \text{——— (2)}$$

$$\mu_1 = \frac{4a^2e^2\nu_1}{kT} \exp -\Delta g_1/kT$$

$$\mu_2 = \frac{4a^2e^2\nu_1}{kT} \exp -\Delta g_2/kT$$

$$\sigma = Ne\ (\mu_1 x_1 + \mu_2 x_2) \qquad \text{——— (3)}$$

From (1), (2) and (3)

$$\sigma = \frac{4Na^2e^2}{kT} \left(\nu_1 \exp -(\Delta g_1 + g/2)/kT\right) + \left(\nu_2 \exp -(\Delta g_2 + g/2)/kT\right) \qquad \text{——— (4)}$$

Where $\Delta g_{1,2} = \Delta h_{1,2} - T\Delta s_{1,2}$

$$g = h - Ts$$

If $\sigma_1 \gg \sigma_2$, the conductivity plot presents a linear region of which the specific conductivity is given by

$$\sigma = \frac{4Na^2e^2\nu_1}{kT} \exp(\Delta s_1 + s/2)/kT. \exp -(\Delta h_1 + h/2)/kT$$

with a slope of $(\Delta h_1 + h/2)k$. If there is an appreciable anion contribution, $\sigma_1 \approx \sigma_2$ and a curvature or breakaway to an increased slope might appear in the intrinsic region, as defined by equation (4). This may explain the large variation in activation energies, Q_1, quoted for sodium and potassium chlorides.

(2) Extrinsic Conduction

At lower temperatures, the conductivity becomes extrinsic, the vacancy concentration being equal to the net concentration of divalent impurities present in the crystal. In the extrinsic range of conduction, anion motion is insignificant and

$$\sigma = Nce\mu_1/kT \qquad \text{——— (5)}$$

$$\sigma = \frac{4Nx_1a^2e^2\nu_1}{kT} \exp\Delta S_1/k. \exp -\Delta h_1/kT \qquad \text{——— (6)}$$

Applying the condition of charge neutrality to equations (2) and (3),

$$x_1 = c + x_2 \qquad \text{——— (7)}$$

we find that at constant temperature

——— (8)

when $c \gg x_o$.

$$\frac{\sigma}{\sigma_o} \approx \frac{c}{x_o(1+\phi)} \qquad \text{——— (9)}$$

For any constant temperature, a plot of σ versus c should be linear for extrinsic conduction.

(3) Diffusion, the Nernst-Einstein Equation and Correlation Corrections

Matter transport in ionic crystals may be studied by diffusion or conductivity. If the same microscopic species is producing the conductivity and diffusion by essentially the same process, then conductivity and diffusivity are related by the Nernst-Einstein equation

$$\frac{\sigma_i}{D_i} = \frac{N q_i^2}{kT}$$

For sodium chloride, where anion and cation vacancies may contribute to conduction

$$\sigma = \frac{Ne^2}{kT} (D_1 + D_2)$$

A correlation factor of 0.7815, appropiate to the f. c.c. lattice of sodium chloride, will be used when utilizing the Nernst-Einstein equation in the present work. It is not necessary to consider correlation effects as contributing to the expressions for conductivity, because the applied electric field removes the randomness associated with the individual jumps. Using the correlation factor, the correct form of the Nernst-Einstein equation becomes

$$\frac{\sigma}{(D_1 + D_2)} = \frac{1.28Ne^2}{kT}$$

(4) Debye-Huckel Corrections

According to the Debye-Huckel theory of inter-ionic attraction in dilute solutions [150], each ion is surrounded by an atmosphere of oppositely charged ions, whose net charge is on average opposite to that of the central ion. When these ions have no external force applied to them, the atmosphere is spherically symmetric about the ion. When an external electric field is applied, the ions are set in motion and changes in the ionic atmosphere arise, which results in a decrease in the velocity of the ions. Debye and Huckel first pointed out that these effects are two-fold, namely:-

(i) A relaxation of the ions surrounding atmosphere. Because of the difference in sign between an ion and its compensating cloud, an electric field will tend to move the central ion in one direction and the atmosphere in the opposite one. In this state, the force exerted by the atmosphere is no longer uniform in all directions, but is greater behind the ion than in front of it. Consequently the ion is slowed down. These retarding effects are much smaller in solid than in liquid solutions, principally because the vacancy concentration in the solid phase is much smaller than the ion concentrations appearing in solvents.

(ii) An electrophoretic effect arises from the interactions between a positive ion, moving towards the cathode, and the high density of negative ions moving in the opposite direction. This does not apply to cation and anion vacancies in ionic crystals.

The inclusion of these Debye-Huckel corrections to vacancy production in the solid state is to fractionally increase the production of vacancies. Equation (2) becomes

$$X_1 . X_2 = \text{exp.} - (g/kT - e^2 i^2/2\ kT + D.N)$$

where $\tau_{D.H.}$ is the characteristic radius of the Debye-Huckel atmosphere surrounding each vacancy, and is given by

Z_i being the number of compensating charges per cation vacancy. This effect is very small, producing a change of approximately 0.033eV. in the measured free energy (g) for sodium chloride, near the melting point.

(iv) The presentation of results

(1) Intrinsic data

The conductivity plot of a pure, single crystal of sodium chloride is presented in Fig. (1.3). The data points were obtained from conductivity determinations performed upon four different specimens cleaved from the same transverse platelet of a pure crystal boule, the crystal specimens being unannealed after cleavage. Except for the data obtained at the highest temperatures, which were sensitive to previous thermal treatment, there is excellent reproduceability. Consistent results were obtained without performing a high temperature anneal of the crystal electrode interface. By using a variable loading electrode, coated with graphite and of sufficient cross sectional area to avoid edge corrections, deformation of the specimen was avoided. This is far more satisfactory than having changes in the crystal's dimensions of up to 10% occurring during conductivity determinations, a situation present in some workers' determinations of conductivity.(52) The intrinsic conductivity should be reproduceable between different investigations on any particular alkali halide: the intrinsic data of other workers is included in Fig. (1.3) and shows that this is apparently not true. It is interesting to see the close agreement between Jain (55) and Etzel and Maurer,(104) who obtained data using a pulsed electric field technique, and the present work's agreement with the results of Bean,(106) which were obtained using an A.C. technique. A.C. results consistently give higher results than D.C. methods at

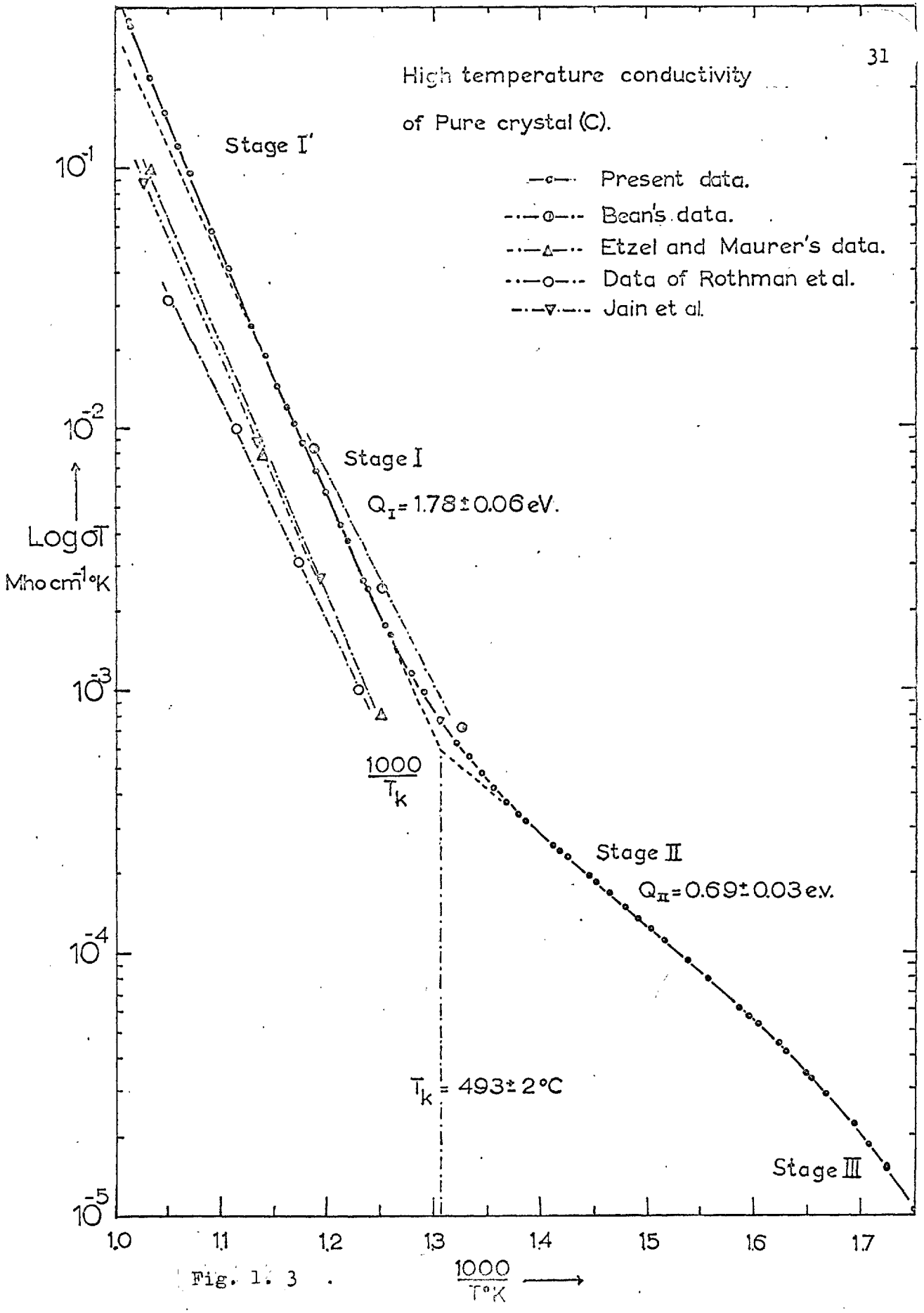
High temperature conductivity
of Pure crystal (C).
Present data.
Bean's data.
Etzel and Maurer's data.
Data of Rothman et al.
Jain et al.
Stage I'
Stage I
$Q_I = 1.78 \pm 0.06$ eV.
Stage II
$Q_{II} = 0.69 \pm 0.03$ e.v.
Stage III
$\frac{1000}{T_k}$
$T_k = 493 \pm 2$ °C
10^{-1}
10^{-2}
10^{-3}
10^{-4}
10^{-5}
Log σT
Mho cm^{-1} °K
1.0
1.1
1.2
1.3
1.4
1.5
1.6
1.7
$\frac{1000}{T°K}$

Fig. 1. 3

elevated temperatures.

The intrinsic region of conductivity, Stage I, shows a definite curvature towards an increased slope at the higher temperatures, Stage I'. Q_I, the slope of the tangent drawn through the low temperature region of intrinsic conduction, has a slope of 1.78± 0.06eV. The values of Q_I were reproduceable to within the limits of experimental error. Table (1.3). Because the values obtained from experiments (4, 5 and 6) produce longer regions of this linear intrinsic conduction (assumed to be purely cationic motion) the best value of Q_I is not necessarily the average value. The most accurate determination of Q_I would appear to be 1.83 ± 0.01eV., which is high when compared with values previously obtained in sodium chloride, and is probably due to the elimination of space charge polarization effects by the use of A.C. measuring techniques.

Q_{II}, the extrinsic conductivity's slope in the pure crystal, is steepened by the onset of the association reaction between the divalent cations and cation vacancies. The conductivity plot starts curving downwards so soon after the commencement of extrinsic conduction that the background impurities must be highly associated. This is reasonable from a consideration of the Law of Mass Action, and is in agreement with the cation diffusion studies of Mapother, Crooks and Maurer,[56] in which the onset of impurity controlled diffusion occurred as soon as intrinsic conduction was finished. A line of minimum slope of 0.69 ± 0.03eV. could be drawn through the extrinsic data. This should represent the best value for the enthalpy of motion of the cation vacancy obtainable from the conductivity data of the pure crystal.

TABLE (1.3).

THE VALUES OF Q_1 OBTAINED FROM DIFFERENT EXPERIMENTS

EXPT.	CRYSTAL STATE	Q_1 eV.
1.	Pure (C), undeformed	1.78 ± 0.06eV.
2.	Pure (C) Diffusion doped with $(OH)^-$	1.83 ± 0.01eV.
3.	Volume doped with $(OH)^-$	1.83 ± 0.01eV.
4.	Pure (C.) Deformed 3%	1.88 ± 0.04eV.
5, 6.	Pure D. Controlled deformation and annealing for 24 hours at 700°C	1.84 ± 0.01eV.

The knee temperature of 493$\pm$ 2°C indicated an effective divalent impurity content of 2.3 $\pm$ 0.1 p.p.m. (expressed as site fraction). This is to be compared with the total divalent impurity content of about 28 p.p.m., as determined by spectrographic analysis. Even allowing for the large systematic errors normally present in the spectrographic analysis, this observation would suggest the presence of small amounts of anion impurities which are complexing with some of the background, divalent, cation impurities.

Fig. (1.4) presents the conductivity of a pure, a manganese, and a manganese plus $(OH)^-$ doped crystal of sodium chloride. The manganese doped crystal shows the additional feature of Stage IV, the precipitation region attributed to the resolution of aggregated manganese with increasing temperature of the crystal. Stage III, the high temperature association region, was found to be curved in all except the most heavily doped crystals. This makes the estimation of an enthalpy of association from the slope Q_{III} a hazardous process. The presence of $(OH)^-$ in the manganese doped crystals reduced the conductivity plot to a gentle curve up to the linear intrinsic region. At low temperatures the conductivity of this crystal was greater than that of the manganese doped crystals, whilst at elevated temperatures the reverse occurred, the crystal behaving, in the extrinsic regions, as if it possessed an effective divalent, cation doping of 36 m.p.p.m. of Mn^{++}. This is presumably evidence for some manganese - $(OH)^-$ complex which is unstable at low temperatures. The fact that the conductivity plot for this crystal presents a continuous curve would indicate that a whole range of associated (Mn^{++} - $(OH)^-$) aggregates or complexes are present. If

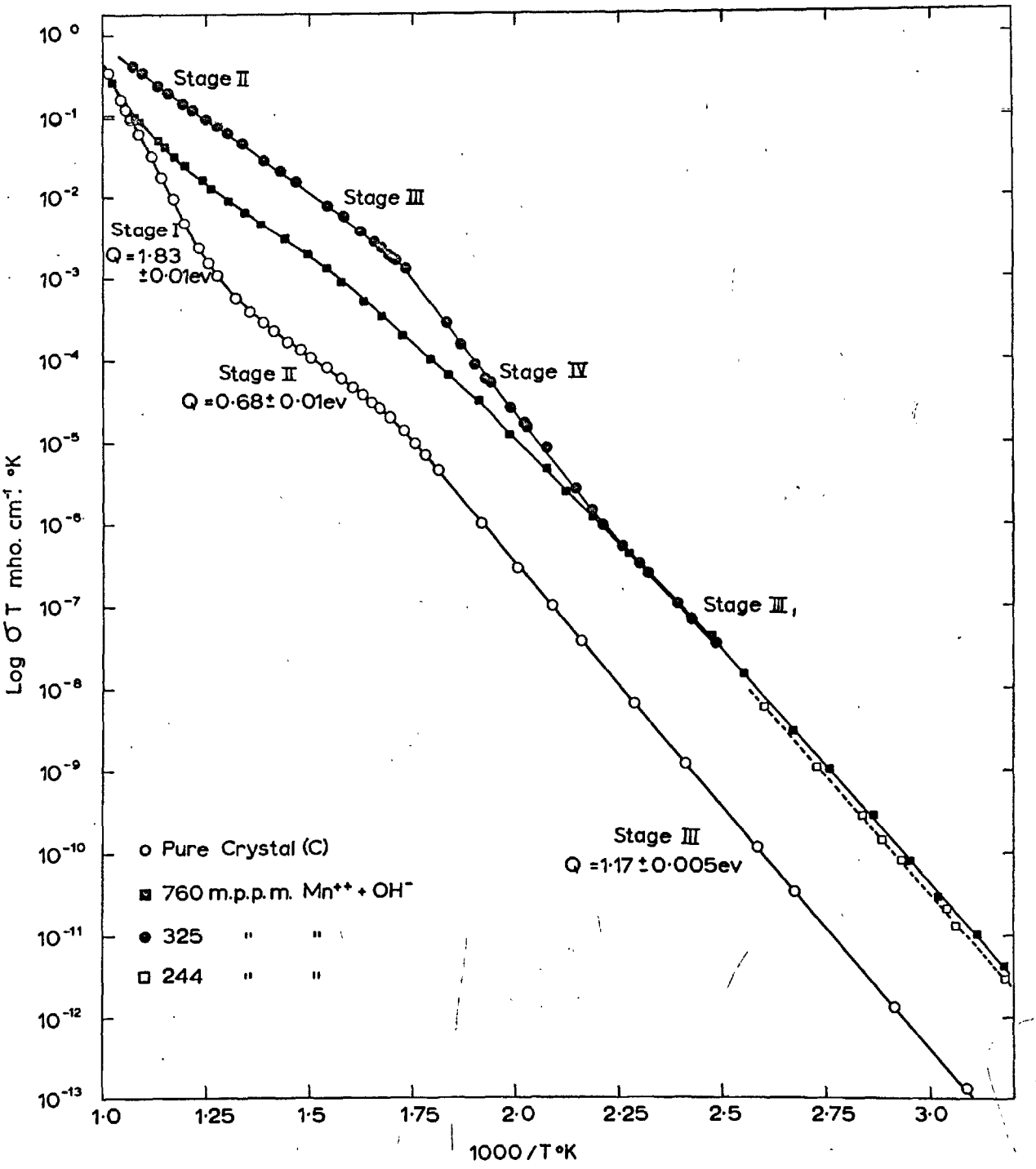

ARRHENIUS CONDUCTIVITY PLOT

Fig. 1.4

there were only one particular species with a well defined structure and binding energy, an irregularity in the curve in the form of a subsidiary knee temperature might be expected.

The association region in the pure crystal gave a value of 1.17 ± 0.005eV. for Q_{III}. Assuming that all the divalent impurity is in solution, a valid assumption for the concentrations and temperatures considered, we may calculate an enthalpy of association from the following relation

$$Q_{III} = \Delta h_1 + ha/_2$$

Using the value of 0.68 ± 0.02eV for Δh_1

$$ha = 0.96 \pm .03eV.$$

This value is far higher than that obtained from any isothermal analysis of sodium chloride intentionally doped with calcium chloride (calcium being the chief background impurity), which yields values from 0.38eV [151-2] to 0.31eV. [153] This discrepancy probably arises from the presence of divalent impurities other than calcium, each with its own association reaction increasing the slope of the association region. The slope Q_{III} of this particular pure crystal is in fair agreement with the values determined by other workers.[154] The absence of any precipitation region in the pure crystals would tend to contradict the recent work of Chang,[155] who calculated the enthalpy of formation of the Schottky pair by observing the limits of the precipitation region in pure crystals subjected to linear heating rates. There is no evidence for precipitation or re-aggregation of the divalent chloride, in crystals with the doping levels present in pure crystals, precipitation of calcium chloride

in the platelet form only appearing with doping levels in excess of 2000 m.p.p.m. (156) At elevated temperatures in the doped crystals, intrinsic conduction is never achieved, the conductivity plot being extrinsic to the melting point.

To obtain better resolution of the curvature of the intrinsic conductivity, which occurred at temperatures in excess of 650°C, a longer region of cation conduction was required. As the chief divalent impurity in sodium chloride is calcium, which has a rejection ratio of 1, the knee temperature could not be reduced by zone refining. Stage I was extended by the addition of $(OH)^-$ ions after the manner of Anger, Fritz and Luty.(101) To control the concentration of $(OH)^-$ in the crystal, attempts were made to diffusion dope the crystals by annealing specimens at 700°C in atmospheres of steam for periods of 120 hours, (Expt.2). This had no apparent effect upon the knee temperature. Crystals were then volume doped by adding controlled amounts of sodium hydroxide to the crystal melt. This reduced the knee temperature to 457°C (Expt.3), with an effective divalent impurity content of 8.9×10^{-1} p.p.m. (site fraction) Fig. (1.5). The high temperature enhancement was much greater in this specimen than for the other pure crystals, and from the data presented so far it is not clear whether this enhancement was brought about by the anion addition or by the deformation the specimen suffered during its preparation. Because it was so soft, the crystal could not be cleaved, and had to be cut by a chemical saw and then water polished. It was not given an annealing treatment and therefore presumably contained much mechanical damage.

To gain insight into the mechanisms of the high temperature

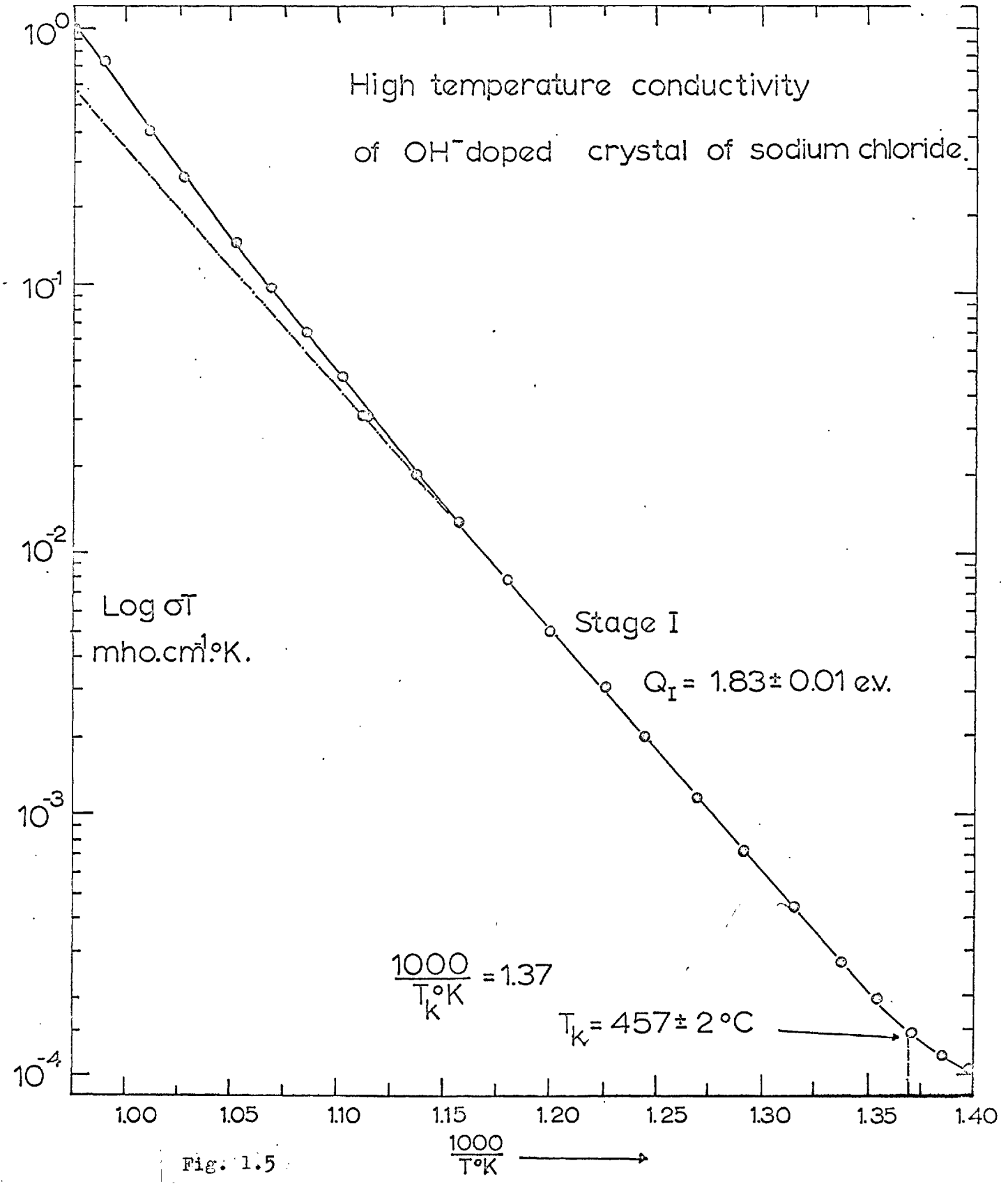
High temperature conductivity
of OH^- doped crystal of sodium chloride.
10^0
10^{-1}
10^{-2}
10^{-3}
10^{-4}
Log σT
mho.cm^{-1}.°K.
Stage I
Q_I = 1.83 ± 0.01 e.v.
$\frac{1000}{T_k °K}$ = 1.37
T_k = 457 ± 2 °C
1.00
1.05
1.10
1.15
1.20
1.25
1.30
1.35
1.40
$\frac{1000}{T °K}$

Fig. 1.5

enhancement, a conductivity curve was computed from the anion and cation diffusion data, using the Nernst-Einstein equation with an appropriate correlation factor of 1.28. The cation diffusion data of Laurent and Benard was chosen as being representative of the sodium ion diffusion. There is much scatter, in both magnitude and energy, in the chlorine ion diffusion data. The anion vacancy contribution to diffusion, as derived by Barr et al, [74] was used for the comparison, this not having been corrected for the effects of vacancy pairs. The calculation shows, Fig. (1.6), that the computed conductivity is effectively a straight line up to 20° or 30°C below the melting point. The agreement between conductivity and diffusion at the lower temperatures is well within the limits of experimental error. This is in direct contrast to the studies of Mapother, Crooks and Maurer, [56] who found agreement between conductivity and diffusion without the use of a correlation factor. At the higher temperatures, there is a considerable enhancement of conductivity above that expected from cation and anion motion through the bulk of the lattice. From this we may conclude that if the enhancement is brought about by anion motion, it is unlikely that the anions are moving through the bulk of the material, but possibly down paths of easy diffusion.

As pointed out in the literature survey, the defect structure may play an important part in the enhancement of intrinsic conduction. With this in mind, two crystals of nominal purity were chosen. Both of these were annealed for twenty-four hours, at 700°C, and then slowly cooled over a period of thirty-six hours. The crystal dimensions were approximately 4.0 x 4.0 x 8.0 m.m. with deformation

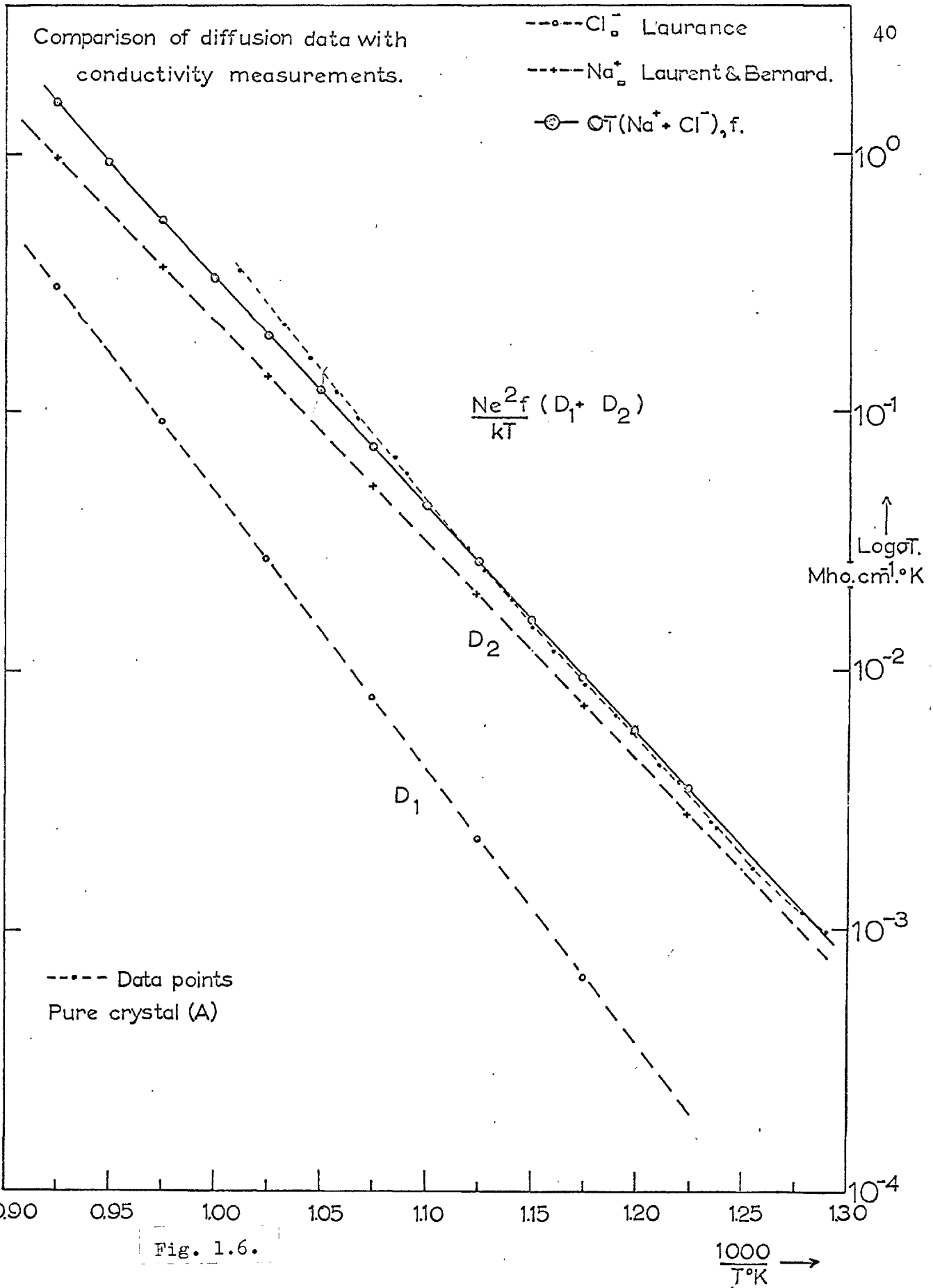
Comparison of diffusion data with conductivity measurements.
---o--- Cl^- Laurance
---+--- Na^+ Laurent & Bernard.
-◎- $\sigma T (Na^+ + Cl^-)$, f.
$\frac{Ne^2 f}{kT}(D_1 + D_2)$
D_2
D_1
---- Data points
Pure crystal (A)
10^0
10^{-1}
10^{-2}
10^{-3}
10^{-4}
Log σT. Mho. cm^{-1}. °K
0.90
0.95
1.00
1.05
1.10
1.15
1.20
1.25
1.30
$\frac{1000}{T°K}$ →

Fig. 1.6.

in compression being performed along the length axis, making the mode of deformation less unambiguous. After being deformed by 1.58% and 4.82%, Fig. (1.7), the high temperature conductivity was measured, Fig. (1.8). It was observed that the deformation considerably enhanced the high temperature conductivity, a much larger enhancement appearing in the crystal suffering the smaller deformation. When these crystals had been removed from the conductivity jig and then annealed for periods of twenty-four hours at $700^{\circ}C \pm 10^{\circ}C$, with a subsequent slow cooling, the enhancement of the conductivity was greatly reduced. The region of intrinsic conduction, assumed to be due to cation motion, was insensitive to the defect state of the crystal, the slope of this region $Q_I = 1.34 \pm 0.01eV$. being in good agreement with that determined for the $(OH)^-$ volume doped crystal. Also, the agreement in magnitude between the different conductivity determinations of this region preclude the possibility of any systematic errors causing the enhancement.

It would be appropriate at this stage to discuss the various mechanisms by which this enhancement of conductivity might occur.

1. Resolution of Polyvalent Impurity

It is possible that some impurity is present in the crystal which only becomes soluble at elevated temperatures. This could explain the enhancement, but would not explain the variation of temperature at which this enhancement occurs and its subsequent disappearance after annealing. The possible change of valence state of the impurities would not explain the effects of annealing

Deformation characteristics of mono-crystals of sodium chloride. Fig. 1.7.

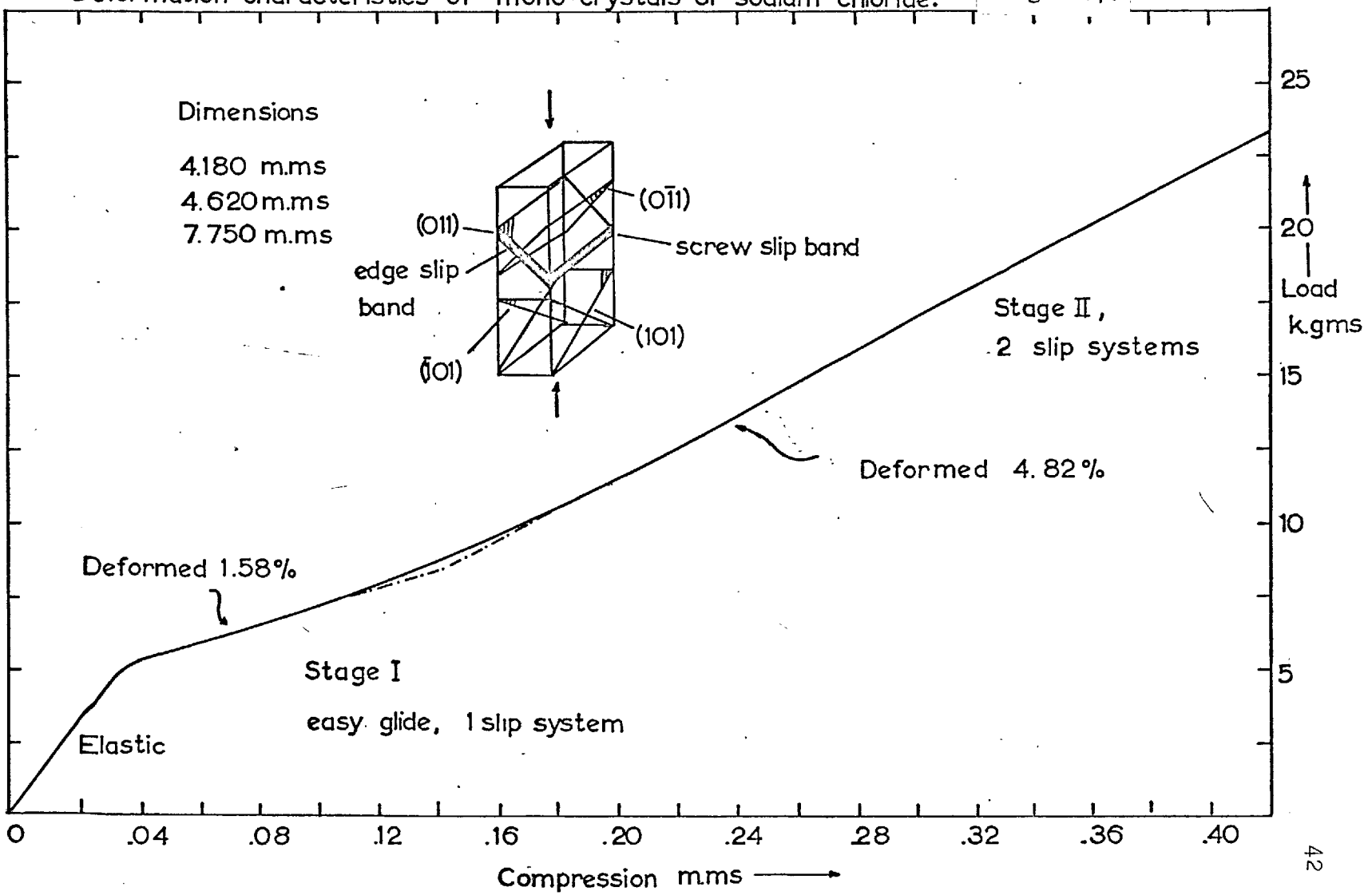

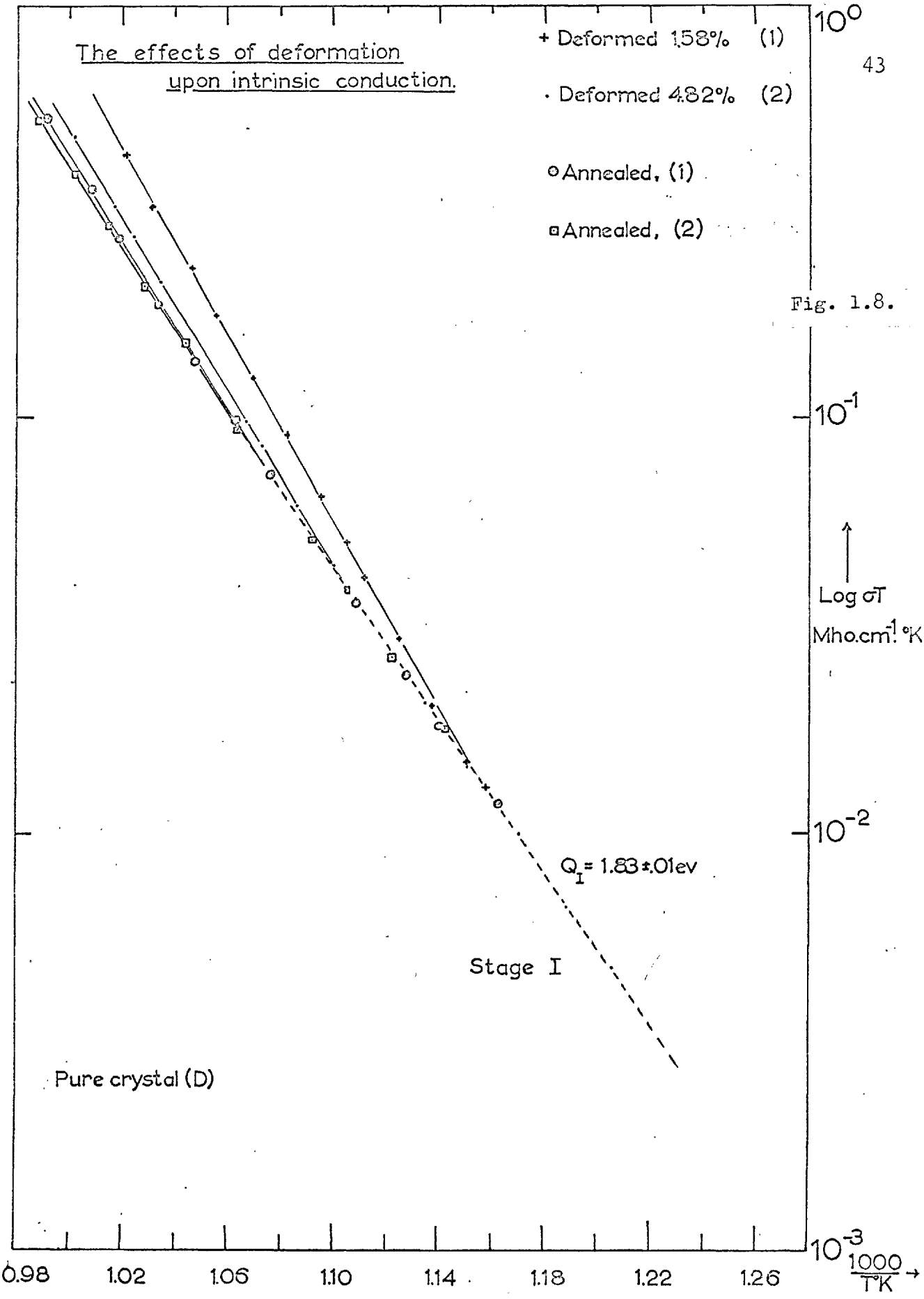
The effects of deformation upon intrinsic conduction.
+ Deformed 1.58% (1)
· Deformed 4.82% (2)
○ Annealed, (1)
□ Annealed, (2)
10^{0}
10^{-1}
10^{-2}
10^{-3}
Log σT
Mho.cm^{-1}.°K
Q_I = 1.83 ± .01ev
Stage I
Pure crystal (D)
0.98
1.02
1.06
1.10
1.14
1.18
1.22
1.26
$\frac{1000}{T°K}$ →

Fig. 1.8.

treatment.

2. Surface Conduction

Any impurity present in the crystal will tend to segregate near the surface, and when the crystal is held at elevated temperatures the impurity will diffuse out to the surface, where it may form paths of lower resistance. This process is unlikely in that its effects would be expected to be random and would be expected to increase with periods of annealing.

3. A Transition Region

Because the transition from extrinsic to intrinsic conductivity may occur over an ill defined temperature region, Stage I may be a transition region from extrinsic conduction to true intrinsic conduction as represented by Stage I'. Given an explicit expression for both intrinsic and extrinsic conduction, a temperature at which the effects of extrinsic conductivity becomes negligible may be calculated. Neglecting any anion contribution,

INTRINSIC:

$$\sigma_I T = \frac{4Na^2e^2\nu_1}{kT} \exp\left(\Delta s_1/k + s/2k\right). \exp - \left(\Delta h_1 + h/2\right)/kT$$

EXTRINSIC:

$$\sigma_E T = \frac{4Nca^2e^2\nu_1}{k} \exp \Delta s_1/k. \exp -\Delta h_1/kT.$$

When $\sigma_E/\sigma_I \lesssim 2.5\%$ extrinsic conduction should not affect the intrinsic data, ie:-

$$\sigma_E/\sigma_I = c. \exp - s/2K \exp. + h/2kT \lesssim 2.5\%$$

Utilizing the values of h and s derived later and assuming a value of 2.3 p.p.m for c, a value of 1140°K is obtained for T_k, a temperature above the melting point. Although this calculation should not be taken too literally, it does show the difficulty of assigning particular regions of the conductivity plot unambiguously to any one process. Only by the agreement in the values of Q_1 for the pure crystals and the $(OH)^-$ doped crystals are we forced to drop the conclusion that Stage I is a transition region. It is difficult to see how the length of a transition region could depend upon the annealing treatment in the way that it does.

4. Change in Energies

It has been assumed that the entropies and enthalpies of formation and motion of the vacancies are independent of temperature. The energy measured upon the Arrhenius plot is given by the relation

$$Q = k \frac{d(\log \sigma T)}{d(1/T)}$$

Assuming that Δs_1 and Δh_1 are possibly temperature dependent, and substituting the expression for σT given by equation (16) into the above, one finds:-

$$Q = T^2 \frac{d\Delta s_1}{dT} + \Delta h_1 - \frac{d\Delta h_1}{dT}$$

utilizing $\Delta H_1 = dU_1 + PdV + T\Delta s_1$ at constant temperature and volume, and

$$T \cdot \frac{d\Delta s_1}{dT} = \frac{d\Delta h_1}{dT}$$

and, hence

$$Q = \Delta h_1$$

This shows that even if the entropy term is variable, any changes in Q would only be indicative of enthalpy changes. It is possible that at the elevated temperatures near the melting point, the lattice structure may become loose. The vacancy may perform a double or "knock-on jump", the momentum of the initial hump carrying it onto the next vacancy position. This effect would result in an enhanced mobility, but would not explain the effects of annealing treatment. The possibility of Debye-Huckel corrections are also ruled out from the previous argument, because a decrease in Q_I would be expected, rather than an increase.

5. Annealing Out of Point Defects Induced by Deformation

The point defects induced by deformation are those of the anion and cation vacancies and possibly the corresponding interstitials, if the deformation is particularly severe. The former defects are found to anneal out rapidly in the temperature range 0°C to 100°C, with the annealing out of the cation vacancy proceeding with a reaction involving first order kinetics.[105] Because the energies of motion of the interstitials are considerably smaller [143] than those of the vacancies, the interstitials would not be expected to remain stable at temperatures in excess of 100°C. The only possible mechanisms which would seem to explain these large unstable enhancements of intrinsic conductivity is the motion of anion or cation vacancies along paths of easy conduction. As the cation diffusion does not appear sensitive to the defect state or the presence of grain boundaries,[58] the analysis will be continued on the assumption that enhanced anion motion is the cause of the increase in the slope of Q_I

to Q_I'.

Having clearly resolved the energy and magnitude of the cation's contribution to intrinsic conductivity, the anion contribution may be obtained by extrapolation. The form of the present enhancement is that of a sharp increase in the slope of the intrinsic conduction similar to that observed by Allnatt et al. [50] in potassium chloride. This is in contrast to the data of Beaumont et al., [52] whose intrinsic region was a continuous curve. It should be added that these workers' crystals were subjected to a constant stress from the spring loaded electrodes, which resulted in a prolonged form of creep. In the present experiments, care was taken to ensure that the electrodes did not increase the dislocation density during the course of the experiment. The anion conductivity, when plotted against reciprocal temperature, yielded an activation energy of 2.70 ± 0.10eV. Fig. (1.9), with a variable magnitude for the enhancement. This energy is high, when compared with values obtained from anion diffusion, Table (1.2), the disagreement increasing when the activation energies obtained from diffusion have been corrected for pair motion. If it is assumed that this activation energy is compounded of enthalpies of formation and motion in the usual manner,

$$Q_{anion} = h/2 + \Delta h_2$$

with

$$h = 2.30 \pm 0.02\text{eV}.$$

an enthalpy of motion (Δh_2) of 1.50 ± 0.20eV. is obtained, again too high a value when compared with the equivalent results from diffusion studies, Table (1.2).

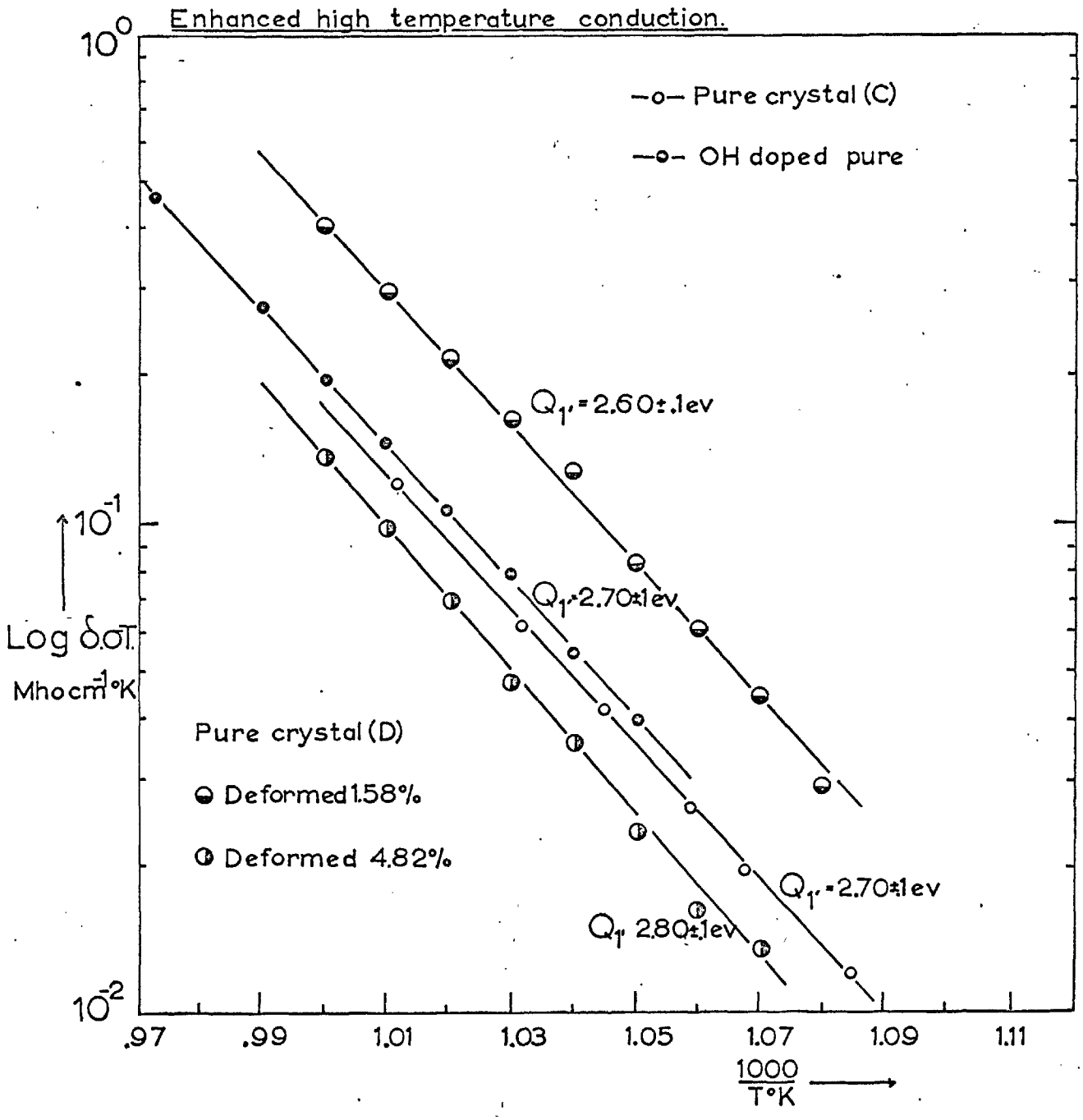
Enhanced high temperature conduction.
10^0
10^-1
10^-2
Log δ.σT.
Mho cm^-1 °K
—o— Pure crystal (C)
—o— OH doped pure
Q1' = 2.60±.1ev
Q1' = 2.70±1ev
Q1' = 2.70±1ev
Q1' 2.80±.1ev
Pure crystal (D)
Deformed 1.58%
Deformed 4.82%
.97
.99
1.01
1.03
1.05
1.07
1.09
1.11
1000/T°K

Fig. 1.9

It is of interest to compare transport numbers determined classically [13] with those derived from diffusion data and the present conductivity studies. This may be done by using the following equation,

$$t_1 = \sigma_1 / (\sigma_1 + \sigma_2) = D_1 / (D_1 + D_2)$$

assuming that the conductivity and diffusion processes are identical a nd in Fig. (1.10) this comparison is made for the crystals showing the enhancement. The transport numbers calculated from diffusion studies suggest that there is an appreciable anion contribution to conductivity occurring over the temperature ranges where we have considered it to be negligible. It is only when the transport numbers are corrected for the contribution from vacancy pairs that the assumption about Region I being purely cationic appears valid. The transport numbers calculated from the conductivity data suggest that the charge contribution carried by the anion vacancy is far greater than would be expected from diffusion studies or the classical determinations of t_1. This would suggest that the enhanced motion of anion vacancies is occurring, possibly down dislocations or grain boundaries. The transport numbers all converge to a limit of 0.97 at the lower temperatures, suggesting that there is a small but possibly electronic contribution to ionic conduction.

It is worthwhile considering the behaviour of dislocations and grain boundaries at elevated temperatures in seeking an explanation for the observed effects. All crystals, no matter how carefully they are prepared, will possess dislocations over and above the grown in dislocation density and the way they behave at elevated

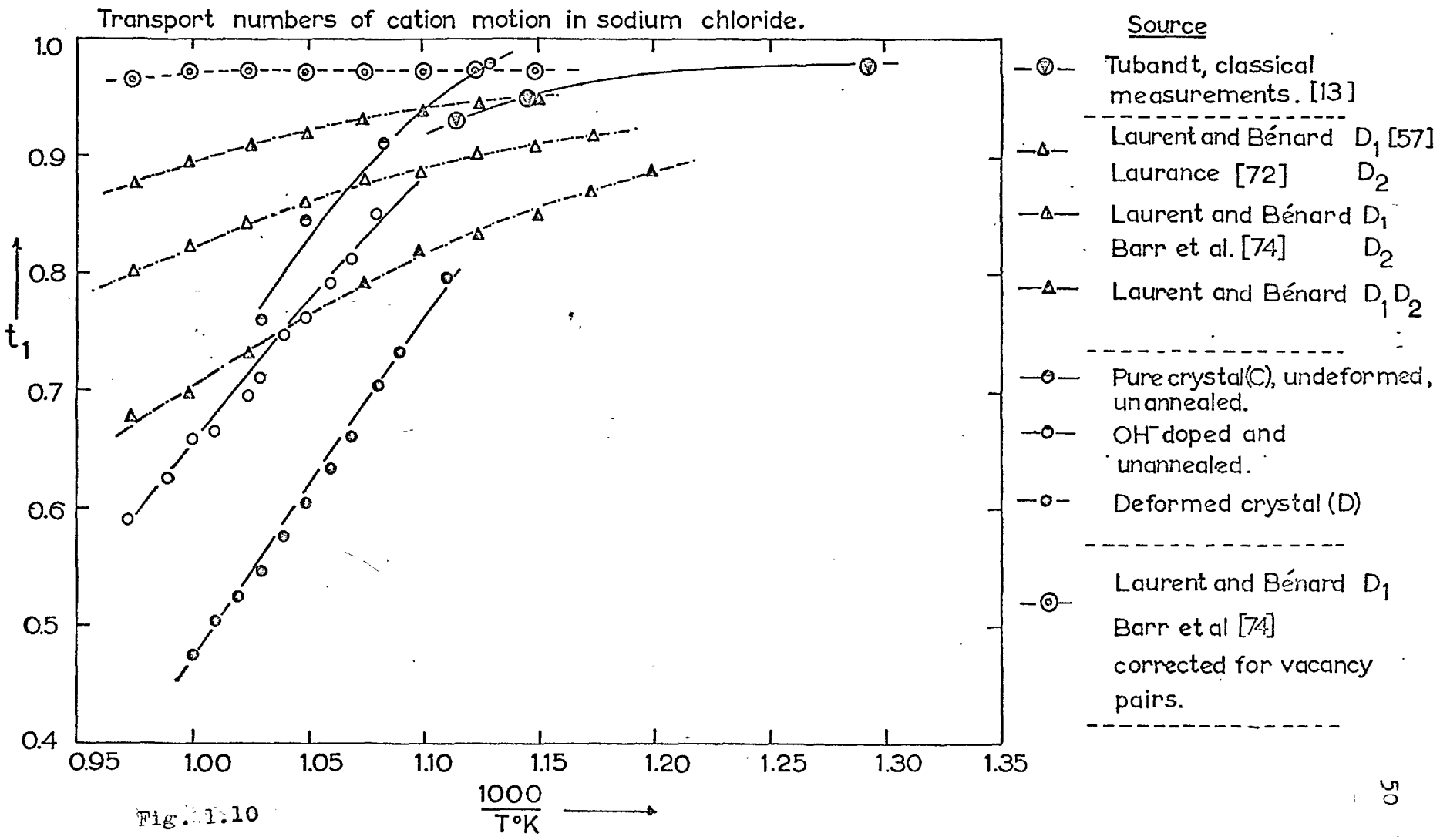
Transport numbers of cation motion in sodium chloride.
1.0
0.9
0.8
0.7
0.6
0.5
0.4
t_1
0.95
1.00
1.05
1.10
1.15
1.20
1.25
1.30
1.35
1000/T°K
Source
Tubandt, classical measurements. [13]
Laurent and Bénard D_1 [57]
Laurance [72] D_2
Laurent and Bénard D_1
Barr et al. [74] D_2
Laurent and Bénard D_1 D_2
Pure crystal(C), undeformed, unannealed.
OH^- doped and unannealed.
Deformed crystal (D)
Laurent and Bénard D_1
Barr et al [74] corrected for vacancy pairs.

Fig. 1.10

temperatures is observable by standard etching techniques. To illustrate this point, the following photographs, Fig. (1.11), are reproduced with the kind permission of Dr. R.W. Davidge.[157] A deformed crystal is a non-equilibrium structure and will return to its former state at elevated temperatures. The photographs show the dislocation arrangements in specimens deformed 10% and then annealed for one hour at 400°C, (a), 500°C, (b), 600°C, (c) and 700°C (d). These specimens were of about the same dimension as those used in the initial deformation-conductivity experiment, and were cleaved in half parallel to the narrow faces, with the new face being etched. Little change is observable in specimens annealed below 400°C, and the specimens annealed at this temperature show the dislocations arranged in roughly parallel dislocation walls. The density of the walls is greatly reduced in specimens annealing at 500°C and annealing at higher temperatures produces the growth of sub-grains. It is seen that the main recovery of dislocation density occurs over the temperature range 400°C - 500°C during an annealing period of one hour, with a subsequent growth of grain and sub-grain boundaries. The high temperature conductivity measurements and subsequent annealing treatment of the conductivity specimens produced the same formation of a grain-like structure, Fig. (1.12). The initial conductivity run on the deformed sample transformed the random dislocation array Fig. (1.12b) to that of parallel lines of dislocation walls Fig. (1.12c). The annealing treatment of twenty-four hours at 700°C resulted in the growth of a grain and sub-grain structure Fig. (1.12d). It is quite feasible that the enhanced conductivity observed is caused by the motion of

Fig. 1.11

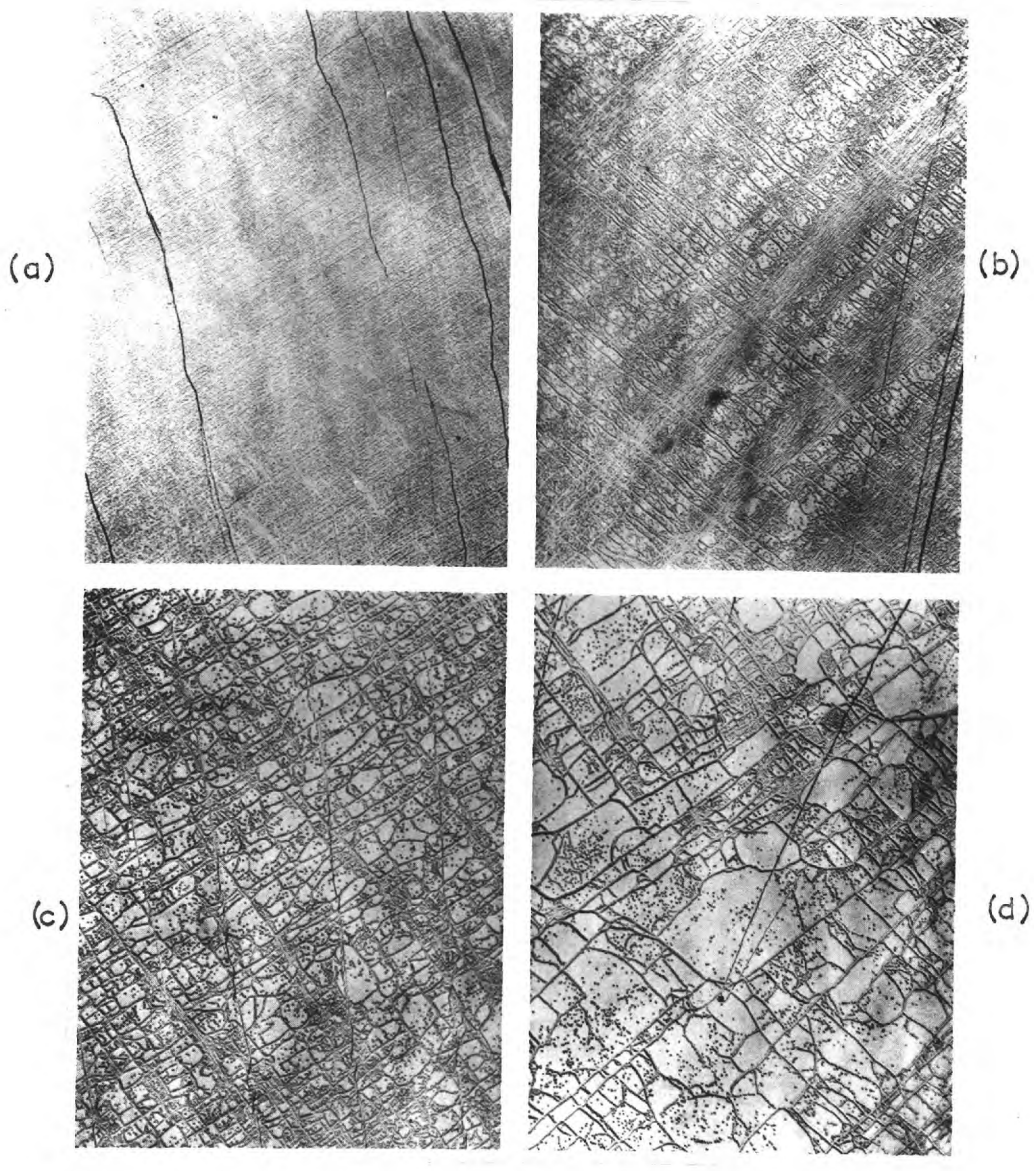

Dislocation arrangements in specimens deformed 10% and annealed 1 hour at (a) 400°C (b) 500°C (c) 600°C (d) 700 °C ×120

After Davidge and Pratt (157)

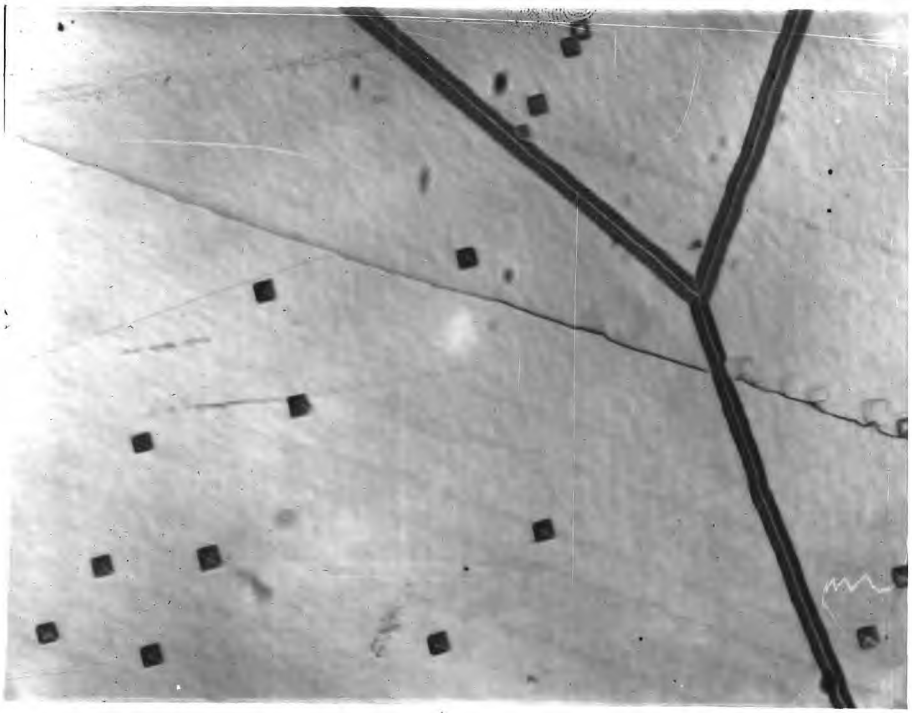

≈ x400

The dislocation arrangements in pure crystals of NaCl, annealed at 700°C and slowly cooled. Fig. 1.12a.

x300

The dislocation arrangements in pure, well annealed single crystal deformed by 4.82 % Fig. 1.13b.

x300

The dislocation arrangement in deformed crystal after completion of conductivity run Fig. 1.12c

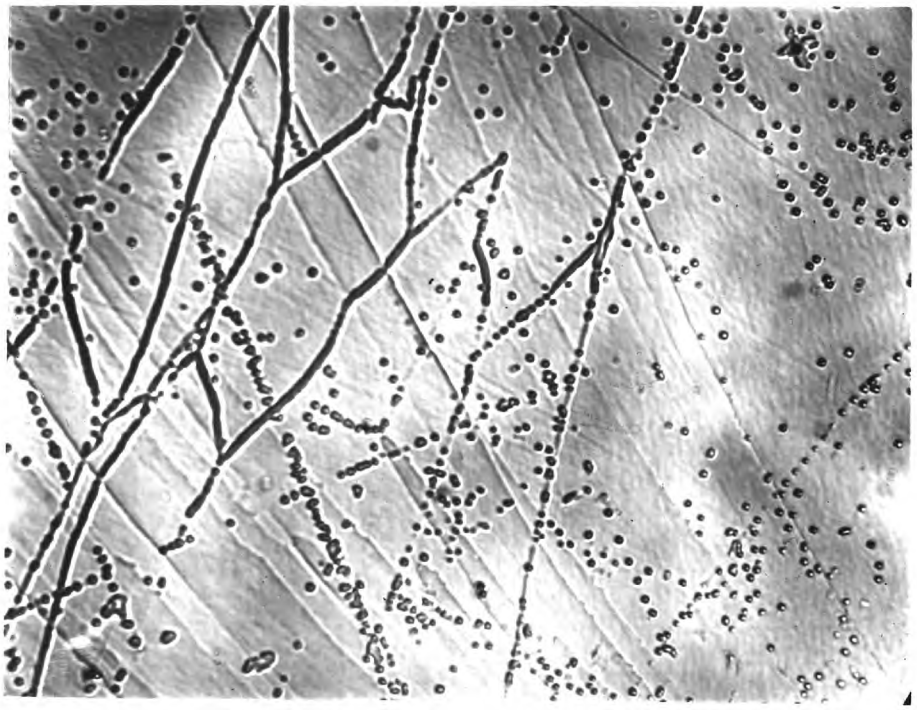

x300

The dislocation arrangement in deformed crystal after annealing at 700°C for 24 hours Fig. 1.12d.

anion vacancies down the grain and sub-grain boundaries, formed by the mechanical and subsequent heat treatment of the crystals. The effect of the prolonged annealing at 700°C is that the individual grains of the structure increase in size, with a decrease in total surface area of grain and sub-grain surfaces. This would explain the subsequent reduction of the enhanced conductivity after annealing treatment. The fact that there is little enhancement in well annealed crystals, where this form of grain structure is absent and the growth in dislocation density is low ($\simeq 10^6/cm^3$), Fig. (1.12a), adds further weight to this argument.

With a knowledge of the anion and cation contributions to conductivity the mobility ratio ϕ may be determined as a function of temperature, Fig. (1.13). The curvature present in these mobility plots could be attributed to an annealing out of paths of enhanced conduction, especially as the limiting slopes of these curves at the lower temperatures all possess the same value. The possible reduction, by annealing, of the high temperature points is also present in Fig. (1.9), the former appearing as a reduction in the value of Q for the crystals showing the greatest enhancement. The mobility plot is apparently more sensitive to these small changes of anion conductivity. From the slope of these plots and a knowledge of Δs_1 and Δh_1, the corresponding enthalpy and entropy of the anion vacancy may be calculated Table (1.4). It would be a little naive to assume that these figures are representative of motion through the bulk of the material. The enthalpy of motion is far too high and the large variation in Δs_2 could be interpreted as a varying magnitude in the anion contribution to conductivity. The

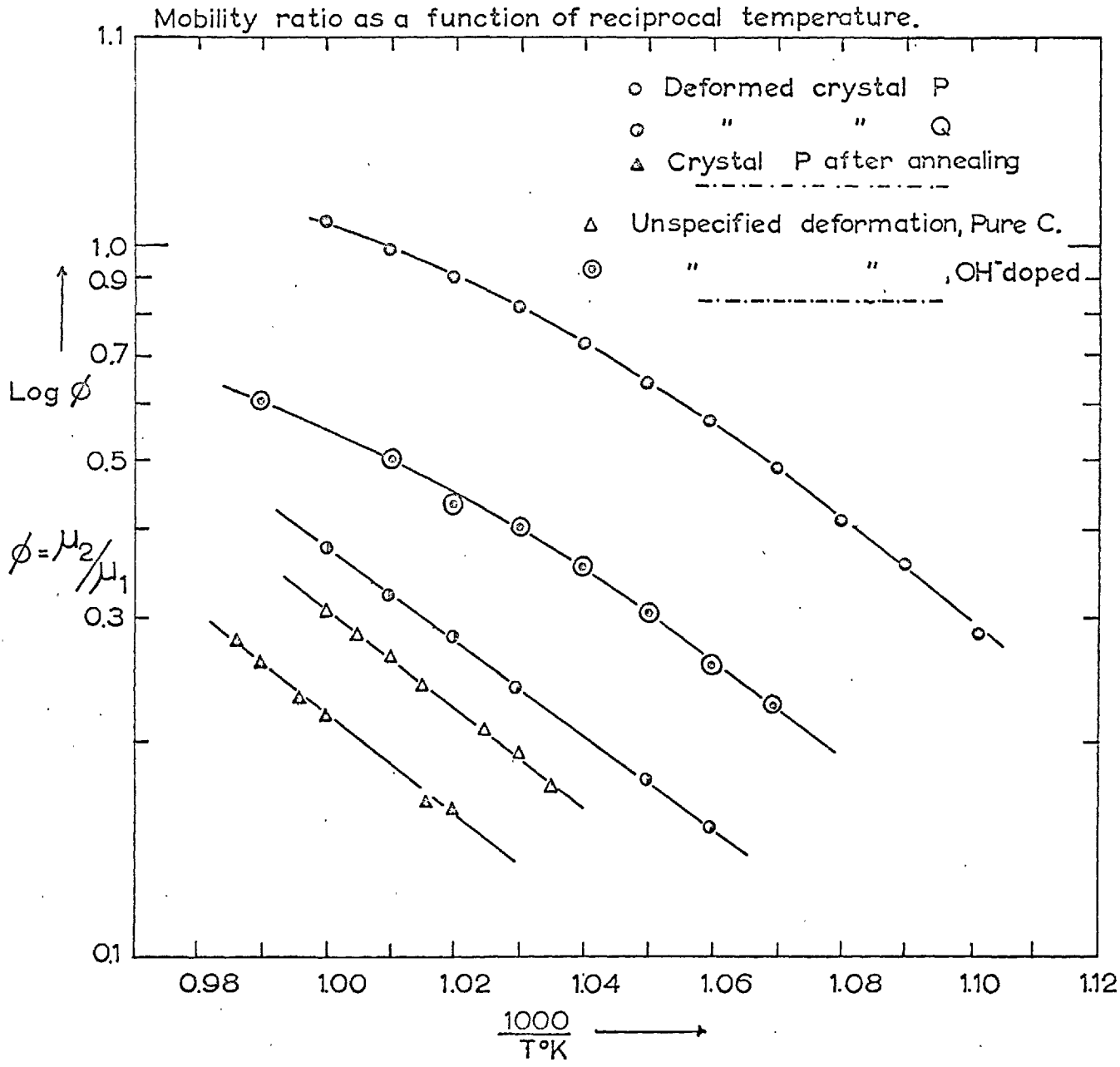
Mobility ratio as a function of reciprocal temperature.
o Deformed crystal P
o " " Q
Δ Crystal P after annealing
Δ Unspecified deformation, Pure C.
" " , OH⁻doped
Log ϕ
ϕ = μ2/μ1
1.1
1.0
0.9
0.7
0.5
0.3
0.1
0.98
1.00
1.02
1.04
1.06
1.08
1.10
1.12
1000/T°K

Fig. 1.13.

TABLE (1.4).

THE ENTHALPY AND ENTROPIES OF ANION MOTION AS DERIVED FROM ENHANCED CONDUCTIVITY AND MOBILITY RATIO

Δh_2 eV.	$\Delta s_2 \times 10^{-3}$ eV./°K	
2.00 ± 0.40	1.53	From mobility plots
2.00 ± 0.40	1.62	
1.98 ± 0.40	1.58	
1.60 ± 0.30	-	From enhanced conduction (average value)

PARAMETERS OF MOTION OF THE CATION VACANCIES - TABLE (1.5).

Debye Frequency $\nu_1^{\circ} = 4.61 \times 10^{12}$ sec.$^{-1}$

Crystal Specimen	Δh_1 eV.	ν_1 sec^{-1}	Δs_1 eV./°K.
686 m.p.p.m. Mn	0.67 ± 0.02	4.70×10^{-13}	0.2 ± 0.05
325 m.p.p.m. Mn	0.68 ± 0.02	4.66×10^{-13}	0.2 ± 0.05
166 m.p.p.m. Mn	0.67 ± 0.02	3.20×10^{-13}	0.17 ± 0.05
90 m.p.p.m. Mn	0.67 ± 0.02	3.48×10^{-13}	0.17 ± 0.05
760 m.p.p.m. Mn, $(OH)^-$	0.73 ± 0.01	-	-
Pure C ———	0.69 ± 0.03	-	-
Mobility Plot ———	0.67 ± 0.01	4.34×10^{-13}	0.19 ± 0.05

possibility of a systematic error in the data is not ruled out, although the weakest point in the analysis - the quantitative description of the cation contribution - was eliminated by the depression of the knee temperature. The resulting errors would not cover the discrepancy between Δh_2, measured by diffusion, and the values obtained from conductivity studies. It may be concluded that the enhancement observed in deformed specimens occurs by the motion of a large number of not very mobile carriers and this large density of carriers could be present at grain and sub-grain boundaries formed by suitable mechanical and heat treatments of the crystal. Charge flow experiments performed during deformation at elevated temperatures suggest that there is an excess of chlorine ion vacancies along the dislocation cores with a compensating Debye-Huckel cloud of sodium ion vacancies surrounding them. The sub-grains and grain boundaries would appear to be in the same condition with the high density of anion vacancies forming the possible anion contribution to conductivity. (126)

(2) Extrinsic data

The enthalpy and entropy of motion of the cation vacancy ($\Delta h_1, \Delta s_1$) may be obtained from Q_{II}, the slope of extrinsic region, or from an Arrhenius plot of the mobility of the cation carriers. The extrinsic regions of conductivity are never clearly resolved because firstly, the change-over from intrinsic to extrinsic processes occurs over a range of temperatures and is never sharply defined for any particular doping level, and secondly, the onset

of the association reaction between divalent impurity ions and cation vacancies produces a gentle change of slope in the conductivity plot at lower temperatures. The association reaction is only marked by a sharp change of slope in heavily doped crystals. To overcome these problems, the extrinsic regions of conductivity were extended by doping with manganese chloride, Fig. (1.14). The limits of extrinsic conductivity were then determined by plotting the isotherms of σ versus c at temperature intervals of $1000/T = 0.025$ Fig. (1.15). For extrinsic conduction, equation (9) requires that the isotherms be linear. This condition is only fulfilled within the temperature range $507^{o}C - 607^{o}C$. This would seem to confirm that manganese occupies a substitutional position in the sodium sub-lattice with an electronic configuration that gives it a divalent character, (159) The manganese ions can have valence states from 1 to 7, except 5. In the valence state of 2 the electronic configuration is 2.8 (2.6.5), so that the third shell is half way between 8 and 18, a factor which accounts for its marked stability. It is interesting that when the extrinsic conductivity isotherms are extrapolated to the origin, they yield a non-zero concentration of impurity. This is presumably evidence for a fixed concentration of anion impurity c_o, which ties up 50 m.p.p.m. of manganese, so that the effective divalent manganese concentration is $(C - C_o)$. m.p.p.m. As the crystals were free of $(OH)^{-}$ and $(CO_3)^{--}$, inferred from the absence of any bands in their optical absorption at 2.8μ and in the ultra violet, the most likely anion impurity was oxygen, this being introduced by the method of growing crystals in air. Watkins (159) has also observed a constant concentration of manganese ions next to divalent anion type

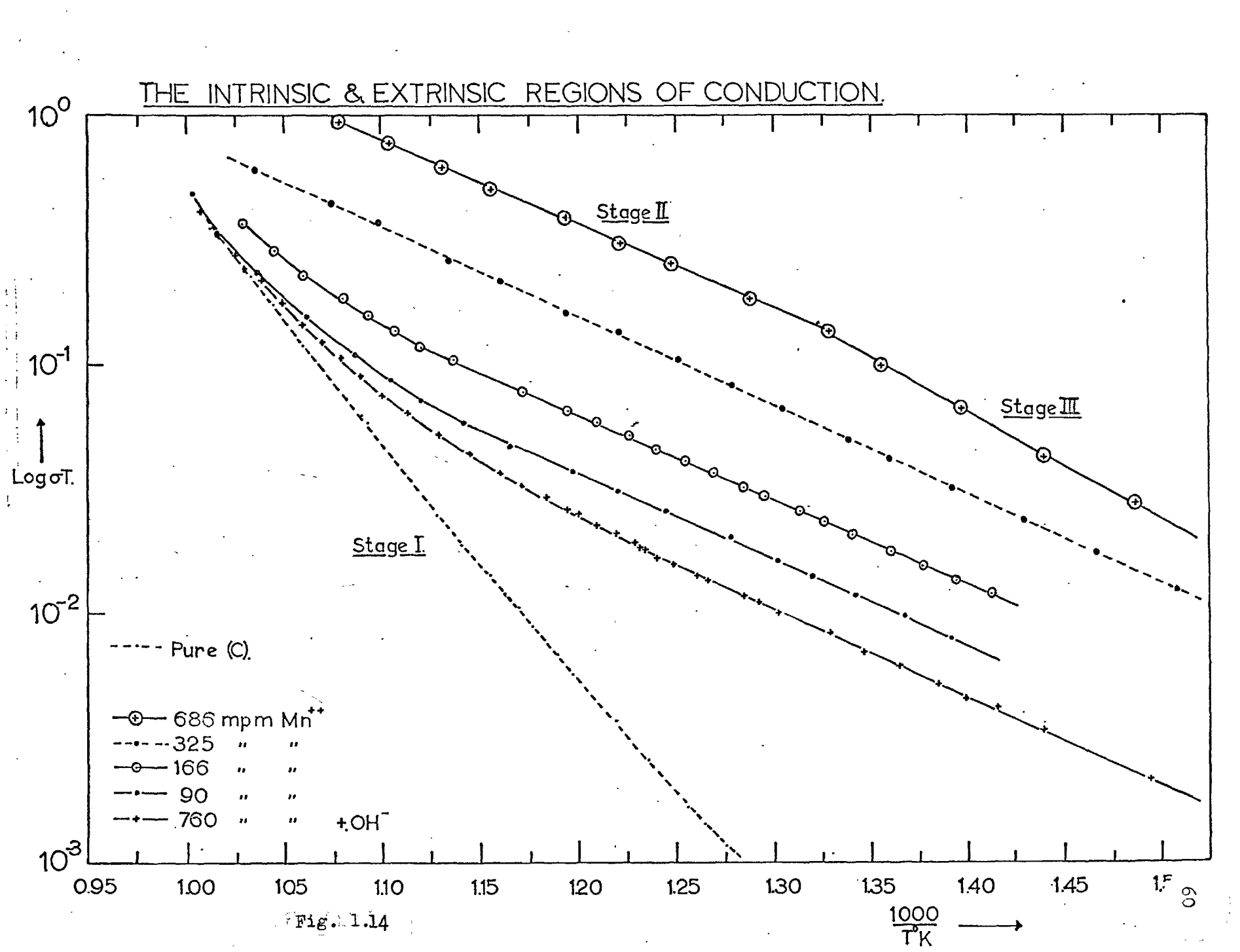
THE INTRINSIC & EXTRINSIC REGIONS OF CONDUCTION.
10^0
10^{-1}
10^{-2}
10^{-3}
Log σT.
Stage II
Stage III
Stage I
Pure (C).
686 mpm Mn^{++}
325 " "
166 " "
90 " "
760 " " $+OH^-$
0.95
1.00
105
1.10
1.15
120
1.25
1.30
1.35
1.40
1.45
1000/T°K
69

Fig. 1.14

Isotherms in the Extrinsic region.

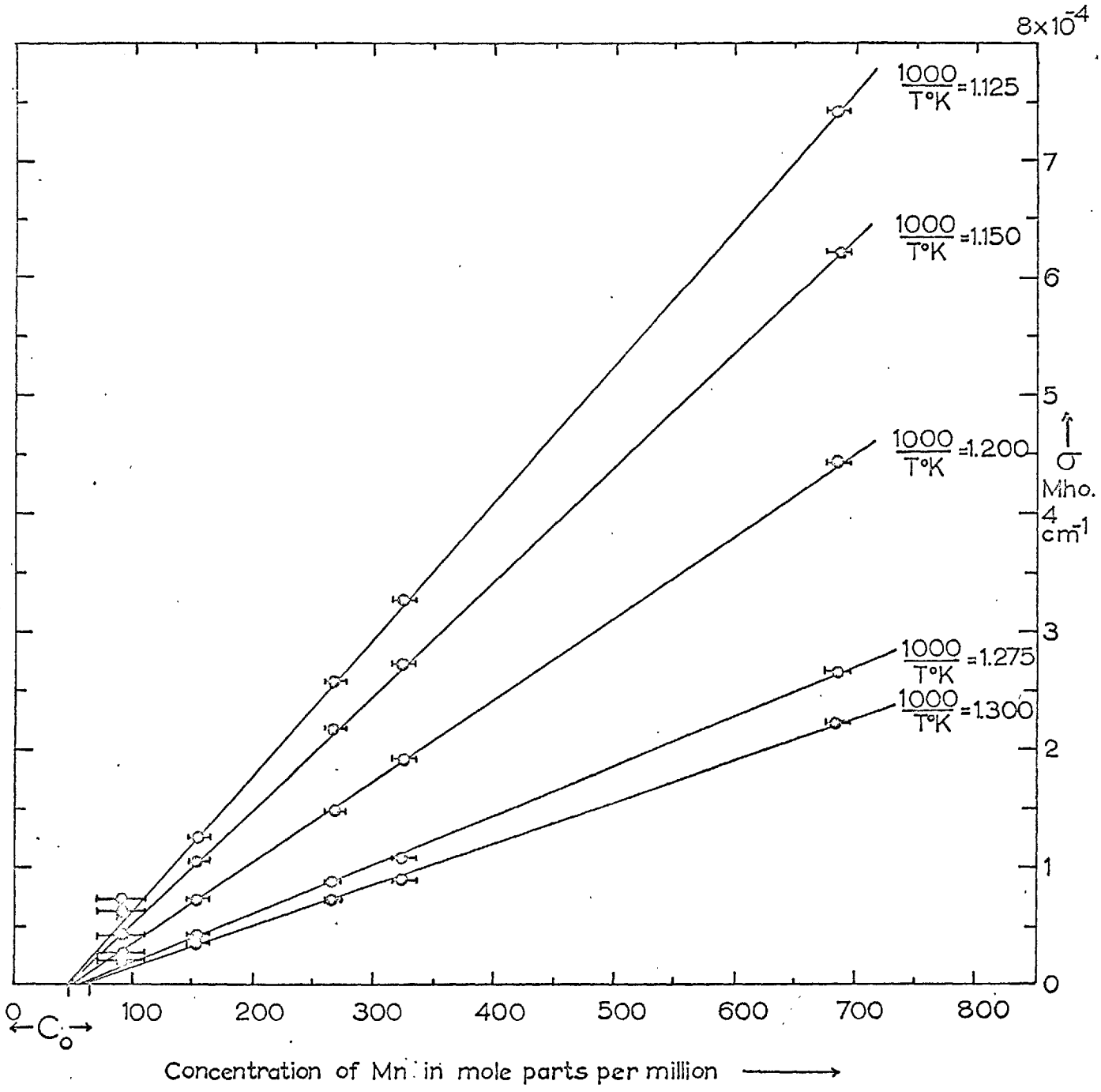

Fig. 1.15

impurity ions in crystals lightly doped with manganese. Having resolved the limits of extrinsic conductivity, the slope Q_{II} of these regions was taken as representing Δh_1. The values of Δh_1 for the different doping levels are tabulated in Table (1.5) and show that consistency is obtained in the values derived by this method. The presence of $(OH)^-$ ions in the Mn^{++},$(OH)^-$ doped crystals increased the value of Q_{II} to $0.73 \pm 0.01eV$, this energy not being representative of Δh_1 but probably involving an energy of association between the manganese ions and the $(OH)^-$ ions. By use of equation (5), and an accurate knowledge of the effective divalent cation concentration, the mobility of the cation vacancy was calculated as a function of temperature. Fig. (1.16). This plot also includes cation mobilities calculated from an analysis of conductivity in the association region, and the values of Δh_1 and Δs_1 obtained, Table (1.5), are in good agreement with the previous calculations. Over the temperature range of 316°C to 650°C, the enthalpy of cation motion seems to be independent of temperature. These measurements were made over a much wider temperature range than those of Etzel and Maurer [104] and are in contrast to Bean's data, which shows a distinct curvature. This curvature probably arose from the assumption that extrinsic conditions existed down to low temperatures. A temperature dependence is predicted on theoretical grounds for the enthalpy of motion of the cation vacancy in sodium chloride in a recent paper by Rice, [160] who related the enthalpy to the normal lattice vibrational modes. The value of 0.68 ± 0.02 obtained for Δh_1 is much lower than that quoted by other workers, Table (1.1). This is not a disturbing feature when it is realized

The mobility of the cation vacancy as a function of temperature.

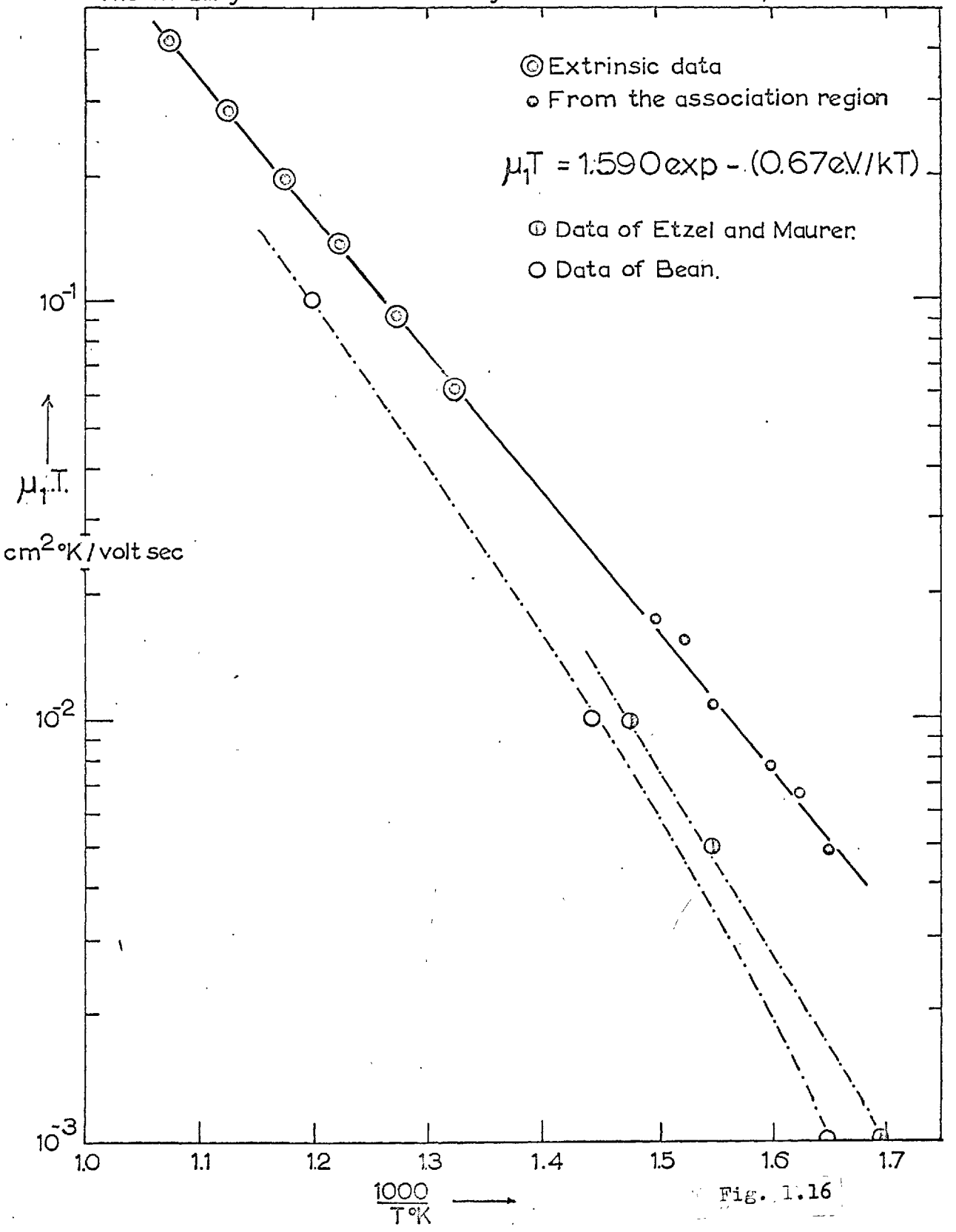

Fig. 1.16

that few systematic attempts to determine the limits of extrinsic conductivity have been made in previous studies. Beaumont's value of 0.709eV. for Δh_1 in potassium chloride is also low by comparison with previous data, and was obtained by the objective use of a computer programme. The value of $\underline{0.68 \pm 0.02eV.}$ for Δh_1 is in good agreement with that obtained from N.M.R. line width broadening, and spin-lattice relaxation time determinations, where the association reaction does not affect the migrational enthalpy obtained.

From a determination of the pre-exponential frequency factor ν_1, the entropy of motion Δs_1 was calculated using the following relation, Table (1.5).

$$\nu_1 = \nu_1^{\circ} \exp \Delta s_1/k$$

It is difficult to know which value to use for ν_1°. One may use the Debye temperature (Θ_D) of 281°K with an associated Debye frequency of $\nu_1^{\circ} = 4.61 \times 10^{12}$ sec^{-1} or the frequency derived from infra-red absorption measurements in sodium chloride, [161] $\nu_1^{\circ} = 4.90 \times 10^{12}$ sec^{-1}. A comparison of the frequency factors ν_1 determined by other workers and the value obtained in the present study is made in Table (1.6). The present value of ν_1 suggests that the cation vacancy will perform 35 jumps/sec. at a temperature of 300°C.

Using the value of $\underline{0.68 \pm 0.02}$ for Δh_1 and $\underline{1.83 \pm 0.01eV.}$ for Q_I, the enthalpy of formation of the Schottky pair was calculated using the following relation

$$Q_I = h/2 + \Delta h_1$$

This yielded a value of $\underline{2.30 \pm 0.02eV.}$, which is high compared with previous theoretical [162] and experimental values, a consequence of the larger value for Q_I, obtained by eliminating space charge

TABLE (1.6).

A COMPARISON OF THE FREQUENCY FACTOR ν_1 : DERIVED BY PREVIOUS WORKERS

Reference	$\nu_1 \times 10^{14}$ sec.$^{-1}$
Etzel & Maurer (104)	2.00
Bierman (164)	1.50
Dreyfus & Howick (105)	0.70
Read & Katz (28)	2.10 (1)
Haven (88)	0.96
Present work	0.434 (2)
Bean (106)	1.40

(1) From Hall effect measurements.

(2) Calculated from Arrhenius mobility plot.

polarization effects and the low values obtained for Δh_1. The most recent theoretical estimation of Q_I made by Boswarva et al. [162] is smaller by about 0.18eV. This situation appears to exist for most of the alkali halides, when a comparison is made of the most recent experimental and theoretical results. An independent estimate of the enthalpy of formation of the Schottky pair, was obtained from the extrinsic conductivity data. This was achieved by determining the knee temperatures from the extrapolated extrinsic and cationic intrinsic regions, and assuming that at these temperatures the effective divalent impurity content was equal to the intrinsic cation vacancy concentration. Hence the cation vacancy concentration was determined as a function of temperature, Fig. (1.17), and the enthalpy and entropy associated with the formation of a vacancy pair derived,

$$h = 2.32 \pm 0.02\text{eV}. \qquad s = 0.52 \times 10^{-3}\text{eV}./^{o}\text{k}$$

An empirical expression for intrinsic vacancy production was also calculated and found to be of the form

$$n_1 = 4.57 \times 10^{23} \times \exp - (1.16 \pm 0.02\text{eV})/kT \text{ vacancies/cc.}$$

The corresponding empirical expression for the cation mobility was

$$\mu_1 T = 1{,}590. \exp * (0.67 \pm 0.01)\text{eV}/kT \text{ cm}^2.{}^{o}\text{K/volt.sec.}$$

The above two results when combined produced an expression for the intrinsic ionic conductivity due to cation vacancy motion and

Cation vacancy concentration as a function of temperature

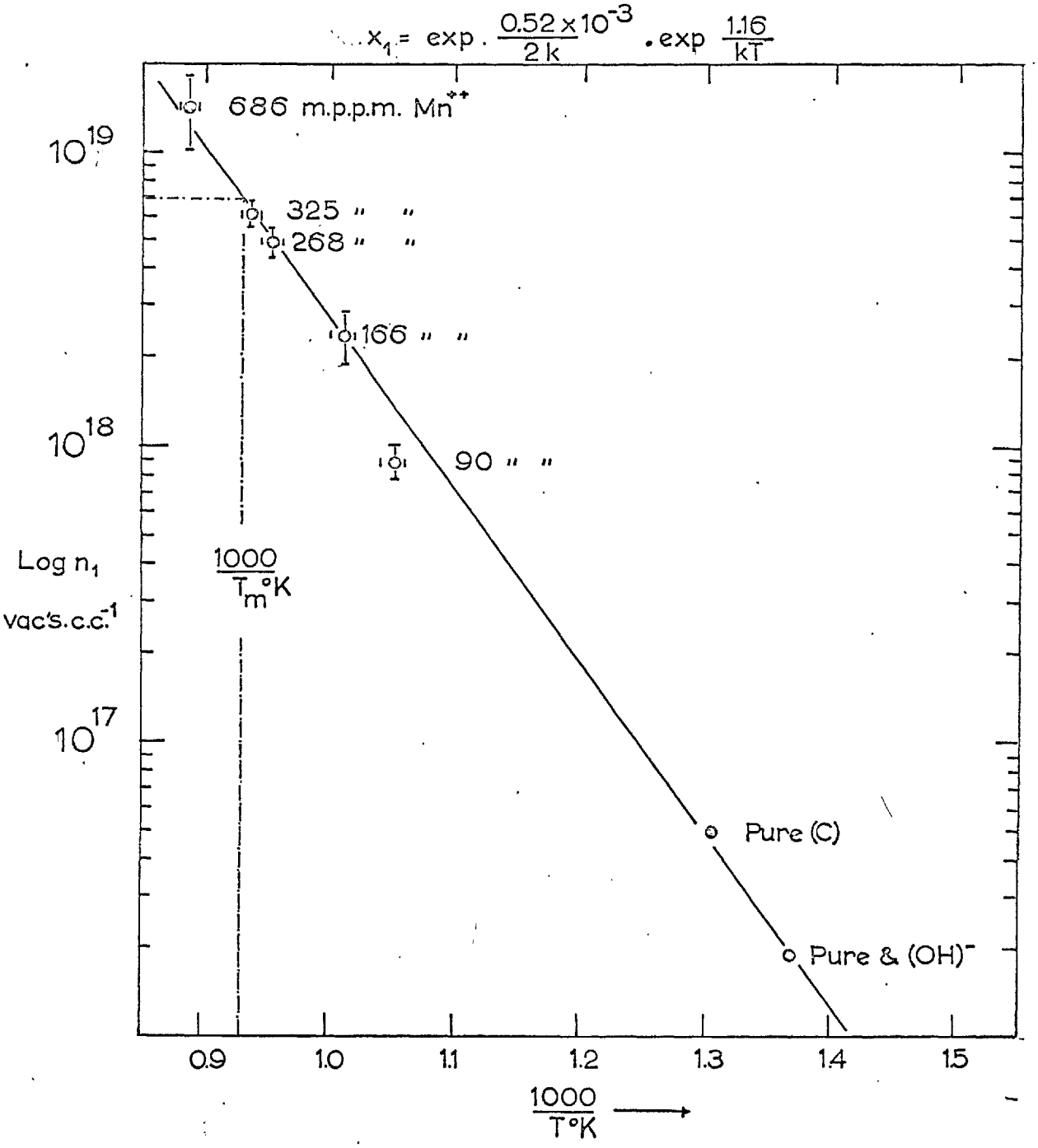

Fig. I.17

formation of

$$\sigma_i T = 1.168 \times 10^8 \times \exp - (1.83 \pm 0.03) eV/kT . Mho . cm^{-1} . {}^oK$$

This when compared with the expression obtained directly from experiment

$$\sigma_i T = (5.5 \pm 3.2) \times 10^8 \times \exp - (1.83 \pm 0.01) ev/kT . Mho . cm^{-1} . {}^oK$$

shows that there is an element of consistency throughout the experimental data.

From the entropy term S the ratio ν_2/ν_1 was determined. This yielded a ratio of 1.655. The fact that this ratio is significantly different from 1.00 would suggest that the values of Δs_1 and Δs_2, calculated by assuming a constant Debye frequency, are incorrect. The effect of the vacancy will be present not only in the nearest atoms surrounding the vacancy, but also in positions distant from the vacancy centre. This will lower the effective lattice vibration frequency and raise the entropy factors.

By observing the concentration of cation vacancies at the melting point, the fractional concentration of vacant lattice sites was found to be

$$\frac{n_1(Tm)}{N} = 3.95 \times 10^{-4}$$

This figure compares well with the value deduced by Dreyfus and Nowick [54] (2.80×10^{-4}) from the extrapolated specific conductivities of a number of different workers, but is much lower than the estimates

obtained from specific heat determinations [11] and dielectric absorption measurements.[76]

(v) Conclusions and suggestions for future work.

A high temperature enhancement of the intrinsic conductivity that occurred in deformed single crystals of nominally pure sodium chloride was explicable in terms of the annealing of dislocations into grain and sub-grain boundaries. These were believed to provide paths of enhanced conduction for anion vacancies at elevated temperatures. The annealing behaviour and the effects of deformation upon the intrinsic conduction were consistent with this model. As a result of this, care should be exercised in the interpretation of intrinsic conductivity data, especially if the crystal growth and method of specimen preparation produces considerable mechanical damage.

The parameters of motion of this anion vacancy, obtained from the analysis of this enhancement, are not representative of ionic motion through the bulk of the crystal. Both the enthalpy and entropy of motion are too high. ($\Delta h_2 = 1.60$eV, $\Delta s_2 = 1.57 \times 10^{-3}$eV/^{o}k), when compared with those obtained from diffusion studies. A logical extension of the present work would be an investigation of the conducting properties of individual dislocations and grain boundaries in higher purity material. This should yield accurate values for the parameters of anion motion down grain and sub-grain boundaries which could be compared with the values obtained from the present study. An investigation of the conductivity of polycrystalline sodium chloride, with particular emphasis being placed upon the grain size dependence and

annealing characteristics, could also provide confirmatory evidence about ionic motion at boundaries in crystalline materials.

Evidence of an anion contribution to the conductivity in undeformed crystals appears in the slight curvature of the intrinsic region. The data of Fig. (1.3) (a pure, undeformed crystal of sodium chloride) when fitted to a theoretical curve involving the eight variables associated with the intrinsic, extrinsic and association regions of ionic conductivity produced the following values: $\Delta h_2 = 0.89eV.$, $\Delta s_2 = 4.33 \times 10^{-4} eV/^{o}k.$ The computer fitting involved a standard I.B.M. least squares minimization routine. These values are in good agreement with the data of Barr et al.(74) and they suggest that in the present work, two distinct types of intrinsic ionic motion have been observed - one associated with anion vacancy motion through perfect regions of the crystal lattice and the other with motion along dislocations and sub-grain boundaries. These present experiments go some way in explaining the differing behaviour of the intrinsic conductivity of potassium chloride, as observed by previous workers and schematically presented in Fig. (1.2).

The extrinsic data of the impure crystals is believed to be the first thorough investigation using manganese as a dopant. It was found to behave as a typical divalent cation impurity occupying a substitutional position in the cation sub-lattice. The value of $0.68 \pm 0.02eV$ for the enthalpy of motion of the cation vacancy is considerably lower than values quoted by previous workers. The reasons for accepting this value, in preference, are two-fold; firstly, it was obtained from the slopes of the extrinsic conductivity plot in which linear isotherms showed the absence of any effects of the association reaction, and secondly, an isothermal analysis of the

association regions of the doped crystals when combined with the extrinsic data of crystals of known manganese impurity levels also produced a mobility whose temperature dependence gave a similar value.

The lowering of the value of Δh_1 automatically results in a higher estimate for h, the enthalpy of formation of the Schottky pair. But the value of 2.30 ± 0.02eV for h is confirmed by an analysis of the extrinsic data which allowed the equilibrium concentration of cation vacancies to be obtained as a function of temperature.

The study of the doped crystals has shown the presence of a significant quantity of anion impurities (possibly O^{--} or $(OH)^{-}$), which fortunately maintained a fixed background level for the crystals investigated. If further progress is to be made, crystals of a lower background impurity level would be desirable. As the behaviour of the divalent manganese ion has been explored in the present work, it would be interesting to extend the measurements of ionic conductivity to cover crystals in which transition metal ions with differing valence states were used as dopants. Valence changes could then be monitored by observing the conductivity.

REFERENCES

Ionic Conductivity

1. A.B. Lidiard: Handbuch der Physik, 20, 246, 1957.
2. R.E. Howard, A.B. Lidiard: Rep.Prog.Phys., 27, 161, 1964.
3. R.J. Friauf: Ionic conductivity of Solid Salts, American Institute of Physics Handbook.
4. W. Schottky: Z. Phys. Chem. Abt., B.29, 335, 1935.
5. J. Frankel: Z. Phys., 35, 652, 1926.
6. W. Lehfeldt: Z. Phys., 85, 717, 1933.
7. E. Koch, C. Wagner: Z. Phys. Chem. Abt., B.38, 295, 1937.
8. H. Pick, H. Weber: Z. Phys., 128, 409, 1950.
9. H. Kelting, H. Witt: Z. Phys., 126, 697, 1949.
10. Strelkow after A.W. Lawson: Phys. Rev., 78, 185, 1950.
11. R.W. Christy, A.W. Lawson: J. Chem. Phys., 19, 517, 1951.

Transport numbers

12. F. Kerkhoff: Z. Phys., 130, 449, 1951.
13. C. Tubandt: Handbuch der Experimental Physik, 12, 383, 1932.
14. Y. Haven: Proc.Brit. Ceram.Soc., July 1964, Conference Report.
15. A.J. Dekker: Solid State Physics, Macmillan and Co.Ltd., 1960.
16. W.T. Read, G.L. Pearson: Rep. of Bristol Con. on Defects in Crystalline Solids, 1954. (Phys. Soc. London).

Electrode effects

17. J.N. Maycock: Thesis, University of London, 1962.

18. C.Z. van Doorn: Rev. sci. Instruments, 32, 755, 1961.

19. J.N. Maycock: Technical report, 64 - 18, R.I.A.S., 1964.

20. S. Csazar: Nature, 181, 1158, 1958.

21. J.R. Hanscomb, K.C. Kao, J.H. Calderwood, J.J. O'Dwyer, P.R. Emtage: Proc. Phys. Soc., 88, 425, 1966.

22. C.A. Bucci, S.C. Riva: J. Phys. Chem. Sol., 26, 363, 1965.

23. J. Beaumont: Ph.D. Thesis, University of London, 1965.

24. J.R. MacDonald: Phys. Rev., 92, 1, 1953.

Electronic conduction

25. A. Redfield: Phys. Rev., 91, 244, 1953.

26. H. Frohlich, N.F. Mott: Proc. Roy. Soc., 171, 496, 1939.

27. F.E. Low, D. Pines: Phys. Rev., 91, 193, 1953.

28. P. Read, E. Katz: Phys. Rev. Letters, 5, 466, 1960.

Thermo-electric powers

29. L. Patrick, A.W. Lawson: J. Chem. Phys., 22, 1492, 1954.

30. R.E. Howard, A.B. Lidiard: Disc. Farad. Soc., 23, 113, 1957.

31. E. Haga: J. Phys. Soc. Japan, 14, 992, 1959.

32. A.R. Allnatt, P.W.M. Jacobs: Proc. Roy. Soc., A.260, 350, 1961.

33. A.R. Allnatt, P.W.M. Jacobs: Proc. Roy. Soc., A.267, 31, 1962.

34. R.W. Christy, Y.W. Hsueh, R.C. Mueller: J. Chem. Phys., 38, 7, 1963.

35. R.E. Howard, A.B. Lidiard: Phil. Mag., 2, 1467, 1957.

36. R.W. Christy: J. Chem. Phys., 34, 1148, 1961.

37. R.W. Christy; E. Fukushima and H.T. Li: J. Chem. Phys., 38, 1647, 1963.

38. Y. Suzuki, S. Endo, E. Haga: J. Phys. Soc. Japan, 14, 729, 1959.

39. I. Ebert, J. Teltow: Ann. Phys. Lpz., 15, 268, 1955.

40. J. Teltow: Ann. Phys. Lpz., 5, 63, 1949.

41. P.L. Tan; Ph.D. Thesis, University of London, 1968.

42. A.R. Allnatt: Ph.D. Thesis, University of London, 1958.

43. H. Curien, Z. Mihailovic: C.R. Acad. Sci., Paris, 248, 2982, 1959.

44. R.E. Howard, J.R. Manning: J. Chem. Phys., 36, 910, 1962.

45. P.G. Shewmon: J. Chem. Phys., 29, 1032, 1958.

46. A. Sawatsky: J. Nuclear Materials, 2, 321, 1960.

47. F.R. Winter, H.G. Drickamer: J. Chem. Phys., 24, 492, 1956.

48. A.R. Allnatt: Manchester Con. on Solid State Phys., Jan. 1967.

49. K. Wirtz: Phys. Z., 44, 221, 1943.

Anion motion and diffusion

50. A.R. Allnatt, P.W.M. Jacobs: Trans. Farad. Soc., 58, 116, 1962.

51. T.E. Phipps, E.C. Partridge: J. Amer. Chem. Soc., 51, 1331, 1929.

52. J.H. Beaumont, P.W.M. Jacobs: J. Chem. Phys., 45, 5, 1966.

53. R.C. Fuller: Phys. Rev., 142, 524, 1966.

54. R.W. Dreyfus, A.S. Nowick: J. Appl. Phys. Suppl., 33, 473, 1964.

55. S.C. Jain, S.L. Dahake: Indian J. Pure App. Phys., 2, 71, 1964.

56. D. Mapother, H.N. Crooks, R.J. Maurer: J. Chem. Phys., 18, 1231, 1950.

57. Y. Haven: J. Chem. Phys., 21, 171, 1954.

58. J.F. Laurent, J.F. Bénard: J. Phys. Chem. Sol., 3, 112, 1958.

59. J.F. Laurent, J.F. Bénard: J. Phys. Chem. Sol., 7, 218, 1958.

60. J.C. Fisher: J. Appl. Phys. 22, 74, 1951.

61. R.T.P. Whipple: Phil. Mag., 45, 1225, 1954.

62. J. Cabané: J. Chem. Phys., 59, 1135, 1962.

63. J.F. Aschner: Thesis, University of Illinois, 1954.

64. M. Chemla: Compt. Rend., 234, 2601, 1952.

65. M. Chemla: Ann. Phys., 1, 959, 1956.

66. H.W. Schamp, E. Katz: Phys. Rev., 94, 828, 1954.

68. J. Owles, S.C. Jain: Proc. Roy. Soc., A423, 353, 1958.

69. L.C. Harrison, J.A. Morrison, R. Rudham: Trans. Farad. Soc., 54, 106, 1958.

70. A.B. Lidiard: J. Phys. Chem. Sol., 6, 298, 1958.

71. J.A. Morrison, R. Rudham: J. Phys. Chem. Sol., 6, 402, 1958.

72. N. Laurance: Phys. Rev., 120, 57, 1960.

73. M.P. Tosi, F.G. Fumi: Nuovo Cimento, 1, 95, 1958.

74. L.W. Barr, J.A. Morrison, P.A. Schroeder: J. App. Phys., 36, 624, 1965.

75. L.W. Barr, I.M. Hoodless, J.A. Morrison, R. Rudham: Trans. Farad. Soc., 56, 697, 1960.

76. P.V. Sastry, T.M. Srinivasan: Phys. Rev., 132, 2445, 1963.

77. H.S. Sack, G.C. Smith: Proc. Int. Con. Crystal Lattice Defects, J. Phys. Soc. Jap., 18, III, 1963.

78. K. Tharmalingham, A.B. Lidiard: J. App. Phys., 33, 473, 1962.

79. K. Tharmalingham, A.B. Lidiard: Phil. Mag., 6, 1157, 1961.

80. R.W. Christy, A.W. Lawson: J. Chem. Phys., 19, 517, 1951 and H. Kanzaki: Phys. Rev., 81, 884, 1951.

81. I.M. Boswarva, A.D. Franklin: Phil. Mag., 11, 335, 1965.

N.M.R. and Line Width Broadening

82. N. Bloembergen: Nuclear Magnetic Relaxation, New York, Benjamin 1961.

83. N. Bloembergen, E.M. Purcell, R.V. Pound: Phys. Rev., 73, 679, 1947.

84. R. Kubo, K. Tomita: J. Phys. Soc., Japan, 9, 888, 1954.

85. J. Itoh, M. Satoh, A. Hiraki: J. Phys. Soc. Japan, 18, 57, 1963 and 16, 343, 1961.

86. M. Eisenstadt: Phys. Rev., 133, 191, 1964.

87. R.R. Allen, M.J. Weber: J. Chem. Phys. 38, 2970, 1963.

88. Y. Haven: Rec. Trav. Chem. Pays. Bas., 69, 1471, 1950

89. M. Eisenstadt: Phys. Rev., 132, 630, 1963.

90. M. Eisenstadt, A.G. Redfield: Phys. Rev., 132, 630, 1963.

91. F. Reif: Phys. Rev., 100, 1597, 1955.

92. D. Ailion: Ph.D. Thesis, University of Illinois, 1964.

93. A.B. Lidiard: Phil. Mag., 46, 815, 1955.

94. J. Hanlon: J. Chem. Phys., 32, 1492, 1960.

95. E. Schone, O. Stasiw, J. Teltow: Z. Phys. Chem., 197, 145, 1951.

96. A.N. Murin, S.N. Banasevich, Yu. S. Grushko: Soviet Phys. Sol. Stat., 3, 1762, 1962.

97. B.G. Lure, A.N. Murin, R.F. Brigevich: Soviet Phys. Sol. Stat., 4, 7, 1957.

98. W.H. Stewart, C.A. Reed: J. Chem. Phys., 43, 2890, 1966.

Anion additions

99. J. Rolfe: Canadian J. Phys., 42, 2195, 1964.

100. B. Redfern, P.L. Pratt: Proc. Brit. Ceram. Soc., 1, 173, 1964.

101. J. Anger, B. Fritz, F. Luty: Z. Physik, 174, 240, 1963.

102. R.W. Dreyfus: App. Phys. Letts., 3, 175, 1963.

103. T.G. Stoebe, J. Phys. Chem. Sol., 28, 1375, 1967.

Association reactions

104. H.W. Etzel, R.J. Maurer: J. Chem. Phys., 18, 1004, 1950.

105. R.W. Dreyfus, A.S. Nowick: Phys. Rev., 126, 1367, 1962.

106. C. Bean: Thesis, University of Illinois, 1952.

107. N. Brown, I.M. Hoodless; J. Phys. Chem. Sol., 28, 2297, 1967.

108. I.A. Parfianovitch: Optics and Spectroscopy, 6, 120, 1959.

109. S.C. Jain, D.C. Parashar: Phys. Lett., 4, 36, 1963.

110. S.C. Jain, S.L. Dahake: Indian Journal of Pure and Applied Phys., 2, 71, 1964.

Charged dislocations and grain boundaries

111. K. Lehovec: J. Chem. Phys., 21, 1123, 1953.

112. P.L. Pratt: Inst. Metals, Monograph and Report, 23, 99, 1957.

113. J.D. Eshelby, C.W.A. Newey, P.L.A. Pratt and A.B. Lidiard: Phil. Mag., 3, 73, 1958.

114. C.A. Plint, O. Theimer, W.A. Sibley: Annal. Phys., 5, 342, 1958.

115. R.W. Davidge: Phil. Mag., 8, 1369, 1963.

116. J.E. Caffyn, J.C. de Freitas, T.L. Goodfellow: Phys. Stat. Sol., 9, 333, 1965.

117. J.S. Koehler, D. Langreth, B. Von Turkovitch: Phys. Rev., 128, 573, 1962.

118. L.M. Brown: Phys. Stat. Sol., 1, 585, 1961.

119. J.C. Macfarlane, C. Weaver: Phil. Mag., 13, 124, 1966.

120. P.L. Pratt: Proc. Brit. Ceram. Soc., 1, 177, 1964.

121. T.W. Adair, C.F. Squire: Phys. Rev., 137, 949, 1965.

122. J.L. Gammel: Phys. Rev., 137, 951, 1965.

123. D. Turnbull, A. Hoffman: Acta. Met., 2, 419, 1954.

124. H. Burgess, R. Smoluchowski: J. App. Phys., 26, 491, 1955.

125. R.L. Tucker, A. Laskar, R. Thomson: J. App. Phys., 34, 445, 1963.

126. R.L. Moment, R.B. Gordon: J. App. Phys., 35, 2489, 1964.

127. F. Bassani, R. Thomson: Phys. Rev., 102, 1264, 1965.

128. H. Kanzaki, K. Kido, T. Kinomiya: J. App. Phys., 33, 482, 1962.

129. H.C. Graham: Dissertation, Ohio State University, 1965.

130. P.L. Pratt: Point Defects in Metals and Alloys, Institute of Metals, 1958.

131. R.W. Whitworth: Phil. Mag., 10,107, 1964.

132. R.W. Davidge: Phys. Stat. Sol., 3, 1851, 1963.

133. D.B. Fishback, A.S. Nowick: J. Phys. Chem. Sol., 5, 302, 1958.

134. W. Deckyser, F. Rueda: Acta. Met., 11, 35, 1963.

135. J.L. Caffyn, T.L. Goodfellow: Proc. Phys. Soc., 79, 1285, 1962.

136. F. Rueda: Phil. Mag., 8, 29, 1963.

137. W.W. Tyler: Phys. Rev., 86, 801, 1952.

138. J.E. Caffyn, T.L. Goodfellow: Nature, 176, 878, 1955.

139. A. Taylor, P.L. Pratt: Phil. Mag., 3, 1015, 1958.

140. R.W. Davidge, C.E. Silverstone, P.L. Pratt: Phil. Mag., 4, 985, 1959.

141. P. Camagni, A. Manara: J. Phys. Chem. Sol., 26, 449, 1965.

142. B.H. Kear, A. Taylor, P.L. Pratt: Phil. Mag., 4, 665, 1959.

143. K. Tharmalingham: J. Phys. Chem. Sol., 25, 225, 1964.

144. P. Camagni, A. Manara: Con. Report on Electrical and Ionic properties of the alkali halides, Luglio, p.219, 1966.

145. C. Wert: Phys. Rev., 79, 601, 1950.

146. A.D. LeClaire: Phil. Mag., 3, 921, 1958.

147. A.D. LeClaire: A.B. Lidiard; Phil. Mag., 1, 518, 1956.

148. L.W. Barr, A.D. LeClaire: Proc. Brit. Ceram. Soc., No. 1, July 1964.

149. G.H. Vineyard, G.J. Dienes: Phys. Rev., 93, 265, 1954.

150. P. Debye, E. Huckel: Z. Phys., 24, 185, 1923.

151. B. Redfern: Thesis, University of London, 1965.

152. J. Quin, B.A.W. Redfern, P.L. Pratt: Proc. Brit. Ceram. Soc., 9, 35, 1967.

153. H. Kanzaki, K. Kido, S. Tamura: J. Phys. Soc. Japan, 20, 2305, 1965.

154. P.H. Sutter, A.S. Nowick: J. App. Phys., 34, 734, 1963.

155. R. Chang: Proc. Brit. Ceram. Soc., 9, 193, 1967.

156. K. Suzuki: J. Phys. Soc. Japan, 13, 179, 1958.

157. R.W. Davidge and P.L. Pratt: Phys. Stat. Sol., 6, 759, 1964.

158. A.R. Kahn: Thesis, University of London, 1967.

159. G.D. Watkins: Phys. Rev., 113, 79, 1959.

160. S.A. Rice: Phys. Rev., 112, 804, 1958.

161. R.B. Barnes: Z. Physik, 75, 723, 1932.

162. I.H. Boswarva, A.B. Lidiard: Int. Con. on Point Defects in Solids, U.S. National Bureau of Standards, May 1 - 4, 1966, Proceedings thereof.

163. A. Taylor: Thesis, University of Birmingham, 1958.

164. N. Biermann: Z. Physik Chem., 25, 253, 1960.

165. F.G. Fumi, M.P. Tosi: Disc. Farad. Soc., 23, 92, 1957.

166. K. Kobayashi, T. Tomiki: J. Phys. Soc. Japan, 15, 1982, 1960.

167. R. Guccione, M.P. Tosi: J. Phys. Chem. Sol., 10, 162, 1959.

PART II

The State of Aggregation and Dispersion of Divalent Manganese in single crystals of Sodium Chloride

GLOSSARY OF SYMBOLS USED.

α_k	Molar concentration of impurity-vacancy dipoles.
n_d	Number of impurity-vacancy dipoles/cc.
Δn	Number of impurity-vacancy dipoles/cc orientated by an applied electric field.
ω_1, ω_2	Jump frequencies of cation vacancy and impurity ion when bound together into a dipole form.
$P(T)$	Electric dipole moment/cc. as a function of temperature.
$\tau(T)$	Dipole relaxation time as a function of temperature.
g_a, h_a s_a	Gibbs free energy, enthalpy and entropy of association.
$\Delta g_o, \Delta h_o$ Δs_o	Gibbs free energy, enthalpy and entropy of recrientation of impurity-vacancy complex.
T_m	Temperature at which I.T.C. peak occurs.

(i) The Scope and Aims of Part II

When a divalent, substitutional cation impurity is dissolved into an ionic crystal it will form a compensating cation vacancy through the condition of charge neutrality. Because of the Coulombic attraction between these oppositely charged defects there will be a tendency to form an I.V. (impurity-vacancy) dipole, a defect which possesses an electrical dipole moment. It is this dipole moment which makes a quantitative study of the associated defect possible through the techniques of dielectric absorption and relaxation. The concentration of these dipoles will, to an approximation, depend upon temperature according to a Law of Mass Action reaction. If the crystal is rapidly cooled from an elevated temperature, these I.V. dipoles will be quenched into the crystal in a non-equilibrium manner. During the subsequent ageing of the crystal, the impurity ions and dipoles will tend to revert to an aggregated or precipitated state.

These dipolar complexes are of considerable importance in explaining the rapid hardening produced in ionic solids containing a divalent impurity. It is believed that the complex produces a tetragonal elastic strain field in the crystal lattice,[1] which increases the hardness of the crystal through elastic interactions with moving dislocations on appropriate slip planes. To obtain a quantitative study of the hardening mechanism, it is essential that a detailed analysis of the parameters describing these dipolar complexes should be resolved; this, when coupled with a knowledge of the state of dispersion of the divalent impurity, as a function of temperature, should lead to an unambiguous interpretation of the

mechanical properties. It was for the former reasons that the present investigation of the system Mn^{++}/NaCl was performed using the techniques of ionic conductivity, dielectric absorption and relaxation and I.T.C. (ionic thermocurrents) measurements. The latter technique is relatively new and can be considered as the D.C. equivalent of dielectric absorption.

(ii) Introduction and Survey of Literature

The association and state of aggregation of the divalent impurities in ionic crystals has been the subject of many investigations, using a wide range of physical techniques. These are briefly reviewed.

(1) X-ray Diffraction

No direct x-ray diffraction studies have been performed upon sodium chloride doped with manganese. The system Cd^{++}/NaCl has been extensively investigated by Suzuki.[2] It is also observed that cadmium and manganese have similar electronic configurations (Mn, 2.8.13.2., Cd, 2.8.18.18.2), phase diagrams[79] and produce a hardening behaviour in which the volume fractions vary in a similar manner with concentration. With these similarities, it is suggested that the aggregated forms of manganese and cadmium in single crystals of sodium chloride are similar.

Suzuki[2] found that by suitably heat treating the crystals, rearrangement of the basic aggregate unit cells could be made to occur. He also observed that three phases may co-exist at low concentrations, namely: (i) The α phase, which is a solid solution

of cadmium in the sodium chloride lattice. (ii) An aggregate phase of $CdCl_2.2NaCl$, which has a unique structure different from that of the divalent chloride. (iii) The Suzuki phase, $CdCl_2.6NaCl$, which is an intermediate structure to that of NaCl and $CdCl_2$. These last two phases may co-exist at room temperatures within a concentration range of 2 - 20 mole %. For the concentrations studied in the present work, the Suzuki phase will be of prime importance when considering aggregation reactions.

The Suzuki phase is not a true chemical compound like $CdCl_2$, but is an intimate conglomeration of cadmium, chlorine, sodium ions and cation vacancies arranged in the manner of Fig. (2.1).

It is interesting that the number of cadmium ions and cation vacancies are equal, the phase remaining electrically neutral. Any formation of this phase would not be observable by density or conductivity studies, as the overall concentration of cation vacancies in the crystal would remain the same. By slowly cooling the crystal from 500°C, this aggregate phase was found to have an f.c.c. structure, with a lattice constant twice that of the matrix. If the crystal were quenched from elevated temperatures, sufficient to put most of the impurity into a dipole form, and then subsequently aged at 200°C, the Suzuki phase formed thin platelets on {100} planes. This presumably represents the initial stages of aggregation of the divalent impurity cadium and possibly manganese.

The Suzuki phase is not a true equilibrium structure. If the concentration of the impurity is increased, the phase becomes metastable with the $CdCl_2.2NaCl$ structure being the stable aggregate. This has a rhombohedral structure with a unit cell of dimension $9.92A^{\circ}$ and $\alpha = 118^{\circ}18'$.

The "Suzuki phase"

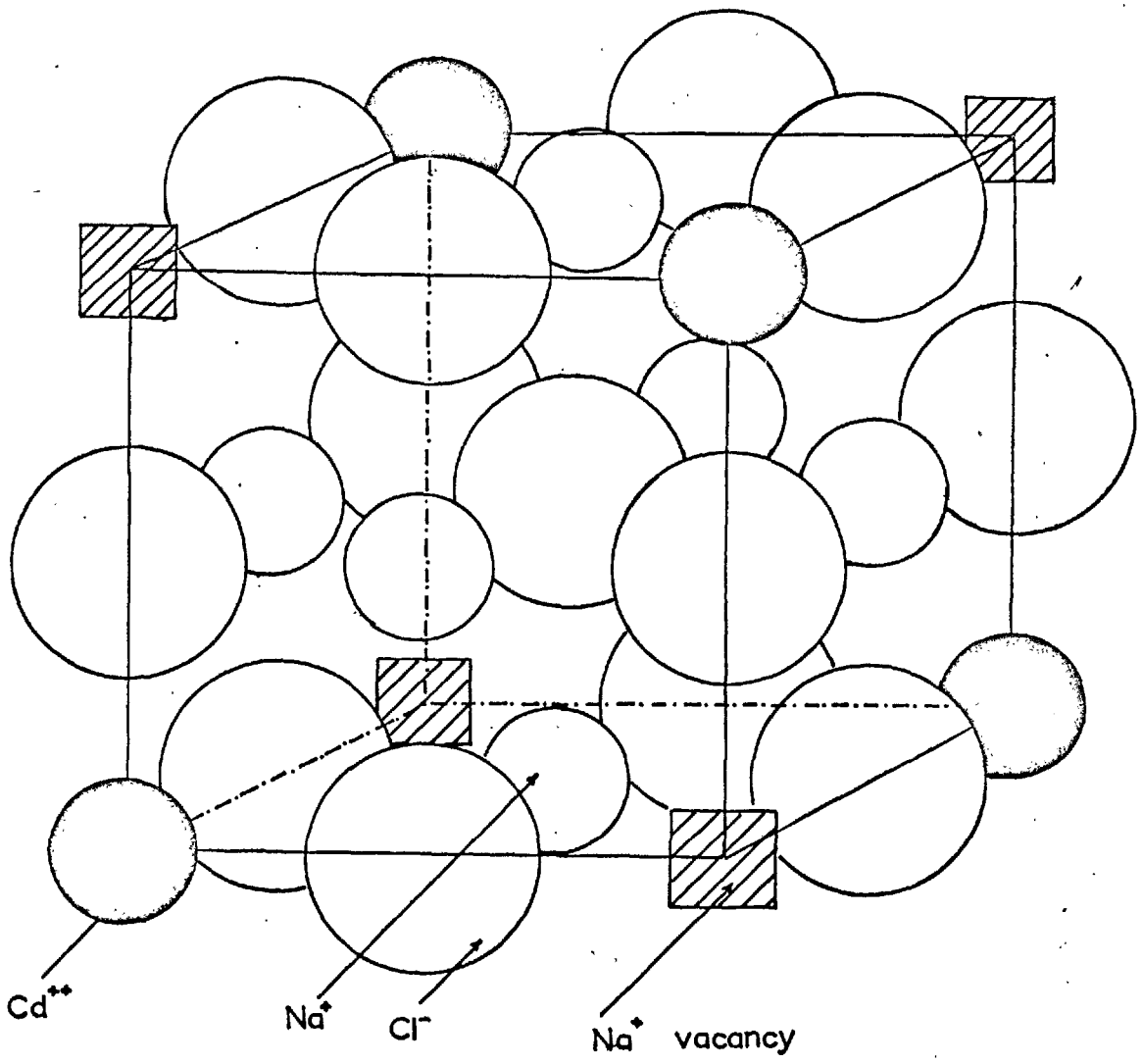

1/8 th the unit cell of $CdCl_2 \cdot 6NaCl$.

Fig, 2.1

Toman [3] extended the work of Suzuki and found that for crystals containing 0.30 mole % $CdCl_2$ the rise of the Suzuki phase aggregates depended upon the rate of cooling from elevated temperatures. Rapidly cooled samples produced regions of 200°A in size, whilst slowly cooled samples presented aggregated phases up to 1000°A in size. The smaller forms appeared coherent with the lattice of the solid solution whilst the larger aggregates were incoherent.

X-ray studies were performed by Suzuki [4,5] on crystals of sodium chloride heavily doped with calcium. The aggregated forms of calcium were found to exist on 111 and 310 planes of the matrix. Of these two forms, the 310 platelets were stable at elevated temperatures.

2) E.P.R. Studies

By investigating the e.p.r. spectra of paramagnetic impurities in diamagnetic crystals, considerable information concerning the electronic states of the paramagnetic atom or ion may be obtained. Because the electronic states depend strongly upon the crystalline electric field, the state of the surrounding crystal environment can be obtained by analyzing the resonance lines. The manganese (Mn^{++}) spin resonance spectrum has been discussed in considerable detail by Bleaney and Ingram.[6] Briefly, the Mn^{++} ion's ground state is $^6S_{5/2}$ and is only slightly affected by its environment. Because of this, in ionic solids its g value is close to 2.0023, the free electron value. (Watkins [14] reports a value of 2.0016 ± 0.0006 for isolated manganese ions in sodium chloride).

Crystalline field splittings are relatively small and relaxation times long, [7] again indicating a rather isolated manganese ion. The isotope Mn^{55} has a nuclear spin 5/2 and as a result, each electronic transition is split into six hyperfine lines.

Impurity vacancy dipole formation can be induced by suitably heat treatment of the doped crystal. From the resulting e.p.r. spectra the relative positions between the impurity ions, vacancies and the crystal field produced by the vacancy can be observed, as well as the relative concentrations of impurity ions in the different environments.

Schneider and Caffyn [8] investigated the e.p.r. spectrum of single crystals of sodium chloride doped with divalent manganese, and found that the spectrum presented a broad single line in the aged state, and a series of fine lines when the crystal was quenched from elevated temperatures. The broad line was considered as arising from the normal Van Vleck [9] broadening (dipole-dipole interactions) between the individual Mn^{++} ions in the aggregated state. The fine line structure was attributed to isolated I.V. dipoles, this spectrum arising from the effects of the tetragonal electric field of the I.V. dipole being superimposed upon the crystalline lattice cubic field. Schneider [10] later discussed this fine line structure in some detail and concluded that the temperature dependent resolution of the manganese occurred to form complexes with cation vacancies, with the impurity occupying substitutional positions in the sodium sub-lattice. His e.p.r. spectra for the aged crystals suggested that resolution and subsequent aggregation proceeded via a dislocation system from and to the aggregates. This work was extended by Morigaki, Fujimoto

and Itoh [11] and Watkins and Walker. [12] These workers investigated specifically the e.p.r. spectrum attributed to manganese ions associated with a cation vacancy, in quenched crystals and observed that this state of manganese was inherently unstable, the complexes diffusing through the lattice to form aggregates or clusters of manganese ions.

The work of Watkins [14] is the most comprehensive investigation of the e.p.r. spectra of the different environments of manganese in ionic crystals. Having considered manganese doped crystals of sodium, potassium and lithium chlorides, the following different spectra were observed for the manganese ion in sodium chloride.

(I) A broad peak:- manganese ions in an aggregated or precipitated state.

(II) A six line spectrum, predominant at temperatures in excess of 400°C, and attributed to isolated manganese ions occupying substitutional positions.

(III & III_1) A complex spectrum attributed to impurity vacancy complexes, with the cation vacancy in the nearest and next nearest-neighbour positions.

(IV) A complex spectrum attributed to divalent charged anion impurity occupying a nearest-neighbour chlorine site.

The binding energies of the n.n. and n.n.n. impurity-vacancy complexes were found to be very similar (ΔE = 0.034eV.) and the thermal disassociation of the complexes was found to obey a simple Law of Mass Action relation, with a Gibbs free energy of 0.4eV.

The detailed ageing characteristics of manganese in sodium chloride were determined by Symmons and Kemp. [16] After a

preconditioning heat treatment at 450°C and then air quenching, nearly all the manganese impurity was found to be present in an I.V. dipole form. The ageing behaviour was consistent with the formation of a trimer, a collection of three dipoles. The process was found to be described by a third order kinetic reaction with an energy of 0.80 ± 0.05eV. for dipole diffusion. The data further showed that the aggregation process continued after the formation of the trimer, with the production of relatively large aggregates. The exact mechanism for this further aggregation process was not clear.

Alzetta, Crippa and Santucci [17] observed the effects of plastic deformation upon the e.p.r. spectrum of manganese present in sodium chloride. Their aged crystals presented a single broad line due to the aggregated state in a crystal containing 600 m.p.p.m. of Mn^{++}. After deformation of the crystal, six hyperfine lines of the Mn^{++} ion occupying substitutional sites were apparent. The concentration of substitutional manganese derived from the intensities of the hyperfine lines was found to be proportional to the percentage of plastic deformation. The results were explained by the partial disassociation of the defect clusters of manganese by moving dislocations.

The composition of the aggregated forms of manganese in sodium chloride has never been determined directly. It is unlikely to be manganese chloride since Schneider [19] found no correlation between the profile of the broad line e.p.r. spectrum of manganese in aged crystals and crystals of manganese chloride. This conclusion is supported by Quin, [20] who observed no density change in crystals of sodium chloride doped with manganese and cadmium, after quenching from elevated temperatures. This latter work again confirms that

the precipitated form contains an equal number of manganese ions and cation vacancies, an impossible situation if the precipitate was composed solely of the divalent metallic chloride.

3) Dielectric Absorption and Relaxation

Because the I.V. dipole has an effective electrical dipole moment, it can be made to orientate under an applied A.C. or D.C electric field. By a suitable choice of temperature and frequency of an applied A.C. field ($\approx$ 1 k.c.p.s. at 30°C for Mn^{++} , Ca^{++} I.V. dipoles) an absorption may be observed, which appears as a peak in the plot of Tan δ versus Log f. This form of absorption is not a true resonant absorption, there being no proper frequency associated with the reorientation of the dipoles, but rather an absorption due to the relaxing dipole system and is described by the classical Debye equations. Lidiard [23] has performed a theoretical analysis of dipole reorientation under the action of variable frequency electric fields. He has considered the effects of nearest-neighbour and next nearest-neighbour I.V. dipole-like complexes and has described their motion in a series of rate equations which are the starting point for any dynamic theory of dipole orientation. Lidiard's analysis shows that the complexes in the n.n.n. positions only produce a slight broadening of the Debye peak, which is usually undetectable within the limits of experimental error.

The first experimental attempt to observe dielectric absorption due to the reorientation of I.V. complexes was made by Breckenridge [24] who, by using an A.C. field of fixed frequency (1 k.c.p.s.) observed peaks in the plot of Tan δ versus 1000/T. He attributed these peaks to the reorientation of I.V. and vacancy-pair dipolar complexes. Part of this interpretation was shown to be incorrect by Lidiard [23]

who pointed out that it would be more convenient to observe the absorption at a fixed temperature with a variable frequency applied field.

Dryden and Rao [25] and Dryden and Meakins [26] observed dielectric absorptions in lithium, sodium and potassium chlorides doped with a wide range of divalent impurities. The impurity was put into a dipole form by annealing at elevated temperatures, to force the impurity into solution and then rapidly cooled by air quenching. Their absorption losses were always superimposed upon a background loss due to the motion of free cation vacancies. All the systems studied exhibited a similar behaviour with respect to the shape and form of the absorption peaks; all, that is, except calcium which presented two absorption losses close together, the high frequency loss being much smaller in magnitude and only appearing in heavily doped crystals. The lower frequency absorption was attributed to the simple impurity-vacancy dipole whilst the high frequency loss was attributed to an absorption possibly present in the aggregated state of the impurity. The work of Burstein, Davidson and Scalar [27] and Jacobs [28] on the systems Sr^{++}/KCl and Ca^{++}/NaCl extended the observations of the I.V. absorption peaks up to temperatures of 150°C and from the shift of the peak height as a function of temperature a more accurate evaluation of the enthalpies of reorientation.

Cook and Dryden [29] measured the intensity of the absorption (and I.V. dipole concentration) as a function of quenching temperature and observed that for Ca^{++}/NaCl, after rapidly cooling from certain critical temperatures, practically 100% of the impurity was to be found in an I.V. dipole form. In contrast Haven [30] found that

in similarly doped crystals of sodium chloride, the sum of the impurity in I.V. dipole form (as determined by dielectric absorption) and that as free ions in solid solution (as determined by conductivity) accounted for only a fraction of the total impurity content at 100°C. The rest was assumed to be in higher complexes or in an aggregate phase. Cook and Dryden [31] observed that for Sr^{++}/KCl, Ba^{++}/KCl, Mn^{++}/NaCl the subsequent ageing and initial reclustering of the I.V. dipoles proceeded by a reaction involving third order kinetics. It was again suggested that the dipoles re-clustered into groups of three to form trimers and then regrouped into larger clusters during further ageing.

Dryden, Morimoto and Cook [33] investigated the relationship between I.V. dipole concentration and the "hardness of the crystal", as revealed by the critical, resolved shear stress. Their principal observations were, that in divalent doped sodium chloride the increase in the critical, resolved shear stress was proportional to the dipole concentration to a 2/3 power. Further, there was no increase in hardness as the I.V. dipoles aggregated into trimers.

The dielectric absorption measurements described previously have observed dipolar complexes at or near room temperature, obtained after suitably heat treating the crystal. Watkins [34] seems to have made the only attempt to observe these complexes at elevated temperatures. Dielectric absorption measurements at radio frequencies revealed a Deby loss peak at 300°C in manganese doped sodium chloride. This was correlated with the reorientational motion of impurity vacancy complexes in n.n. and n.n.n. positions. An energy of 0.63 ± 0.05eV. was obtained for the average enthalpy of reorientation of n.n. and n.n.n. complexes.

Dielectric absorption measurements are solely concerned with a resonance absorption of energy by the I.V. dipoles under A.C. field conditions. Dielectric relaxation involves the measurement of the displacement current produced when an impurity dipole is reorientated by a steady electric field. Measurements can only be performed when the dipolar relaxation time is greater than 1 sec: for relaxation times less than this, the reorientation is achieved too rapidly for a quantitative analysis of the displacement current to be made. Dreyfus [35] observed these relaxation currents for a wide range of divalent impurity dopants (Mg^{++}, Mn^{++}, Ca^{++}, Zn^{++}, Sr^{++}) in sodium chloride. The dipolar reorientation was seen as an exponential decay in the current-time curve. A very fast relaxation was attributed to the reorientation of n.n.n. impurity vacancy complexes, whilst a slow background decay was probably caused by the relaxations seen by Sutter and Nowick [36] in pure ionic crystals. The dominant jump mechanisms were inferred from the way in which the relaxation time varied with the radius of the impurity ion, for a fixed temperature. It was suggested that the decrease in relaxation time with decreasing radius of the impurity ion showed a strong dependence of the jump rate of the impurity ion upon the ionic radius.

Dreyfus and Laibowitz [37] extended this work by observing the mechanical relaxation of I.V. dipoles. This was performed by observing the stress induced reorientation of I.V. dipoles in the systems Ca^{++}/NaCl, Mn^{++}/NaCl using the technique of internal friction. A mechanical loss peak was observed at 100°C for a vibrational frequency of 10 k.c.p.s. This was attributed to the stress reorientation of the complex. Data obtained for longitudinal strain

along <100>and <111> directions gave information concerning the mechanism of the relaxation modes.

Lozovoskii [38] and Franklin, Shorb and Watchman [39] have performed a relaxation mode analysis, using group theory, that includes the "excited states" of the I.V. dipole. For the binding energies of each particular excited state, Lozovoskii chose purely Coulombic values arising from the electrostatic interactions between point charges. He showed that there could be four active relaxation modes, of which the slowest one would be predominant. Under A.C. conditions, this would result in a close agreement with a Debye absorption peak characterized by a single relaxation time. In the case of Dreyfus' data [35] the fast and very fast relaxations could be described by the dominant mode and a superposition of the other three. The other slow relaxation must be attributed to some process not connected with I.V. dipole orientation.

4) Ionic Conductivity

The primary effect of the association reaction between impurity ions and cation vacancies is to reduce the free cation vacancy concentration, through the formation of electrically neutral complexes and to subsequently steepen the slope of the Arrhenius conductivity plot. It is often implicitly assumed that the association reaction is represented by a linear region of the conductivity plot, the slope of which is related to the enthalpy of formation of the complex by the following relationship:-

$$Q_{III} = \Delta h_1 + h_{a/2}$$

It can be shown that this assumption is only valid if all the impurity is in solution and the crystal contains a relatively large doping level. More significant estimates of the enthalpy of association can be obtained from an isothermal analysis of the conductivity data.

The equations and processes governing the association reactions in ionic solids are very similar to the reactions occurring in ionized solutions of sodium chloride. Thus the association theories of Stasiw and Teltow, [40] which were developed for electrolytic solutions, can be transferred quite readily to the charged point defects appearing in the solid state. This simple theory only considers nearest neighbour interactions and is seen to describe well the behaviour of Co^{++}, Ni^{++}, [41] in sodium chloride. Refinements to this simple model have been introduced by Lidiard [42] and Allnatt and Cohen. [43, 44] Lidiard took into account the Coulombic interactions between the unassociated point defects by the use of activity coefficients, as first introduced into the Debye-Huckel [45] theory of ionic solutions. The principal result of this analysis was to introduce a curvature in the plot of $(c - c_o)/\sigma$ versus σ, for small values of concentration. The simple Stasiw-Teltow theory predicts a straight line relationship. Allnatt and Cohen [44] treated the distribution of impurity ions and point defects by the cluster expansion methods of Statistical Mechanics, as initially formulated by Mayer for ionic solutions and found agreement with Lidiard at very small concentrations but slight differences at finite concentrations. Due to theoretical limitations the predictions could not be extended to higher doping levels, which would have been useful for comparison with the present work.

Etzel and Maurer [46] measured the ionic conductivity of sodium

chloride containing cadmium chloride as an added impurity. They analyzed their conductivity isotherms and deduced a value of 0.85eV. for Δh_1 and 2.02eV. for h. They deduced an enthalpy of association of 0.3eV. for each I.V. complex. Their work was one of the first attempts to derive conductivity parameters from a more rigorous analysis than that of determining slopes of conductivity plots. Whilst Etzel and Maurer's work showed considerable evidence for association, Bean's [47] data for calcium doped sodium chloride presented linear isotherms, normally attributable to extrinsic conductivity free of association, down to temperatures of 161.0°C. The results are anomalous in that dielectric absorption [26] and mechanical [37] and dielectric relaxation [35] indicate a large degree of association in these Ca^{++} doped crystals. Recently, Quin, Redfern and Pratt [48] using the techniques of dielectric absorption and ionic conductivity studied the association reaction of the calcium ion in sodium chloride. They disagreed with Bean in that a considerable curvature of the isotherms was observed which yielded a Gibbs free energy of association of 0.36eV. Kanzaki, Kido and Tamura [49] repeated the measurements on Ca^{++} doped sodium chloride. At a temperature of 300°C a curvature of the reduced isotherm c/σ versus σ was detected which was attributed to the presence of higher order I.V. complexes. They obtained a free energy of association of 0.31 ± 0.01eV. for the n.n. impurity vacancy complex.

Rothman, Barr, Rowe and Silwood [50] measured conductivity and diffusion in the system Zn^{++}/NaCl. They observed a free energy of association of 0.47eV. for the I.V. dipole at a temperature of 976°K. This is much higher than that predicted on purely theoretical grounds; a lower free energy was obtained when n.n.n. impurity dipoles were

considered. The effects of precipitation interfered with the results at high temperatures and low zinc concentration, a heat of solution of 0.97eV. being obtained for the zinc ion in NaCl. The binding of a small concentration of zinc ions with possibly $(OH)^-$ ions was also observed.

Dreyfus and Nowick [51] measured the conductivity in the association regions of ionic conduction for Mg^{++}, Mn^{++}, Cd^{++}, Ca^{++}, Sr^{++}, Ba^{++} dopants in sodium chloride. Their quoted enthalpies of association were obtained from the "linear" regions of the conductivity plot. In consequence, not too much significance can be placed upon their numerical results.

Jain and Dahake [41] investigated the conductivity of nickel doped sodium chloride and deduced a free energy of association of 0.32eV. for the nickel-vacancy dipole from the conductivity isotherms. Table (2.1) presents the enthalpies and free energies of association as determined by other workers for different divalent dopants in sodium chloride.

The only systematic measurements of ionic conductivity in the temperature regions concerned with precipitation and low temperature association are those of Dreyfus and Nowick.[51] These workers successfully related the marked steepening of the Arrhenius plot to the aggregation or precipitation of the divalent impurity. Dreyfus,[52] in a later paper, showed that the precipitation phenomena only appeared in crystals grown in air. He suggested that the presence of $(OH)^-$ or (H_2O) molecules was necessary as nucleating centres for the start of aggregation.

GIBBS FREE ENERGIES AND ENTHALPIES OF ASSOCIATION FOR DIFFERENT DIVALENT DOPANTS, AS DETERMINED BY OTHER WORKERS - TABLE (2.1).

Dopant $^{++}$	h_a eV.	g_a eV.	Method and Author
Mn, 0.80A°	0.40 ± 0.1	0.30 ± 0.1	Present Work
	-	0.39	C.D.W.[14] e.p.r
	0.32	-	D.N.[51]
Ca, 0.90A°	-	0.31	K.K.T.[49]
	-	0.36	Q.R.P.[48]
	0.38	-	B.F.[62] Th.
	0.36	-	D.N.[51]
Cd, 0.97A°	-	0.34	E.M.[46]
	0.38	-	B.F.[62] Th.
	0.42	-	D.N.[51]
Ni, 0.69A°	0.32	-	J.D.[41]
Co, 0.72A°	0.30	-	J.D.[77]
Zn, 0.74A°	-	0.47	R.B.R.S.[50] Diff.
Mg, 0.65A°	0.36	-	D.N.[51]
Sr, 1.13A°	0.45	-	B.F.[62] Th.
Ba, 1.35A°	0.78	-	D.N.[51]

5) Other Techniques

(a) Microscopy[53]

The technique of ultra microscopy has been used by Bansigir and Schneider [22] to observe the aggregated form of manganese in sodium chloride. The aggregates had dimensions of a few hundred angstrom units and were visible as diffraction images from the branch points of a semi-organized network of dislocations. As the temperature increased, the concentration and relative size of the aggregates were reduced, due to the impurity entering into solution.

(b) Bulk Density Studies

As a cation vacancy can effectively reduce the density of the sodium chloride lattice the monitoring of the bulk density presents a quantitative method of observing changes in the cation vacancy concentration. Quin [20] has compared the density of slowly cooled and air quenched samples of manganese, calcium and cadmium doped sodium chloride. Only in crystals heavily doped with calcium was there evidence for the precipitation of the divalent cation chloride. Differences between measured density changes and calculated changes with increasing calcium content were interpreted in terms of lattice relaxations. $(Cl)^-$ ions also contributed to the observed density changes. As no density change was observed in the manganese doped crystals, precipitation would be expected to occur by the impurity ion taking its charge compensating vacancy from solid solution into the precipitate or aggregate phase.

(c) Electron Miscroscopy

The normal thin film techniques of electron miscroscopy are not applicable to sodium chloride. Although the material may be successfully thinned, the electron beam induces so much radiation damage that the information obtained is not representative of the bulk lattice.[54] To overcome this, a replica technique has been used by Khan[55] which involves cleaving a crystal under vacuum and then depositing a thin layer of carbon or gold upon the freshly cleaved surface. This film presents a replica of this surface and when removed it can be subjected to the normal methods of electron microscopy. Using this method, Khan has observed the shape and planes of occupation of the aggregates of divalent dopants Mg^{++}, Zn^{++}, Cd^{++}, Mn^{++}, Ca^{++} in sodium chloride. The aggregates in well aged crystals possessed well defined geometrical forms. If the crystal was slowly cooled, as opposed to air quenched, the aggregates were found to have varying dimensions.

(iii) Theoretical Considerations (Equations Used in Analysis of Data)

(1) The Association of Reaction

The simple theories of association between mobile, oppositely charged defects moving in a medium of uniform dielectric constant have been thoroughly covered in the theories developed for dilute ionic solutions. (58, 59, 60) Fortunately many of the equations describing the Coulombic interactions between the defects can be transferred, with a few modifications, from solutions to the solid state. The simplest empirical description of association reactions occurring in solid state sodium chloride is that due to Stasiw and Teltow, (40) which is an application of the Law of Mass Action to the following reaction:-

(Divalent cation^{++})$^{+}$ + cation vacancy^{-} $\rightleftharpoons$ Impurity vacancy complex

$(c - x_k)$ + x_1 $\rightleftharpoons$ x_k

$$x_k/(c-x_k)x_1 = Z_1 \exp + g_a/kT = K_2(T) \qquad \text{——— (1)}$$

where g_a is the free energy of association and Z_1 is the number of distinct orientations of this n.n. impurity vacancy dipole. This form of reaction produces an expression for the conductivity of

$$\sigma T = Ne\left(\frac{x_k}{Z_1}\right)^{\frac{1}{2}} \frac{4a^2\lambda^2\nu_1}{k} \cdot \exp\left(\Delta S_1 + S_a/2\right)/k \cdot \exp\left(\Delta h_1 + h_a/2\right)/kT \qquad \text{—— (2)}$$

which is derived by assuming that the anion vacancy concentration becomes negligible at temperatures below intrinsic conduction

$$x_1 \simeq (c - x_k) \qquad \text{——— (3)}$$

If x_k becomes independent of temperature the association reaction will be represented by a linear region of the Arrhenius plot whose

slope is given by

$$Q_{III} = \Delta h_1 + ha/2 \qquad \text{——— (4)}$$

This could happen if the degree of association were large and x_k became equal to c. The appropriate expression for the conductivity isotherms is

$$c/\sigma = A\sigma + B \qquad \text{——— (5)}$$

where

$$A = (x_o/\sigma_o), \qquad B = (x_o/\sigma_o)K_2(T) \qquad \text{——— (6)}$$

Coulombic interactions between the unassociated point defects will influence the degree of association and the cation vacancy mobility. Both these factors will influence the resulting conductivity, making it difficult to analyze the data for the separate effects. Fortunately, the Debye-Huckel [45] theory for non-ideal ionic solutions has been applied to the present case.

Lidiard [63] has considered the Coulombic interactions between the impurity ion and the cation vacancy as defining the free energy of association

$$g_a = \frac{\mu^2}{\sqrt{5}\epsilon a} = kT_o \qquad \text{——— (7)}$$

Using this energy, he has included Debye-Huckel corrections in a calculation of the degree of association as a function of concentration and temperature

$$\frac{p}{(1-p)^2} = 2_1 c \exp\left[\frac{T_o}{T} - \frac{2(2\pi\sqrt{2})^{1/2}(T_o/T)^{3/2}[(1-p)c]^{1/2}}{\{1+4(\pi\sqrt{2})^{1/2}[(1-p)c\,T_o/T]^{1/2}\}}\right] \qquad \text{——— (8)}$$

The principal effect of including these corrections is to increase

the decay of p with increasing temperature and concentration. The corresponding expression for σ is

$$\sigma = \left(\frac{\mu d}{2a^3}\right) c(1-p)\left[1 - \frac{2(2\pi\sqrt{2})^{1/2} c^{1/2}(1-p)^{1/2}(T_0/T)^{3/2}}{3(\sqrt{2}+1)(1+2H_a)(\sqrt{2}+2H_a)}\right] \qquad (9)$$

$$2H_a = 4(\pi\sqrt{2})^{1/2} c^{1/2}(1-p)^{1/2}(T_0/T)^{1/2}$$

This does not bear a simple parabolic relationship between c and σ which the Stasiw-Teltow model predicts, but shows that the reduced isotherms (c/σ vs. σ) should be curved, the curvature being more marked for small concentrations of impurity. This curvature is present in the data of Etzel and Maurer, [42, 46] who investigated Cd^{++}/NaCl, but is absent in Ni^{++} and Co^{++} dopants. [41]

(2) The Dielectric Absorption and Relaxation of the Impurity Vacancy Dipole

(a) The Reorientation of Impurity-Vacancy Dipoles by the Application of a Steady Electric Field

The relaxation of a n.n. impurity vacancy complex is considered; the nomenclature appropriate to this model is presented in Fig. (2.2). As the equations describing such a relaxation process have been considered in detail by Lidiard [23] only the more important features will be presented. Because there are four equivalent positions for the vacancy in the c plane occupying n.n. positions, the total number of dipoles n_d, is given by

$$n_d = 4(N_a + N_b + N_c)$$

The jump frequencies w_1, w_2 represent the appropriate jump probabilities in the absence of an electric field. Assuming that a

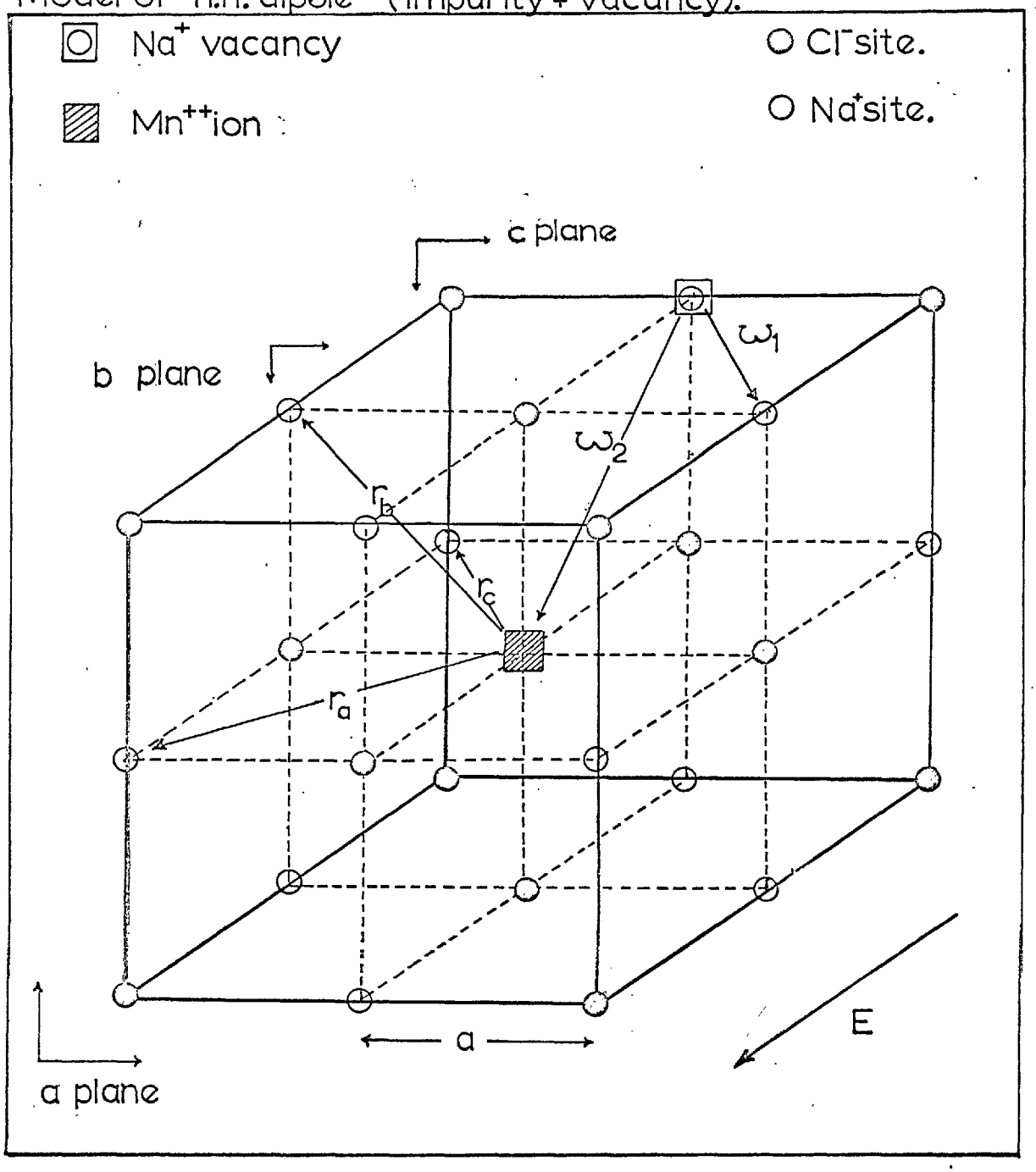
Model of n.n. dipole (Impurity + vacancy).
Na+ vacancy
Mn++ion
O Cl⁻site.
O Na⁺site.
c plane
b plane
a plane
ω1
ω2
rb
rc
ra
a
E

Fig. 2.2

direct interchange of the impurity and the vacancy, and vacancy jump are restricted to the n.n. positions, the rates of change of the vacancy population in the various positions are described by a series of rate equations, the solutions of which are:-

$$\left.\begin{aligned} N_a &= N - n\,(1 - \exp -\lambda t) \\ N_b &= N \\ N_c &= N + n\,(1 - \exp -\lambda t) \end{aligned}\right\} \qquad \text{——— (10)}$$

with $\lambda = 2(\omega_1 + \omega_2)$ ——— (11)

$$n = N a \mu E / kT \qquad \text{——— (12)}$$

$$n_d = 12N$$

at any instant

$$P(t) = \mu a\,(4N_a - 4N_c)$$

and

$$j(t) = \frac{4 n_d a^2 \mu^2 (\omega_1 + \omega_2)}{kT} \exp -2(\omega_1 + \omega_2)t \qquad \text{——— (13)}$$

The reorientation of the impurity-vacancy complex is observed as an exponentially decaying displacement current with a relaxation time given by

$$\tau^{-1} = 2(\omega_1 + \omega_2)$$

If n.n.n. dipoles are considered in addition to the n.n. configurations it can be shown that the current density is given by

$$j(t) = \lambda_1 P_1 \exp -\lambda_1 t + \lambda_2 P_2 \exp -\lambda_2 t \qquad \text{——— (14)}$$

where

$$P_1 = \frac{4 n_d a^2 \mu^2 E\,[2(\omega_0 + \omega_4) - \lambda_2 (1 + \omega_4/\omega_3)]}{3kT\,(2 + \omega_4/\omega_3)\,[(\omega_0 + \omega_4 - 2\omega_3)^2 + 4\omega_3\omega_4]^{1/2}}$$

and

$$P_2 = \frac{4 n_d a^2 \mu^2 E\,[\lambda_2 (1 + \omega_4/\omega_3) - 2(\omega_0 + \omega_4)]}{3kT\,(2 + \omega_4/\omega_3)\,[(\omega_0 + \omega_4 - 2\omega_3)^2 + 4\omega_3\omega_4]^{1/2}}$$

$$\lambda_{1,2} = (\omega_0 + \omega_4 + 2\omega_3) \pm [(\omega_0 + \omega_4 - 2\omega_3)^2 + 4\omega_3\omega_4]^{1/2}$$

$$\omega_0 = (\omega_1 + \omega_2)$$

with w_3 and w_4 representing the jump probabilities for a vacancy to move from a n.n.n. to a n.n. configuration and vice versa. Equation (14) suggests that if there is a considerable contribution from n.n.n. dipoles to the relaxation process, the displacement current observed should be a sum of two exponentials.

The number of dipoles orientated by the electric field, Δn, is the excess present in configuration c above that of the field free concentration. The number orientated after the initial application of the electric field is given by

$$\Delta n = \frac{n_d a u E}{3kT}\left(1 - \exp -t/\tau\right) \qquad \text{(15)}$$

Assuming that saturation of the system has occurred, $t \gg \tau$, the fraction of dipoles orientated is given by

$$\Delta n / n_d = \frac{a u E}{3kT} \approx 4.4 \times 10^{-3}$$

assuming

E = 10,000 volts/cm.

T = 243°K.

Less than 1% of the impurity vacancy dipoles are effectively orientated by the applied electric field. However, this small number is implicitly related to total dipole content, applied electric field strength and temperature, by the equations given.

(b) Resonance Absorption under Variable Frequency Electric Fields

When the impurity-vacancy dipole is subjected to a sinusoidally varying electric field of the form

$$E = E_0 \exp j\omega t$$

the resulting current density due to dipole reorientation is (23)

$$j(t) = \frac{2a^2u^2n_d}{3kT}\left[\frac{-j\omega}{1 - \frac{1}{2}j\omega(\omega_3 + \omega_4)}\right] \qquad \text{(16)}$$

the appropriate loss angle being

$$\tan\delta = \frac{8\pi a^2 u^2 n_d}{3\epsilon kT}\left[\frac{\omega\tau}{1+\omega^2\tau^2}\right] \qquad \text{——— (17)}$$

The peak height occurring when

$$\omega = \tau^{-1} = 2(\omega_1 + \omega_2) \quad , \quad \tan\delta_{MAX} = \frac{4\pi a^2 u^2 n_d}{3\epsilon kT}$$

Lidiard [23] has considered the effects of n.n.n. dipoles contributing to the absorption loss and has shown that their only effect is to produce a slight, but usually undetectable broadening of the Debye plot.

(3) Ionic Thermocurrent Phenomena (I.T.C.)

The ionic thermocurrent technique is based upon the alignment of impurity-vacancy dipoles, by using an electric field applied along a [100] direction. This alignment process is performed at a temperature where the relaxation time for reorientation of the dipole is of the order of seconds or more. In the system, studied, Mn^{++}/NaCl, the dipoles were aligned at -30.0°C and then frozen into the crystal with a non-random distribution of orientations by rapidly cooling to liquid nitrogen temperatures. After removal of the electric field, the crystal was warmed, using a linear heating rate (2.041°C/min.). As the energy for the reorientation of the dipoles from the non-random positions became available from the crystal lattice, the dipoles flipped and produced a displacement current which was measured. The collective effect of the dipoles reorientation was to produce a peak in the plot of crystal current versus temperature. By polarizing the crystals at elevated temperatures and then slowly cooling them, all the relaxation processes

present in the crystal were quenched in. Then, by careful choice of subsequent polarizing temperatures, individual relaxation processes were resolved and studied in detail. This technique has been used to study the space charge polarizations present in strontium doped potassium chloride, [56] and dipole relaxations in the systems $Sr^{++}/NaCl$, Sr^{++}/KCl.

Again the model used in this analysis is that of a simple n.n. impurity-vacancy dipole, there being little evidence for impurity-vacancy dipoles existing in the n.n.n. configuration over the temperature range investigated ($-50^{\circ}C$ to $-10^{\circ}C$), with the heat treatment used. The ionic thermocurrent produced during the heating of the crystal is subject to the following conditions

$$j(T) = \frac{dP(T)}{dt} = -\frac{P(T)}{\tau(T)} \qquad \text{(18)}$$

It is also assumed that the electric moment produced by the dipole relaxation at any temperature obeys an equation of the form

$$P(T) = P_0(T)[1 - \exp(-t/\tau)] \qquad \text{(19)}$$

with

$$\tau = \tau_0 \exp \Delta h_0/kT \quad , \quad \Delta g_0 = \Delta h_0 - T\Delta s_0 \qquad \text{(20,21)}$$

If the crystal is subjected to a linear heating rate after the reorientated dipoles have been quenched in,

$$T = bt \quad , \quad b = \frac{dT}{dt} \qquad \text{(22,23)}$$

then it may be shown that the displacement current peak produced by the relaxation is given by

$$j(T) = \frac{a^2u^2n_d E}{3kT_p}\left[\tau_0 \exp \Delta h_0/kT\right]^{-1} \exp -\int_0^{T/b} (\tau_0 \exp \Delta h_0/kT)^{-1} dT \qquad \text{(24)}$$

This describes the shape and magnitude of the I.T.C. peaks. The principal features of interest are

(i) Peak Maxima

The peak maximum is defined by

$$\frac{\Delta h_o \cdot b \cdot \tau(T_m)}{k T_m^2} = 1 \qquad \text{——— (25)}$$

Hence T_m is independent of the applied electric field and the temperature of polarization.

(ii) Peak Height as a Function of Dipole Concentration

When $T = T_m$

$$j(T_m) = K(n_d) \cdot K'(T_m) \cdot \exp I(T_m) \qquad \text{——— (26)}$$

where $K'(T_m)$ represents a constant and $I(T_m)$ an integral, both of which are solely dependent upon T_m for any given impurity-vacancy dipole studied and $K(n_d)$ represents a constant which depends solely upon the dipole concentration n_d. Hence if T_p and E are fixed and because T_m is independent of n_d, T_p and E, the maximum current density is proportional to the dipole concentration. From equation (4)

$$\frac{a^2 e^2 n_d}{3kT_p} = \int_o^\infty j(T).dT$$

an absolute value for the dipole concentration may be obtained from the area enclosed by the I.T.C. peak.

(iii) Estimation of Δh_o

From equation (18),

$$\tau(T) = - \frac{\int_o^T j(T).dT}{j(T)} \qquad \text{——— (27)}$$

By plotting Log e $\left\{\int_o^T j(T)dT / j(T)\right\}$ versus $1000/T$ estimates of Δh_o and Δs_o may be obtained. Alternatively, when $T \to o$ the low temperature tail of the peak approximates to

$$j(T) \approx \frac{a^2 l^2 n_d E}{3kT_p} \left[\tau_o \exp \Delta h_o / kT\right]^{-1} \qquad \text{——— (28)}$$

and the tail of the I.T.C. peak, when plotted logarithmically, will yield an estimate of Δh_o.

It has been assumed, in the previous discussion, that the

effective field determining the relaxation phenomena is the same as the microscopic applied field E, and that no internal field corrections are present. There are, however, two significant internal field effects that should be included. These are the interactions between individual impurity-vacancy dipoles and also the interactions between the effective charges on each vacancy and the polarized ions in its vicinity. Boswarva and Franklin (68) have considered these effects. They have approached these problems by treating the interactions amongst the dipoles with a method using the Onsager approximation. In a crystal dielectric of the configuration studied, the local field is given by the well known Lorentz relationship

$$E_L = E + 4\pi P/3$$

Allowing for the aforementioned interactions, Boswarva et al. found that the deviations from the simple theory, which assumes $F = F_1$, were only appreciable for anion-cation vacancy pairs. For impurity-vacancy complexes in a n.n. configuration the differences between the more refined and simple theory were indistinguishable. It would appear that for impurity-vacancy dipoles, the polarization term in the Lorentz expression for the local field is compensated for by these interactions.

(iv) Presentation of Results

(1) Conductivity Data

The regions of the Arrhenius plot attributed to the precipitation and association reactions are presented in Fig. (2.3). These regions are clearly defined for the heavily doped specimens, but the conductivity plot for the lightly doped specimens presents a continuous curve rather than a series of segmented linear regions. Evidence for association appears from the positive curvature of the isotherms in this region Fig. (2.4). These plots also show a displaced origin of 50 m.p.p.m. Mn^{++}, similar to the extrinsic isotherms, which suggests that the "effective" manganese content is still being reduced by a fixed level of anion impurity c_o. With this in mind, the effective impurity content of $(c-c_o)$m.p.p.m. Mn^{++} will be used in the subsequent analysis.

By using the values of the cation vacancy mobility, obtained in Part I, the degree of association of the impurity ions with the cation vacancies was calculated as a function of temperature. Fig. (2.5). This analysis is performed for the heaviest doped crystal and shows the degree of association to be large at low temperatures, with considerable thermal disassociation occurring at the higher temperatures. Fig. (2.5) only presents data above the precipitation regions. The degree of association for this crystal does not seem to be characterized by a constant Gibbs free energy of association. This energy is calculated from the data in Fig. (2.5), assuming a simple Law of Mass Action relationship, and produces a temperature dependence presented in Fig. (2.6). The sharp

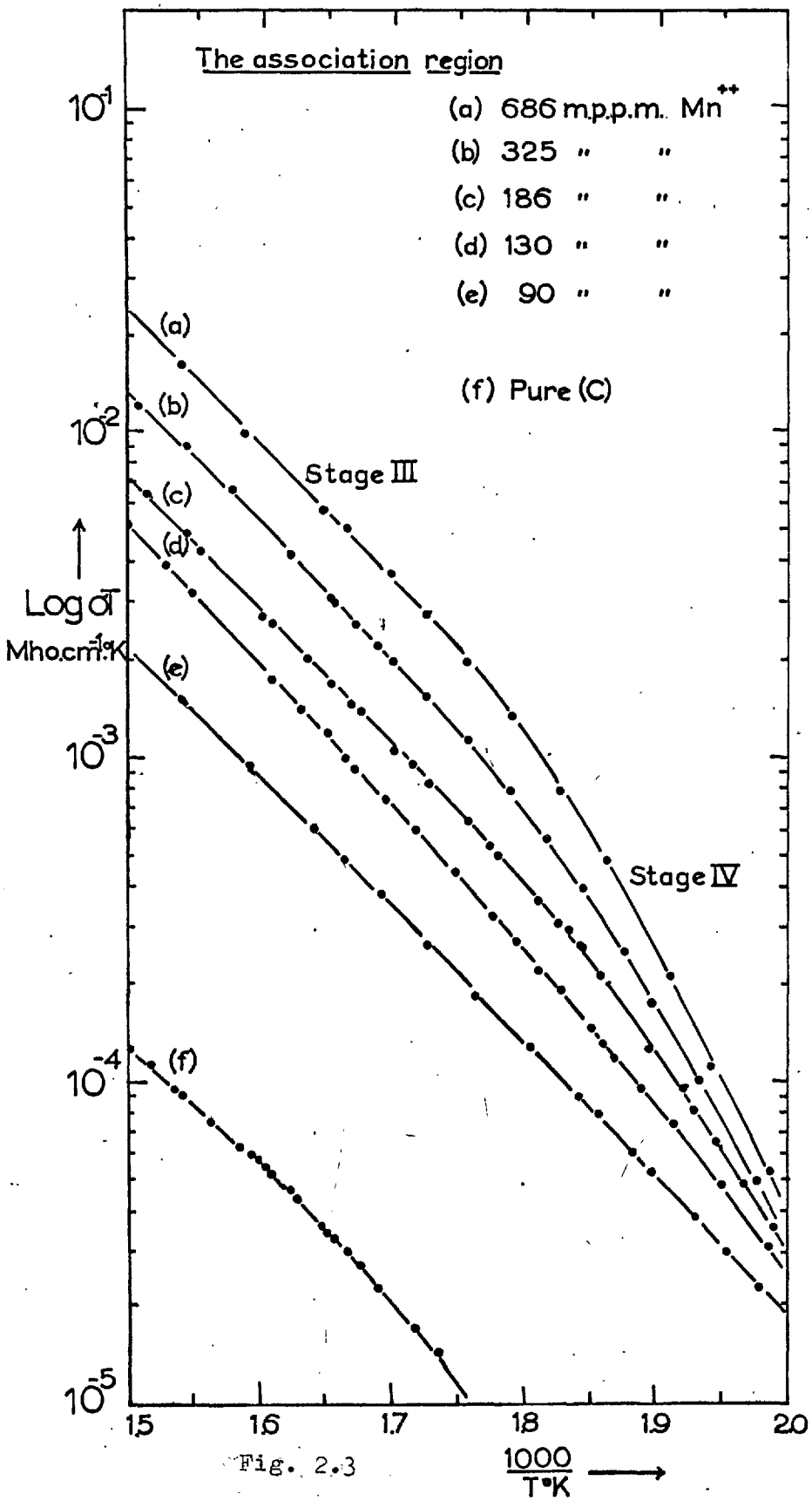
The association region
(a) 686 m.p.p.m. Mn++
(b) 325 " "
(c) 186 " "
(d) 130 " "
(e) 90 " "
(f) Pure (C)
Stage III
Stage IV
Log σT
Mho.cm⁻¹.°K
10⁻¹
10⁻²
10⁻³
10⁻⁴
10⁻⁵
1.5
1.6
1.7
1.8
1.9
2.0
1000/T°K

Fig. 2.3

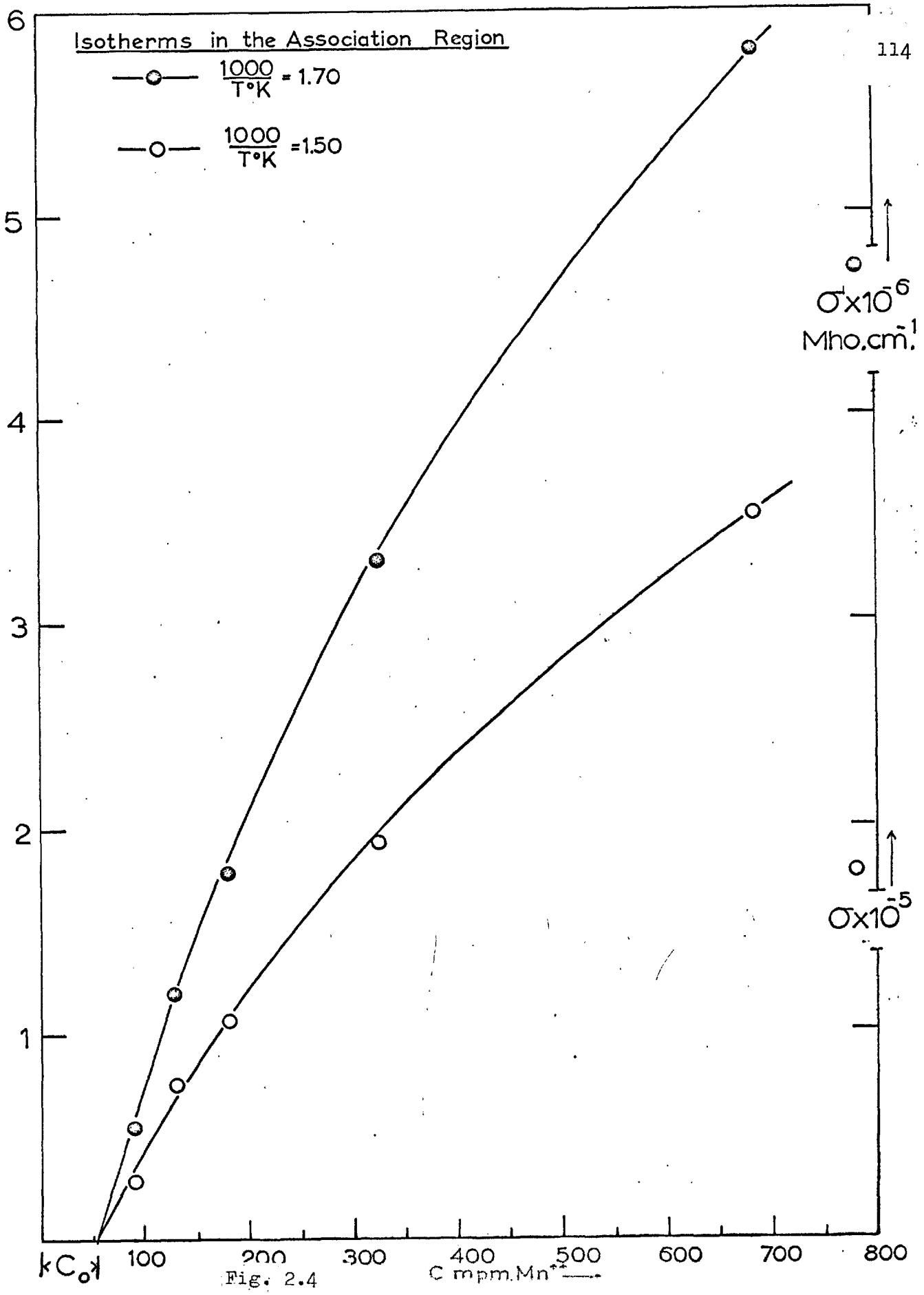
Isotherms in the Association Region
1000/T°K = 1.70
1000/T°K = 1.50
σ x10⁻⁶ Mho.cm⁻¹
σ x10⁻⁵
6
5
4
3
2
1
100
200
300
400
500
600
700
800
kC₀
C mpm.Mn⁺⁺

Fig. 2.4

The degree of association as a function of temperature for crystal of 686 m.p.p.m. Mn^{++}

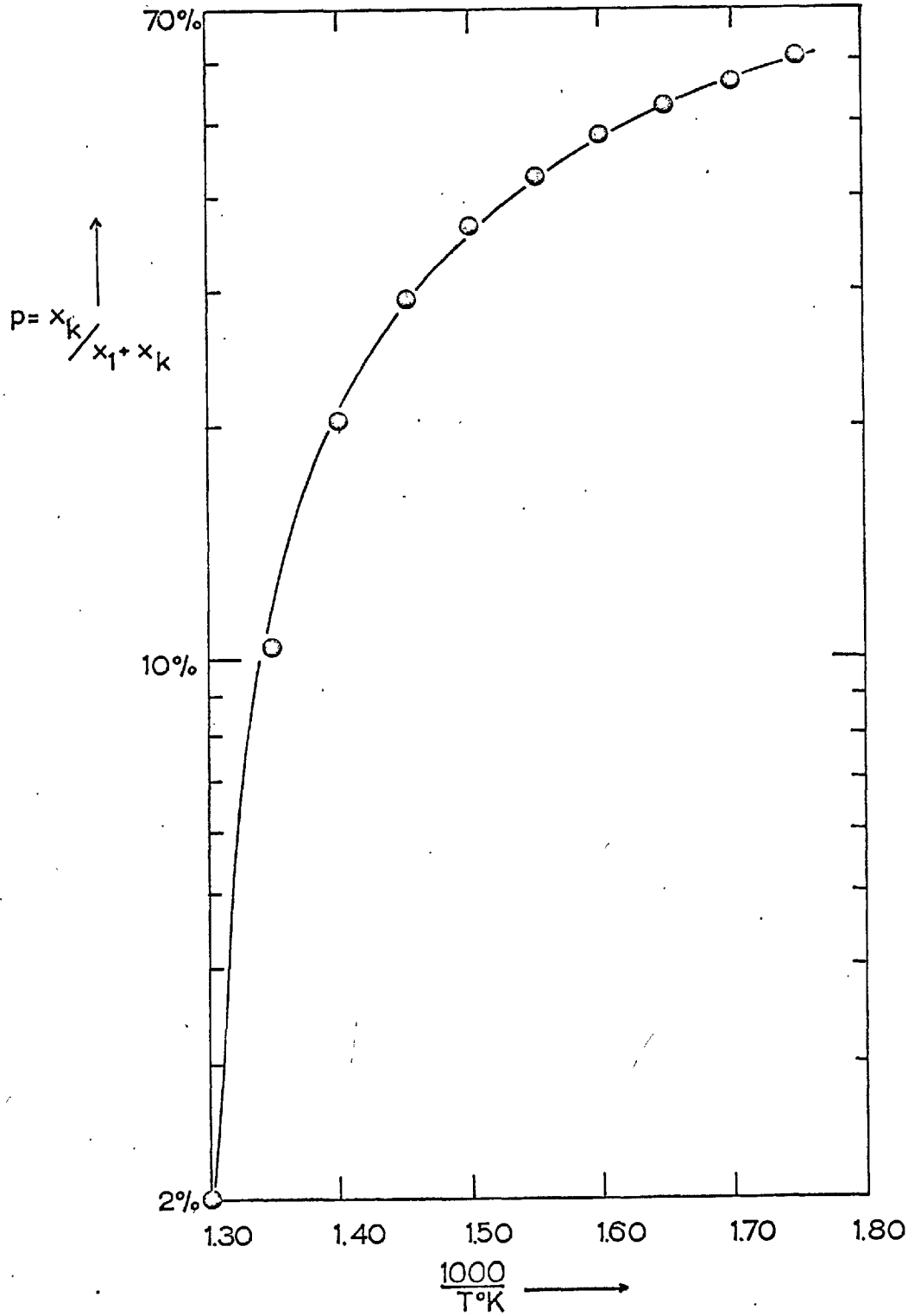

Fig. 2.5

drop in the value of g_a could be attributed to the commencement of thermal disassociation, where the description of the association reaction by a simple Law of Mass Action breaks down, due to the presence of higher order complexes. Allnatt [69] observed a much larger variation in the value of g_a for the association between strontium ions and cation vacancies in potassium chloride. The large variation observed at lower temperatures was probably due to the precipitation or aggregation of the divalent impurity. Repeating the analysis for crystals of different doping levels at fixed temperatures, the degree of association may be observed as a function of concentration Fig. (2.6). This analysis was performed for region A of Fig. (2.6), which shows a fairly constant free energy of association. It is difficult to make a comparison with the theoretical predictions of Allnatt et al., [44] as they were only able to calculate the degree of association up to concentrations of approximately 100 m.p.p.m. of Mn. This is below the levels that are considered in the present work.

From the data obtained so far, it would appear unwise to analyze the results obtained in excess of 680°C in terms of the simple Stasiw-Teltow model of ionic association. Confining this method of analysis at present to the regions of $1000/T = 1.50$ to 1.70 ($T = 588°C$ to $667°C$), the simple Stasiw-Teltow model for association predicts parabolic isotherms and linear "reduced" isotherms, equations (5) and (6).

By using a least squares method to fit the data to equation (5), the parameters A and B may be determined. Alternatively, a plot of $(c - c_o)/\sigma$ versus σ should yield a straight line of slope and intercept equal to A and B. The former method of analysis weights

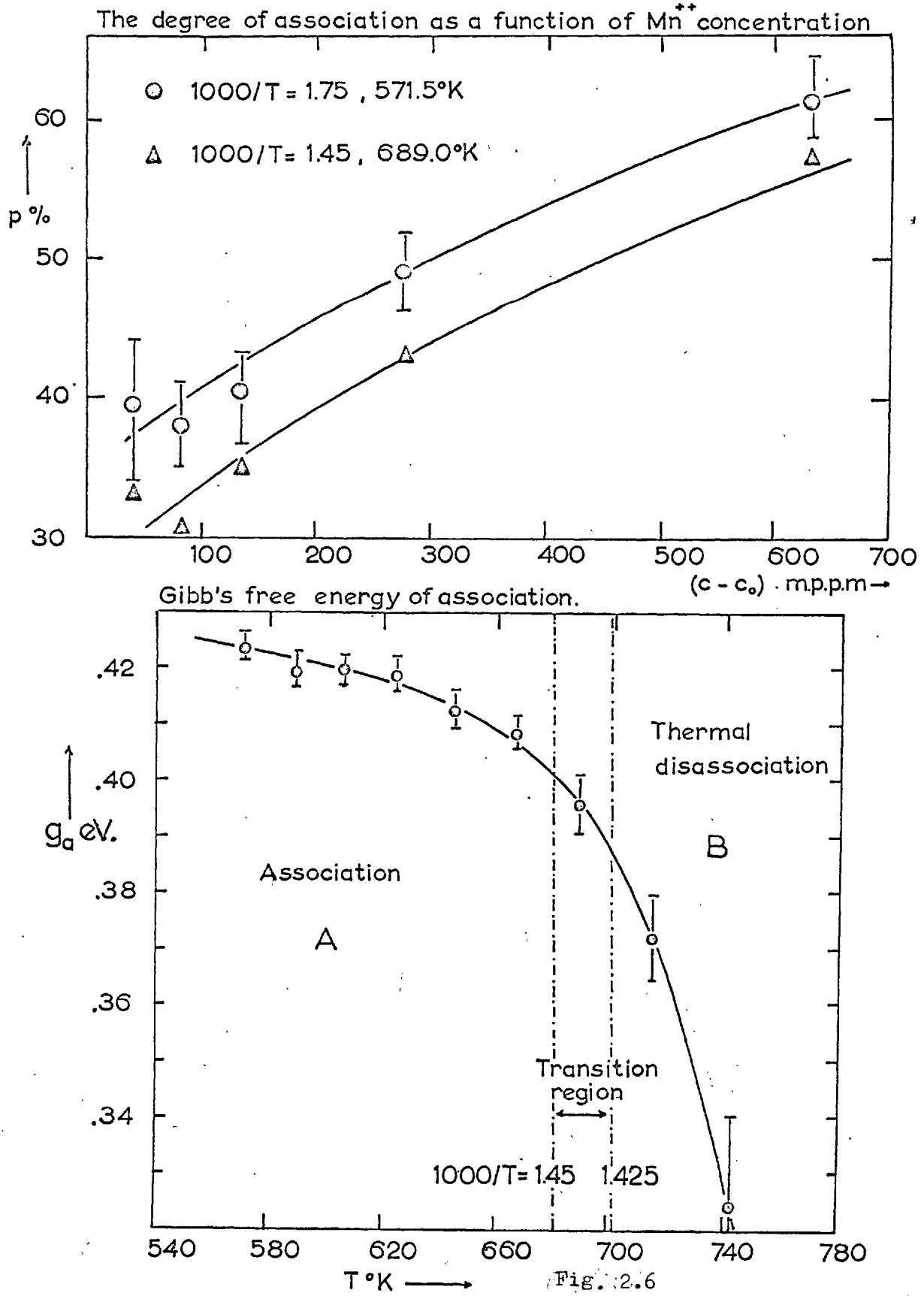
The degree of association as a function of Mn++ concentration
1000/T = 1.75 , 571.5°K
1000/T= 1.45 , 689.0°K
p %
60
50
40
30
100
200
300
400
500
600
700
(c - c₀) · m.p.p.m
Gibb's free energy of association.
.42
.40
.38
.36
.34
g_a eV.
Association
A
Thermal
disassociation
B
Transition
region
1000/T= 1.45
1.425
540
580
620
660
700
740
780
T °K

Fig. 2.6

the data points from the crystals containing larger impurity concentrations, whilst the latter analysis takes more account of the data points obtained from the smaller doping levels. Plots of $(c - c_o)/$ versus are presented in Figs. (2.7) - (2.9) for temperatures in the association and extrinsic regions of ionic conduction. Over the temperature range 1000/T = 1.50 to 1.70, the reduced isotherms present a series of straight lines of differing slopes and intercepts, Fig. (2.7), as predicted by the simple Stasiw-Teltow model of association. The cation vacancy's mobility ($\mu_i T$) was determined from the slopes and intercepts and is presented as a function of temperature in Fig. (1.18). There is good agreement with the extrinsic data, an enthalpy of motion of 0.67 $\pm$ 0.01eV. being obtained. The equilibrium constant's ($K_2(T)$) temperature dependence Fig. (2.10) yields an enthalpy and entropy of association of 0.40 $\pm$ 0.10eV. and 1.40 $\pm$ 0.30x10^{-4}eV/^{o}K respectively. The corresponding Gibbs free energy of 0.30 $\pm$ 0.10eV. at a temperature of 660^{o}C is in fair agreement with the values presented in region A of Fig. (2.6). The enthalpy obtained agrees, within the limits of experimental error, with the value determined from the slope of the linear region of Stage III, the association region.

$$Q_{III} = \Delta h_1 + h_a/2 = 0.83 \pm 0.01\text{eV}.$$

$$\Delta h_1 = 0.68 \pm 0.01\text{eV}.$$

$$h_a = 0.30 \pm 0.02\text{eV}.$$

Values of $K_2(T)$ were also derived by fitting the data to the parabolic relation defined by equation (5). This was performed for two temperatures and the values obtained are compared below, with the other method of analysis. There is a slight disagreement

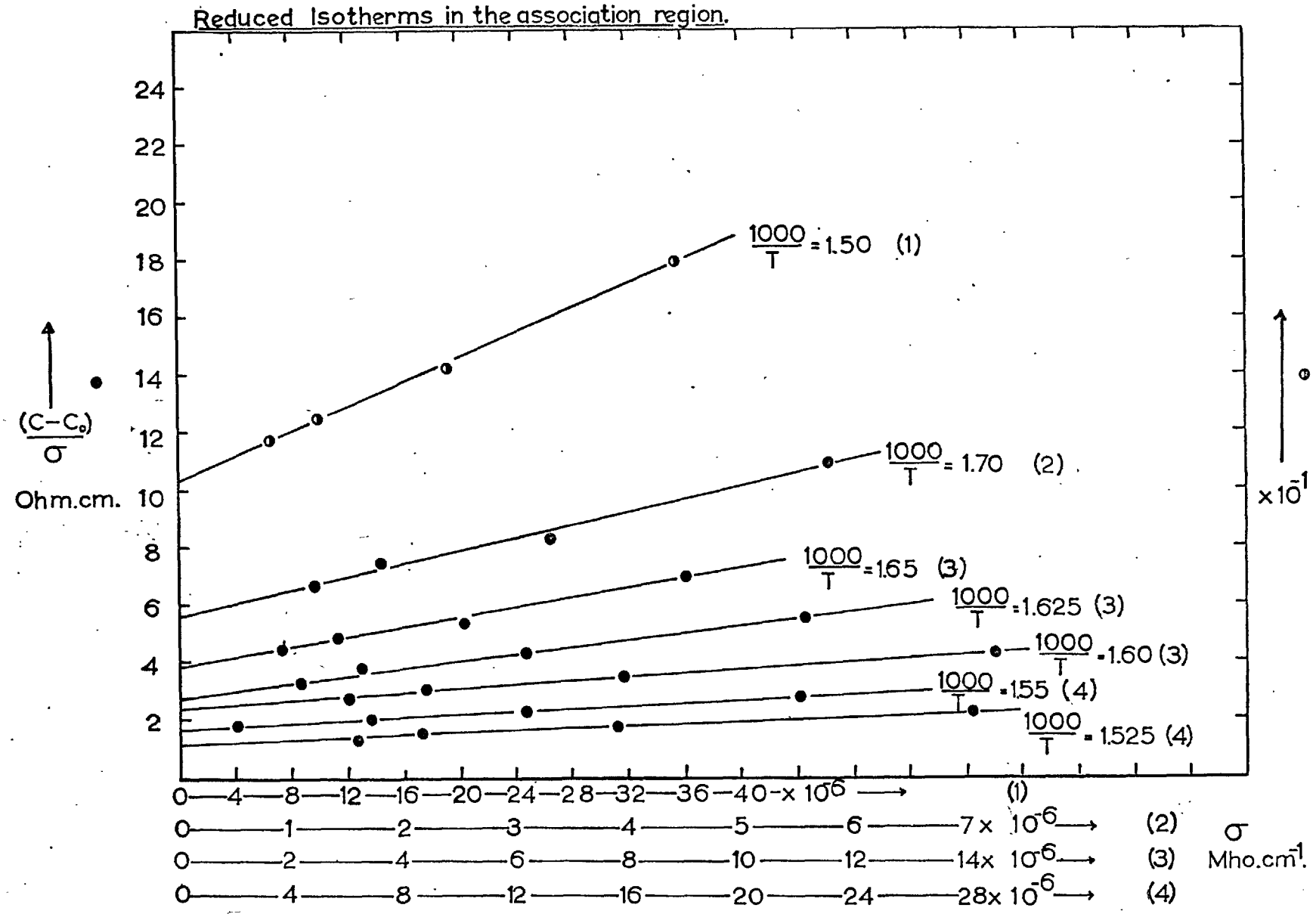
Reduced Isotherms in the association region.
(C−C₀)/σ
Ohm.cm.
24
22
20
18
16
14
12
10
8
6
4
2
1000/T = 1.50 (1)
1000/T = 1.70 (2)
1000/T = 1.65 (3)
1000/T = 1.625 (3)
1000/T = 1.60 (3)
1000/T = 1.55 (4)
1000/T = 1.525 (4)
x 10⁻¹
0—4—8—12—16—20—24—28—32—36—40—x 10⁻⁶ → (1)
0—1—2—3—4—5—6—7 x 10⁻⁶ → (2)
0—2—4—6—8—10—12—14x 10⁻⁶ → (3)
0—4—8—12—16—20—24—28x 10⁻⁶ → (4)
σ
Mho.cm⁻¹.

Fig. 2.7

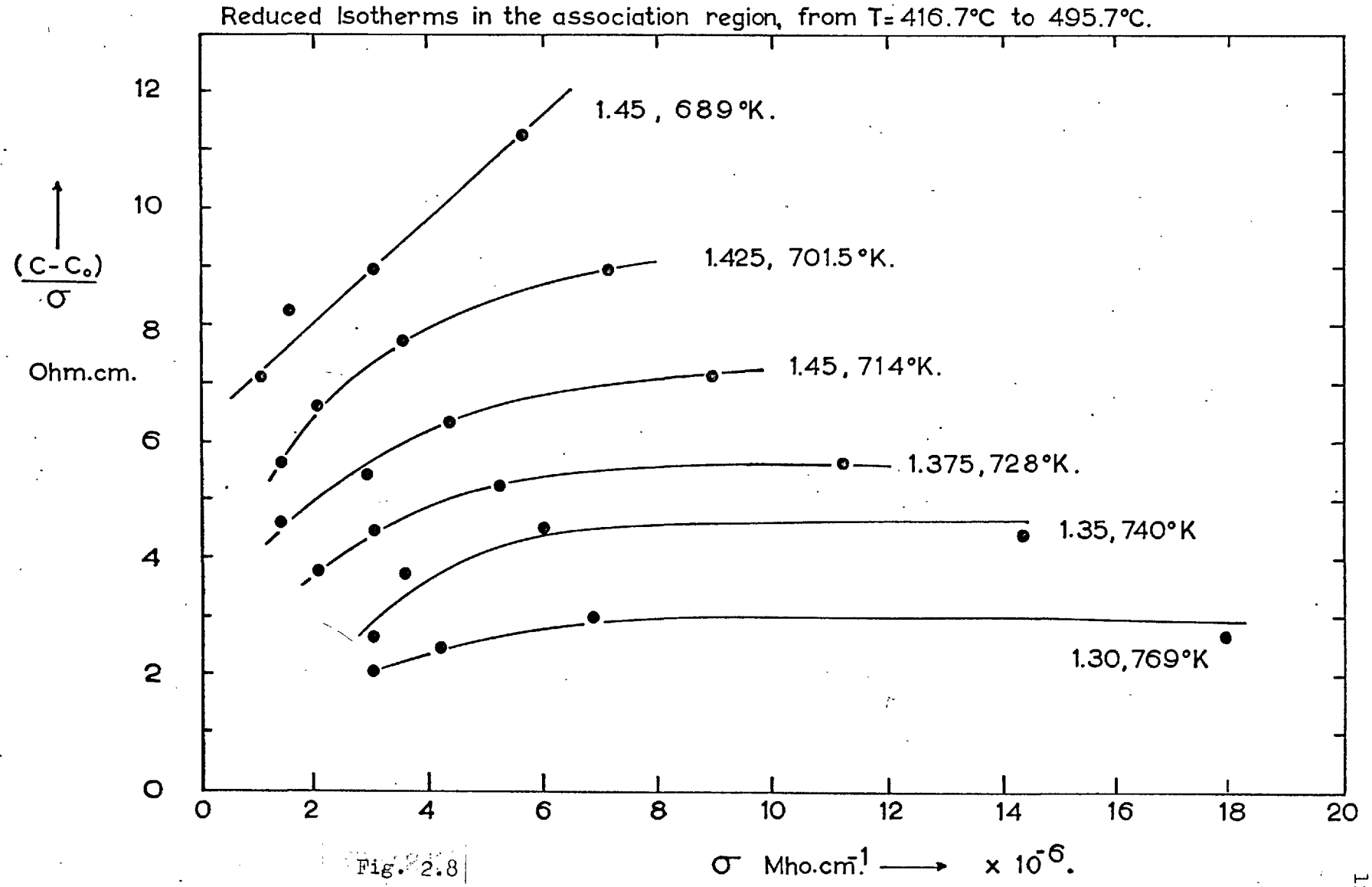
Reduced Isotherms in the association region, from T= 416.7°C to 495.7°C.
(C-C₀)/σ
Ohm.cm.
1.45 , 689°K.
1.425, 701.5°K.
1.45, 714°K.
1.375, 728°K.
1.35, 740°K
1.30, 769°K
σ Mho.cm⁻¹ → x 10⁻⁶.
0
2
4
6
8
10
12
14
16
18
20

Fig. 2.8

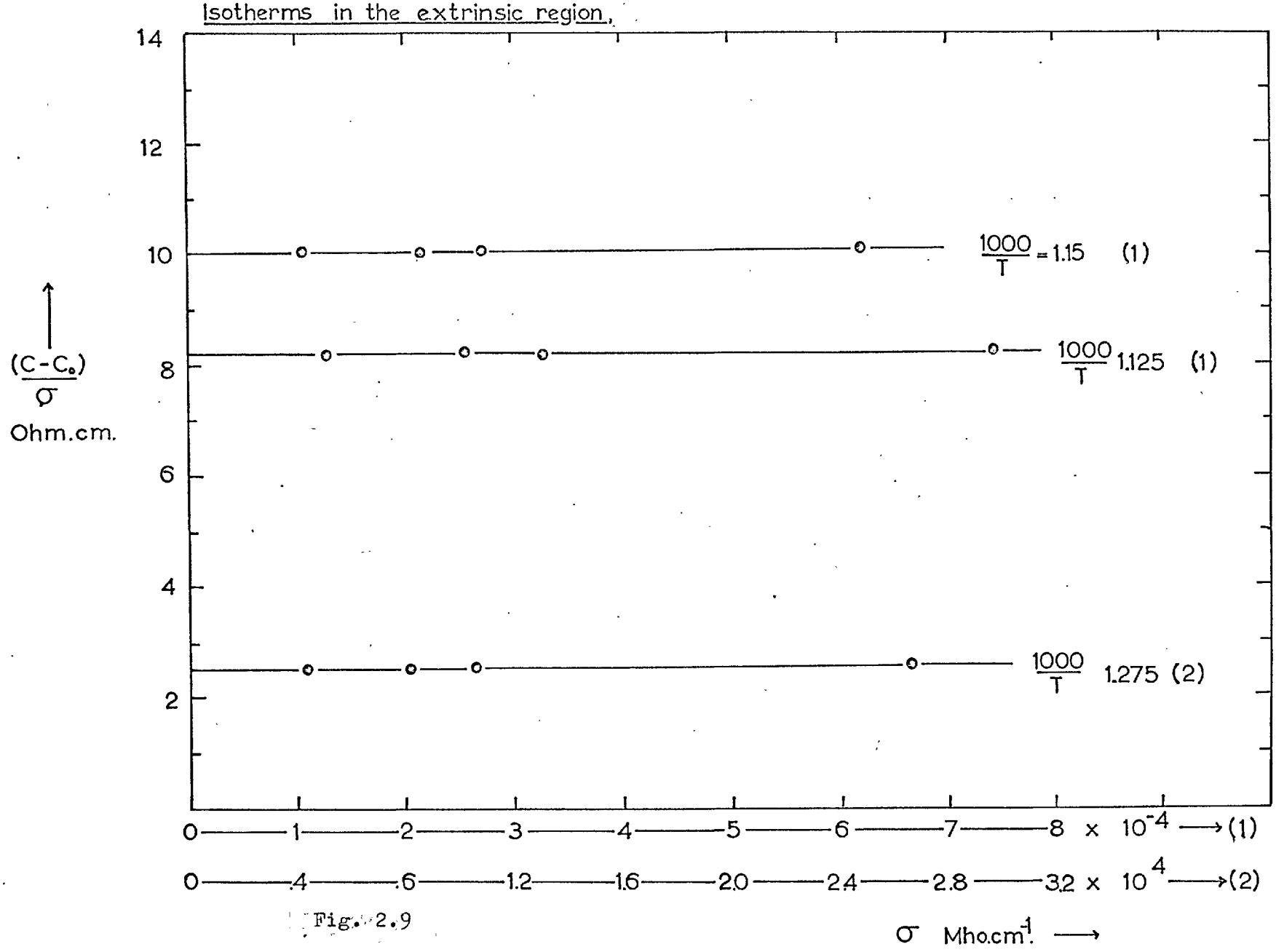
Isotherms in the extrinsic region,
14
12
10
8
6
4
2
(C-C₀)/σ
Ohm.cm.
1000/T = 1.15 (1)
1000/T 1.125 (1)
1000/T 1.275 (2)
0 1 2 3 4 5 6 7 8 x 10⁻⁴ → (1)
0 .4 .6 1.2 1.6 2.0 2.4 2.8 3.2 x 10⁴ → (2)
σ Mho.cm⁻¹. →

Fig. 2.9

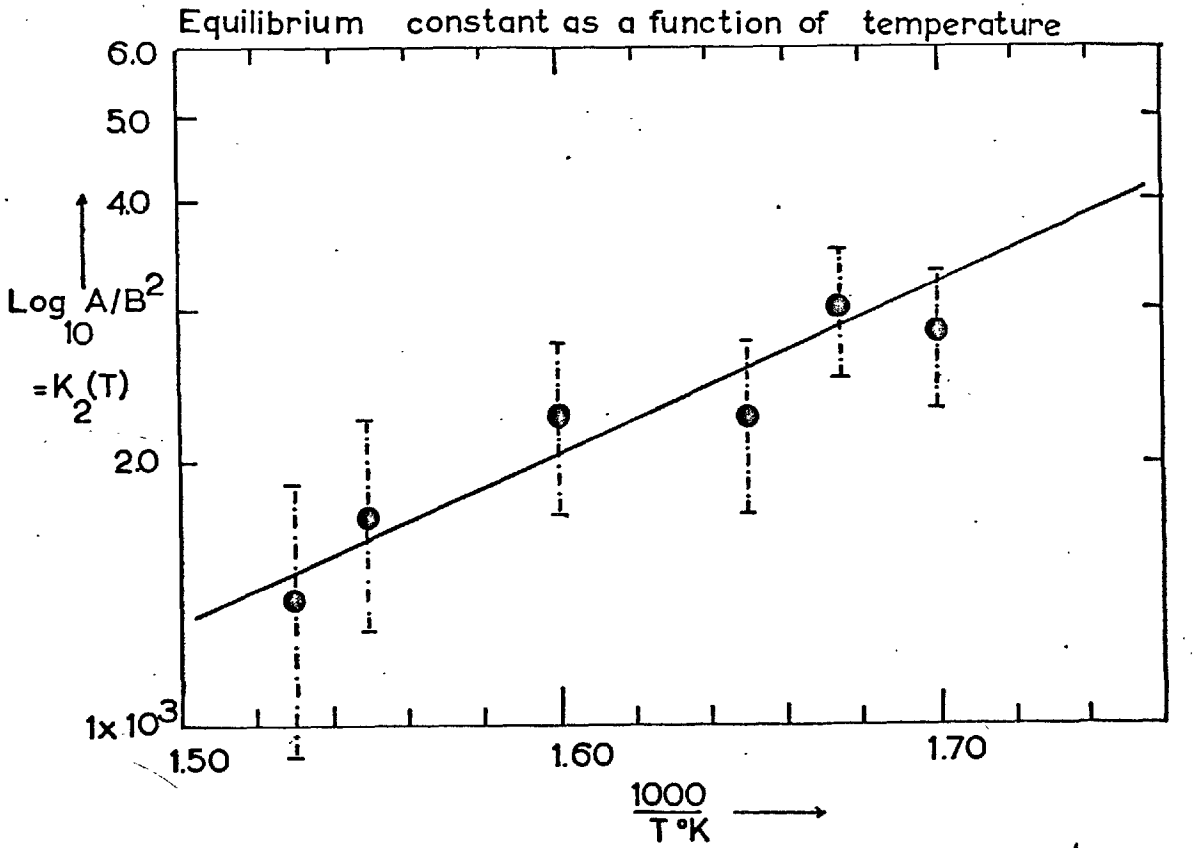
Equilibrium constant as a function of temperature
6.0
5.0
4.0
2.0
1x10^3
Log10 A/B2
=K2(T)
1.50
1.60
1.70
1000/T °K
K2(T) = 12 exp[(0.40±0.1) eV. − T(1.40±0.3) x10^-4 eV./°K]

Fig. 2.10

between the two methods of analysis, presumably due to a systematic error in the data.

1000/T	PARABOLIC FITTING $K_2(T)$	LINEAR ISOTHERMS $K_2(T)$
1.5	——— 1.165×10^3	——— 1.445×10^3
1.70	——— 2.892×10^3	——— 2.92×10^3

As the temperature increased, the form of the reduced isotherms changed markedly. Within the temperature range of 1000/T = 1.30 to 1.45 (T = 690°K to 769°K), a curvature appears which is caused by Coulombic interactions between the unassociated defects and the subsequent existence of higher order impurity-vacancy complexes.

The onset of this curvature, 1000/T = 1.425 to 1.45 correlates with the sharp decrease in g_a that occurred in Fig. (2.6) and it would be pointless to analyze this higher temperature data in terms of the simple association theory used previously. It may be concluded that the thermal disassociation proceeds via the break-up of the nearest neighbour impurity-vacancy dipole into higher order complexes, rather than the complete break-up of the simple complex into an isolated vacancy and impurity ion. It is very easy to attribute a curvature of the "reduced" isotherm to what is in effect a poor determination of impurity content. With this in mind, the data points for the lowest impurity concentrations have been omitted from all the reduced isotherms, as they have the largest error. The "reduced" isotherms over the temperature range 1000/T = 1.275 to 1000/T = 1.15 (T = 785°K to 870°K) present a series of lines which

are parallel to the σ^- axis, showing that association is absent in the extrinsic regions of ionic conduction.

If it is assumed that regions IV of the Arrhenius plots are due to resolution of the aggregated or precipitated phases of manganese in sodium chloride, a temperature may be obtained from the extrapolation of regions III and IV, which represents the lowest temperature at which all the impurity of that particular concentration is in solution. By observing the variation of this temperature with different concentrations of impurity, the temperature limits for the onset and finish of resolution may be observed. From this, a crude form of solvus curve may be drawn. Fig. (2.11). This reproduces a portion of the phase diagram for the system $Mn^{++}/NaCl$ and is in qualitative agreement with the curve derived by Schneider.[19] This solvus curve represents the free vacancy solubility, the true solubility being somewhat higher, as a fraction of the impurity not in an aggregated state will be in an associated form with cation vacancies. Haven[70] has determined the free vacancy solubility for the same system and has shown that the solubility of divalent manganese is represented by an equation of the form

$$c = 2 \exp - 0.44eV/kT$$

with

$$h_s = 0.88eV.$$

This expression represented the solubility over ranges of concentration and temperature of 10 to 10,000 m.p.p.m. of Mn^{++} and 100°C to 600°C. In the present work, the enthalpy of solution had a value of $0.88 \pm 0.10eV$, which is in fair agreement with a value of $0.77 \pm 0.10eV$. derived by Kahn[71] from the observation

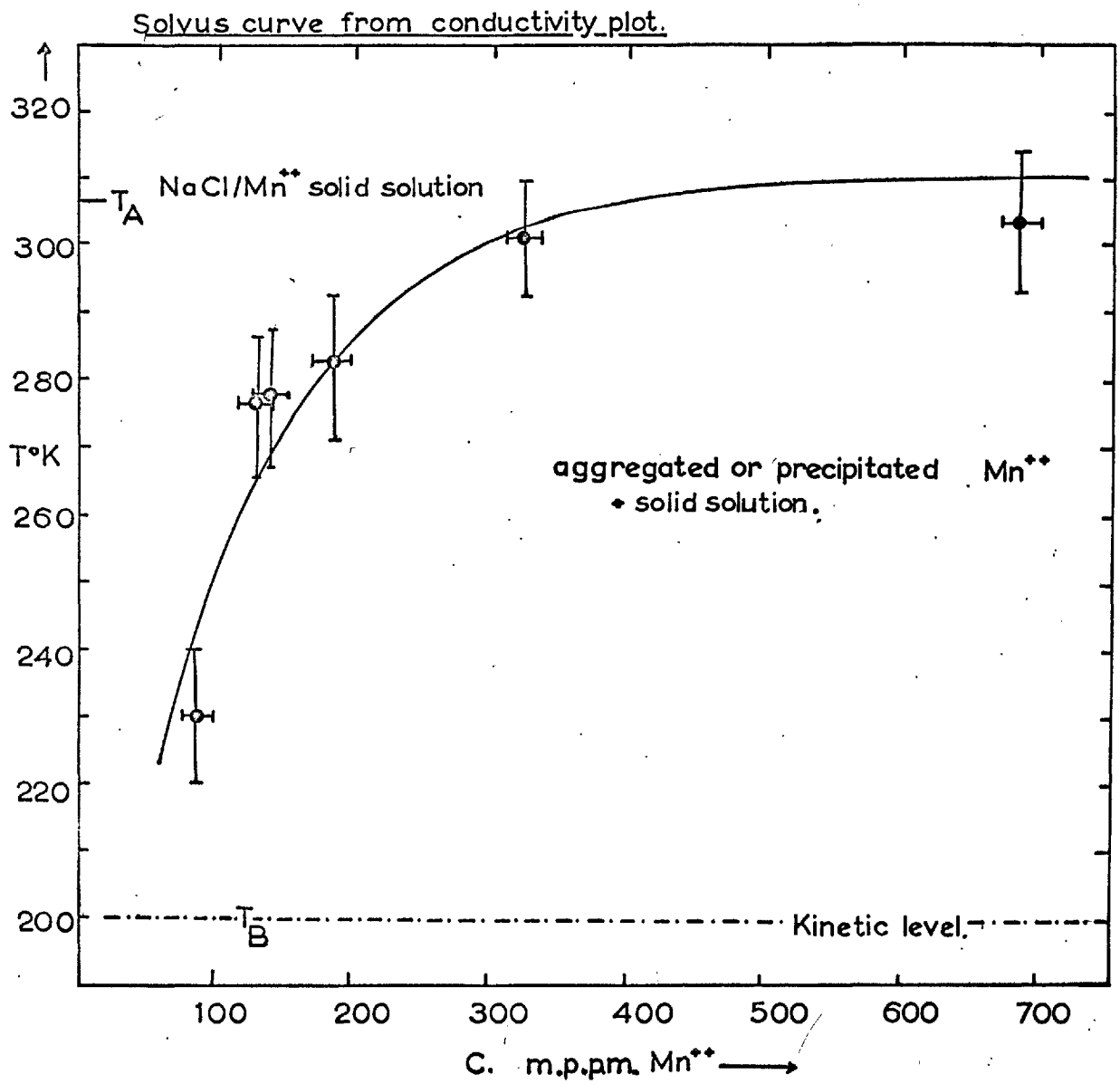
Solvus curve from conductivity plot.
320
300
280
T°K
260
240
220
200
T_A
T_B
NaCl/Mn^{++} solid solution
aggregated or precipitated Mn^{++}
solid solution.
Kinetic level.
100
200
300
400
500
600
700
C. m.p.pm. Mn^{++} ⟶

Fig. 2.11

of the size of manganese precipitates as a function of temperature. With the present studies there was also a low temperature "kinetic level" which corresponded to a sharp increase in the slope of the A rrhenius plot at the onset of Stage IV. This kinetic level corresponded to a temperature region around $200 \pm 10^{\circ}C$ and was characterized by the Stage IV and Stage III_1 conductivity plots diverging from and converging to a region near this temperature. Fig. (2.12).

The kinetic level presumably represents a temperature above which the process of resolution is possible. It is interesting to compare the solvus curve in Fig. (2.11) with the effect of quenching temperature upon the 0.1% proof stress in manganese doped crystals. Fig. (2.14). The sharp rise in proof stress which occurs between the temperature limits T_A and T_B, for the particular doping level, corresponds well to the equivalent points in Fig. (2.11), confirming that resolution is occurring between these temperatures. The slopes Q_{IV} of the precipitation region were observed to increase with larger concentrations of divalent impurity, Table (2.2), indicating that the enthalpy of solution is possibly concentration dependent, if the following relation is true.

$$Q_{IV} = \Delta h_1 + h_{s/2}$$

The rate of resolution should depend on the form taken by the impurity once it enters solution (e.g. dipoles, trimers, pentamers) and could thus be concentration dependent. This would explain the dependence of Q_{IV} upon concentration. Haven's derivation of free vacancy solubility incorrectly assumes that the precipitated phase of manganese is $MnCl_2$. Over the range of concentrations studied, $MnCl_2.6NaCl$ and $MnCl_2.2NaCl$. would represent the precipitate phases.

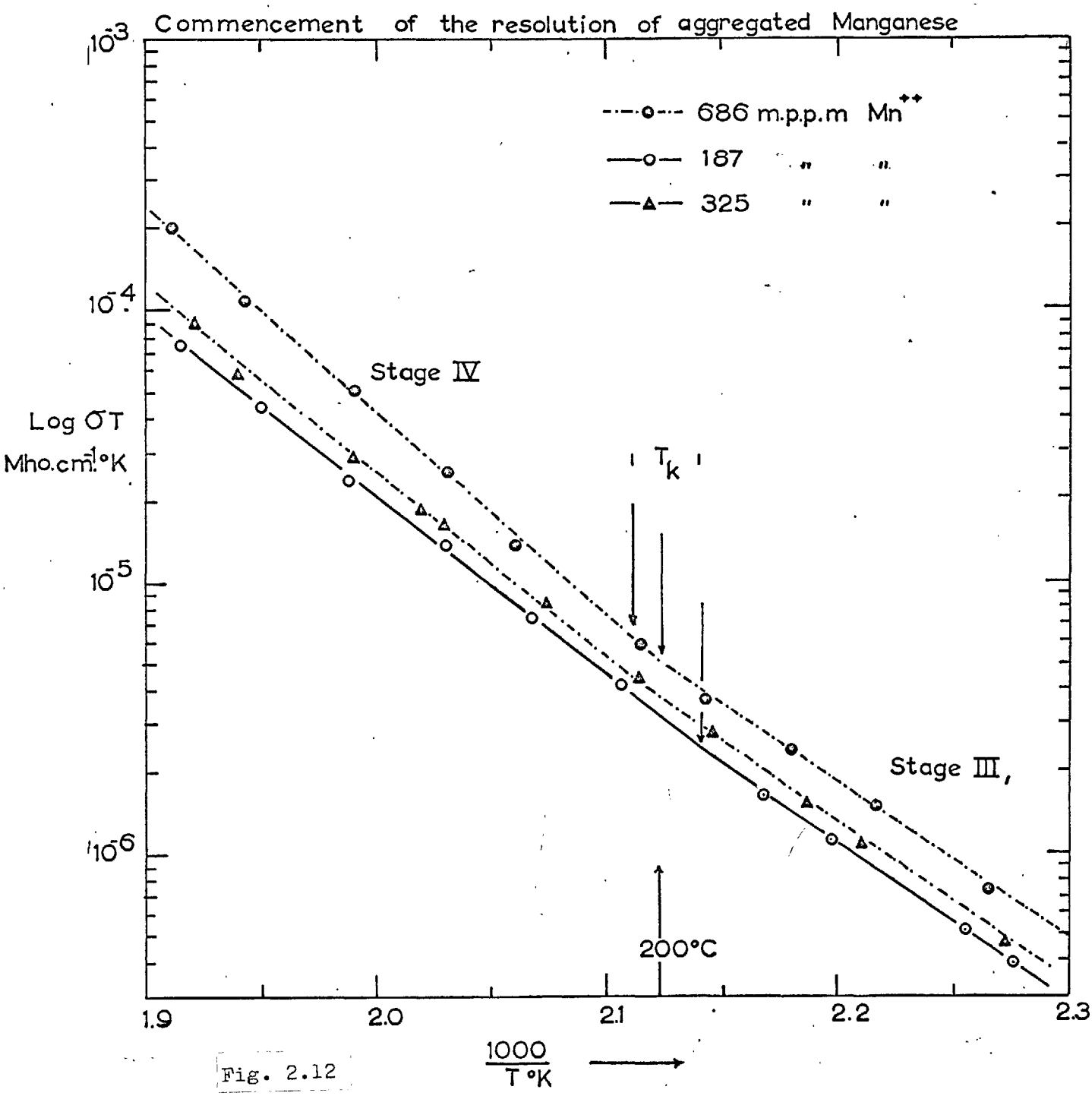
Commencement of the resolution of aggregated Manganese
686 m.p.p.m Mn++
187 " "
325 " "
Stage IV
Stage III
Tk
200°C
Log σT
Mho.cm-1°K
10-3
10-4
10-5
10-6
1.9
2.0
2.1
2.2
2.3
1000/T °K

Fig. 2.12

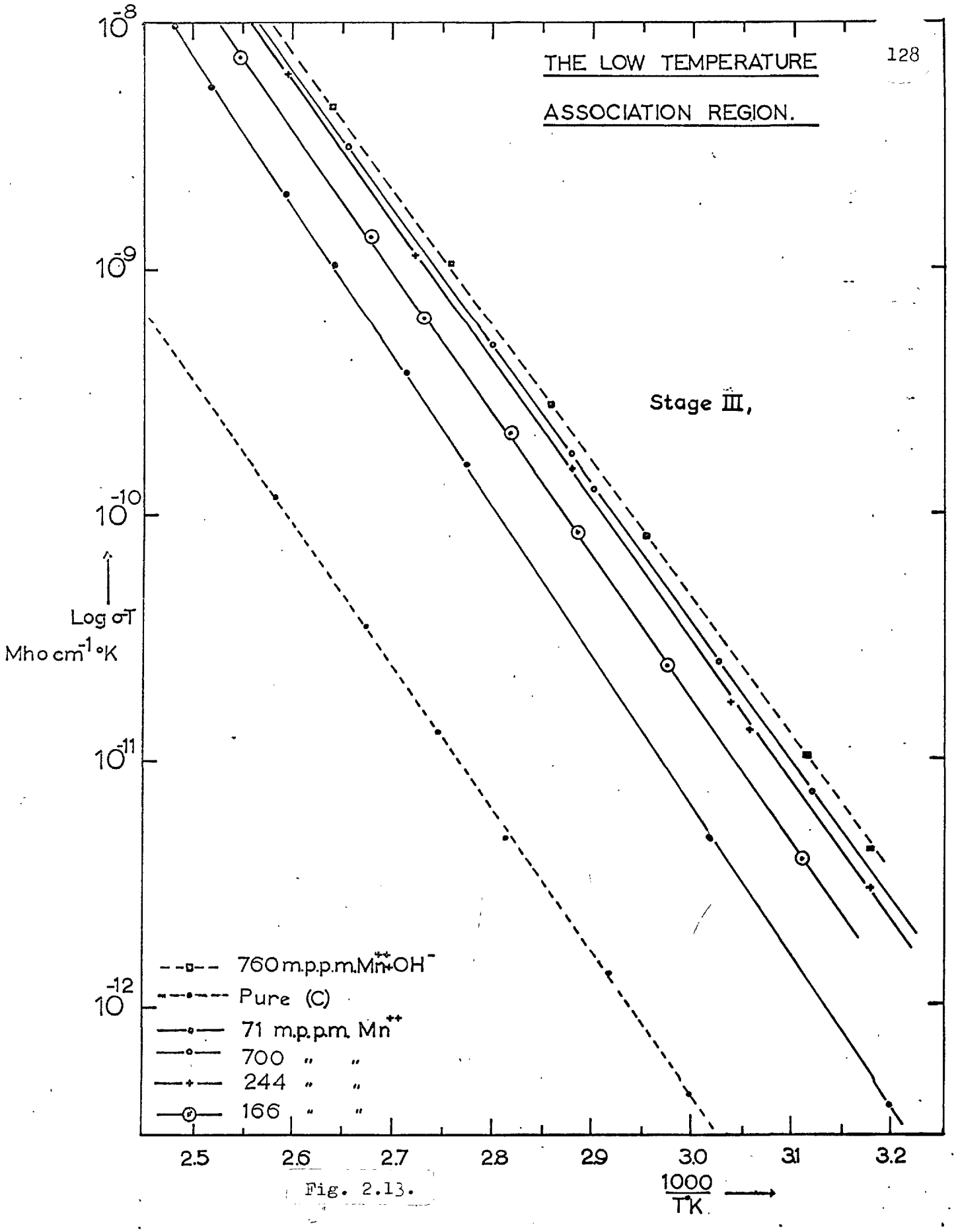
THE LOW TEMPERATURE
ASSOCIATION REGION.
Stage III,
10^{-8}
10^{-9}
10^{-10}
10^{-11}
10^{-12}
Log σT
Mho cm^{-1} °K
760 m.p.p.m. Mn^{++} OH^-
Pure (C)
71 m.p.p.m. Mn^{++}
700 " "
244 " "
166 " "
2.5
2.6
2.7
2.8
2.9
3.0
3.1
3.2
1000/TK

Fig. 2.13.

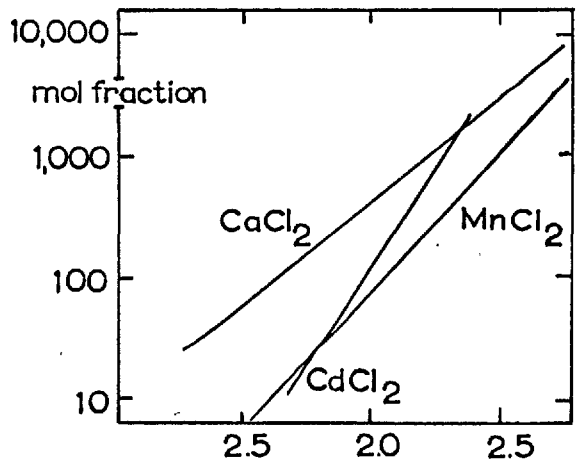

Free vacancy solubility,
After Haven

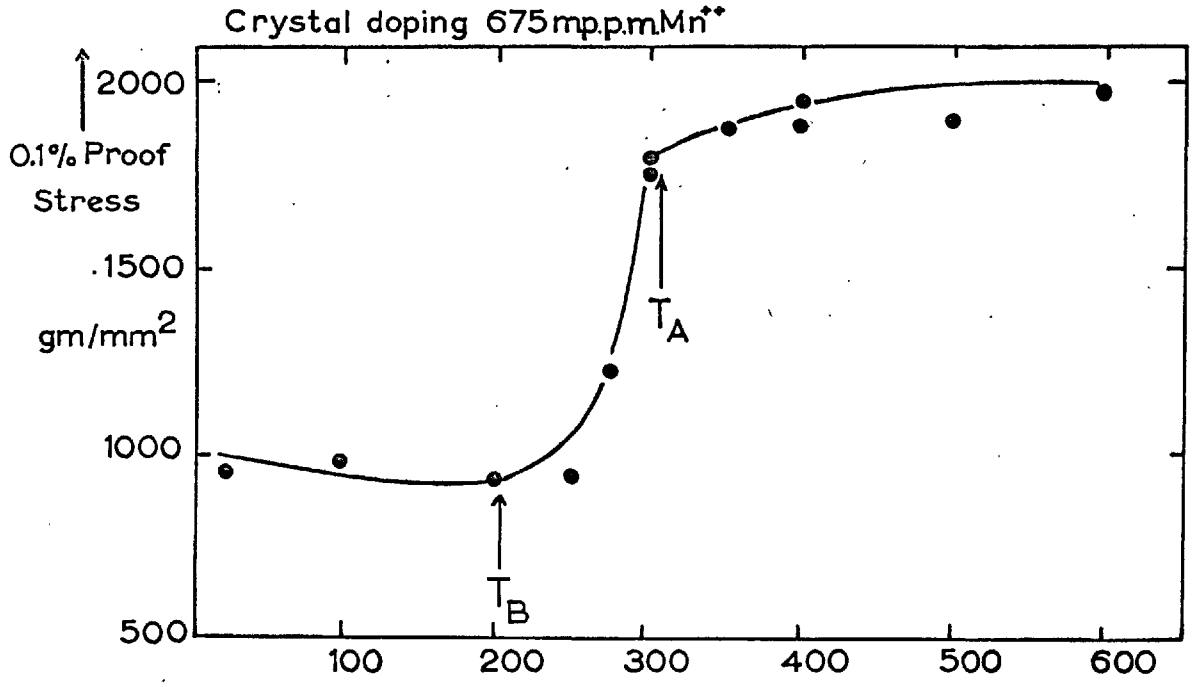

Mechanical properties of Manganese doped sodium chloride.
After Harrison(74)

Fig. 2.14.

TABLE (2.2).

Crystal	Q_{IV}, eV	End of Precipitation, °K
686 ± 10 m.p.p.m. Mn	1.48 ± 0.01	303°K
325 ± 10 m.p.p.m. Mn	1.29 ± 0.01	302°K
130 ± 10 m.p.p.m. Mn	1.16 ± 0.01	276°K
90 ± 20 m.p.p.m. Mn	1.21 ± 0.01	229°K

TABLE (2.3).

Crystal	Q_{III_1} eV.
Pure	1.17
71 ± 20 m.p.m. Mn	1.22
166 ± 10 m.p.m. Mn	1.16
244 ± 10 m.p.m. Mn	1.15
700 ± 10 m.p.m. Mn	1.13

It should be pointed out that all the conductivity data obtained in the present study were "equilibrium readings", that is, well aged crystals were taken from the dessicator and warmed up by steps of $5^{o}C$ and the conductivity allowed to reach an equilibrium value before the reading was taken. To obtain equilibrium in the lightly doped crystals, waiting periods in excess of twenty four hours were required.

The regions of the conductivity plot attributed to the association reactions, occurring below the precipitation regions, are shown in Fig. (2.13). These presented an interesting feature, a decreasing slope Q_{III_j} with increased doping level. Table (2.3). If this region were solely due to a low temperature association reaction, the conductivity plots would be characterized by a well defined slope, independent of doping level. This concentration dependence of the activition energy appears in the data of Schneider and Caffyn. [8] The only reasonable explanation would be that partial resolution of the precipitated phase is occurring below the kinetic level of $200^{o}C$, and this resolution is temperature dependent. The magnitude of the conductivity at any fixed temperature also increased with doping level up to a saturation value. This is consistent with there being a solubility limit for the solid solution, above which the divalent impurity will go into the aggregated or precipitated phase.

(2) Ionic Thermocurrent Results

The complete I.T.C. spectra of a manganese doped crystal is presented in Fig. (2.15). This was obtained by holding the crystal

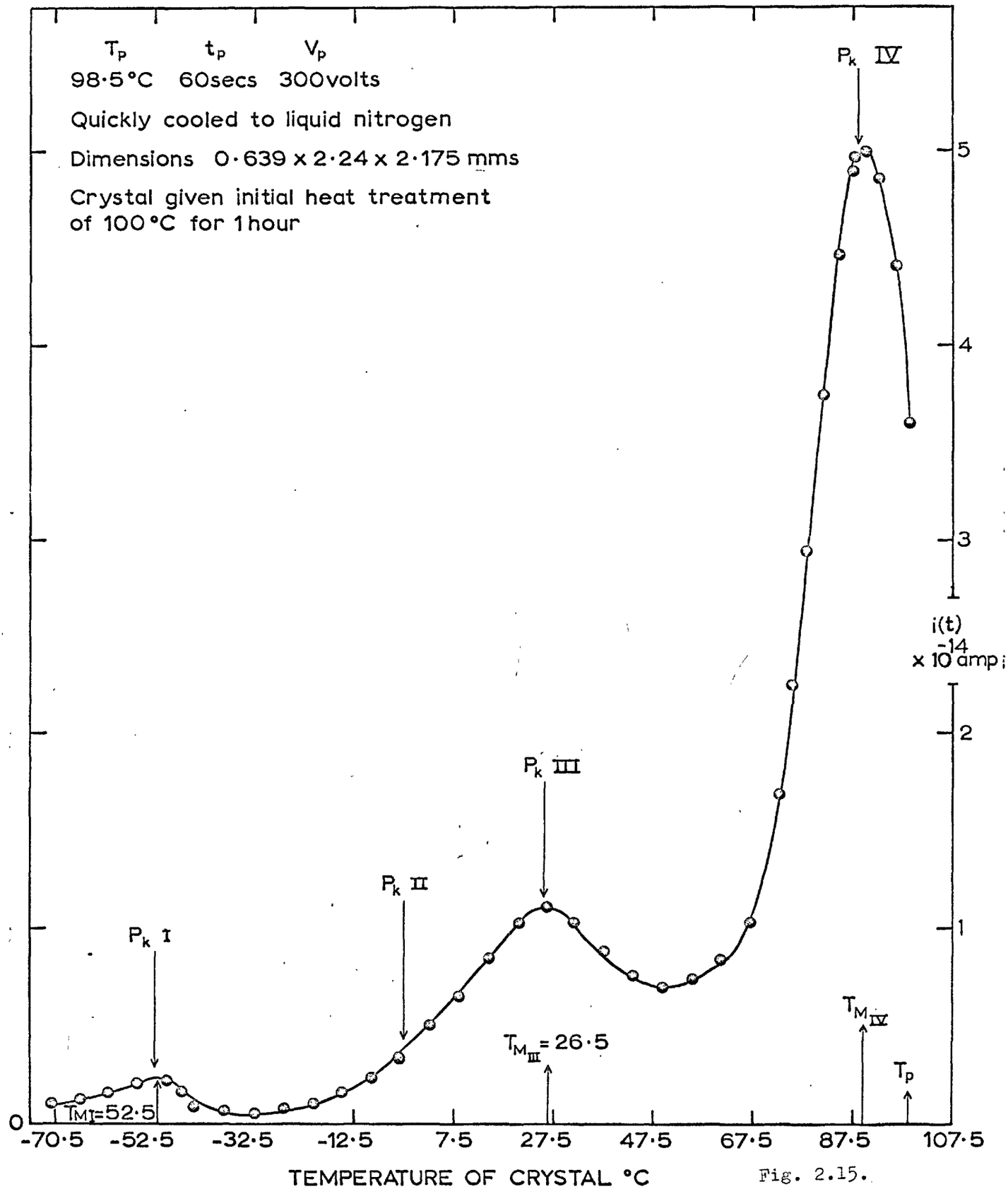
T_p t_p V_p
98·5°C 60secs 300volts
Quickly cooled to liquid nitrogen
Dimensions 0·639 x 2·24 x 2·175 mms
Crystal given initial heat treatment
of 100°C for 1 hour
P_k I
P_k II
P_k III
P_k IV
T_{M_I}=52·5
$T_{M_{III}}$=26·5
$T_{M_{IV}}$
T_p
i(t)
-14
x 10 amp
0
1
2
3
4
5
-70·5
-52·5
-32·5
-12·5
7·5
27·5
47·5
67·5
87·5
107·5
TEMPERATURE OF CRYSTAL °C

Fig. 2.15.

at a temperature of 98.5°C for a period of one hour, polarizing the crystal with an electric field and then slowly cooling it to liquid nitrogen temperature in order to quench in all the relaxation processes. During the subsequent linear heating of the crystal, three peaks (I,III and IV) were produced, with Peak II only appearing in the later experiments. The same experiment was repeated upon a pure crystal and produced the results of Fig. (2.16). As both crystals were subjected to the same polarizing times and temperatures, Peaks I, II and III could be attributed to the presence of the divalent, manganese impurity.

All the I.T.C. discharge peaks were superimposed upon a background of a constant discharge current, which was related to the volume of the crystal. This discharge was not thermal noise but was attributed to the change of dielectric constant of the material with increasing temperature. Similar discharge currents have been observed by Matsonashvili [72] in heated crystals of the alkali halides. By suitable choice of polarizing temperatures, the individual peaks could be isolated and investigated. For example, by polarizing the manganese doped crystals at about -30°C for more than five minutes and then cooling the crystals suddenly, Peak I could be observed, free from the effects of the other peaks.

(a) Peak I

It is feasible that Peak I was produced by the reorientation of impurity-vacancy dipoles, especially as the peak height of this particular discharge occurred at a temperature where the impurity-vacancy dipole had a relaxation time of greater than 1 sec. With

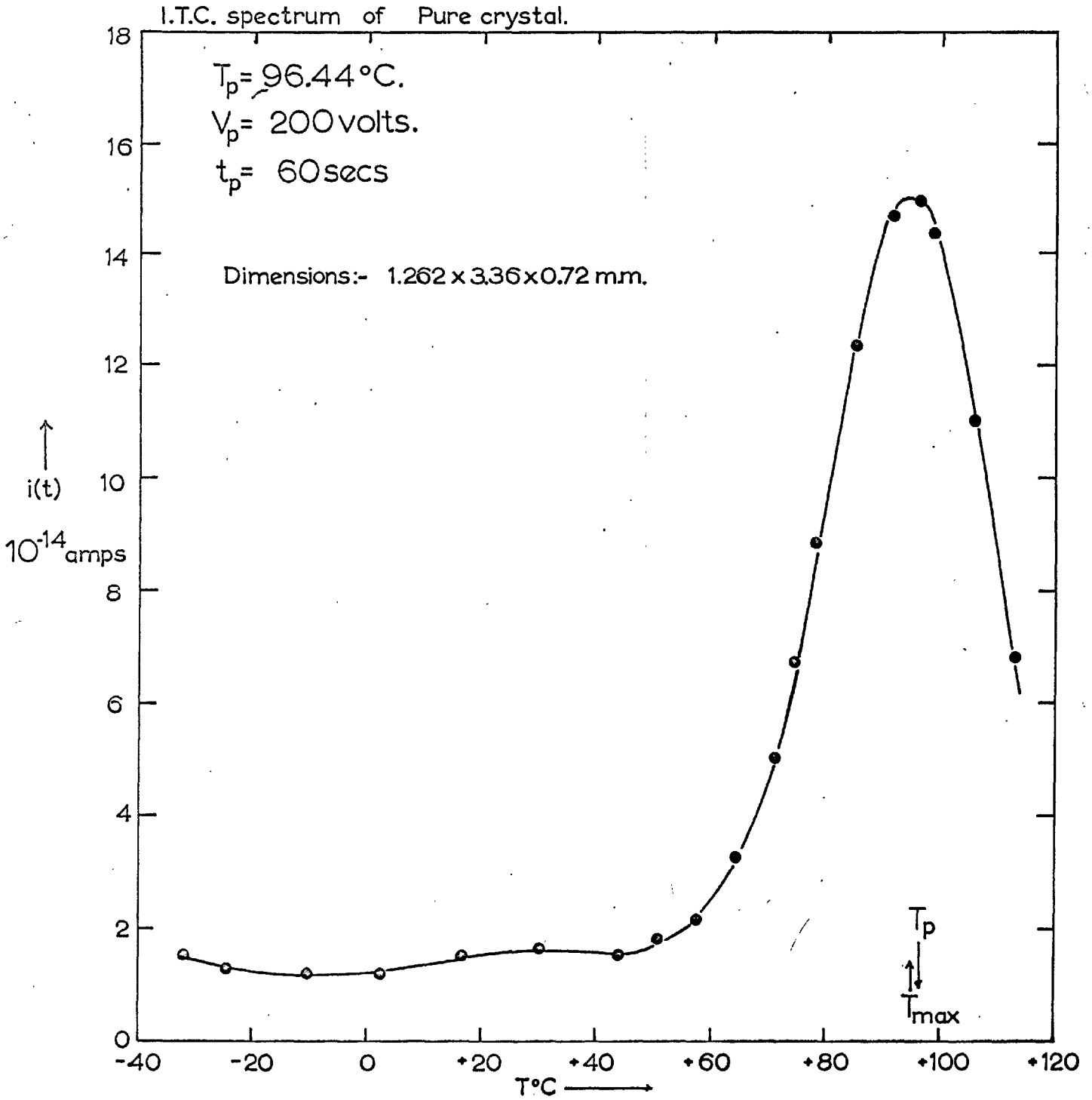
I.T.C. spectrum of Pure crystal.
T_p= 96.44°C.
V_p= 200 volts.
t_p= 60 secs
Dimensions:- 1.262 x 3.36 x 0.72 m.m.
i(t)
10^{-14} amps
18
16
14
12
10
8
6
4
2
0
-40
-20
0
+20
+40
+60
+80
+100
+120
T°C
T_p
T_{max}

Fig. 2.16.

this in mind, a manganese doped crystal was given a preliminary heat treatment of two hours at 300°C and then air quenched onto a block of asbestos. It was hoped that this treatment would put a large proportion of the impurity into dipole form. The specimen was then polarized at -30°C for a period of 300 secs., quickly cooled to liquid nitrogen temperature and the I.T.C. discharge observed. This process was repeated for different polarizing field strengths, Fig. (2.17). If different specimens of the same doping level had been used, the current density would have been observed in order to make a quantitative comparison. In Fig. (2.18), the maximum current density is plotted against the applied electric field strength, for two different specimens of the same manganese content. The linear relationship observed is in agreement with the predictions of equation (24), for constant dipole concentration , and polarizing temperature T_p. The temperature at which the peak height occurred (-52.5°C) was independent of the applied polarizing field strength, as suggested by equation (25). Using this equation a nd a value of 0.70eV. for the reorientational energy, a value of $\log_{10}\tau = 1.31$ is obtained at T_m. Dielectric relaxation experiments performed on the same crystals, Fig. (2.29) suggest a value of $\log_{10}\tau = 1.65$. The discrepancy between these values could indicate some systematic lag between the temperature of the chamber and the specimen.

By keeping the polarizing temperature and times constant, the impurity-vacancy dipole concentration was varied by using different heat treatments. Then, by plotting the current density/unit field strength as a function of temperature, the comparative effects of quenching temperature upon dipole concentration for different crystals

Dipole peaks as a function of applied field strength.

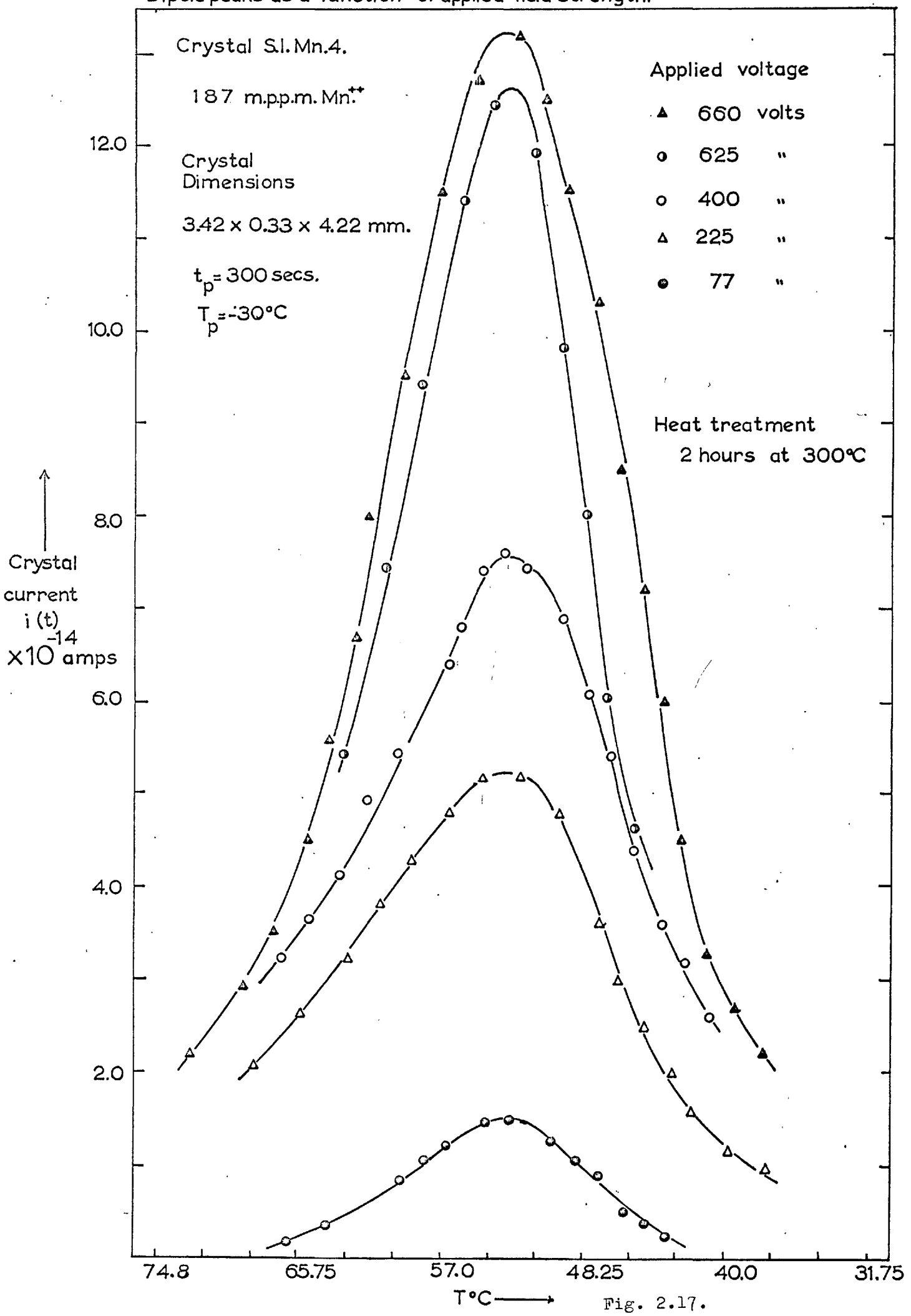

Fig. 2.17.

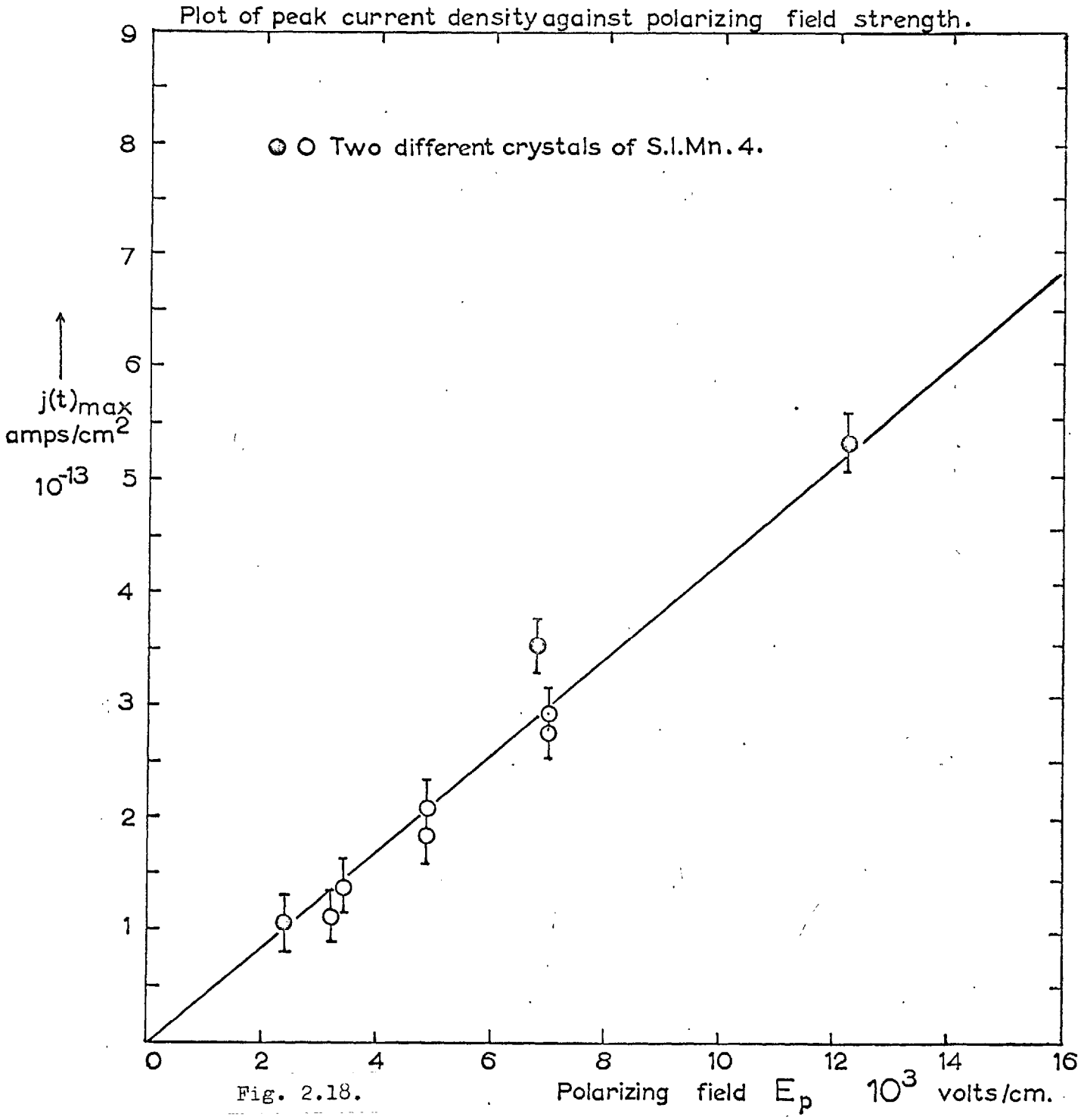
Plot of peak current density against polarizing field strength.
⊙ O Two different crystals of S.I.Mn.4.
$j(t)_{max}$ amps/cm^2
10^{-13}
9
8
7
6
5
4
3
2
1
0
2
4
6
8
10
12
14
16
Polarizing field E_p 10^3 volts/cm.

Fig. 2.18.

of the same doping level were observed. Fig. (2.19). Again the peak temperature of 53.2 ± 0.9°C would appear to be independent of dipole concentration.

An estimation of the enthalpy of reorientation was obtained by analysing the low temperature tail, using the method suggested in equation (28). This is performed in Fig. (2.20) and yields an energy of reorientation of 0.67 ± 0.01eV. An independent estimate was obtained by analysing the whole peak in the manner suggested by equation (27). Fig. (2.21). This analysis yields a relation for of the form

$$\tau(T) = 5.0 \times 10^{-12} \cdot \exp(0.65 \pm 0.04)\text{eV}/kT \cdot \text{sec}.$$

with

$$\Delta h_o = 0.65 \pm 0.04\text{eV} \qquad \Delta s_o = 5.0 \times 10^{-4}\text{eV}/^{\circ}\text{K}$$

Having resolved variations in dipole concentration in a quantitative manner, a crystal platelet of a known manganese content was split up into a series of specimens of similar impurity content. These well aged crystals were air quenched after being subjected to different annealing temperatures for periods of time in excess of two hours, and their relative impurity-vacancy dipole content determined by the I.T.C. technique Fig. (2.22). This result shows a gradually increasing dipole content up to temperatures of about 220 ± 10°C, where a sharp increase occurs, just above the kinetic level, due to the onset of the resolution of the aggregated phase. The gradual increase in dipole concentration below this temperature is due to the partial resolution of the aggregated state. At a temperature of 320 ± 20°C, all the impurity would appear to be in solution. The subsequent decrease in dipole concentration at

Effective peaks as a function of dipole concentration. Fig. 2.19.

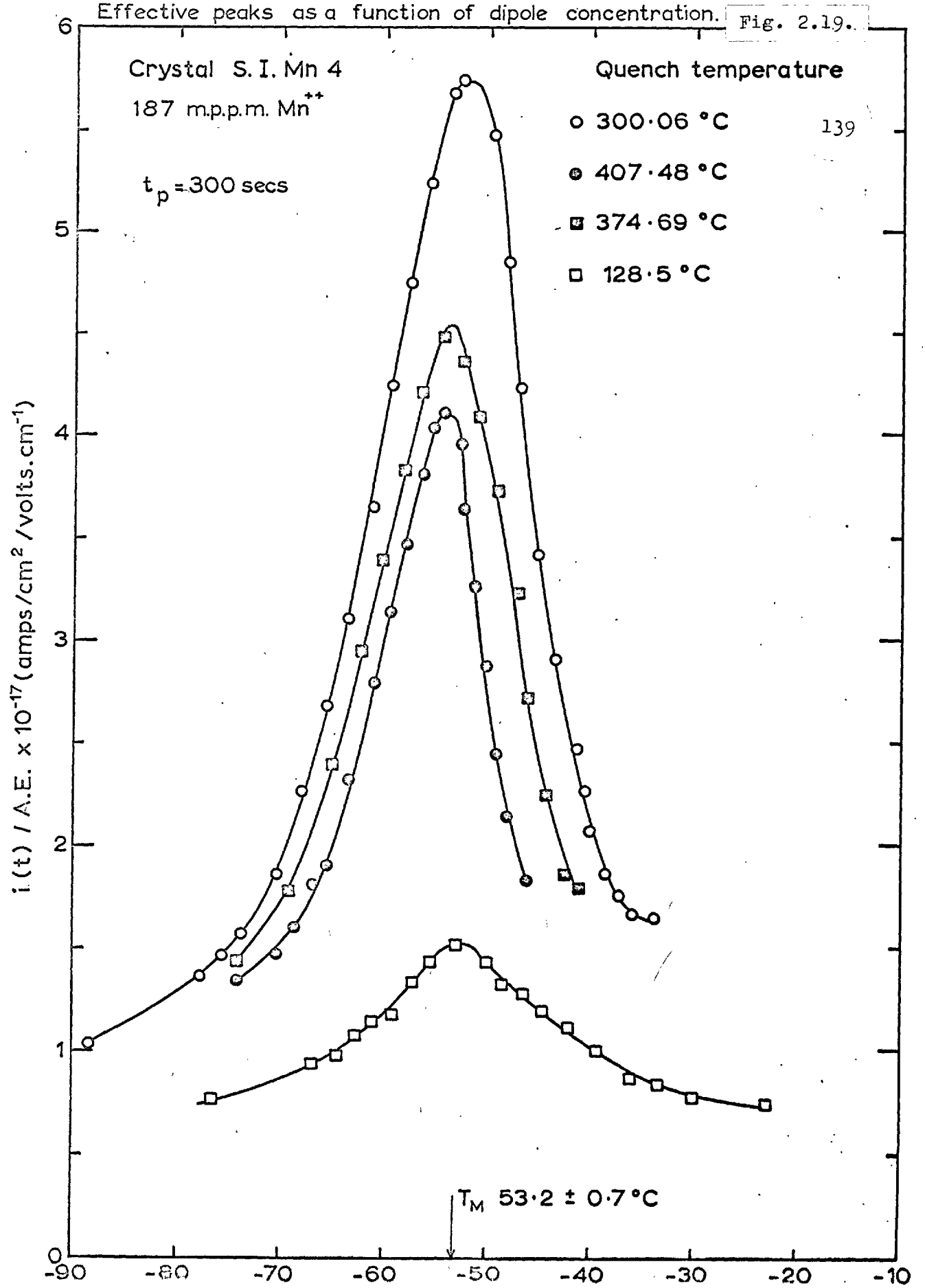

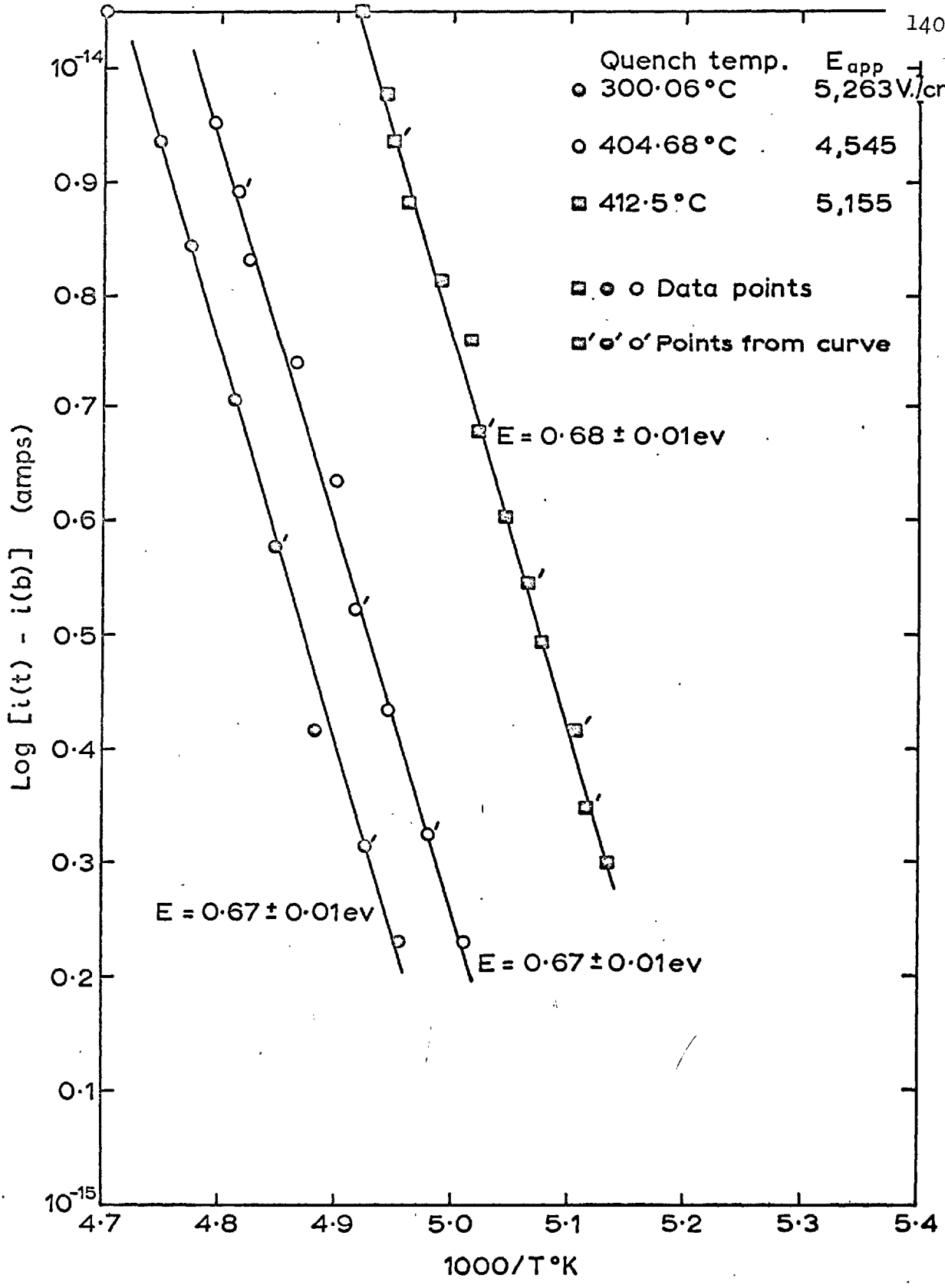

ANALYSIS OF LOW TEMPERATURE TAILS OF CURVES

Fig. 2.20.

Relaxation time as a function of temperature, from I.T.C. peak.

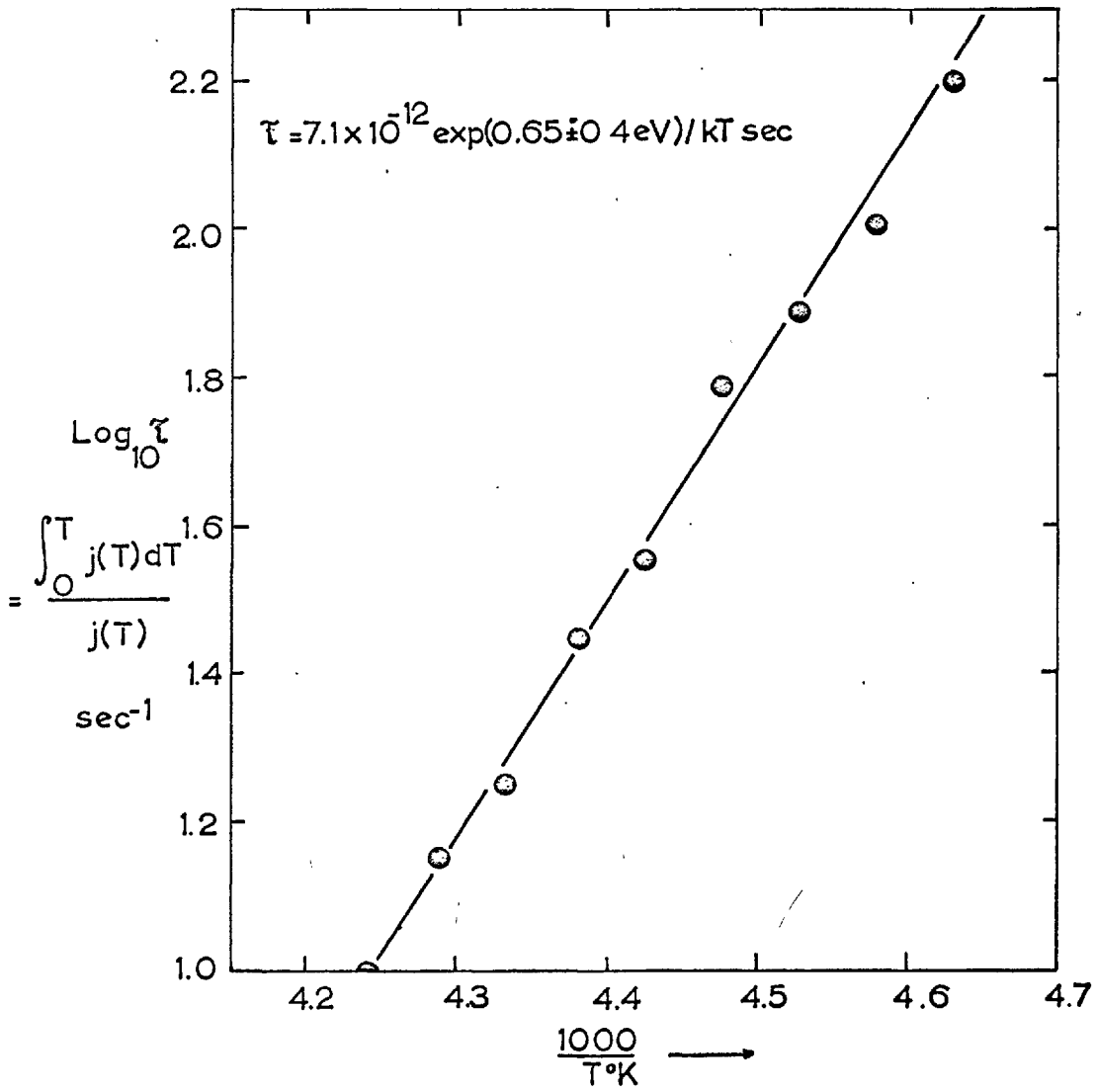

Fig. 2.21.

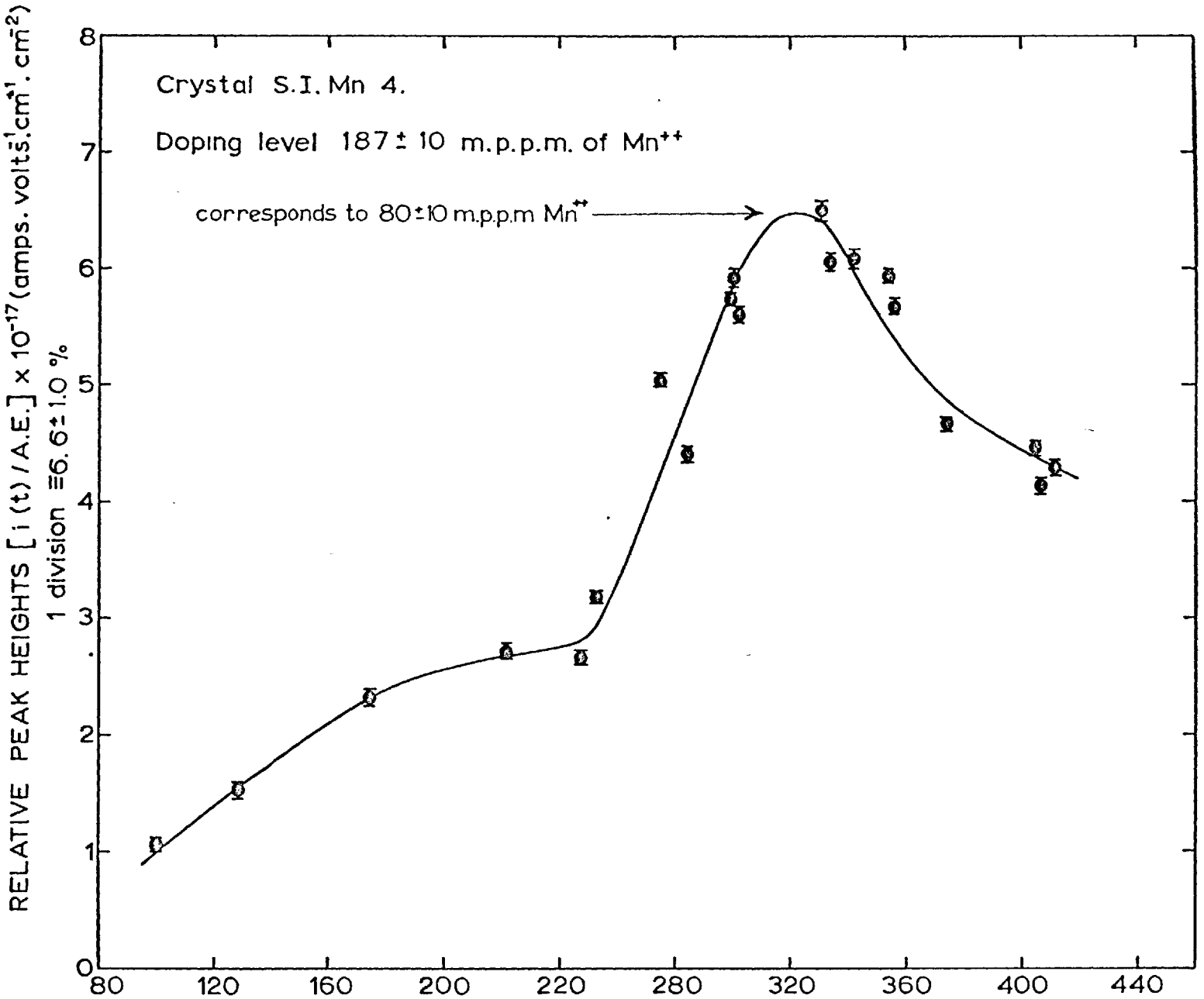
Crystal S.I. Mn 4.
Doping level 187 ± 10 m.p.p.m. of Mn++
corresponds to 80±10 m.p.p.m Mn++
RELATIVE PEAK HEIGHTS [i (t) / A.E.] x 10-17 (amps. volts-1.cm-1. cm-2)
1 division ≡6.6± 1.0 %
0
1
2
3
4
5
6
7
8
80
120
160
200
220
280
320
360
400
440

higher temperatures may be attributed to thermal disassociation of the complexes. For temperatures in excess of 420°C the results were not reproduceable, probably because the cooling in air was not rapid enough to quench in the equilibrium dipole concentration. In order to obtain the drop in dipole concentration, attributed to thermal disassociation, the specimens had to be quenched from the annealing temperature to -30°C in a period of less than five seconds. The specimens were less than 0.3mm thick and presumably followed the cooling chamber's rapid changes in temperature with little thermal lag. If thicker specimens, or a normal air quench were used, inconsistent results were obtained at the higher temperatures. The maximum dipole concentration would appear to be achieved at quenching temperatures of 320 ± 20°C, this concentration accounted for only 42.5% of the total divalent impurity. The rest is presumably present as free ions or tied up with anions. This result is in contradiction to the results of Cook and Dryden, [29, 31] who claim that after suitable heat treatments, 100% of the divalent impurity may appear in dipole form. If this were so, the air quenched crystals would be expected to have intrinsic conductivity at the quenching temperature.

Having observed the dipole concentration as a function of temperature, the conductivity of a similarly doped specimen was measured over the same temperature range. Fig. (2.23). Using the expression for the cation vacancy mobility, determined in Part I, the molar concentration of free vacancies x_1 and hence the number of free impurity ions was determined. Then, by using the following

Low temperature precipitation region of conduction.

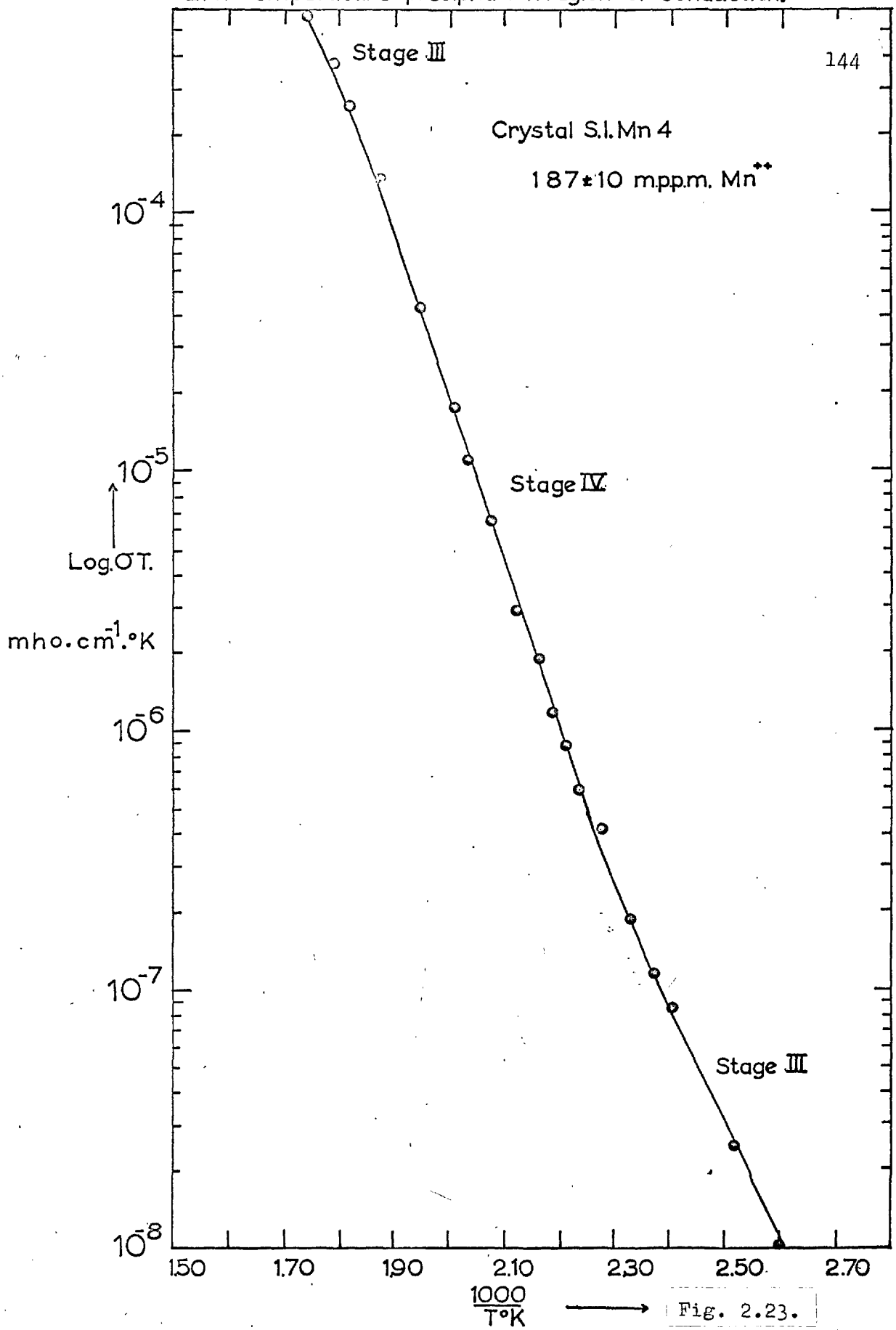

Fig. 2.23.

relation,

X_o	=	X_1	+	X_k	+	σ_o	+	X_p
CHEMICAL ANALYSIS		IONIC CONDUCTIVITY		I.T.C.		EXTRINSIC CONDUCTIVITY		

the molar concentration of the impurity in aggregated form was determined as a function of temperature Fig. (2.24). There appears to be considerable resolution of the precipitate occurring below the kinetic level. This resolution probably helps determine the slope of Stage III_1.

(b) Peaks II, III and IV

The other I.T.C. peaks were not subjected to such an intensive investigation as Peak I. Peak III was observed by polarizing at room temperature and then rapidly cooling to liquid nitrogen temperature. Fig. (2.25) presents the effect of increasing electric field strength, and shows that there is a linear relation between peak height and the polarizing electric field. A subsidiary peak (Peak II) was attributed to partly orientated states of the impurity vacancy complex, produced during the rapid cooling process. It must be confessed that the position of this subsidiary peak does not occur at the normal temperature of the dipole peak, a fact which could argue against the above suggestion. No definite model can be suggested for the relaxation process producing Peak III. It is most unlikely that it is caused by a dipolar relaxation of an aggregated or precipitated phase, as the prior heat treatment of two hours at 350°C was performed to remove any aggregated form of the impurity.

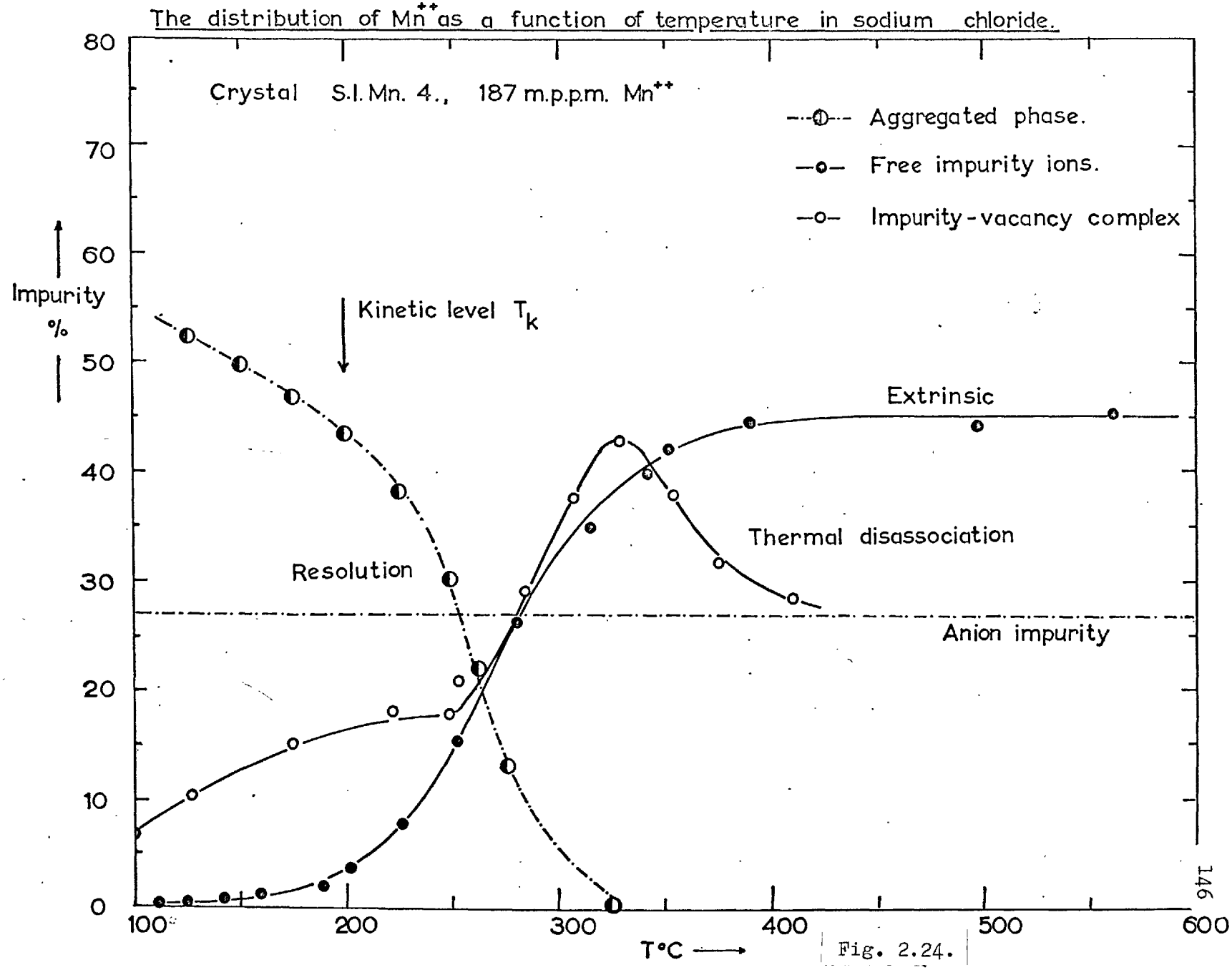
The distribution of Mn++ as a function of temperature in sodium chloride.
Crystal S.I. Mn. 4., 187 m.p.p.m. Mn++
Aggregated phase.
Free impurity ions.
Impurity-vacancy complex
Impurity %
Kinetic level T_k
Extrinsic
Thermal disassociation
Resolution
Anion impurity
80
70
60
50
40
30
20
10
0
100
200
300
400
500
600
T°C

Fig. 2.24.

I.T.C. spectra of peak III. Fig. 2.23.

T_p	t_p	V_p	Curve
23°C	180sec.	200 volts.	(1)
23°C	"	150 "	(2)
23°C	"	100 "	(3)

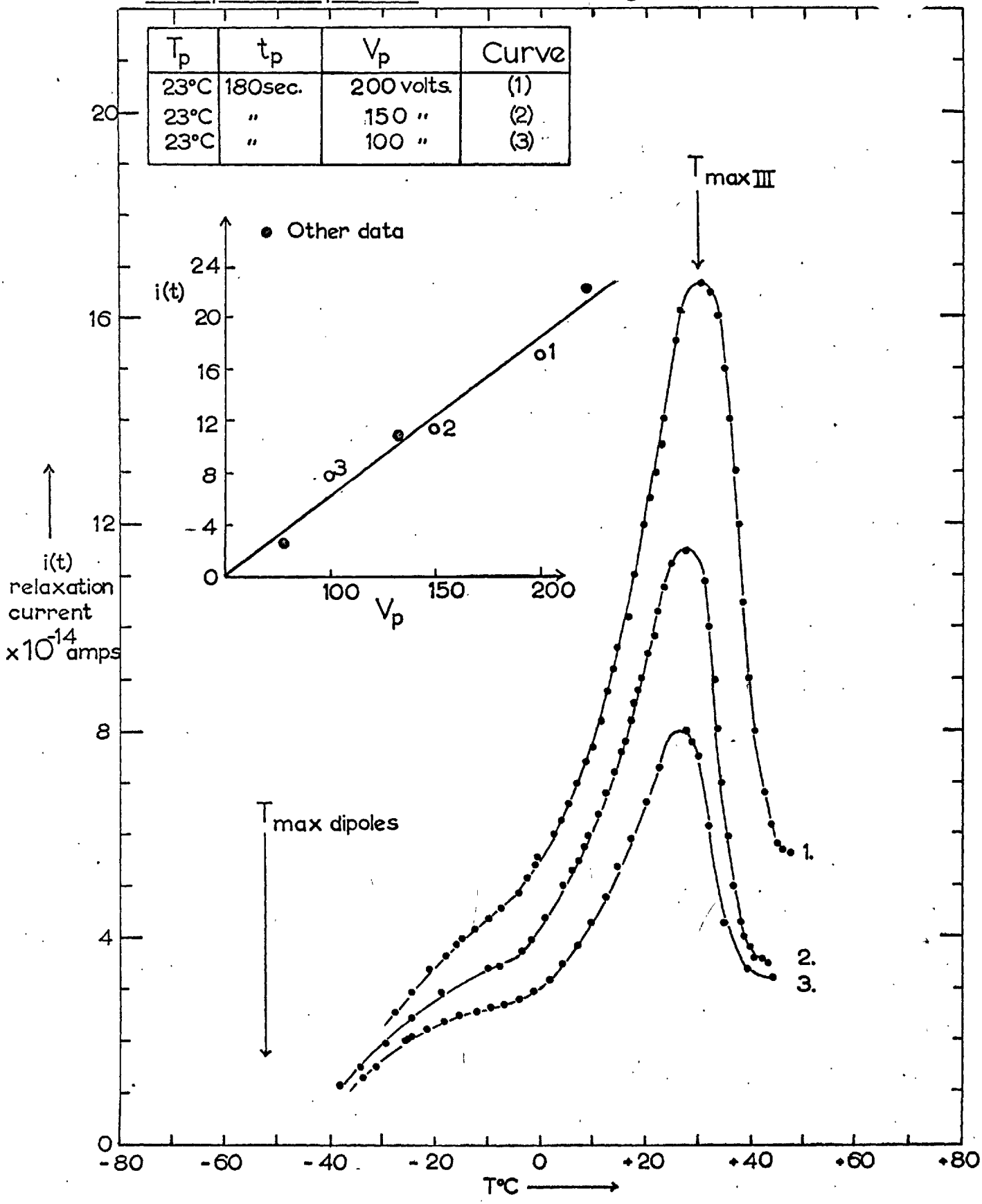

The possibility of polarization of the charge clouds around dislocation cores might be an interesting line to pursue.

Peak IV was attributed to space charge polarization at the crystal-electrode interface. This form of relaxation had been the subject of an investigation by Bucci and Riva, [56] who first used the I.T.C. technique to investigate space charge effects in ionic crystals.

(3) Dielectric Absorption and Relaxation

The techniques of dielectric absorption and relaxation are alternative methods of observing the reorientational motion of impurity-vacancy dipoles. The I.T.C. techniques suggests that in the crystals investigated the dipolar relaxation is accurately described by the relaxation of a n.n. impurity-vacancy complex. As these alternative techniques cover essentially the same temperature range of investigation, with perhaps different resolution of the higher order complexes, they were used to investigate crystals of the same doping level. Dipole reorientation under an applied steady state electric field is observed as a decay in current which is related exponentially to time by equation (13). Fig. (2.26) presents current decays for crystals at different temperatures. These show that there is a linear region of the current decay curve which may be attributed to the relaxation of the nearest neighbour impurity-vacancy dipole. These transient currents were obtained from crystals which had been air quenched from a temperature of 300°C, and were in marked contrast to those obtained from well aged crystals, Fig. (2.27),

Dipole relaxations in quenched crystals.

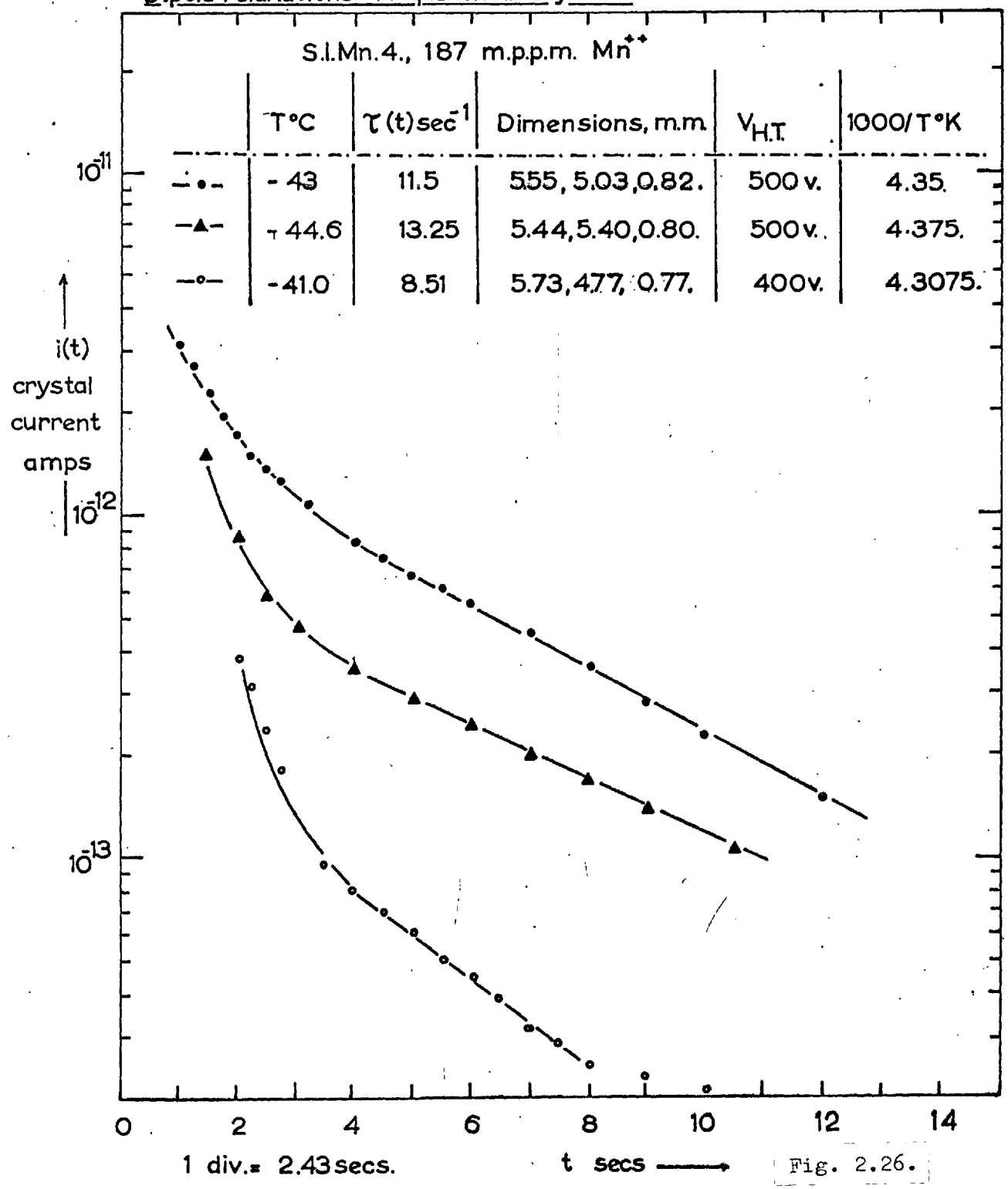

Fig. 2.26.

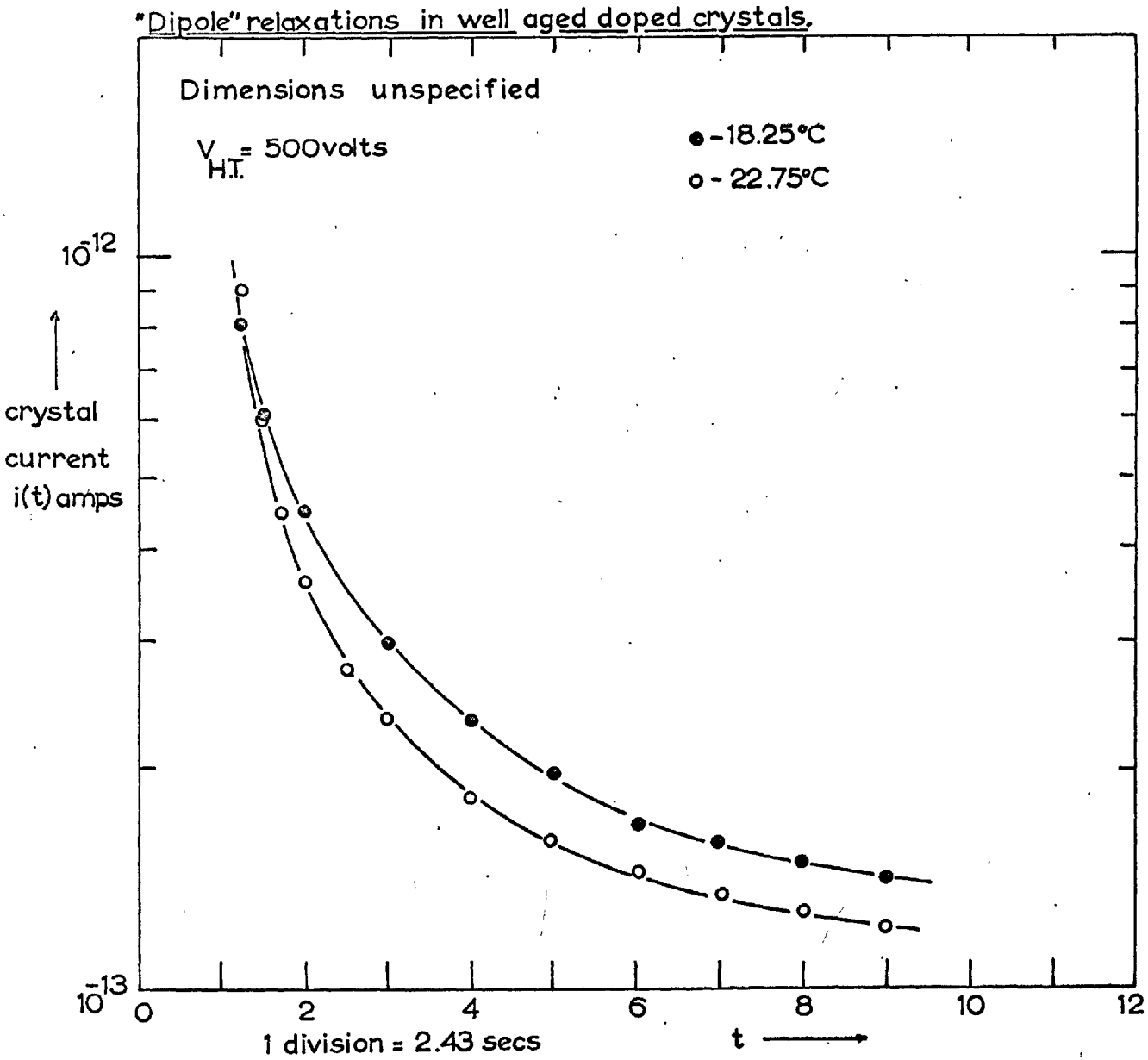
"Dipole" relaxations in well aged doped crystals.
Dimensions unspecified
$V_{H.T.}$ = 500volts
● - 18.25°C
o - 22.75°C
10^{-12}
crystal current i(t) amps
10^{-13}
0
2
4
6
8
10
12
1 division = 2.43 secs
t

Fig. 2.27.

which do not show a well defined relaxation time. The relaxation process in the well aged crystals may be attributed to the polarization of the Suzuki phase, which, although electrically neutral, does contain divalent manganese ions with cation vacancies arranged to form ordered electrical dipoles Fig. (2.1). The "very fast" relaxations observed in the air-quenched crystals were attributed, by Dreyfus, to the relaxation of the n.n.n. impurity-vacancy complexes. Even though the current decay appeared to be a sum of two exponential processes, as suggested by equation (14) which takes into account the presence of n.n. and n.n.n. impurity-vacancy complexes, there was no systematic relation between the temperature and relaxation time for this "very fast" relaxation. An effect similar to that of the very fast relaxation could be produced by a poor response time of the current detecting system or failure to obtain complete resolution of the impurity. The temperature dependence of the n.n. relaxation is presented in Fig. (2.28) and shows that the relaxation time, τ , for this particular process obeys a relationship of the form

$$\tau = 3.0 \times 10^{-14} \exp (0.71 \pm 0.01eV)/kT.sec.^{-1}.$$

The value of $0.71 \pm .01eV$. for the enthalpy of reorientation is very similar to the enthalpy of motion of the cation vacancy (0.68eV). This would suggest that dipolar reorientation is occurring predominantly by vacancy motion, rather than direct impurity-vacancy exchange, and that this enthalpy of motion is not greatly affected by the close proximity of the manganese ion. From the pre-exponential term τ_o, the entropy involved in the vacancy making a jump may be derived, assuming that the vacancy movement is the predominant process.

$$\tau_o^{-1} = \lambda . \nu_1 \exp \Delta s_{o/K.sec.}$$

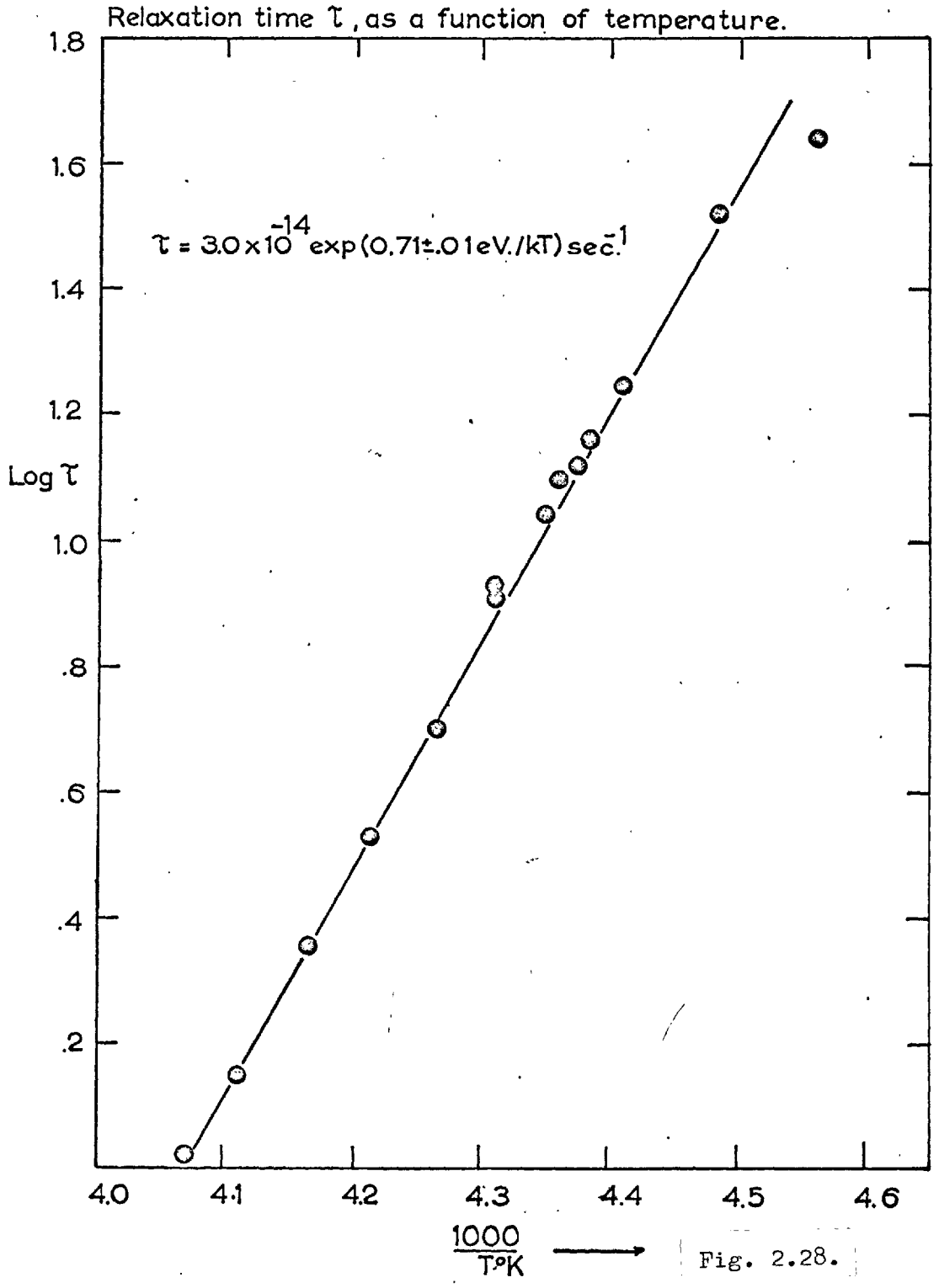
Relaxation time τ, as a function of temperature.
τ = 3.0 x 10^-14 exp(0.71±.01eV./kT) sec.^-1
Log τ
1.8
1.6
1.4
1.2
1.0
.8
.6
.4
.2
4.0
4.1
4.2
4.3
4.4
4.5
4.6
1000/T°K

Fig. 2.28.

In the above expression, ν_1 is the ionic vibrational frequency, taken to be the Debye frequency and λ is the number of similar jumps capable of producing the relaxation. The value of 3.00×10^{-4} eV/°K for Δs_o is similar to the values obtained for Δs_1, the entropy of motion for the cation vacancy ($\Delta s_1 = 1.70$ to 2.00×10^{-4} eV./°K). No attempt was made to measure relaxation times for temperatures in excess of -20°C, as the form of the current decay curve appeared to change markedly in the temperature range -20°C to -15°C. The exponential decay of current was replaced by a decay that was related to time by a power law of the form

$$-\left\{ j(t) - j(\infty) \right\} = A_o t^{-n}$$

No discussion of this will be included, as a similar form of current decay has been observed by Sutter and Nowick [36] in pure crystals of sodium chloride.

The dielectric absorption peak produced by manganese impurity-vacancy dipoles appears in Fig. (2.29). From the magnitude and position of the peak maxima, which is decribed in the Debye absorption of equation (17), the peak obtained may be compared with that predicted for a Debye loss characterized by a single relaxation time. The agreement between the two curves is well within the limits of experimental error and is in contrast to the rather broad absorption peaks observed by Haven [73] in manganese doped sodium chloride. The absence of any appreciable broadening of the peak would rule out any large contribution to the loss from n.n.n. impurity-vacancy complexes. By observing the variation in the position of the peak maxima for different temperatures, the

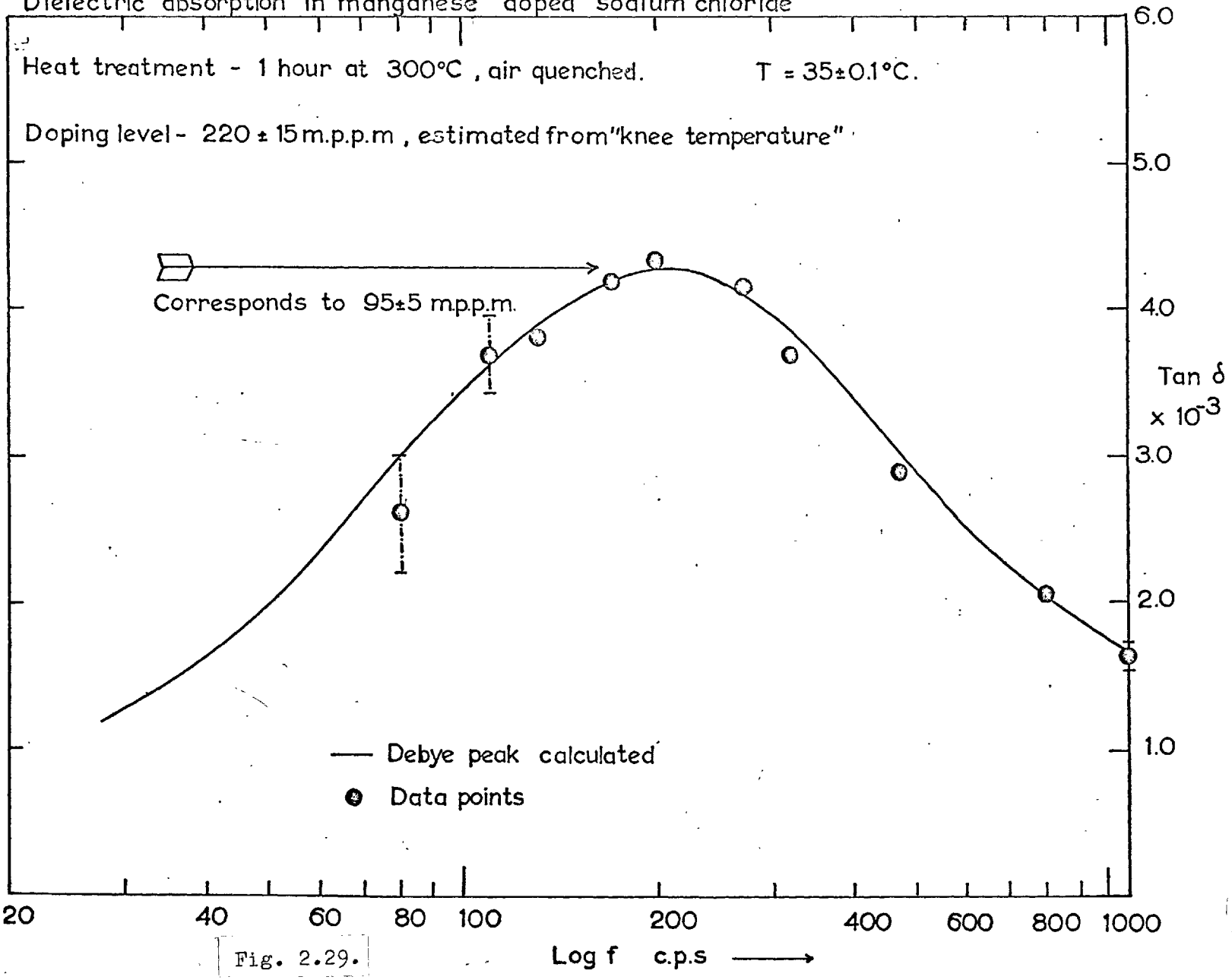
Dielectric absorption in manganese doped sodium chloride
Heat treatment - 1 hour at 300°C , air quenched.
T = 35±0.1°C.
Doping level - 220 ± 15 m.p.p.m , estimated from "knee temperature"
Corresponds to 95±5 m.p.p.m.
Debye peak calculated
Data points
Tan δ
x 10⁻³
6.0
5.0
4.0
3.0
2.0
1.0
20
40
60
80
100
200
400
600
800
1000
Log f c.p.s

Fig. 2.29.

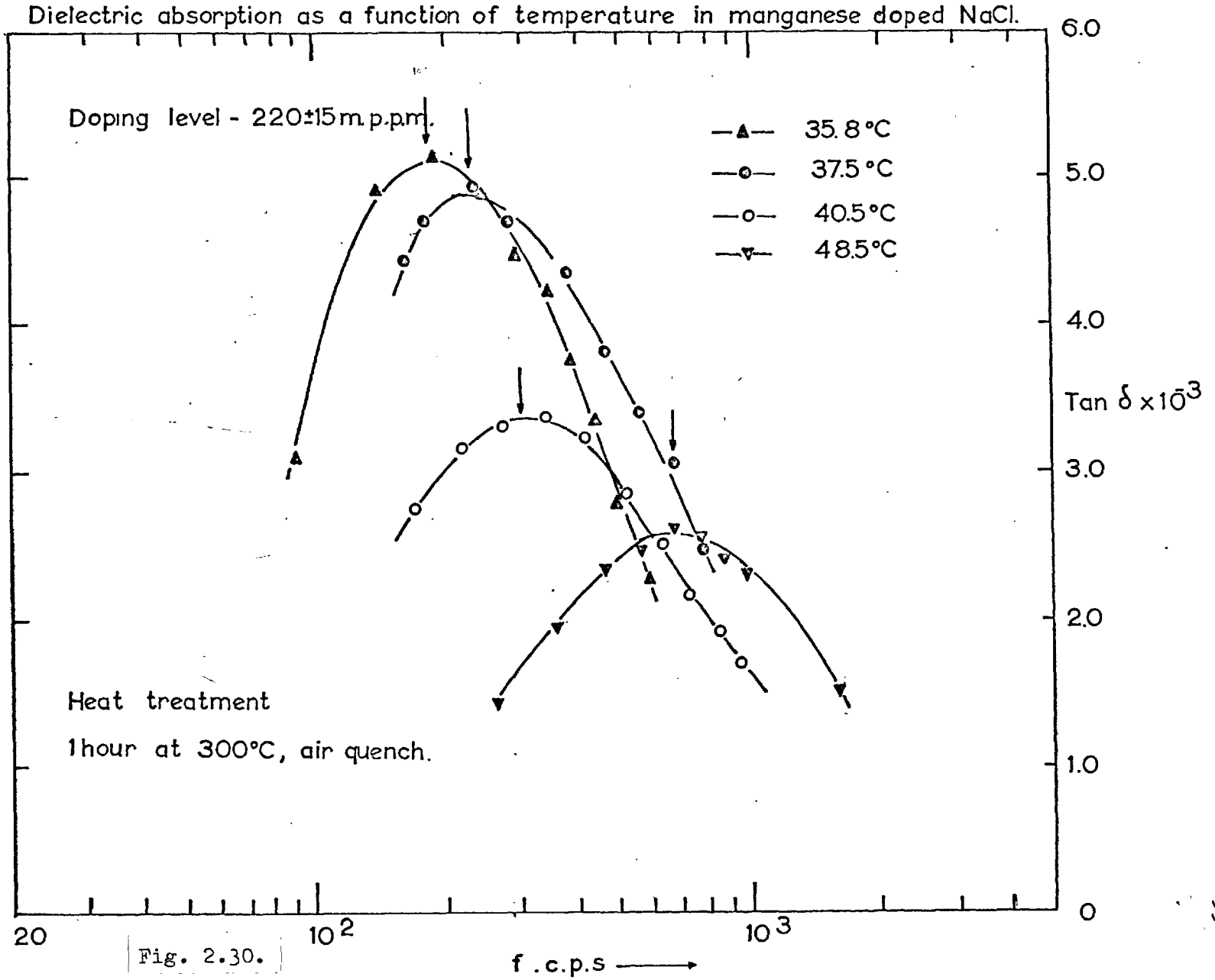
Dielectric absorption as a function of temperature in manganese doped NaCl.
Doping level - 220±15 m.p.p.m.
35.8 °C
37.5 °C
40.5 °C
48.5 °C
Heat treatment
1 hour at 300°C, air quench.
Tan δ x 10^3
6.0
5.0
4.0
3.0
2.0
1.0
0
20
10^2
10^3
f .c.p.s

Fig. 2.30.

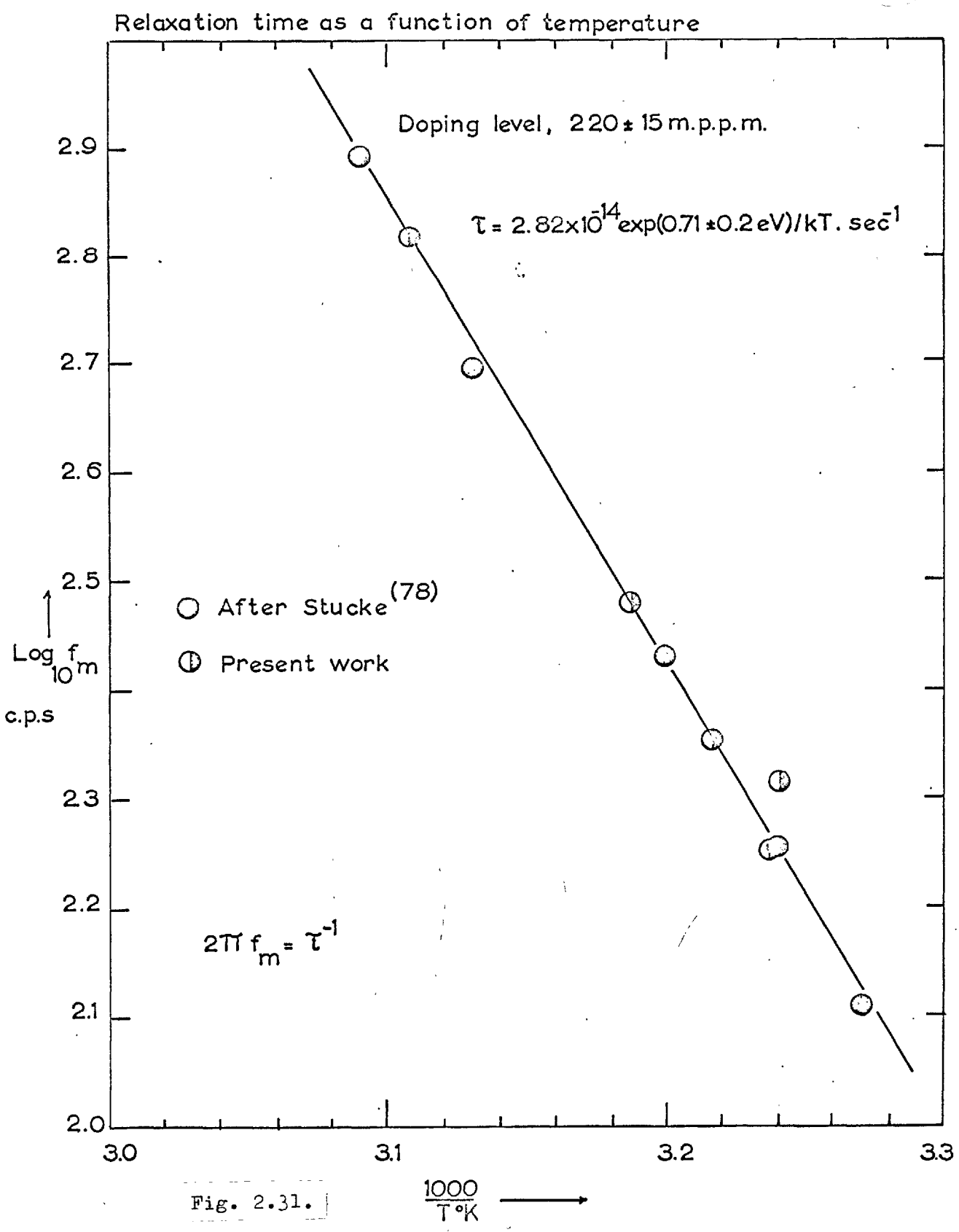
Relaxation time as a function of temperature
Doping level, 220 ± 15 m.p.p.m.
τ = 2.82x10⁻¹⁴ exp(0.71 ±0.2 eV)/kT. sec⁻¹
After Stucke (78)
Present work
2π f_m = τ⁻¹
Log 10 f_m
c.p.s
2.9
2.8
2.7
2.6
2.5
2.3
2.2
2.1
2.0
3.0
3.1
3.2
3.3
1000/T °K

Fig. 2.31.

temperature dependence of the relaxation time τ may be obtained Fig. (2.30), Fig. (2.31) and an enthalpy and entropy of reorientation of 0.71 ± 0.02eV. 0.116 x 10^{-3}eV/^{o}K obtained. The enthalpy value is in good agreement with those derived from the other techniques, but there does seem to be a difference in the values derived for Δs_o. This could be attributed to different systematic errors associated with each technique. The dipole concentration was obtained from the peak height and for the heat treatment used, two hours at 300^{o}C and then air quenched, about 45 ± 5% of the impurity was in dipole form. This value is in good agreement with the value derived from the I.T.C. peaks of crystals of approximately the same doping level, although the error quoted on the present figure is probably larger, due to ageing of the dipoles during the course of the experiment. The values for the enthalpies of reorientation are almost identical to those obtained by Dryden and Meakens [26] for calcium doped sodium chloride, 0.68eV. This is not unreasonable since the ionic radii of calcium and manganese are similar (Mn^{++} 0.80Å, Ca^{++} 0.99Å) and the relative interactions between the impurity ion and the vacancy would be expected to be similar.

(v) Conclusions and Suggestions for Future Work

The I.T.C. technique is a powerful tool for the study of impurity-vacancy dipoles in dielectric crystals and it could be usefully extended to investigate these defects in the alkaline earth fluorides (CaF_2, SrF_2, BaF_2). The technique is an order of magnitude more sensitive to the concentration of dipoles than that of dielectric absorption and it is more selective in resolving the particular relaxation processes that may be occurring. Only when preliminary experiments are performed in conjunction with the I.T.C. measurements to define the mechanism of any particular relaxation peak can the technique be used to its full advantage. In the present study, an I.T.C. peak (Peak I) appearing at a temperature of $-52.5 \pm 0.7^{\circ}C$ was attributed unambiguously, with the aid of dielectric absorption and relaxation, to the reorientation of manganese ion-cation vacancy dipoles.

The parameters associated with the reorientation of this defect (Δh_o, Δs_o) were consistent with a n.n. model, in which the motion under an applied electric field, between -60 and $60^{\circ}C$, occurred by the movement of the cation vacancy about the impurity ion. This is not an unreasonable conclusion, since the contribution to the relaxation process from a direct interchange of impurity ion and cation vacancy at these low temperatures should only be important when the radius of the impurity ion is significantly smaller than that of the alkali metal ion (Mn^{++}, $0.80A^{\circ}$; Na^{+}, $0.95A^{\circ}$). The consistency amongst the values of Δh_o, Δs_o, as determined by the different techniques, show that quantitative estimates of the parameters obtained from I.T.C. measurements are reliable.

The exact mechanisms producing Peaks II and III have not been clearly resolved. There is the possibility that the latter peak could be attributed to the polarization and subsequent relaxation of the Debye-Huckel vacancy clouds which surround the dislocation cores; if this were so, much useful information could be obtained by studying this peak as a function of the mechanical state and doping level of the crystal. Additional work, not included in this thesis, has indicated that the dielectric relaxations appearing above room temperature in these crystals are intimately connected with this peak.

The I.T.C. technique itself could be developed in one or two interesting ways. The present work has shown that the degeneracy associated with the three possible orientations of the impurity-vacancy complex can be removed by the application of an electric field. This produces three distinct energy states for dipole occupation, the relative population of these states being governed by a classical Boltzman distribution. It should be possible to use this technique in the study of Z centres where the presence of a neighbouring F centre may produce changes in the relative population of these states when compared with that of I.V. dipoles in uncoloured crystals.

Alternatively, one could perform an I.T.C. experiment in which a mechanical stress is used to produce dipole reorientation, rather than an electrical stress. The principal differences between mechanical and dielectric relaxation arise from the appropriate expressions for the relaxation rates being different. Further, the expressions for the mechanical relaxation have different

forms for stresses applied along the <100> and <111> , in marked constrast to dielectric relaxation which does not show this orientational dependence. The application of a small mechanical stress below the onset of plastic deformation would result in a repopulation different to that produced by an electric field and would produce different decays in the displacement currents or I.T.C. peaks when the crystal was allowed to relax.

The present work has also helped to determine, in a quantitative manner, the state of aggregation and dispersion of divalent manganese in sodium chloride as a function of temperature. This, coupled with previous work on the ageing characteristics of impurity-vacancy dipoles for this sytem [32] and the form of the aggregated phase,[5] has enabled a detailed picture of the behaviour of manganese in single crystals of sodium chloride to be drawn, Fig. (2.31). This will be useful in devising future experiments in which the role played by the impurity ion can significantly affect the physical properties of the crystal (mechanical properties, ionic conductivity and colour centre reactions).

The conductivity studies of Mn^{++}/NaCl over the temperature range 20°C to 600°C have provided estimates of h_a and s_a. They have also revealed that thermal dissociation of the n.n. manganese ion-vacancy dipole proceeds via the formation of intermediate higher order dipoles (n.n.n.). Evidence for this appears in the curvature of the reduced isotherm $\sigma/\sigma_s.\sigma$ over the temperature range 416°C to 496°C. The association reaction between 320°C and 393°C was described by a simple Stasiw-Teltow model with an enthalpy and entropy of association of 0.40 ± 0.10eV. and 1.40 ± 0.30 x 10^{-4}eV./°K. Fig. (2.31) also confirms that with the quenching temperatures used

The dispersion of Mn^{++} in sodium chloride.

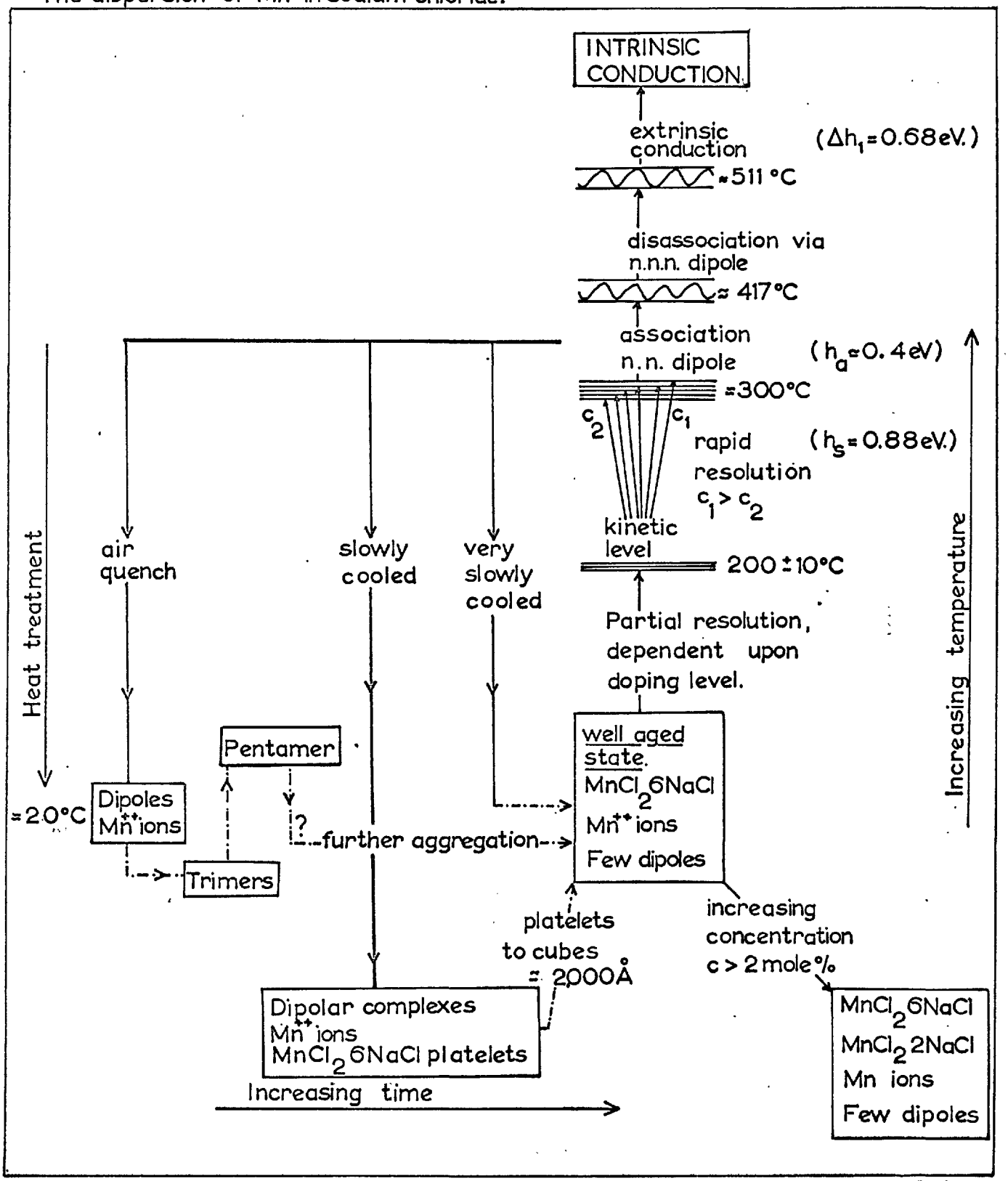

Fig. 2.32.

TABLE (2.4) – A SUMMARY OF NUMERICAL RESULTS OBTAINED IN THE PRESENT WORK

Units of enthalpy, eV.	Units of entropy, eV./^{o}K
h, Enthalpy of formation of Schottky pair 2.30 $\pm$ 0.02eV.	s, Entropy of formation of Schottky pair 0.52 x 10^{-3}eV./^{o}K
Δh_1 = 0.67 $\pm$ 0.01eV. = 0.69 $\pm$ 0.03eV. = 0.67 $\pm$ 0.02eV.	The enthalpy of motion of the cation vacancy. Obtained from three independent sets of data.
Δs_1 = 0.18 x 10^{-3}eV./^{o}K	Entropy of motion of cation vacancy.
Δh_2 = 1.60 $\pm$ 0.30eV. 2.00 $\pm$ 0.40eV.	Two independent estimates of the enthalpy of motion of the anion vacancy along sub-grain and grain boundaries.
Δs_2 = 1.57 x 10^{-3}eV./^{o}K	Entropy of motion of the anion vacancy along sub-grain and grain boundaries.
ν_r/ν_i = 1.655	Ratio of jump frequencies of ion in the bulk and ion next to vacancy.
$\mu_1 T$ = 1,590 x exp-(0.67 $\pm$ 0.02)/kT volt^{-1}.sec^{-1}.cm^{2}.^{o}K. n_1 = 4.57 x 10^{23} x exp-(1.16 $\pm$ 0.02)/kT vacancies/c.c.	
h_a = 0.30 $\pm$ 0.02eV. (θ_{III}) h_a = 0.40 $\pm$ 0.10eV. Isoth'ms s_a = 1.40 x 10^{-4}eV/^{o}K	Enthalpy and entropy of association for manganese ion and cation vacancy
Δh_o = 0.71 $\pm$ 0.01eV (D.R.) = 0.71 $\pm$ 0.02eV. (D.A.) = 0.65 $\pm$ 0.04eV. (I.T.C.) = 0.67 $\pm$ 0.01eV. (I.T.C.)	Enthalpy and entropy of re-orientation of manganese ion-cation vacancy complex Δs_o = 0.50 x 10^{-3}eV/^{o}K
h_s = 0.88 $\pm$ 0.10eV.	Enthalpy of solution of manganese ion into sodium chloride lattice.

in the I.T.C. experiments (400°C), there was little chance of observing the presence of n.n.n. impurity-vacancy dipoles. The isothermal analysis of the conductivity data suggests that their concentration only becomes appreciable in excess of 417°C. Extension of the I.T.C. studies to crystals quenched from these higher temperatures couldprove interesting, although devising a reproduceable and consistent quenching technique could present some difficulty.

The nature of the bonding and the physical properties of the aggregated Suzuki phase $MnCl_2.6NaCl$ present an interesting problem as yet unstudied. Isolation of this phase by careful control of impurity content, heat treatment and its subsequent detection by x-ray methods could lead to an unambiguous study. The e.p.r. results in the past have shown that only limited information about its structure can be obtained from the broad resonance signal associated with this phase. To confirm and investigate Suzuki's model the ENDOR technique would have to be applied to such a spectrum.

In conclusion, it may be said that a thorough investigation of ionic motion in sodium chloride and of the state of dispersion of divalent manganese in sodium chloride has been made over a temperature region from 20°C to 780°C and the principal numerical results to come from this investigation are finally summarized in Table (2.4).

REFERENCES

1. R.L. Fleischer: J.App.Phys., 33, 3504, 1962.

X-ray Studies

2. K. Suzuki: J.Phys.Soc. Japan, 16, 67, 1961.

3. K. Toman: Czech.J. Phys., 13, 296, 1963.

4. S. Miyake, K. Suzuki: J. Phys.Soc. Japan, 9, 702, 1954.

5. K. Suzuki: J.Phys.Soc. Japan, 10, 9, 1955.

E.P.R. Methods

6. B. Bleaney, D.J.E. Ingram: Proc.Roy.Soc., A.208, 143, 1951.

7. G.E. Pake: Paramagnetic Resonance, W.A. Benjamin, New York, 1962.

8. E.E. Schneider, J.E. Caffyn: Report of the Conference on Defects in Crystalline Solids, Phys.Soc., London, 1955.

9. J.H. Van Vleck: Phys. Rev., 74, 1168, 1948.

10. E.E. Schneider: Conference on Radio & Microwave Spectroscopy, Duke University, 1957.

11. K. Morigaki, M. Fujimoto, J. Itoh: J. Phys.Soc. Japan, 13, 10, 1958.

12. G.D. Watkins, R.M. Walker: Bull.Amer.Phys.Soc., 1, 324, 1956.

13. B. Bleaney: Phil Mag., 42, 441, 1951.

14. G.D. Watkins: Phys. Rev., 113, 79, 1959.

15. C.N. Owston: Proc. Phys.Soc., 88, 205, 1966.

16. H.F. Symmons, R.C. Kemp: B.Jour.App.Phys., 17, 607, 1966.

17. G. Alzetta, P.R. Crippa, S. Santucci: Phys.Stat.Sol, 12, 2, 1965.

18. K. Kawamura, Okuba: J.App.Phys. 33, 376, 1962.

19. E. E. Schneider: Proc. University of Durham Phil.Soc. XIII, 1961.

20. J. Quin: Ph.D. Thesis, University of London, 1967.

21. K. Oshima, H.Abe, H. Nagano, H. Nagusa: J. Chem.Phys. 23, 9, 1955.

22. K.G. Bansiger, E.E. Schneider: J.App.Phys., 33, 383, 1962.

Dielectric relaxation and absorption

23. A.B. Lidiard: Report of the Conference on Defects in Crystalline Solids, Phys. Soc., London, 1955.

24. R.G. Breckenridge: J.Chem.Phys., 16, 959, 1948.

25. J.S. Dryden, J. Rao: J.Chem.Phys., 25, 222, 1956.

26. J.S. Dryden, R.J. Meakens: Disc. Faraday Soc., 23, 39, 1957.

27. E. Burstein, J.W. Davidson, H. Scalar: Phys. Rev., 96, 819, 1954.

28. G. Jacobs: Naturwissenschaften, 42, 575, 1955.

29. J.S. Cook, J.S. Dryden: Aust. J. Phys., 13, 260, 1962.

30. Y. Haven: Report of the Conference on Defects in Crystalline Solids, Phys. Soc., London, 1955.

31. J.S. Cook, J.S. Dryden: Proc. Phys. Soc., 80, 479, 1962.

32. J.S. Dryden: Proc. Int. Con. on Crystal Lattice Defects, Con. J. of Phys. Soc. Japan, 1962.

33. J.S. Dryden, S. Morimoto, J.S. Cook: Phil. Mag., 12, 116, 1965.

34. G.D. Watkins: Phys. Rev., 113, 91, 1959.

35. R.W. Dreyfus: Phys. Rev., 121, 6, 1961.

36. P.H. Sutter, A.S. Nowick: J. App. Phys., 34, 734, 1963.

37. R.W. Dreyfus, R.B. Laibowitz: Phys. Rev., 135, 1413, 1964.

38. V.N. Lozovoski: Izv. Akad. Nauk. S.S.S.R., 24, 161, 1960.

39. A.D. Franklin, A. Shorb, J.B. Watchman: J. Res. National Bureau of Standards, 68A, 5, 1964.

Ionic Conductivity

40. O. Stasiw, J. Teltow: Ann. Physk., 1, 261, 1947.

41. S.C. Jain, S.L. Dahake: Indian Jour. Pure & App. Phys., 2, 3, 1964.

42. A.B. Lidiard: Phys. Rev., 94, 29, 1954.

43. A.R. Allnatt, M.H. Cohen: J. Chem. Phys., 40, 1860, 1964.

44. A.R. Allnatt, M.H. Cohen: J. Chem. Phys., 40, 1871, 1964.

45. P. Debye, E. Huckel: Physikalische Zeitschrift, 24, 185, 1923.

46. H.W. Etzel, R.J. Maurer: J. Chem. Phys., 18, 8, 1950.

47. C. Bean; Thesis, University Illinois, 1952.

48. J. Quin, B. Redfern, P.L. Pratt: Proc. Brit. Ceram. Soc., 9, 35, 1967.

49. H. Kanzaki, K. Kido, S. Tamura: J. Phys. Soc. Japan, 20, 2305, 1965.

50. S.J. Rothman, L.W. Barr, A.H. Rowe, P.G. Silwood: Phil. Mag. 14, 501, 1966.

51. R.W. Dreyfus, A.S. Nowick: 126, 1367, 1962.

52. R.W. Dreyfus: App. Phys. Letts., 3, 175, 1963.

53. G.D. Miles: J. App. Phys., 36, 1471, 1965.

54. K. Yagi, G. Hunjo: J. Phys. Soc. Japan, 19, 1892, 1964.

55. R.A. Kahn, Thesis, University of London, 1967.

56. C.A. Bucci, S.C. Riva: J.Phys.Chem.Sol., 26, 363, 1965.

57. C. Bucci, R. Fieschi, G. Guidi: Int. Symp. Colour Centres in Alkali Halides, University of Illinois.

58. S.H. Maron, C.F. Prutton: Principles of Physical Chemistry, The Macmillan Company, New York, 1958.

59. L. Onsager: Physik. Zeit., 27, 388, 1926.

60. H. Falkenhagen: Electrolytes, Oxford University Press, New York, 1934.

61. J.R. Reitz, J.L. Gammel: J. Chem. Phys., 19, 7, 1951.

62. F. Bassani, F.G. Fumi: Phil.Mag., 45, 228, 1954.

63. A.B. Lidiard: Phys. Rev., 94, 1, 1954.

64. N. Bjerrum: Kgl. Danske Videnskab., 7, No. 9, 1926.

65. L. Onsager: Z. Phys., 28, 286, 1927.

66. E. Pitts: Proc. Roy. Soc., A217, 43, 1953.

67. A.J. Dekker: Solid State Physics., Macmillan & Co. Ltd., 1963.

68. I.M. Boswarva, A.D. Franklin: Phil.Mag., 11, 335, 1965.

69. A.R. Allnatt, P.W.M. Jacobs: Trans. Farad. Soc., 58, 116, 1962.

70. Y. Haven: Rec. Trav. Chem. Pays. Bas., 69, 1471, 1950.

71. A. Khan: Private Communication.

General Topics.

72. B.N. Matsonashvili: Bull. Acad. Sciences, U.S.S.R., 22, 294, 1958.

73. Y. Haven: J. Chem. Phys., 21, 171, 1953.

74. R.P. Harrison: Thesis, University of London, 1965.

75. F.M. Johnson, A.H. Nothercot: Phys. Rev., 114, 705, 1959.

76. R.A. Erickson: Phys. Rev., 90, 779, 1953.

77. S.C. Jain, D.C. Parashar: Phys. Letts., 4, 36, 1963.

78. M. Stucke: Report, Metallurgy Dept., Imperial College, 1967.

79. C. Sandonnini, G. Scarpa: contained in Phase Diagrams for Ceramacists, E.Levin, C. Robbins, H.F. MacMurdie, American Ceram. Soc., 1964.

PART III

EXPERIMENTAL CONSIDERATIONS.

PART III - EXPERIMENTAL CONSIDERATIONS

(i) Crystal Growth

Both pure and doped single crystals of sodium chloride were grown from the melt, using a modified Kyropoulos technique.[1] It would appear that there are significant differences in the mechanical and electrical properties of crystals grown in air, and those grown in vacuum.[2] As previous work on mechanical properties had been concerned with crystals grown in air,[3] the advantage of correlating mechanical properties with information obtained from electrical properties would have been missed if vacuum-grown crystals had been introduced. The crystal growing rig is presented in Fig. (3.1). Analytical grade sodium chloride was contained in a Vitreosil silica beaker. Before crystal growth, the powder was held at 400°C overnight to drive off any moisture. After the sodium chloride had been melted, a single crystal seed was inserted into the melt. A "foot" was allowed to grow onto this seed, and when it had grown to a sufficient size was gradually pulled from the melt by the rotating, water-cooled, nickel-plated chuck. The rotation evened out any temperature gradients in the melt and produced a crystal free of grain boundaries. Fig. (3.2) [4]. To reduce the silicon content of the crystals, any given melt was only used twice to produce crystals. If the melt was left in contact with the beaker for periods of days, the beaker surface was attacked and dissolved, producing crystals of high background impurity content. All doped crystals were produced by adding known amounts of analytical grade manganese chloride to the melt.

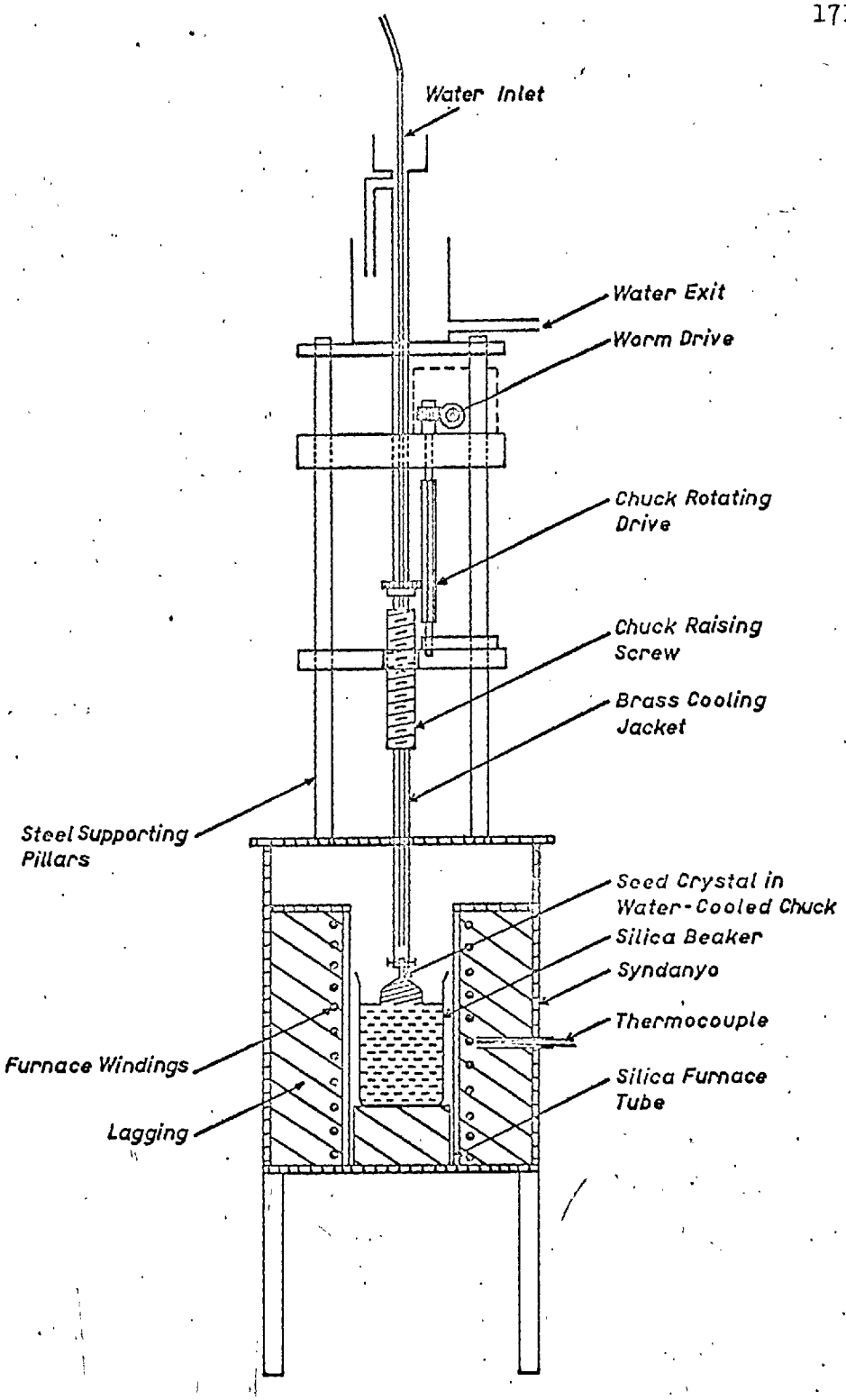

The crystal growing rig Fig. 3.1.

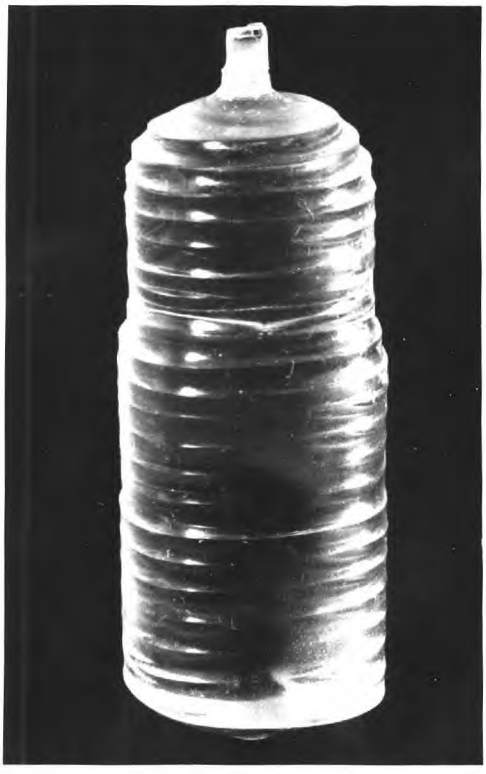

A Typical single crystal Fig.(3.2)

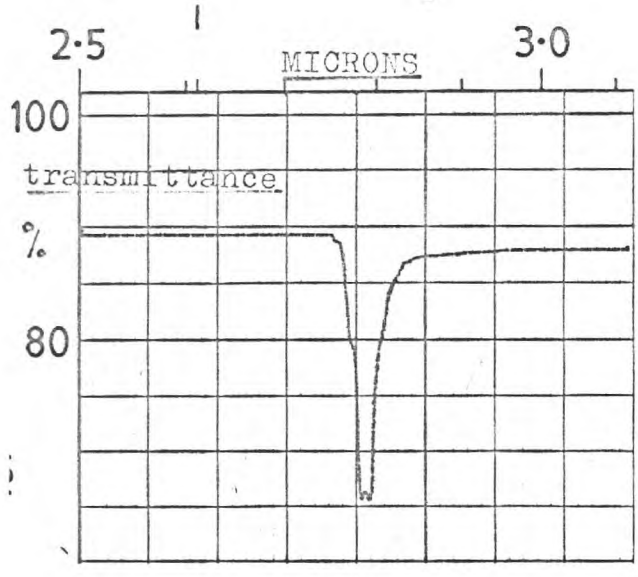

The form of optical absorption in Ca^{++}, $(OH)^{-}$ doped NaCl Fig. 3.2.

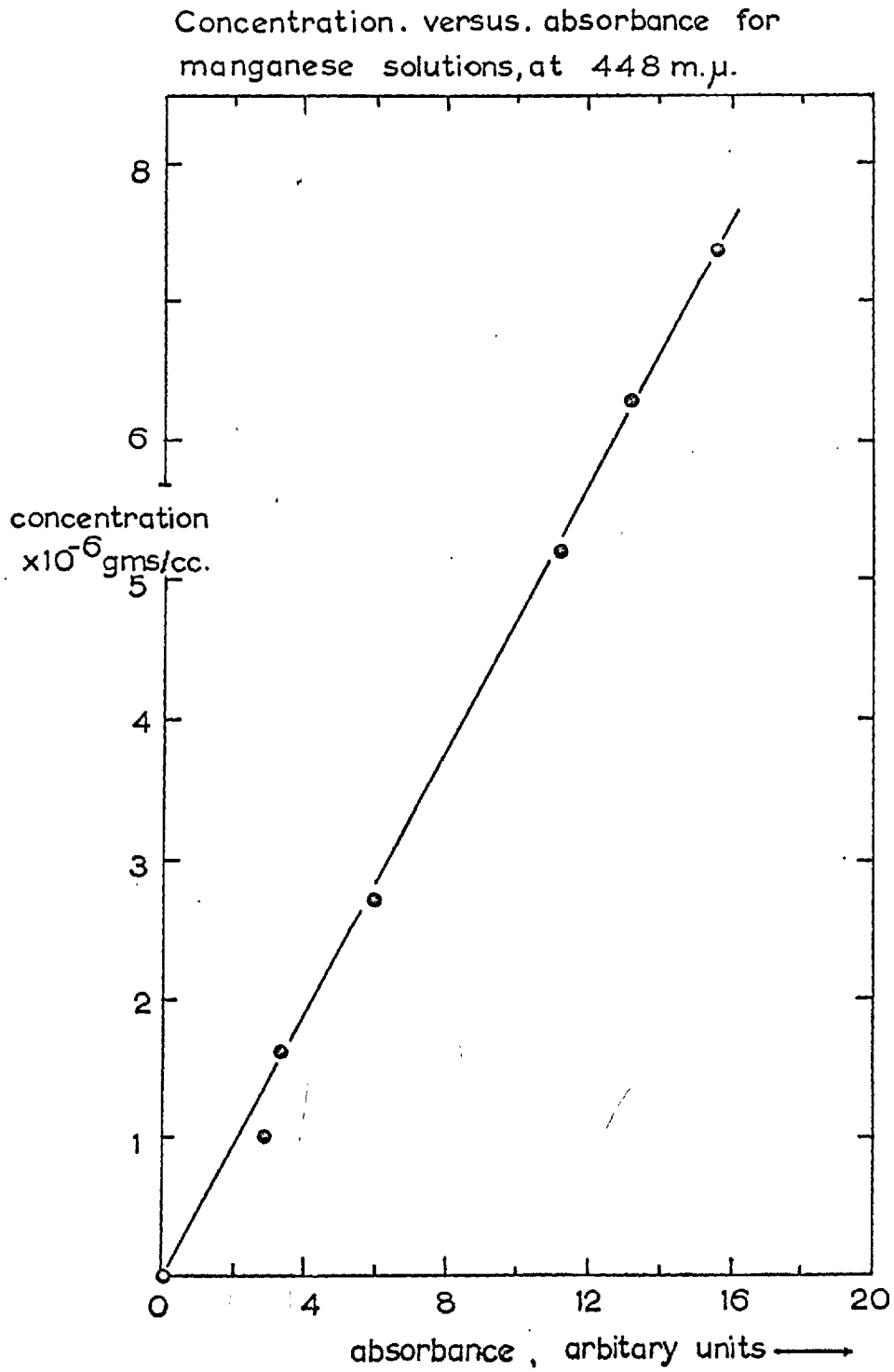
Concentration. versus. absorbance for
manganese solutions, at 448 m.μ.
concentration
x10⁻⁶gms/cc.
8
6
5
4
3
2
1
0
4
8
12
16
20
absorbance, arbitary units

Fig. 3.3.

Two methods of impurity analysis were applied to the crystals. Spectrographic analysis determined, in a semi-quantitative manner, the total background impurities present in the crystal. This analysis was performed commercially, and from it the crystals possessing the smallest background impurity content were chosen. To determine the manganese content, a colorimetric method was used.

(ii) Analysis of Manganese Impurity Content

The quantitative estimation of manganese content in the crystals was based upon the use of formaldoxime as an indicator. Manganese in alkaline solution gives a soluble, reddish brown colouring with formaldoxime ($H_2C - NOH$). The coloured compound is said to be $(CH_2NO)_3$ Mn. with manganese present in the trivalent state.[5] Indicator solutions were prepared by dissolving 10 gms. of paraformaldehyde and 23.5 gms of hydroxylamine in 75 c.c. of deionized water, and boiling gently. The solution was allowed to cool and then made up to 100 c.c. with deionized water. Standard solutions were obtained by dissolving pure manganese in dilute nitric acid, and then boiling the solution to drive off oxides of nitrogen. The weight of the dissolved manganese was measured to six significant figures, using a micro-balance. A known quantity of the sample solution was placed in a 100 c.c. standard flask. The solution was made alkaline by the addition of 5 c.c. of ammonia solution (S.G.0.88). 1 c.c. of the indicator was added and the solution made up to 100 c.c. with deionized water. The absorbance was then measured on a Perkin Elmer spectrophotometer at a wavelength of 448 mμ. Beer's Law was obeyed over the range of concentrations used. Fig. (3.3). The

process was then repeated using a known weight of the sodium chloride, in place of the pure manganese.

The presence of the anion impurity, $(OH)^-$, was detected by measuring the optical absorption in the infra-red at 2.8 . Only in one heavily doped manganese crystal was there any indication of $(OH)^-$ not intentionally present. This crystal was rejected.

The typical impurities present in the crystals are shown in Table (3.1). In the pure crystals, calcium is the main impurity. This could not be removed by zone-refining, as the calcium ion has equal solubility in the melt and the solid phase of sodium chloride.

(iii) Conductivity and Transient Current Instrumentation

Equipment for measuring conductivity at room temperature and below was developed. This enabled the measurement of small currents of the order of 1 femtoamp (10^{-15} amps) upwards. With this a cell was constructed, which provided adequate electrical screening, high insulation resistance, constant temperature and an inert atmosphere surrounding the crystal. The need to have a current detecting system with a fast response time, posed an additional problem when measuring the transient currents produced by the dielectric relaxations.

To obtain conductivity data at high temperatures (300°C to the melting point), equipment was designed and built to measure the crystal's capacity and conductance as a function of the frequency of an applied alternating electric field, for any fixed temperature. In this way space charge effects were eliminated at high temperatures by measuring the A.C. conductivity at a frequency greater than 1.5kc/s.

TABLE (3.1)

Spectrographic Analysis of Pure

and Doped Sodium Chloride Crystals.*

Impurity	Pure (C) (NaCl)	Pure (D) (NaCl)	700 m.p.p.m. Mn^{++} (Doped NaCl)
Ca^{++}	0.001%	0.0005%	0.001%
Si^{++}	-	-	-
Mn^{++}	-	-	0.30%
Mg^{++}	-	-	-
Fe^{++}	-	-	0.005%
Al^{++}, Al^{+++}	Less than 0.001% in both		-
Cu^{++}	0.0008%	0.0005%	0.0005%
Ba^{++}	-	-	-
Cd^{++}	-	-	-

* Quantitative spectrographic analysis performed by

American Spectrographic Laboratories, Inc.,
557, Minna,
San Francisco.

(1) Low Temperature Conductivity and Dielectric relaxation measurements

The conductivity probe used for measurements at low temperatures is shown in Fig. (3.4). Readings at room temperature and below were achieved by filling the large Dewar with siutable coolants. Although this particular probe possessed excellent thermal stability ($\pm \frac{1}{2}^{o}$C over a period of one hour), its input capacity was large enough to make its response time too slow for the measurement of very fast relaxation currents. Temperature control was achieved by using an anticipatory controller to regulate the power supplied to a nichrome wire, wound furnace. The insulation resistance was maintained in excess of 10^{15} Ohm cm.$^{-1}$ by the use of carefully prepared silica glass supports for the electrodes and P.T.F.E. mounting blocks for the electrometer valve and the connections.

All other leads (high tension, thermocouple, power leads) were carefully screened by flexible copper sheathing, the screening being connected to a good earth point. The probe unit was enclosed by a gas-tight copper can. Into this a constant flow of high purity argon gas was maintained. It was essential that all traces of moisture were removed from this gas flow, as it would have condensed out upon the crystal's surface, when working below room temperature. The gas was dried by first passing it through drying tubes containing phosphorous pentoxide and then through a liquid nitrogen vapour trap. The electrodes were constructed from nickel blocks whose surfaces had been ground optically flat. This surface was painted with a colloidal graphite suspension to ensure good Ohmic contact between the electrode

Low temperature conductivity probe. Fig. 3.4.

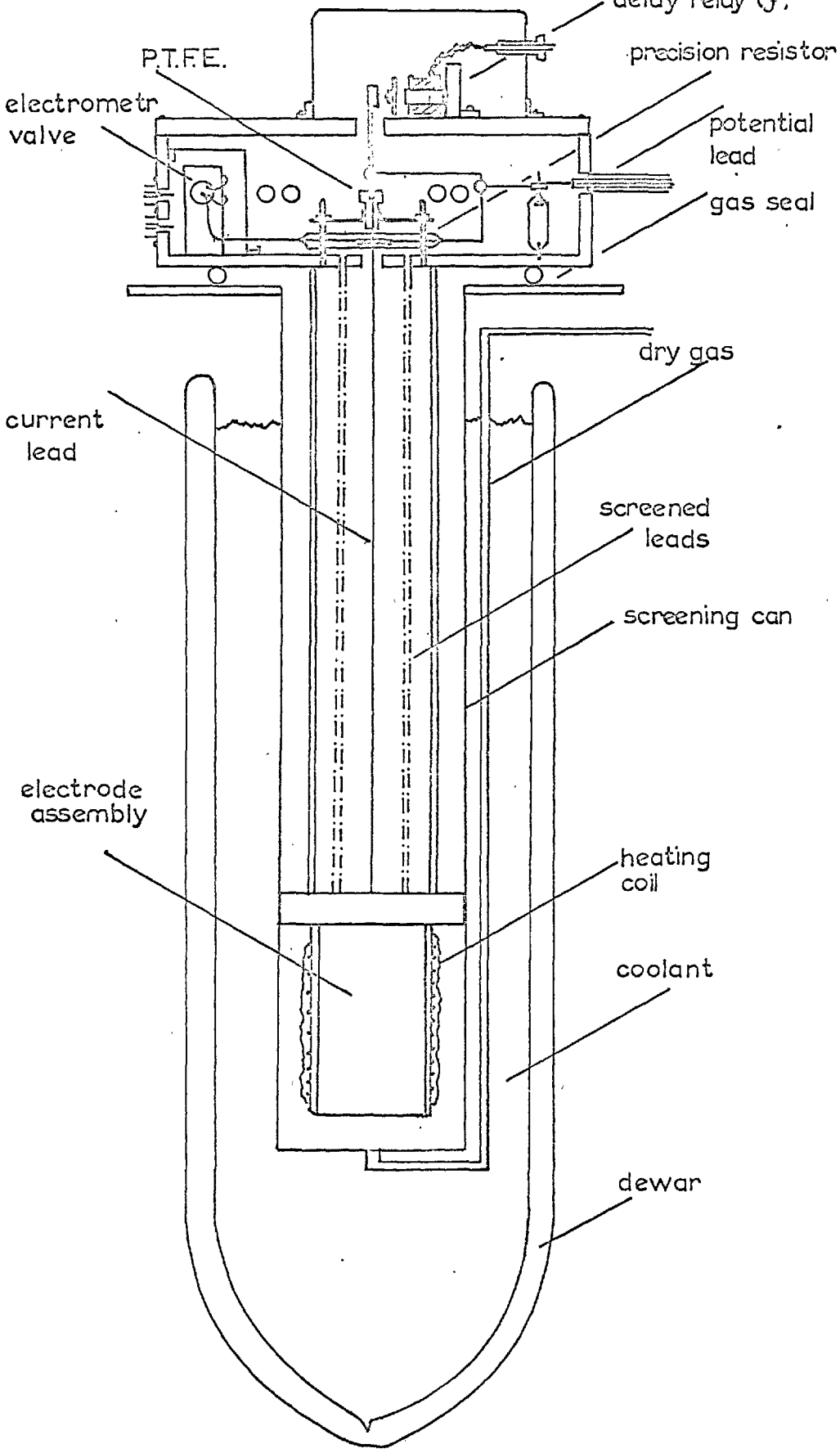

Low temperature probe

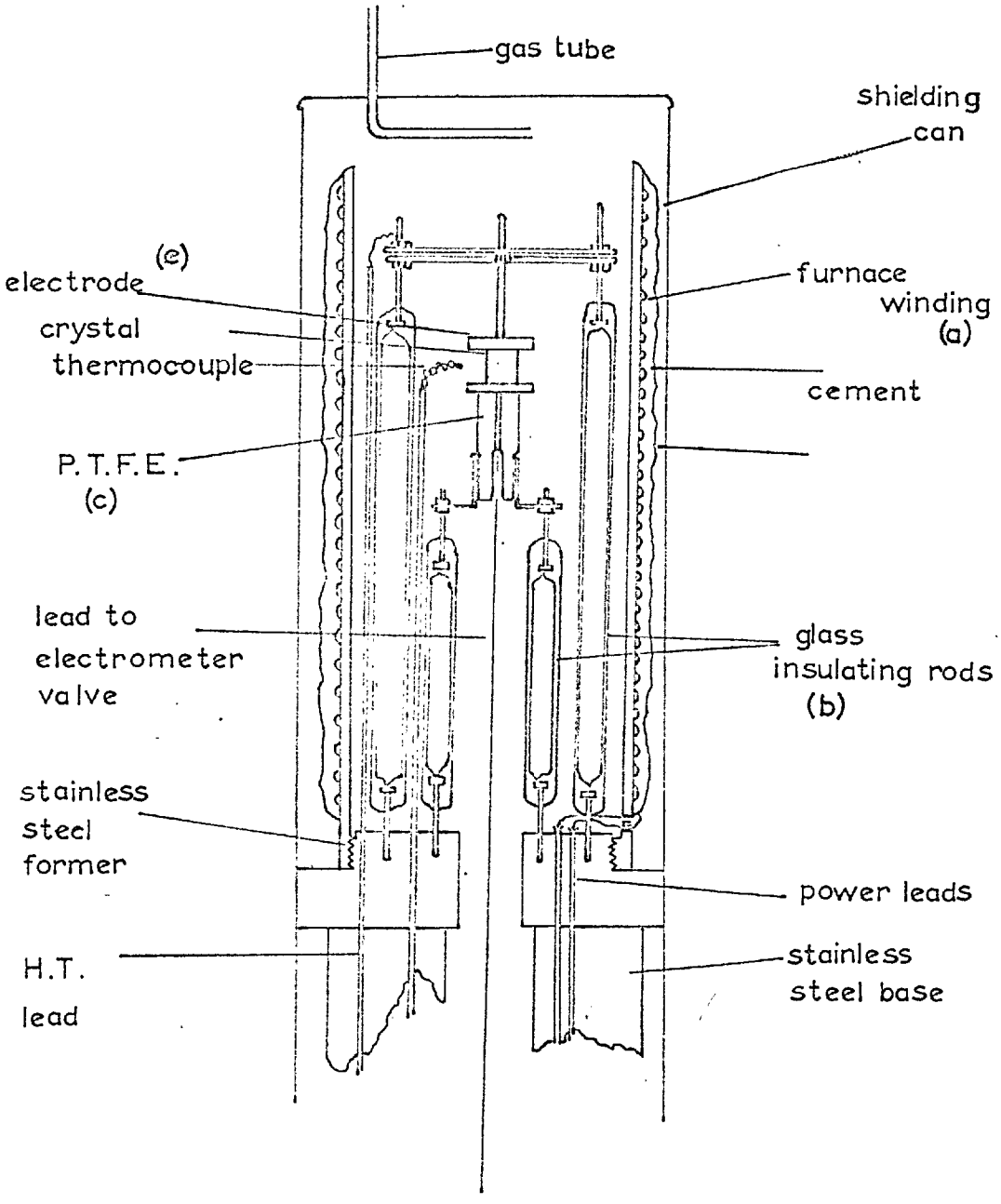

Fig. 3.4.

surface and the crystal. An electrometer valve was used in preference to a vibrating reed electrometer, because of its relative cheapness and fast response time.(6) Its disadvantages were its susceptibility to vibration and light, and a tendency to "zero drift" when subjected to thermal fluctuations. These defects were minimized by enclosing the valve in a light tight box in the head of the probe unit.

The current to be measured was fed through a precision resistor. The value of the resistors used, ranged from 10^6 Ohms to 10^{11} Ohms and were calibrated with respect to a Welwyn standard resistor. The voltage developed across this resistor was then applied to the grid of the electrometer valve, and because the input impedance of the valve is greater than 10^{16} Ohms, the signal was not shorted out. This variation in grid voltage produces a variation in the anode current. By choosing a linear region of the V_g/I_a characteristic, these variations are directly related, Fig. (3.5). The variation in anode current I_a produces a variation in Va and it is this voltage variation which monitors the successive stages of amplification, Fig. (3.6). Differential negative feedback was applied from the amplifier output to the base of the grid resistor. The principal effect of feedback being applied to any D.C. amplifying element, is a reduction in gain and response time, with an increase in the length of linearity of its amplifying characteristics. Care must be exercised when measuring small transient currents, as these could readily be produced by the transient response of the valve's input impedance; for this reason, when observing transient currents, the value of the input resistor was kept to a minimum value for the particular current being measured.

Block diagram of low temperature equipment.

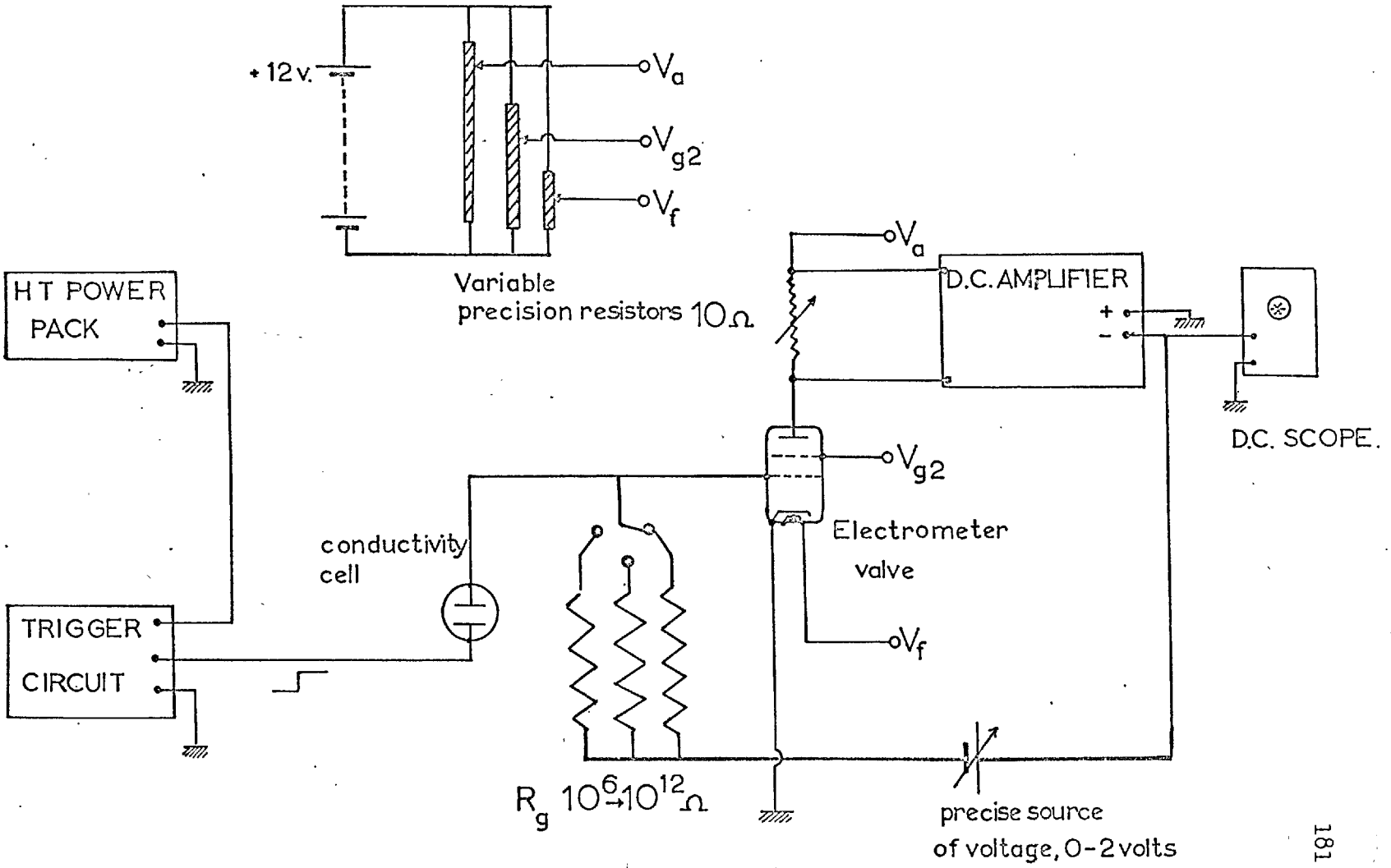

Fig. 3.6.

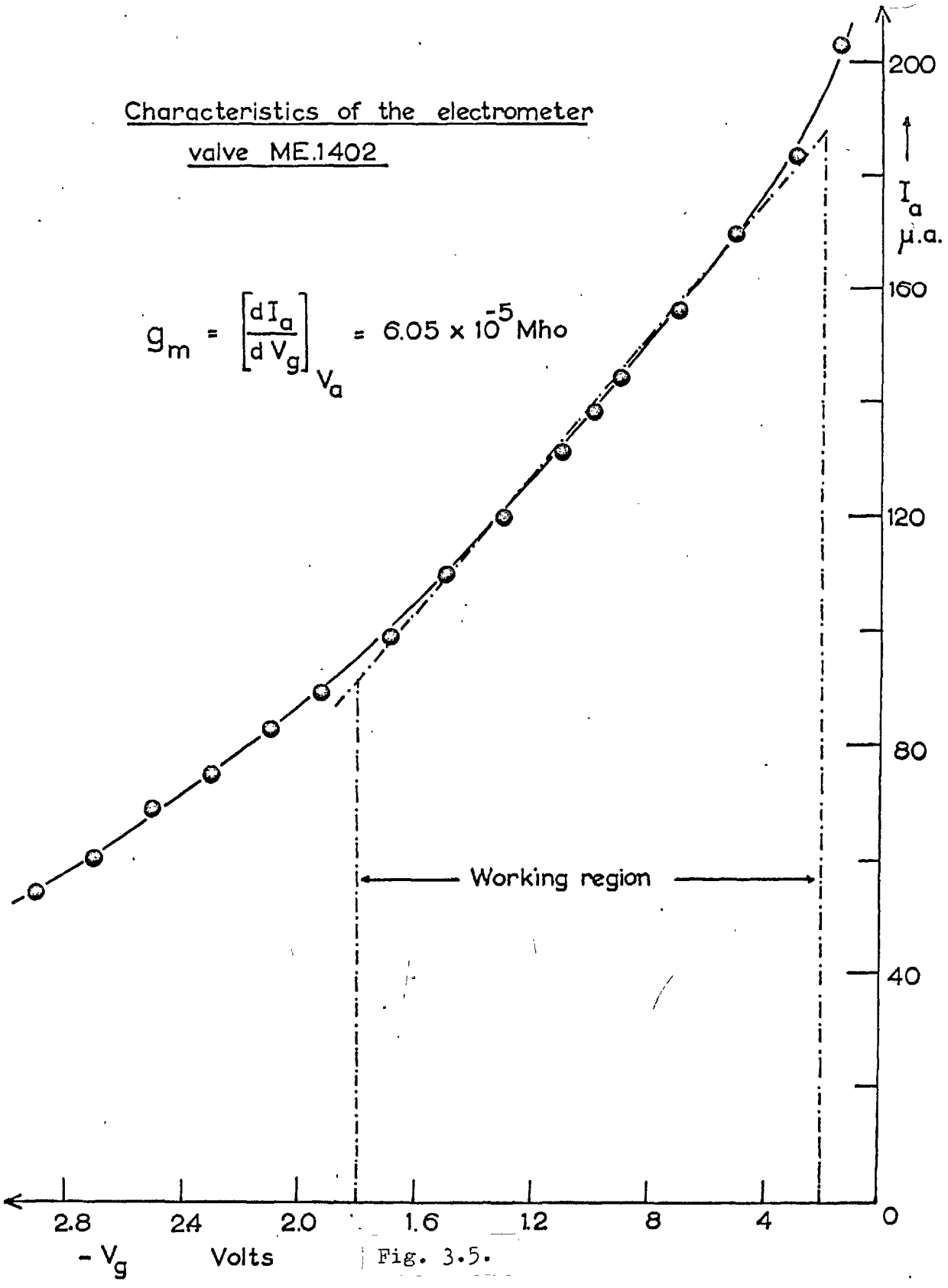
Characteristics of the electrometer valve ME.1402
$g_m = \left[\frac{dI_a}{dV_g}\right]_{V_a} = 6.05 \times 10^{-5}$ Mho
200
160
120
80
40
0
I_a μ.a.
Working region
2.8
2.4
2.0
1.6
1.2
8
4
$-V_g$ Volts

Fig. 3.5.

Further amplification was achieved by using a D.C. transistorized amplifier. A D.C. amplifier should have a gain which is linear over the working range of input voltage plus a negligible zero drift. The transistor amplifier shown in Fig. (3.7) was constructed and had the characteristics shown in Fig. (3.8). The original design utilized germanium transistors. These were rejected because of the appearance of a large zero drift when the temperature of the transistors changed. A considerable reduction in zero drift was achieved, Fig. (3.9), by the substitution of silicon transistors, which were less susceptible to thermal fluctuations, and by mounting these in a copper block to thermally isolate them. The output transient signals were recorded upon a Honeywell recorder and a Nagard Oscilloscope.

To calibrate the equipment, a vernier potentiometer was inserted in the feedback line. For calibration, a zero position was chosen on the oscilloscope and recorder, and any deflection produced by a steady state crystal current was annulled by varying the voltage in the feedback line. This gave an accurate value for the voltage drop produced across the resistor by the crystal current. In a similar manner, calibration charts were obtained to analyze transient crystal currents.

The electric fields applied to the crystal were produced by a commercial power pack supplying stabilized voltages up to 500 volts. A "Schmit" trigger circuit and thyratron valve used in conjunction with this power pack produced a well defined step voltage, with a rise time of less than 1 m.sec., Fig. (3.10). This circuit also supplied the power to the relay situated on the probe head: the purpose of this relay was to short out the input circuitry for a period

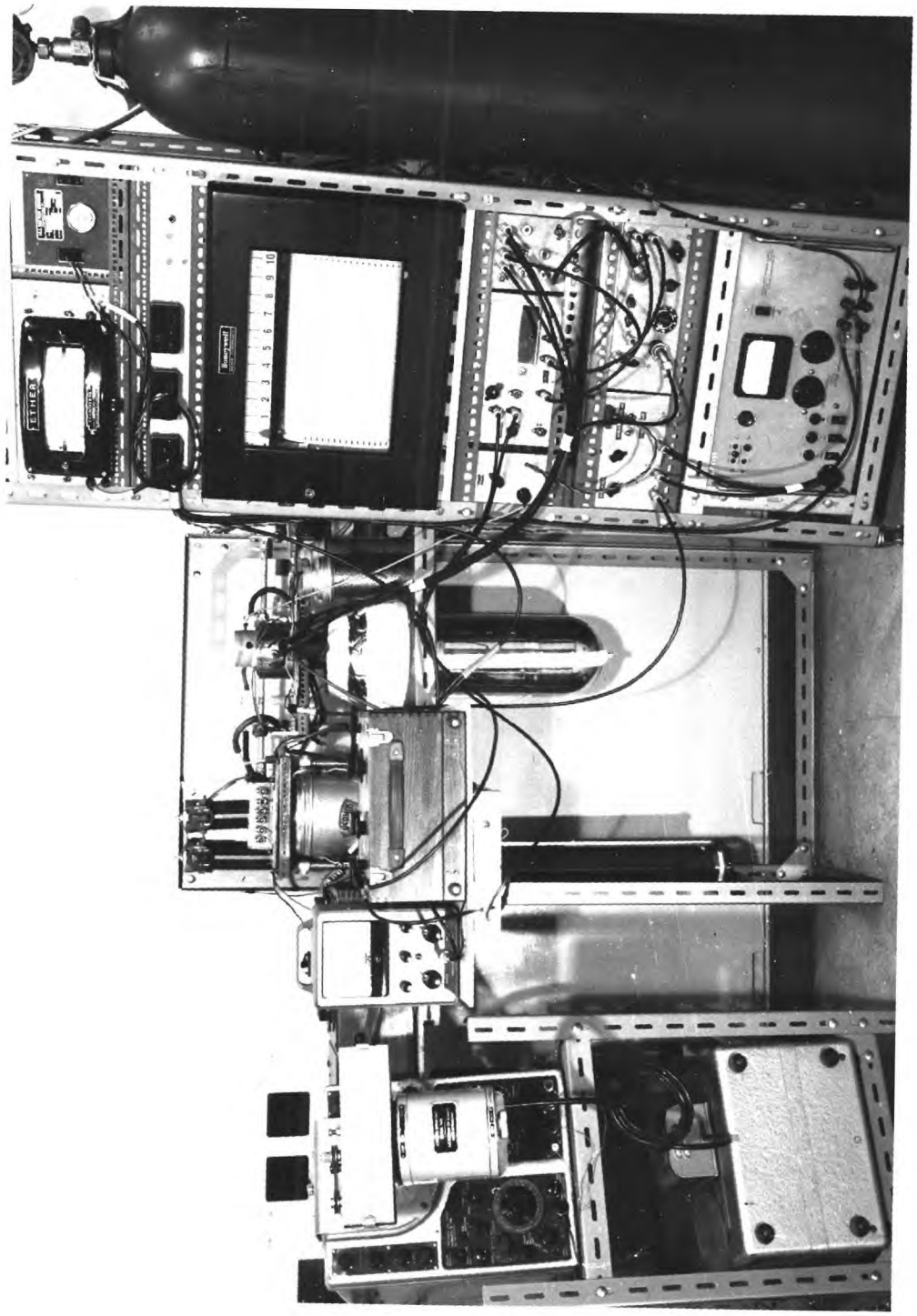

Low temperature conductivity rig.

DC TRANSISTORISED PUSH-PULL AMPLIFIER.

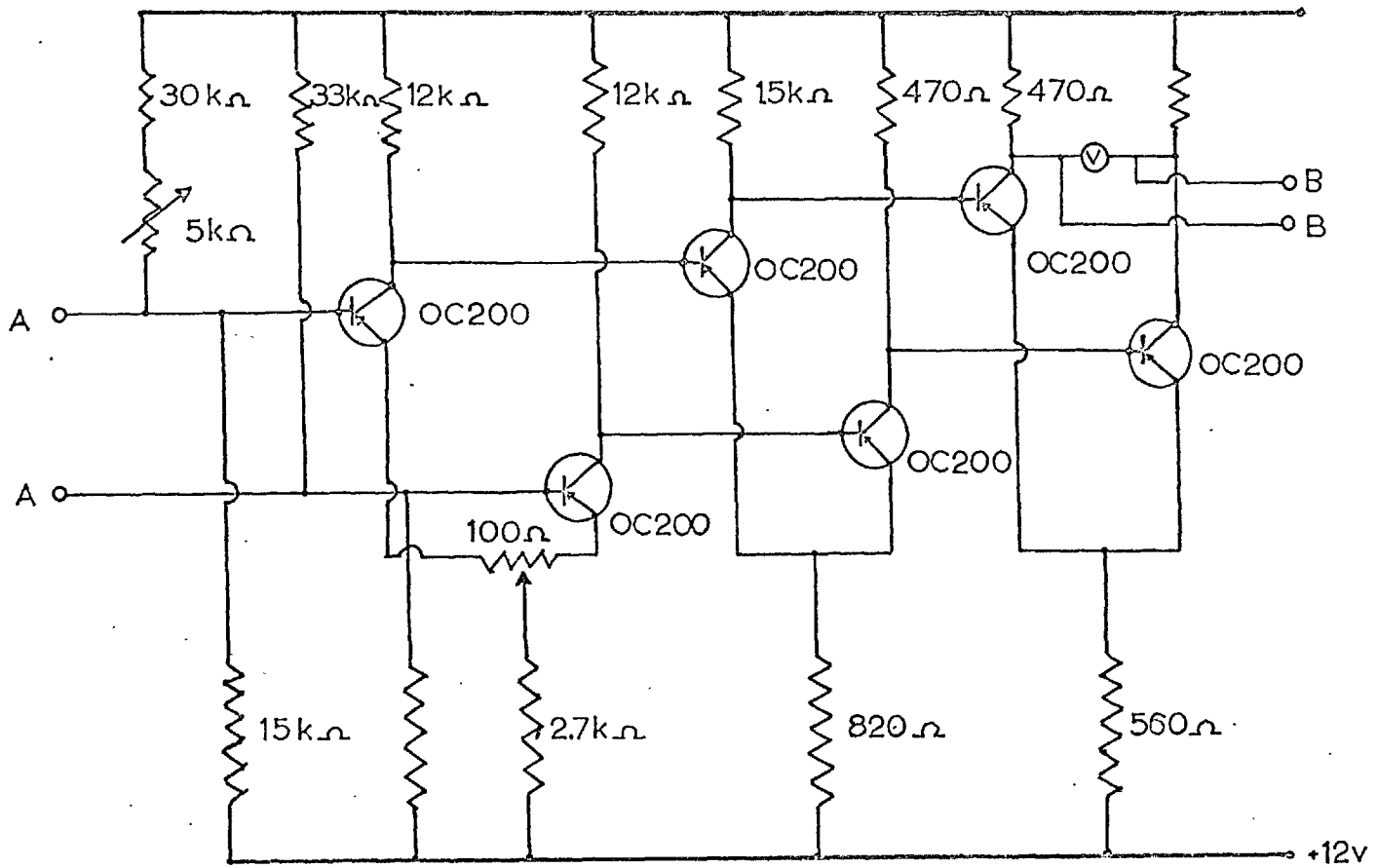

Fig. 3.7.

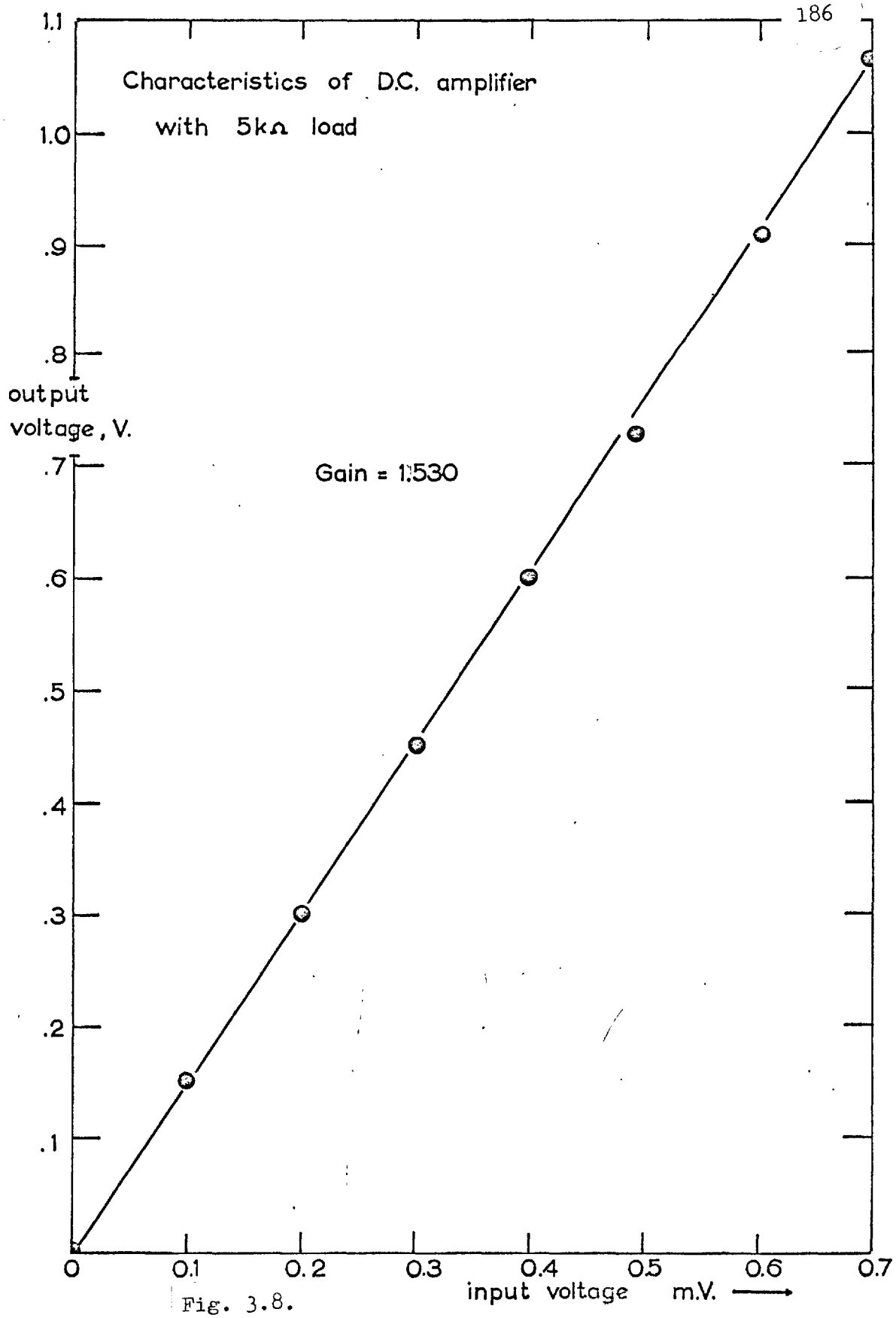
Characteristics of D.C. amplifier
with 5kΩ load
Gain = 1:530
output voltage, V.
1.1
1.0
.9
.8
.7
.6
.5
.4
.3
.2
.1
0
0.1
0.2
0.3
0.4
0.5
0.6
0.7
input voltage m.V.

Fig. 3.8.

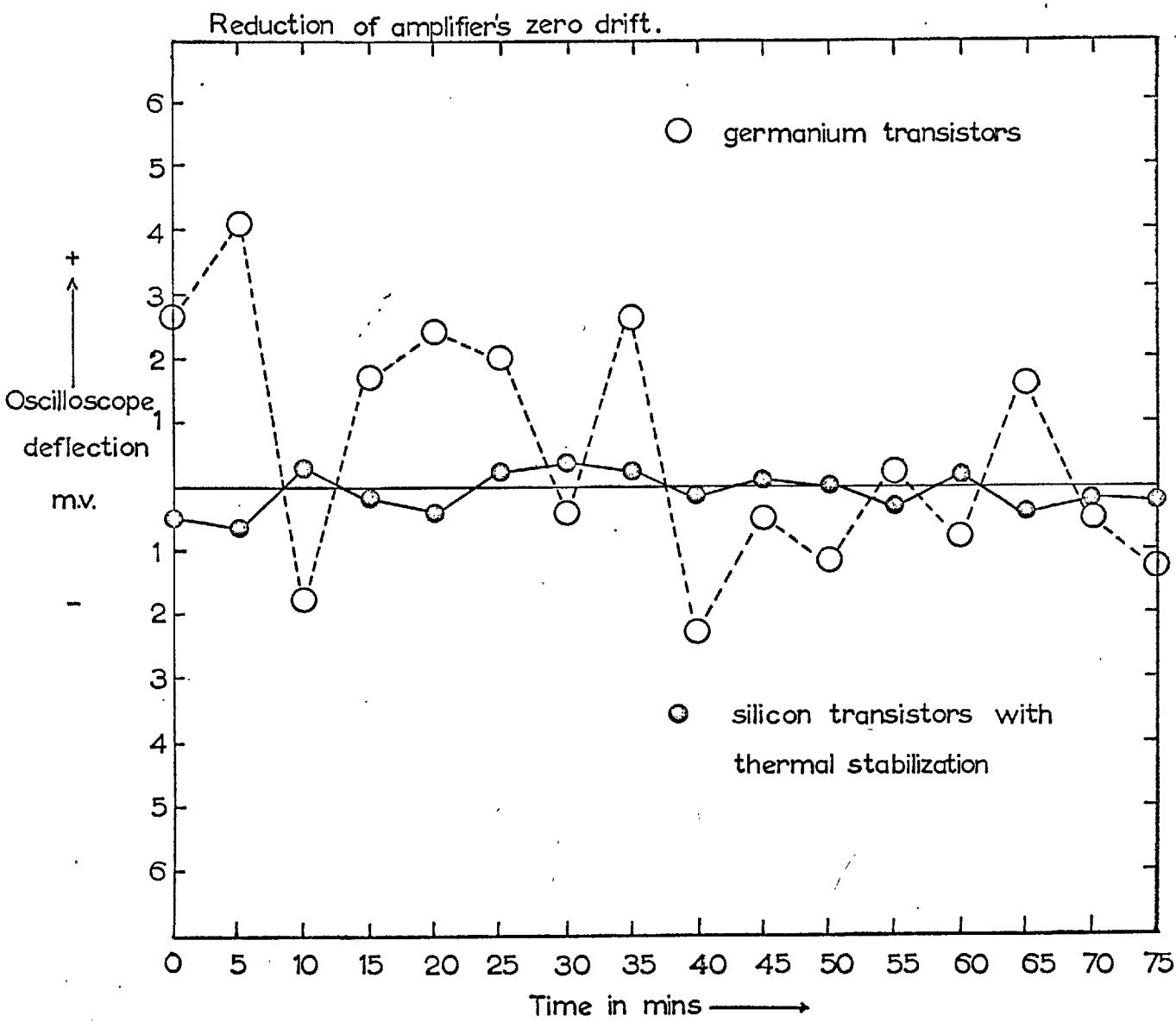
Reduction of amplifier's zero drift.
germanium transistors
silicon transistors with thermal stabilization
Oscilloscope deflection m.v.
+
-
6
5
4
3
2
1
1
2
3
4
5
6
0
5
10
15
20
25
30
35
40
45
50
55
60
65
70
75
Time in mins

Fig. 3.9.

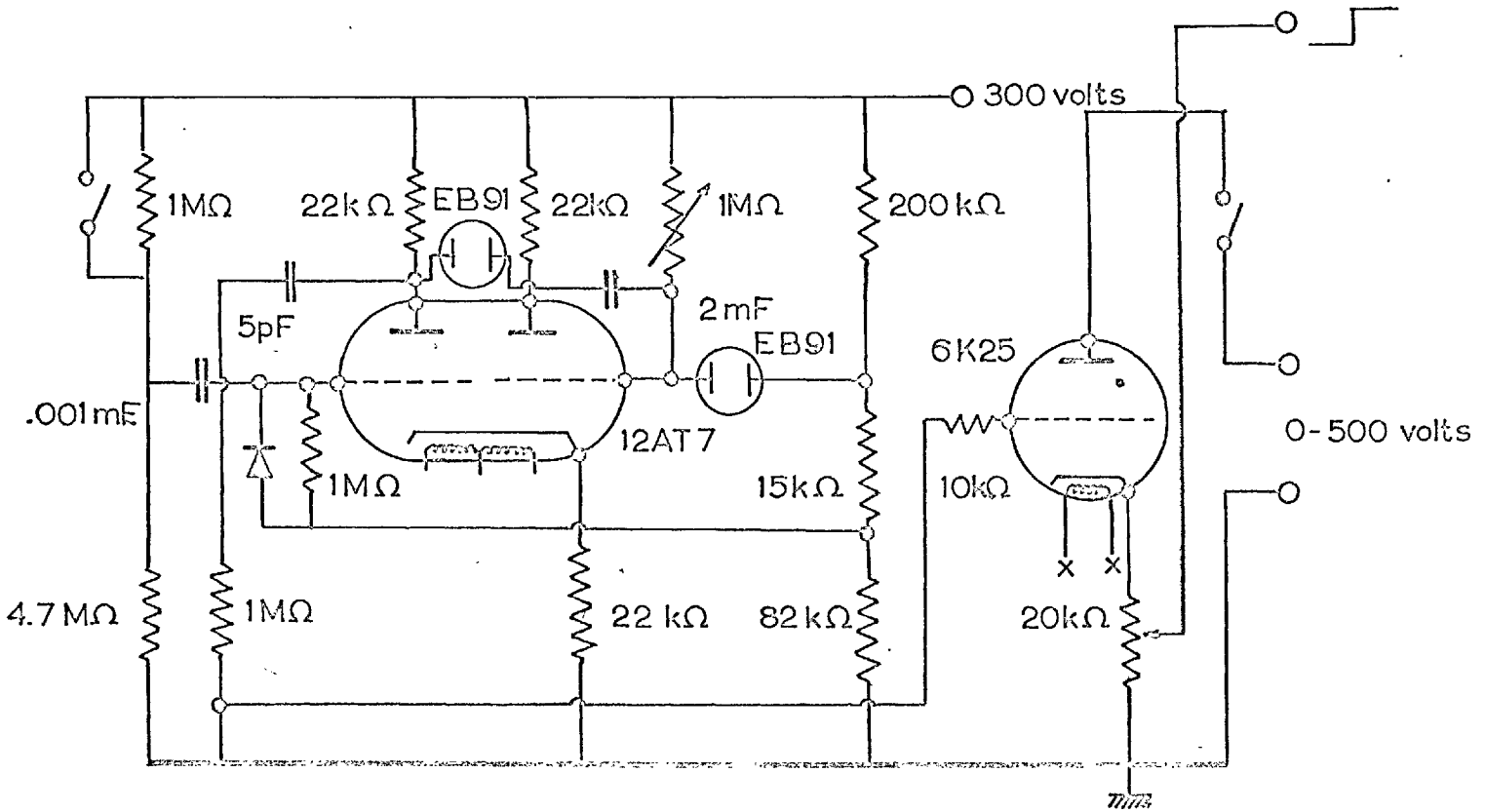

H.T. switching and delay circuit. Fig. 3.10.

of 10 m.sec., thus discharging any spurious charges induced by the switching on or off of large electric fields. Power for both the amplifier and electrometer valve was obtained from 12 volt, heavy duty, Mallory cells. These were convenient in that they possessed long term stability and were small enough to be mounted in the instrument cases, where they were free from the effects of pick-up.

Temperatures were measured with a chromel-alumel thermo-couple, with a compensating lead immersed in an ice-water mixture at $0^{\circ}C$. All thermo-couples used were calibrated with a platinum - platinum rhodium standard thermo-couple. A source of possible error was the difference between the crystal temperature and that recorded by the thermo-couple. To examine this error, an auxiliary thermo-couple was placed into a hole drilled in a sodium chloride specimen. The crystal's temperature was then monitored while the crystal environment was subjected to a sharp change in temperature. The heating curve Fig. (3.11) shows the need to maintain the crystal at its test temperature for at least one hour, in order to achieve thermal equilibrium throughout the crystal. This effect presumably arises from the poor thermal conductivity of sodium chloride, and may be partly avoided by the use of thin specimens.

As mentioned previously, the large input capacity of the conductivity probe made it unsuitable for the measurement of fast relaxation currents. To reduce the input capacity and hence the response time, the probe shown in Fig. (3.12) was constructed. This was an improvement in that the input capacity was only that of the electrometer valve's electrode leads (order of 3pF), resulting in an order of magnitude decrease in the response time. (600 m.sec. as compared with 5 secs.). The electrometer valve and calibrated

The thermal lag involved in heating a crystal to 305°C. Fig. 3.11.

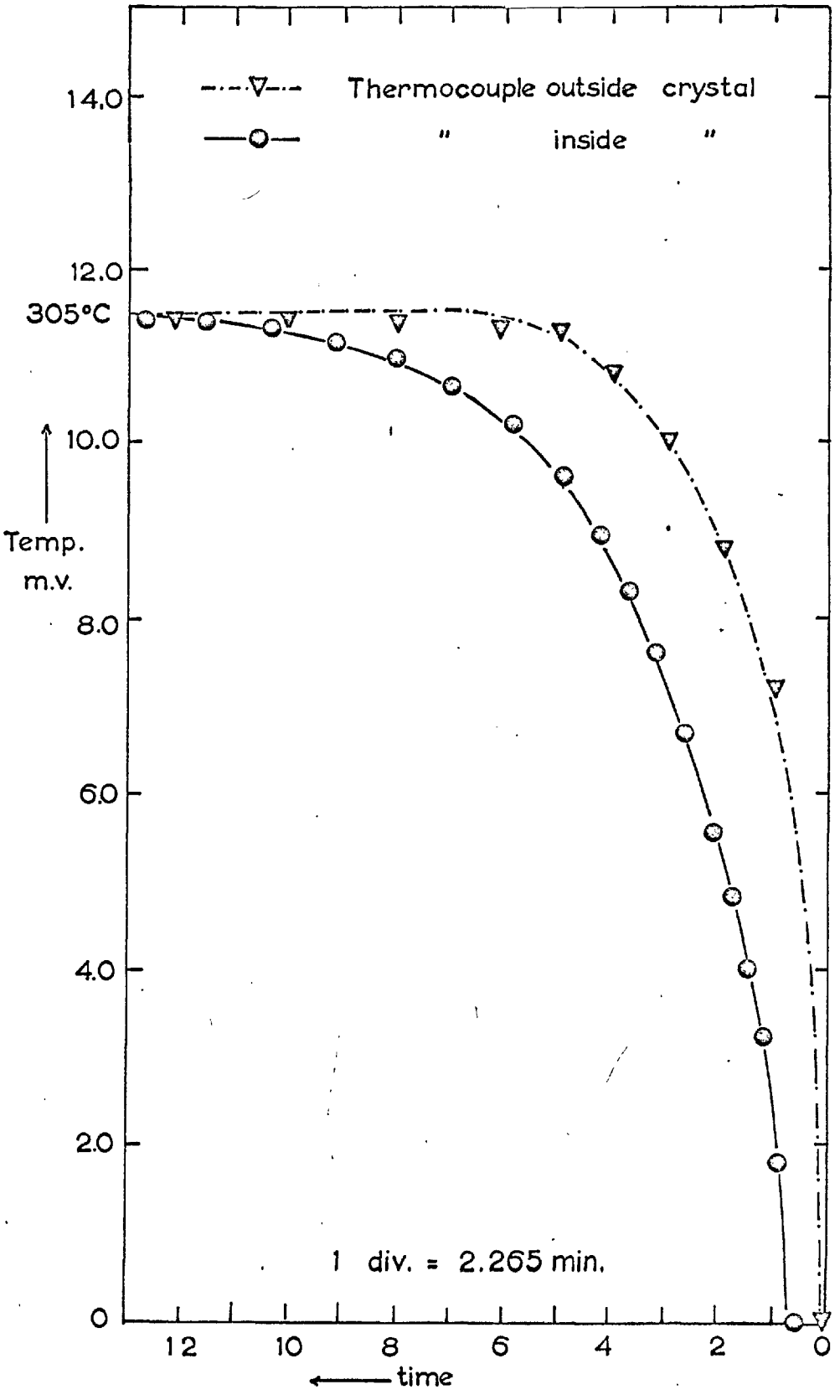

Conductivity rig with fast response time.

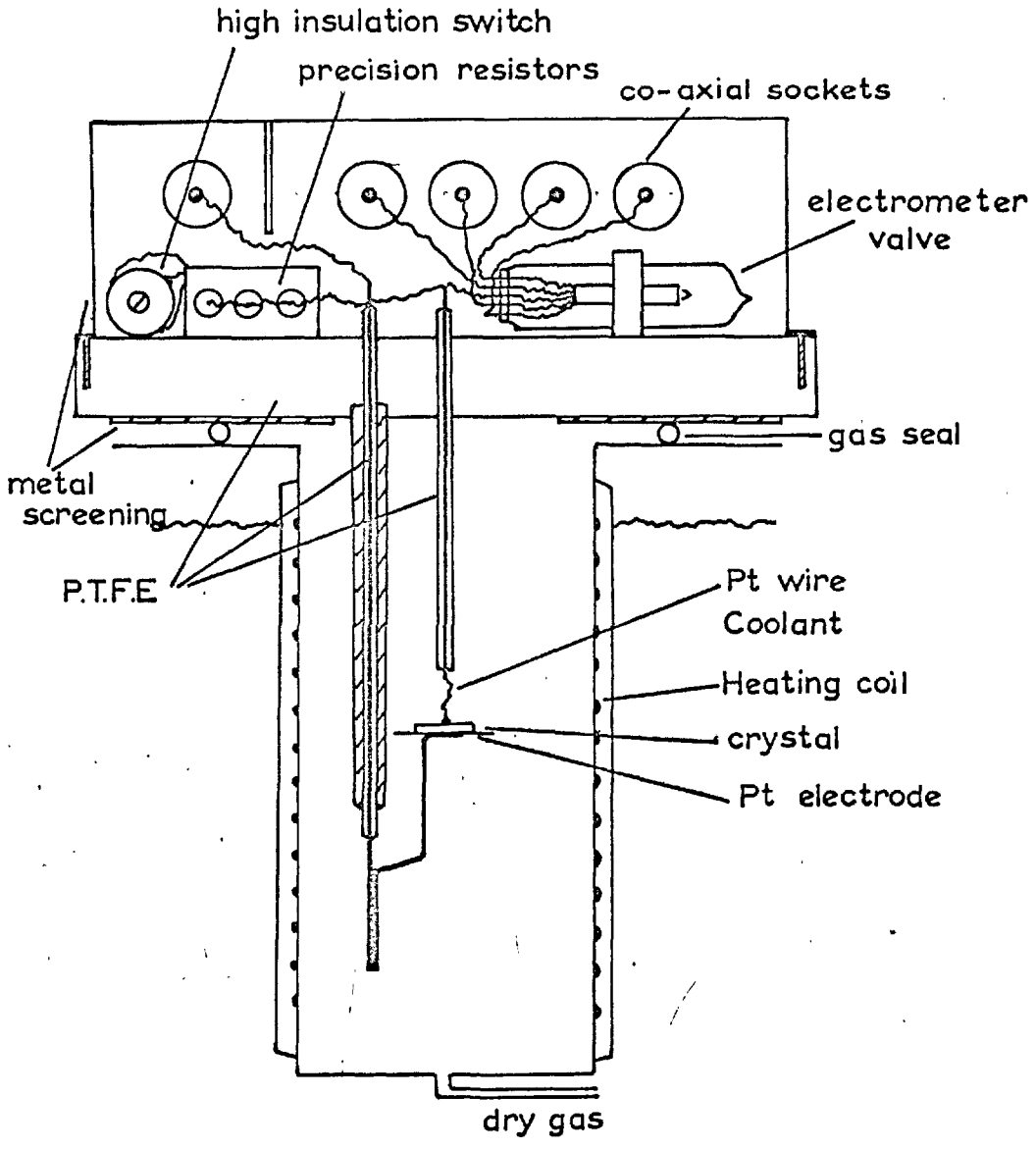

Fig. 3.12.

resistors were housed in a "mu" metal can and were thermally isolated from the cooling chamber by a $\frac{1}{2}$ inch thick slab of P.T.F.E. A piece of platinum foil soldered to the H.T. lead formed the lower electrode and the crystal was mounted onto this, using a colloidal silver suspension. The screen grid connection on the electrometer valve formed the upper electrode, it being held in place on the uppermost surface of the crystal with a droplet of the colloidal suspension. The cooling chamber consisted of a cylindrical copper enclosure surrounded by suitable constant temperature baths. Inside this enclosure a nichrome furnace was wound upon a cylindrical copper former which surrounded the crystal and its electrodes. The whole enclosure was gas tight, and was supplied with a dried, high purity argon atmosphere. Temperature control was achieved in the usual manner, an anticipatory controller regulating the D.C. power supplied to the furnace. The crystal temperature was measured using a chromel-alumel thermo-couple placed near the crystal. The same stages of amplification and detection were used on both the probes.

(2) A.C. Conductivity Measurements

The conductivity cell and associated electronics used at high temperatures ($> 300^{\circ}C$) isshown in Fig. (3.13). The insulation resistance of the cell was maintained by using Sintox discs and recrystallised alumina tubes as electrode supports. Because the flow stress of sodium chloride is small at elevated temperatures, the rig was designed to provide a variable loading electrode. In this way the minimum load to maintain contact without deformation was used. The cell also possessed a small thermal capacity, allowing thermal

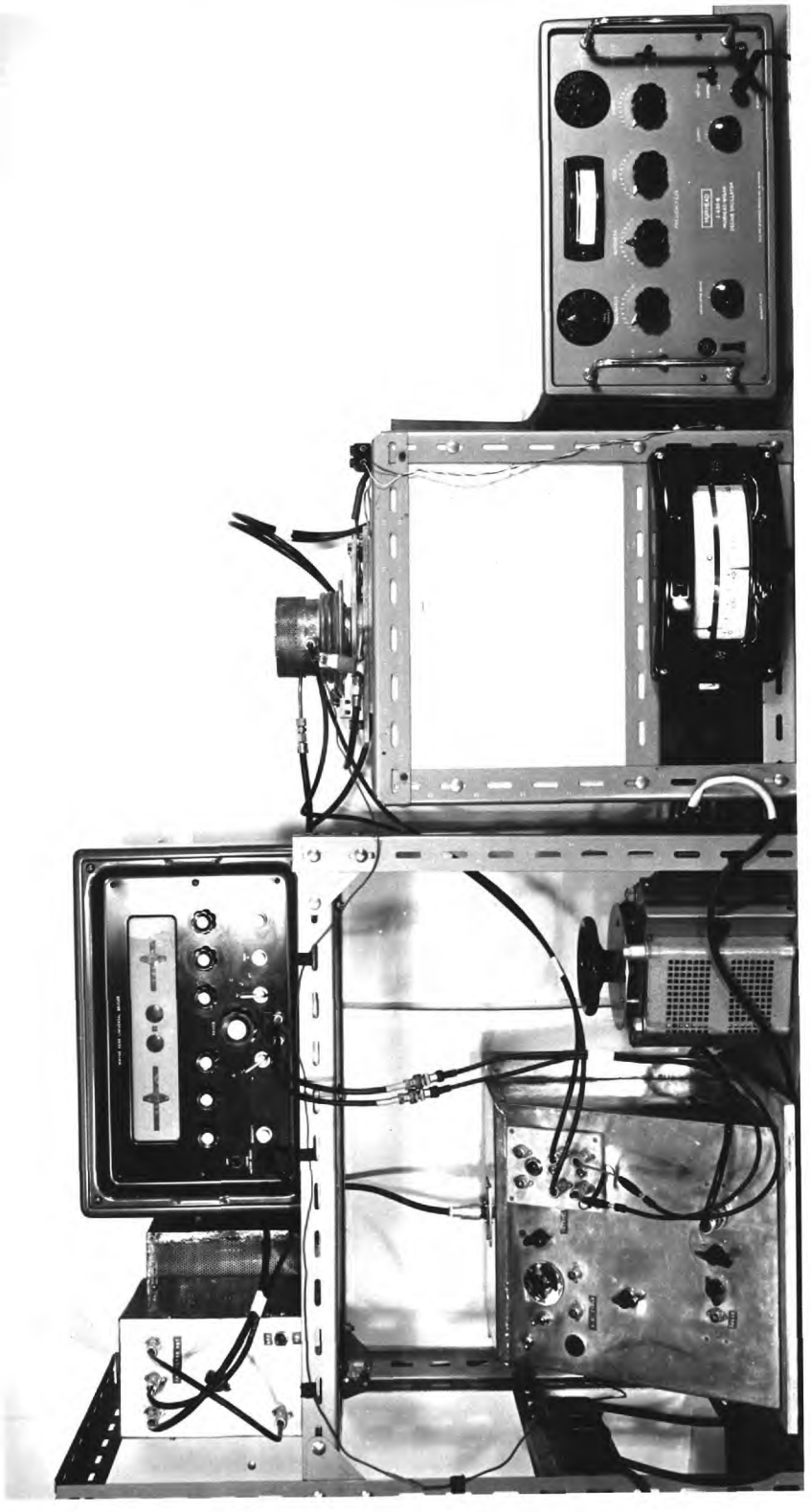

High temperature conductivity rig.

High temperature probe.

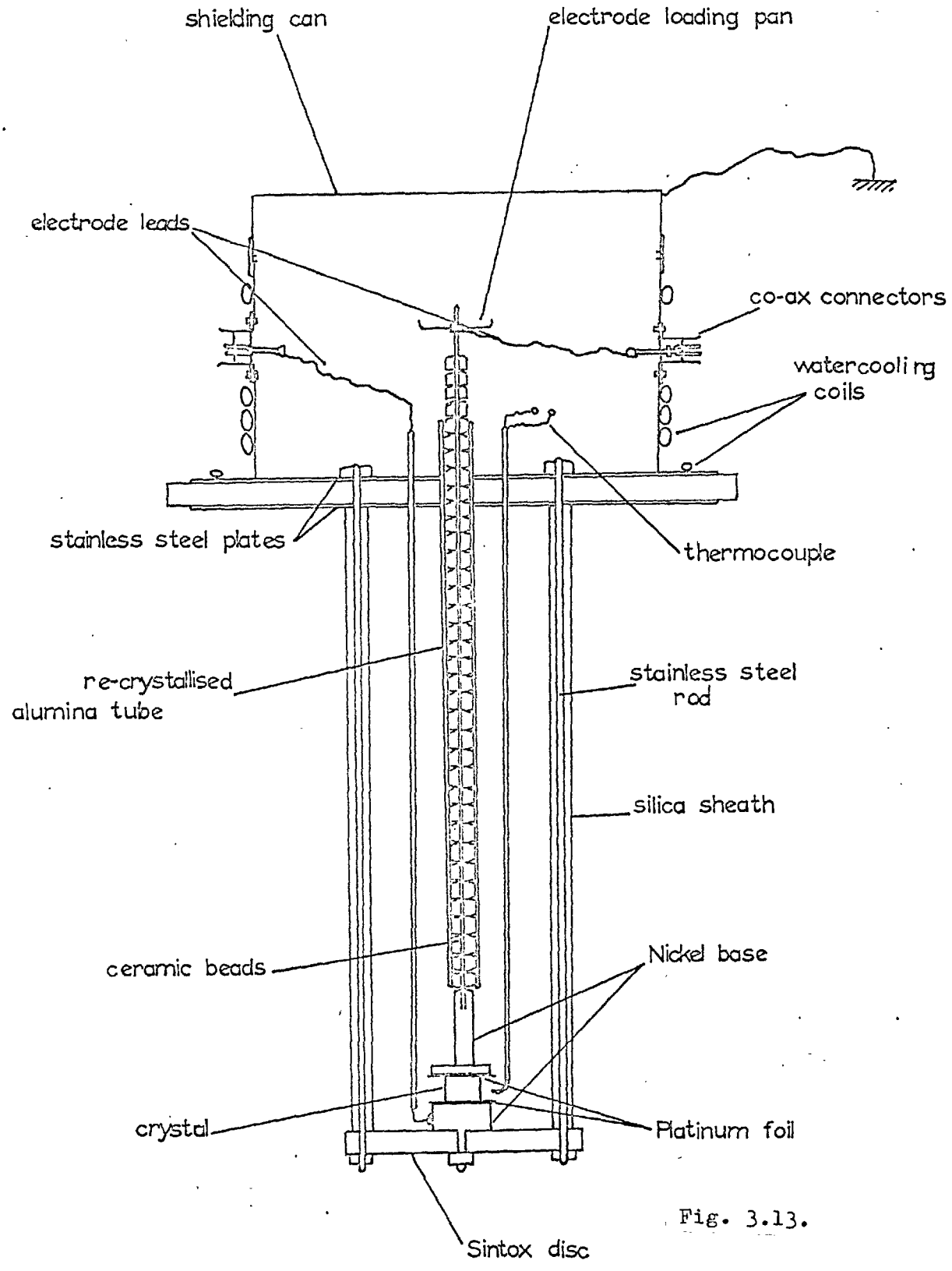

Fig. 3.13.

High temperature furnace.

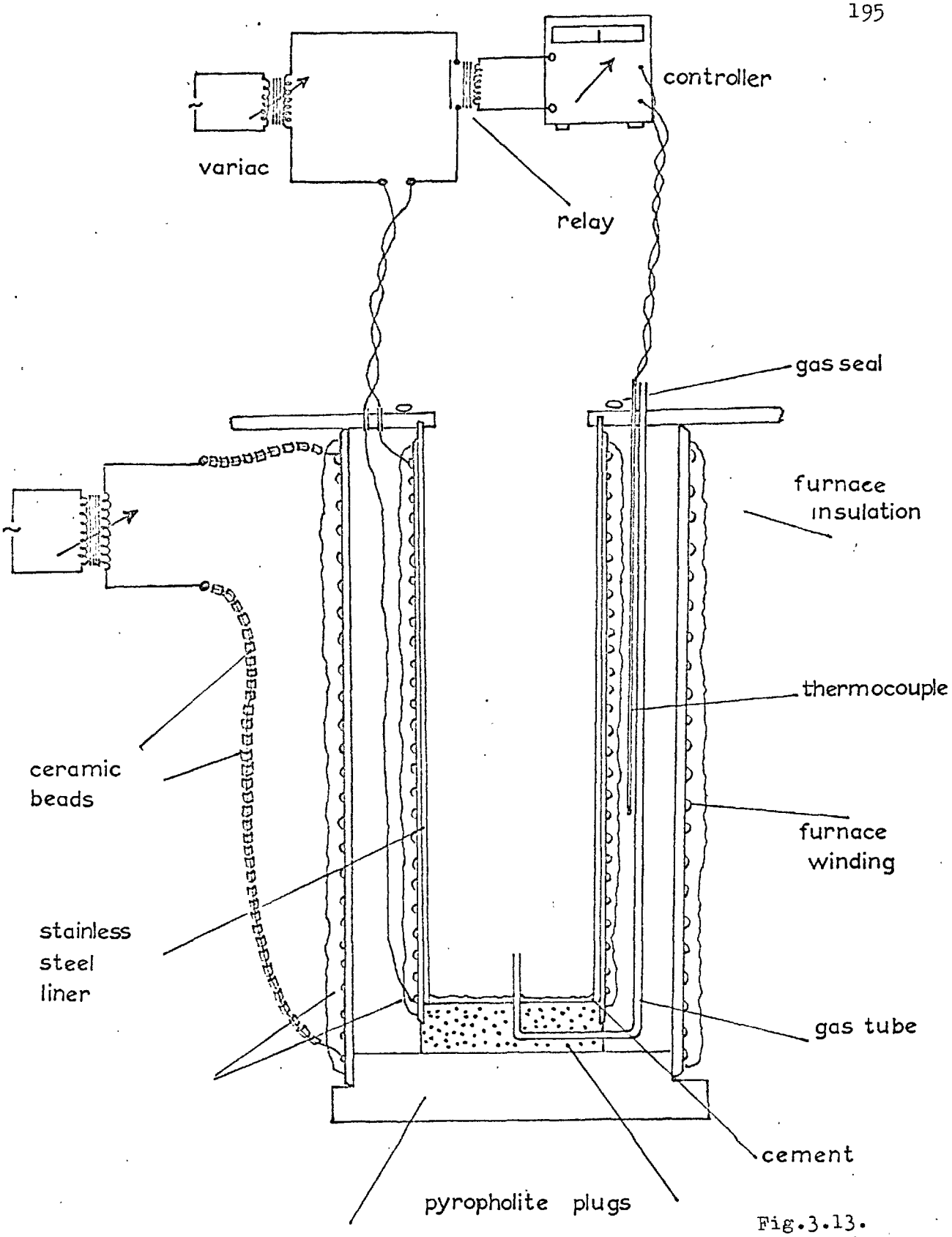

Fig.3.13.

BLOCK DIAGRAM FOR A.C. CONDUCTIVITY WORK.

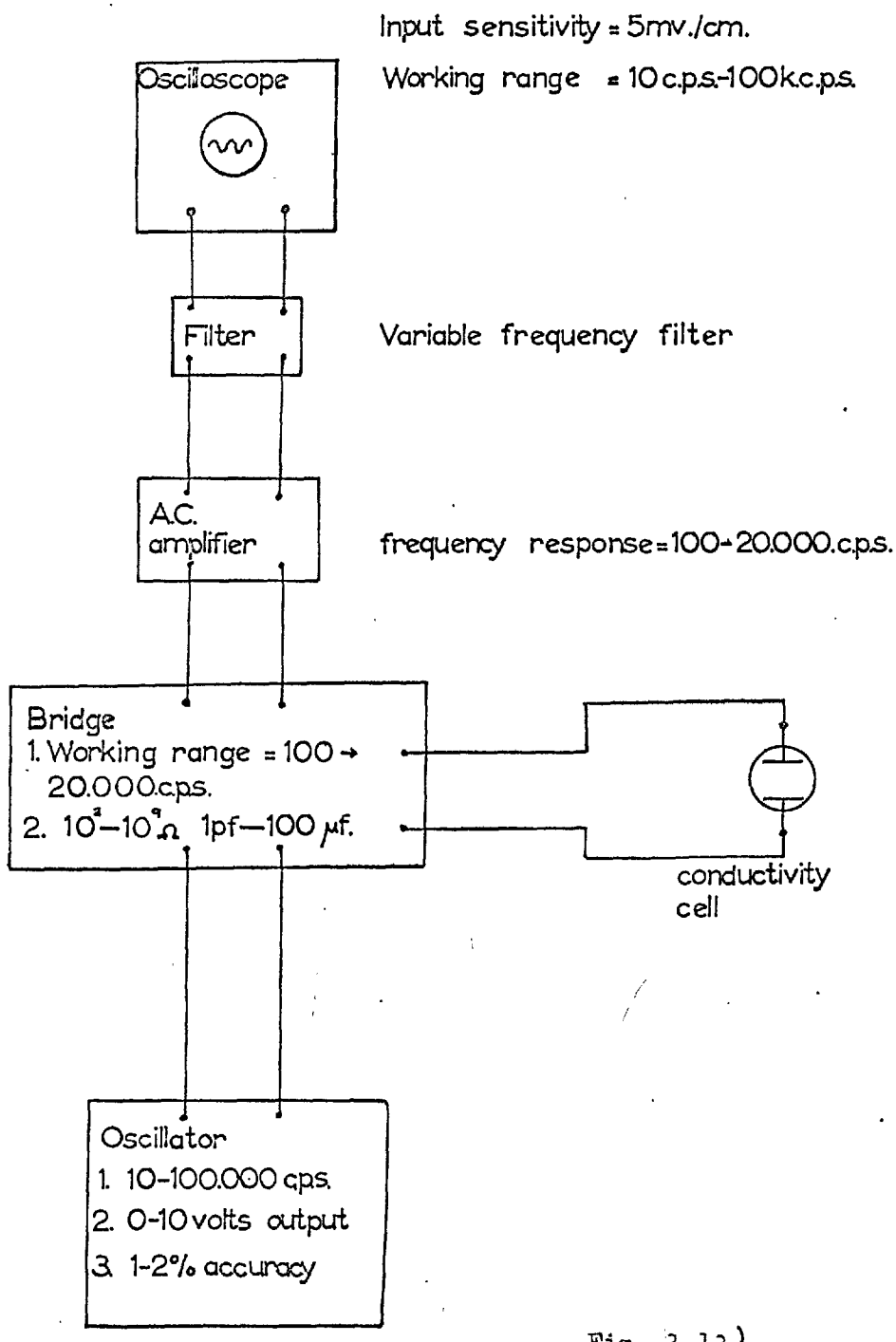

Fig. 3.13)

equilibrium to be quickly attained. A flow of high purity argon gas was maintained from the top and the bottom of the cell. This prevented oxidation of the colloidal graphite coating on the electrodes and of the stainless steel support rods. Nevertheless, some oxidation of the support rods did occur at high temperatures. To prevent this, the rods were subsequently enclosed in silica sheaths. This may appear an unnecessary precaution, but the presence of iron or iron oxide, possibly in the vapour phase, must be avoided in measurements made at high temperatures, as surface conduction, produced by contamination, could easily produce inconsistent results. Electrodes were constructed of platinum foil brazed onto flat nickel blocks, the blocks providing a solid base for support of the crystal. The electrode and crystal surfaces were coated with colloidal graphite to maintain good electrical contact. Platinum wires welded onto the top and the bottom electrodes were connected to co-axial sockets in the head of the probe. These sockets were the connecting points for the A.C. bridge. Temperatures were again measured with a calibrated chromel-alumel thermo-couple placed near the crystal face.

The electrode materials used most widely in the past have been platinum, rhodium, nickel and stainless steel. For experiments conducted a t high temperatures, platinum foil was found to be the most suitable, this material not combining chemically with the crystal during the course of the experiment. Any tendency for chemical combination, between the chlorine ions and the platinum metal was further inhibited by the graphite coating between the surfaces of the crystal and the electrodes. The electrode material also had to possess a high electron affinity, so that few electrons were introduced into the surface of the crystal, to prevent the formation of F centres.

Again platinum was deemed a suitable choice of material.

After checking that the single crystal specimens were free from damage and sub-grain boundaries, good electrical contact was made between the crystal and electrodes by painting both surfaces with a conducting medium. Different forms of contact media were used, the main features of which are tabled as follows:-

COLLOIDAL GRAPHITE	Suitable for use at high and low temperatures. (0°C to 750°C).
COLLOIDAL PLATINUM	Ideal for high temperature work.> 300°C.
COLLOIDAL SILVER	Suitable at temperatures less than 300°C. Above this temperature the silver film breaks up.
VACUUM DEPOSITED SILVER OR GOLD	Low temperature work only. Tends to flake off at high temperatures.

The procedure adopted was to paint one of the specimen platelets on both sides with one of the above colloidal suspensions. After allowing the suspension to dry, a suitable specimen was cleaved from this platelet. This ensured that the sides of the platelet did not get accidentally painted. To ensure that proper contact had been made at low temperatures, Ohm's Law was tested at room temperature. Practically all crystals obey Ohm's Law [7] at low temperatures, up to field strengths of 5000 volts/cm. Any large deviations in linearity of the current/voltage plot were usually caused by poor electrical contact between the crystal and the electrode.

Some workers in the past [8] have annealed their crystals in

contact with the electrode material. These annealing treatments have been conducted at elevated temperatures (600°C to 700°C) for periods of several days. The aim of the heat treatment was to produce consistency of results in the high temperature intrinsic region. This treatment was found to be unnecessary using the weighted electrode with graphite coatings described above. The initial measurements performed upon pure crystals were found to be identical, within the limits of experimental error, to those obtained after periods of twenty-four hours and forty-eight hours. The situation was not the same in doped crystals, where after leaving the crystal at elevated temperatures for long periods of time, inconsistencies and in some cases random results were obtained. Upon examination underthe microscope, the manganese impurity was observed to have diffused out from the surface and become oxidised, thus forming paths of low resistance across the edge of the crystal.

Most of the conductivity data was obtained at a frequency of 1592 c/s. (10,000 rads/s.), which was the frequency of the internal oscillator of the A.C. bridge. Only at temperatures near to the melting point in pure and doped crystals did the conductivity show the frequency dependence associated with the formation of a space-charge region at the crystal-electrode interface. The effects of the space-charge of cation vacancies were eliminated by working at higher frequencies (10 kc/s.). Space-charge formation also produced a large difference between the A.C. and D.C. conductivity, the A.C. values being higher than those obtained with D.C. or pulsed electric fields.

(3) D.C. and Pulsed D.C. Field Measurements

Conductivity measurements under steady and pulsed electric field conditions were obtained at elevated temperatures using the circuit configuration of Fig. (3.14). Potentials, of less than 4 volts were applied to the crystal, and the crystal current observed by measuring the voltage drop it produced across a series of calibrated resistors. Both of these potentials were measured with a vibrating reed electrometer. A square wave generator Fig. (3.15) gave varying magnitude pulses of repitition rates from 10 to 1000 pulses/sec. The transient response of the crystal current was observed with an oscilloscope possessing a fast rise time. The high temperature cell and furnace, Fig. (3.13a, b) used in the A.C. measurements was found to be suitable for the measurements of D.C. conductivity at elevated temperatures.

(iv) Ionic Thermocurrent Instrumentation.

To obtain decent I.T.C. spectra, the equipment had to be able to measure crystal currents of 10^{-16} amps in magnitude, in a vacuum of less than 10^{-5} m.m. of mercury. The vacuum limit was imposed by the level of background interference produced by the evacuated gas molecules colliding with the electrometer head. The crystal was mounted in a stainless steel chamber, which was evacuated with a standard diffusion and rotary pump. The degree of vacuum was measured with a Penning gauge. A lead from the crystal was taken through a high insulation ceramic seal to the head of the commercially available reed electrometer. (E.I.L. Model No. 33C). The chamber,

High temperature D.C. and Pulsed conductivity.

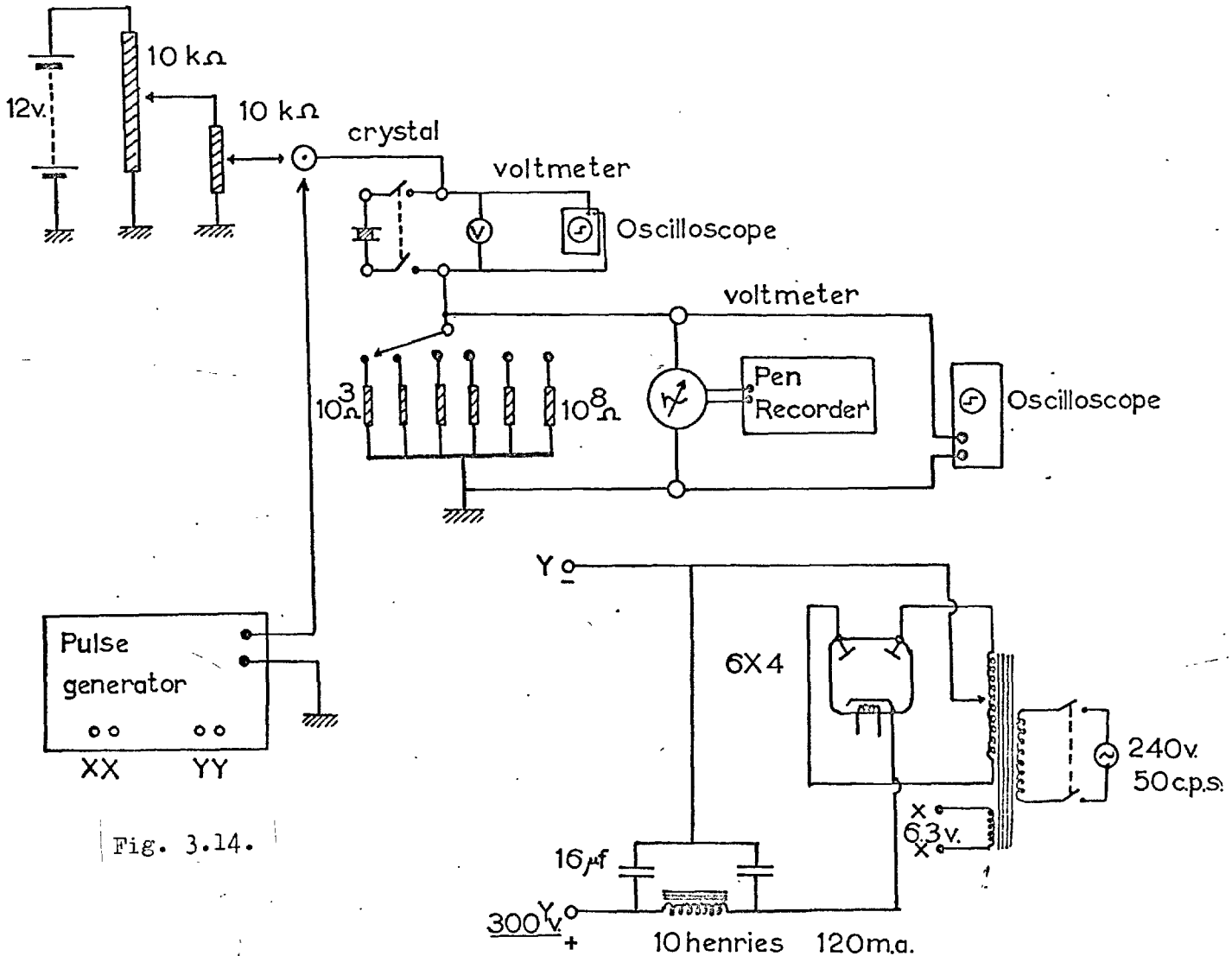

Fig. 3.14.

PULSE GENERATOR.

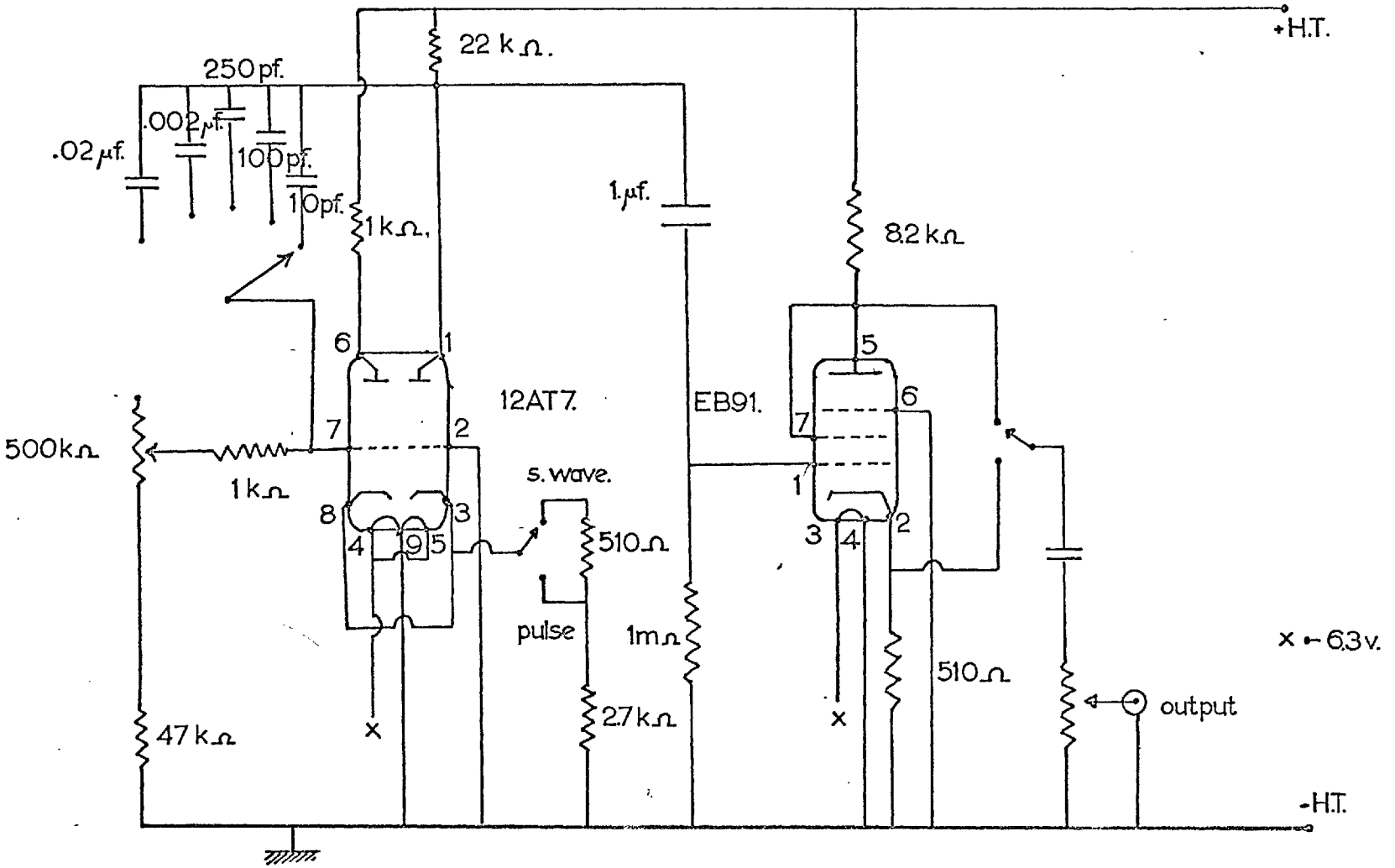

Fig. 3.15.

being made completely of stainless steel, eliminated photocurrents, spurious induced charges and mains pick-up. To reduce any variations in background interference, brought about by variations in pumping speed, a cylindrical copper sheath enclosed the crystal mount and its heating chamber. The H.T. polarizing field was applied to the crystal current lead by the use of a specially constructed, high insulation switch, mounted on the top of the chamber.

The mount for the crystal had to provide a constant temperature surface, an ability to be rapidly cooled from room temperature to liquid nitrogen temperature and also an accurately linear heating rate for the crystal. The device shown in Fig. (3.16) provided these conditions. It consisted of a hollow, copper cylinder whose thermal capacity was variable by the addition of lead shot to its interior. Liquid nitrogen or cooled air was carried through the chamber by cryogenic stainless steel tubes. Around the cylinder was wound a nichrome wire heating coil which in turn was coated with a layer of heat-proof cement. The cement was painted with several layers of a colloidal suspension of silver. This shielded the heating coil from the electrometer input. All other electrical connections were made through ceramic vacuum seals mounted in the base plate. By varying the thermal capacity of the chamber, different heating rates were obtained. By the use of a programmed controller regulating the power supplied to the heating coil, linear heating rates from liquid nitrogen temperature to 200°C could be achieved. Fig. (3.17). A transistorized power pack was built to provide the power for the heating coil, Fig. (3.18). This did not possess the current decay normally associated with batteries used over long periods of time, and was sufficiently stable to be free of mains interference. The

I.T.C. Specimen chamber.

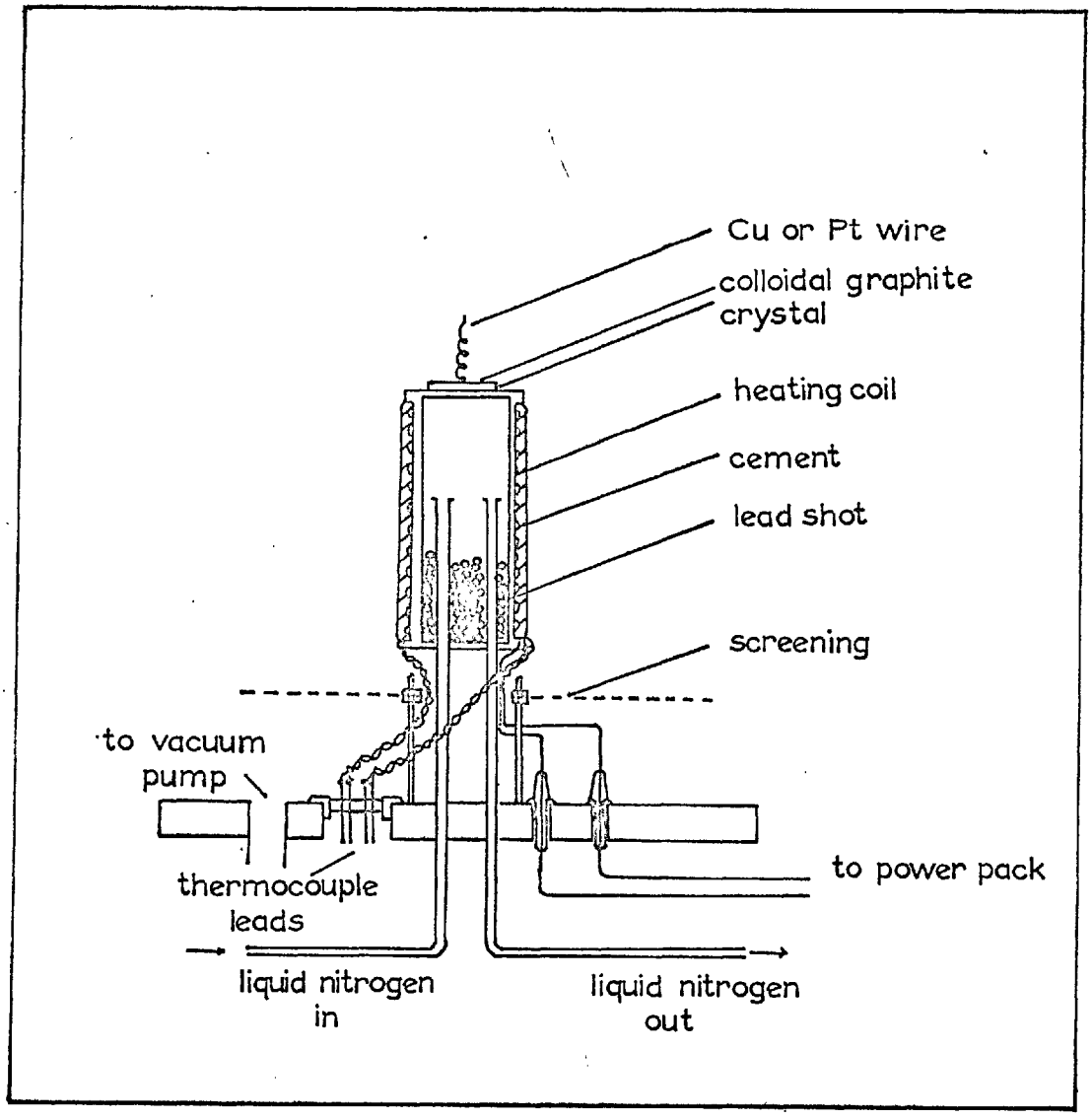

Fig. (3.17)

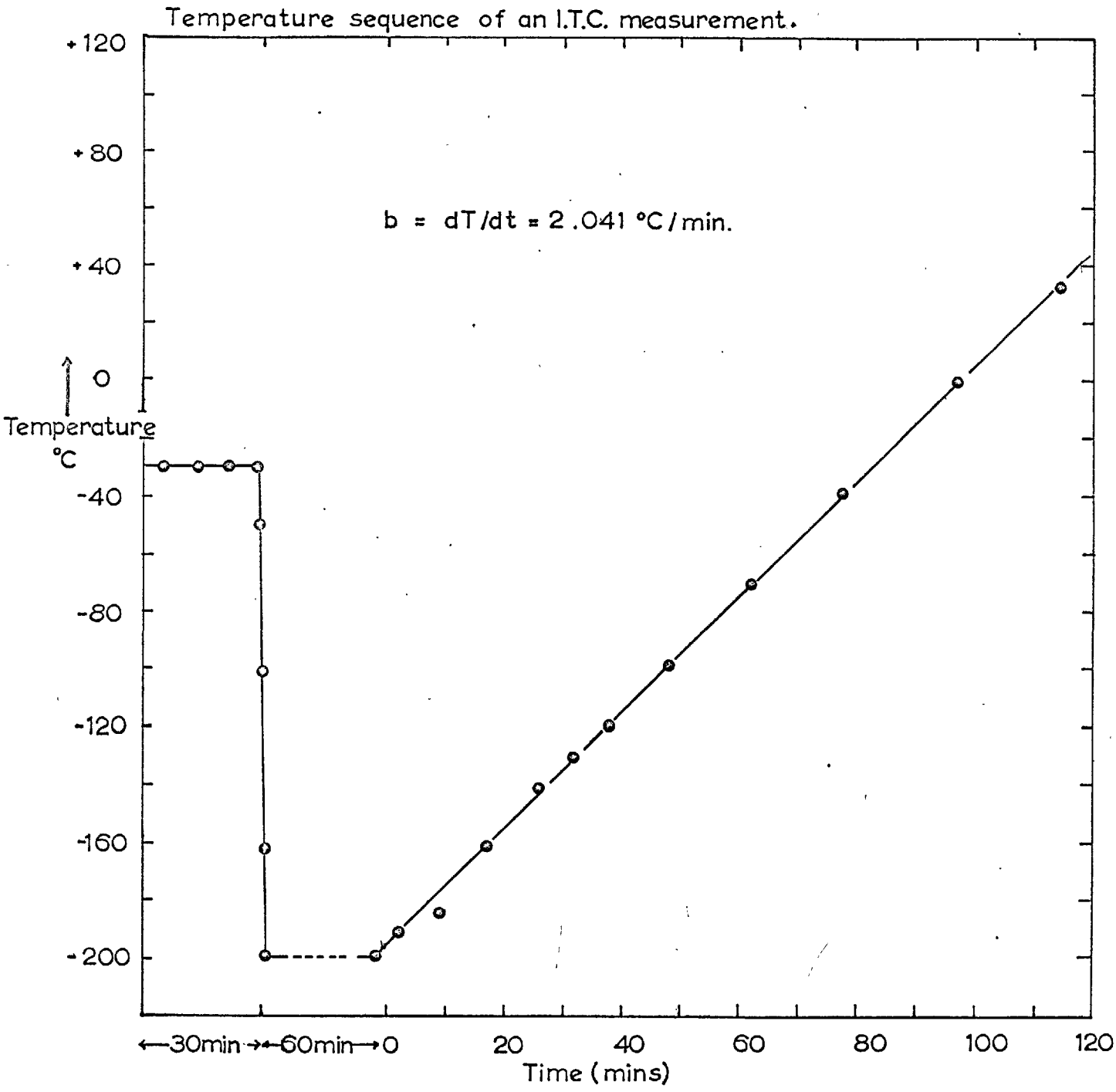
Temperature sequence of an I.T.C. measurement.
+120
+80
+40
0
Temperature °C
-40
-80
-120
-160
-200
b = dT/dt = 2.041 °C/min.
←30min→←60min→0
20
40
60
80
100
120
Time (mins)

Fig. (3.18)

12 volt D.C. power supply

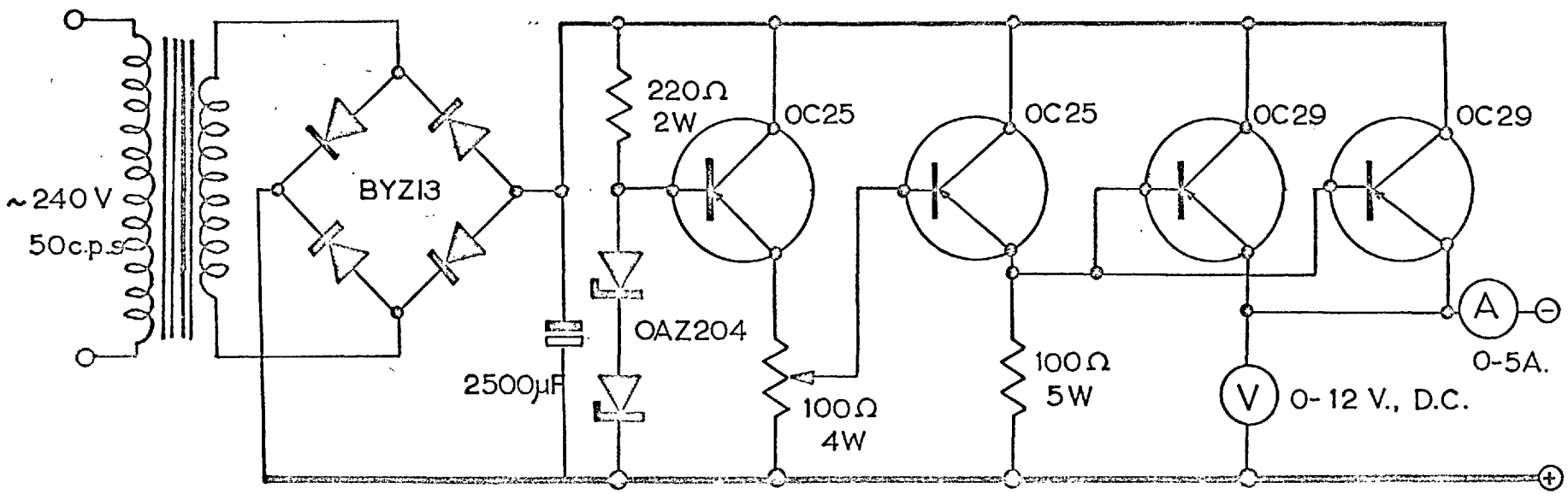

Fig. (3.19)

chamber could be rapidly cooled to liquid nitrogen temperature by the pumping of liquid nitrogen into its interior, the surface of the crystal mount reaching 77°K within 5 seconds. The temperature was monitored by two thermo-couples placed under the lip of the crystal mount's upper surface. Constant temperatures below room level were maintained by pumping suitable coolants into the chamber, e.g. Inceon compounds and other freezing mixtures. Higher temperatures wereachieved by using the controller to regulate the power supplied to the heating coil.

The crystals used were 0.3 m.m. to 0.6 m.m. thick. Crystals thicker than this produced inconsistent results, attributable to the lag in temperature between that of the crystal and the crystal mount's surface. The crystal surfaces were coated with a suspension of colloidal graphite and then attached to the mount with the same suspension. A small lead of fine copper wire was then joined to the top surface of the crystal with the aid of a small droplet of colloidal graphite. When the crystal mount was in place inside the vacuum chamber, the fine copper lead was soldered to the main current and H.T. lead. The polarizing fields were sufficiently large to require a voltage source operating at 1 kV. or more. As the current drain was negligible, when polarizing the crystal, a system utilizing the principal of a Cockcroft-Walton voltage doubling circuit was used. Fig. (3.19). This circuit was essentially an Eccles-Jordan multi-vibrator, oscillating at 1Kcs. and linked to the voltage doubling circuit by a step-up transformer with a turns ratio of approximately 40:1. This provided stable voltages up to 1.5 kV.

The ionic-thermocurrents produced by the crystal when it was heated were measured with the vibrating reed electrometer. The output from

H.T. GENERATOR.

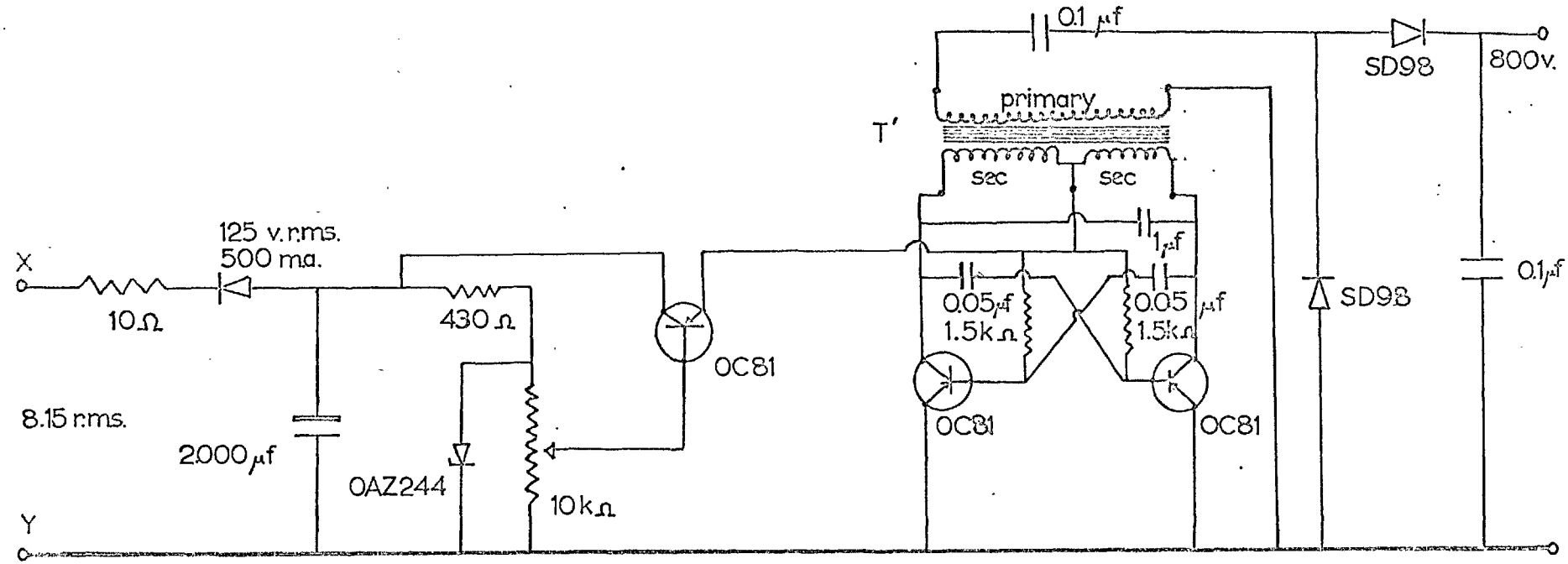

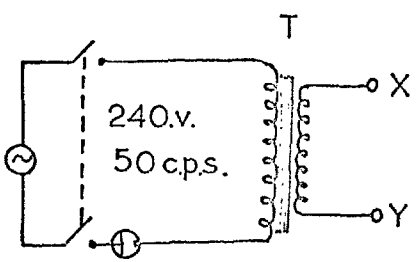

T' ⟶ 6.3 v. centre tapped filament transformer

T ⟶ 8.15 v. secondary

Fig. (3.21)

this electrometer was fed into a Honeywell pen recorder so that the continuous spectrum of ionic thermocurrents was recorded in chart form. This made the process of analysis that much more accurate.

(v) Dielectric absorption

The dielectric absorption experiments were performed using an experimental set-up similar to that presented in Fig. (3.13c). In place of the high temperature conductivity cell, a commercially available Wayne Kerr permitivity cell, with guard ring, was used. This had to be corrected for background losses (as a function of frequency) which were always present. The cell was placed inside a cabinet which maintained any given temperature from room temperature to 50°C with a deviation of ± 0.05°C, thus enabling the absorption peaks to be observed as a function of temperature. For better resolution, the oscilloscope was replaced by a Wayne Kerr harmonic analyser which gave a better determination of the null point for any given frequency.

REFERENCES

1. E. Kyropoulos: Z. Anorg. Allg. Chemic., 154, 308, 1926.

2. R.W. Dreyfus: Appl.Phys. Letts., 3, 175, 1963.

3. R.P. Harrison, P.L. Pratt, C.W.A. Newey: Proc. Brit. Ceram. Soc., 1, 197, 1964.

4. R.W. Dreyfus: The Art and Science of Growing Crystals, Wiley, New York, 1964.

5. E.B. Sandell: Colorimetric Determination of Traces of Metals, Interscience Inc., New York, 1959.

6. Mullard Pamphlet, "The Electrometer valve" ME. 14102.

7. C.A. Buoci, S.C. Riva: J. Phys. Chem. Sol., 26, 363, 1965.

8. A.R. Allnatt, P.W.M. Jacobs: Trans.Farad. Soc., 58, 116, 1962.